Surface fluxes in heterogeneous landscape

Hasager, Charlotte Bay

Publication date:
1997

Document Version
Publisher's PDF, also known as Version of record

Surface Fluxes in Heterogeneous Landscape

Risø-R-922(EN)

Charlotte Bay Hasager

Risø National Laboratory, Roskilde, Denmark
January 1997

Abstract The surface fluxes in homogeneous landscapes are calculated by similarity scaling principles. The methodology is well established. In heterogeneous landscapes with spatial changes in the microscale range, ie from 100 m to 10 km, advective effects are significant. The present work focus on these effects in an agricultural countryside typical for the midlatitudes.

Meteorological and satellite data from a highly heterogeneous landscape in the Rhine Valley, Germany was collected in the large-scale field experiment TRACT (Transport of pollutants over complex terrain) in 1992. Classified satellite images, Landsat TM and ERS SAR, are used as basis for roughness maps. The roughnesses were measured at meteorological masts in the various cover classes and assigned pixel by pixel to the images.

The roughness maps are aggregated, ie spatially averaged, into so-called effective roughness lengths. This calculation is performed by a microscale aggregation model. The model solves the linearized atmospheric flow equations by a numerical (Fast Fourier Transform) method. This model also calculate maps of friction velocity and momentum flux pixelwise in heterogeneous landscapes.

It is indicated how the aggregation methodology can be used to calculate the heat fluxes based on the relevant satellite data ie temperature and soil moisture information.

This thesis was submitted to the University of Copenhagen in partial fullfillment of the requirements for the Ph.D. degree in October 1996 and defended in December 1996. A few corrections are included in the present version of the report.

ISBN 87-550-2218-9
ISSN 0106-2840

Information Service Department • Risø • 1997

Contents

Notation and acronyms

$\overline{\ }$	time average
$< >$	spatial average

A	function in drag law (in neutral ~ 1.8)
B	function in drag law (in neutral ~ 4.5)
B^{-1}	excess resistance parameter (-)
c	concentration of a scalar (kg m^{-3})
c_1	constant (- ~ 100)
c_2	constant of intercept from linear regression (mm)
c_3	constant of slope from linear regression (mm K^{-1})
c_4	constant (s m^{-1} K^{-1})
c_5	constant (mm $K^{-3/2}$)
c_6	radiation constant (W μm^4 m^{-2} $=3.7413*10^8$)
c_7	radiation constant (μm K $=1.4388*10^4$)
c_8	speed of light ($3*10^8$ m s^{-1})
c_9	specific radar system constant
c_{10}	constant (kg s^{-2} m^{-1} K^{-1} ~ 0.046)
c_{11}	constant (kg s^{-2} m^{-2} K^{-1} ~ 1.791)
c_{12}	constant (-)
C_i	subgrid coefficient of patch i (-)
C_E	equilibrium transfer coefficient for heat (-)
C_H	bulk transfer coefficient for heat (Stanton number) (-)
C_{HN}	bulk transfer coefficient for heat at neutral stability (-)
CH_4	methane
C_M	bulk transfer coefficient for momentum (-)
C_Q	bulk transfer coefficient for humidity (-)
C_S	bulk transfer coefficient for passive scalar (-)
c_p	specific heat capacity at constant pressure for moist air (m^2 s^{-2} K^{-1} ~ 1004)
d	displacement height (m)
D	diffusion coefficient of gas (m^2 s^{-1} for O_3 and NO_2 $\sim 14*10^{-6}$)
DN	digital number (-)
E	latent heat flux (kg H_2O m^{-2} s^{-1})
E_λ	radiant exitance (W m^{-2} μm)
E_{SB}	radiant exitance of all wave lenght (W m^{-2})
ET_d	daily evaporation (mm day^{-1})
f	frequency (s^{-1})
F	flux
f_c	Coriolis force (s^{-1}).
f_i	fractional area (-)
F_R	value of resolution cell
g	acceleration of gravity (m s^{-2} ~ 9.82)
g	conductance (m s^{-1})
G_R	gain in specific radar antenna
G	geostrophic wind speed (m s^{-1})
g_i	conductance in patch number i (m s^{-1})
h	convective boundary layer height (m)
H	sensible heat flux (J m^{-2} s^{-1})
h_c	canopy height (m)
h_c^*	effective canopy height (m)
$\Im$	imaginary number
$\overline{k_h}$	wave vector in Fourier space
HH	horizontally received, horizontally transmitted

HV	horizontally received, vertically transmitted
k	wavenumber in x-direction (rad m^{-1})
K_e	turbulent exchange coefficient for moisture (-)
K_h	turbulent exchange coefficient for heat (-)
K_m	turbulent exchange coefficient for momentum (-)
K_s	turbulent exchange coefficient for passive scalars (-)
K_x	turbulent exchange coefficient horizontally (-)
K_z	turbulent exchange coefficient vertically (-)
l	wavenumber in y-direction (rad m^{-1})
l	leaf dimension (m spruce ~0.005, deciduous ~0.01)
L	Monin Obukov mixing lenght (m)
l_b	blending height (m)
L_c	horizontal length scale (m)
l_d	diffusion height (m)
L_d	domain lenght (m)
l_e	lenght scale of the main eddies (m)
L_e	horizontal adjustment scale (m)
L_p	patch length (m)
L_x	horizontal lenght scale (m)
M	magnitude in roughness step change logarithmic ratio (-)
m(x,y)	roughness pertubation (-)
$\hat{m}(k,l)$	roughness pertubation in Fourier space (m^{-1})
N_L	number of looks (-)
NO	nitrogen dioxide
0_3	ozone
P_R	power received in radar per pixel (Volt)
p_j	parameter with j variables
Pr	Prandtl number (for heat 0.71)
q'	humidity pertubation (g H_2O g^{-1} air)
q_*	humidity scale (g H_2O g^{-1} air)
Q	grid air specific humidity (g H_2O g^{-1} air)
q	specific humidity (g H_2O g^{-1} air)
q_{sg}	subgrid specific air humidity (g H_2O g^{-1} air)
QG_d	daily ground heat flux (mm day^{-1})
QH	sensible heat flux (W m^{-2} K^{-1})
QH_d	daily sensible heat flux (mm day^{-1})
$q_{i,sg}$	subgrid air specific humidity (g H_2O g^{-1} air)
q_{sat}	saturated surface humidity (g H_2O g^{-1} air)
$\Re$	real number
r_a	aerodynamic resistance (s m^{-1})
r_b	excess resistance (s $^{-1}$)
r_c	canopy resistance (s m^{-1})
r_h	heat resistance (s m^{-1})
r_q	humidity resistance (s m^{-1})
r_s	surface resistance (s m^{-1})
R	resolution element
Ra	radar range
Ri	Richardsons number (-)
Rn_d	daily net radiation (mm day^{-1})
Ro	Rossby number (-)
r_q	humidity resistance (s m^{-1})
r_s	surface resistance (s m^{-1})
S	scalar flux (kg m^{-2} s^{-1})
Sc	Schmidt number (for water vapour 0.60)
T	time since dawn (s)
t_*	convective eddy time scale (s)

T_a	air temperature (K)
T_{ai}	subgrid air temperature of patch i (K)
T_g	grid ground temperature (K)
T_0	basic state temperature (K)
T_s	surface radiant temperature (K)
T_{si}	subgrid surface radiant temperature (K)
T_{gi}	subgrid ground temperature of patch i (K)
u	streamwise wind speed (m s^{-1})
u'	streamwixe velocity pertubation (m s^{-1})
U	magnitude of streamwise wind (m s^{-1})
u_*	friction velocity (m s^{-1})
u_{*0}	friction velocity for equilibrium flow (m s^{-1})
v	lateral wind speed (m s^{-1})
v'	lateral velocity pertubation (m s^{-1})
VH	vertically received, horizontally transmitted
VV	vertically received, vertically transmitted
w	vertical wind speed (m s^{-1})
w'	vertical velocity pertubation (m s^{-1})
w_*	vertical velocity scale in CBL (m s^{-1})
w_i	weighting coefficient of patch i (-)
W^i	subgrid surface soil moisture of patch i (%)
W	surface soil moisture (g H_2O per g soil)
w_{temp}	weighting coefficient for temperature (~ 0.8)
w_q	weighting coefficient for humidity (~ 0.25)
X	dynamic patch lenght scale (m)
z	level above ground (m)
z_d	level above ground (m)
z_{0a}	average equilibrium roughness length for momentum (m)
z_0	roughness lenght for momentum (m)
z_{0q}	roughness lenght for humidity (m)
z_{0s}	roughness length for passive scalar (m)
z_{0t}	roughness lenght for temperature (m)
z_{0ta}	average equilibrium roughness lenght for temperature (m)
$z_{0t,r}$	radiometric roughness length for temperature (m)
z_r	computational height above ground (m)
æ	silhouette area of average obstacle (m^2)
Æ	cross-wind area (lot area) (m^2)

α	wetness factor (-)
β	Bowen ratio (-)
Δ	difference
δ_i	internal boundary layer height (m)
ϵ	emissivity (-)
θ'	potential temperature pertubation (K)
θ_*	temperature scale (K)
κ	the von Karman constant (~ 0.4)
λ	electromagnetic radiation wave length (m)
ν	kinematic viscosity of air (m^2 s^{-1} $\sim 15*10^{-6}$)
Π_R	effective parameter set for resolution cell
ρ	density of air (kg m^{-3} ~ 1.2)
ρ_{corr}	correlation coefficient
σ^0	backscatter coefficient (-)
σ^0_{dB}	backscatter coefficient (dB)
$\sigma_{\sigma 0}$	standard deviation on backscatter coefficient (-)

ρ_ϕ	standard deviation on angular direction (°)
σ_{Ri}	standard deviation of bulk Richardsons number (-)
σ_{SB}	Stefan-Boltzmann radiation constant (W m^{-2} K^{-4} $=5.6693*10^{-8}$)
σ_{Ts}	standard deviation of radiation temperature (K)
σ_u	standard deviation of streamwise wind speed (m s^{-1})
σ_v	standard deviation of lateral wind speed (m s^{-1})
σ_w	standard deviation of vertical wind speed (m s^{-1})
τ	momentum flux (kg m^{-1} s^{-2})
τ	shear stress (Pa)
τ_0	surface shear stress (Pa)
τ_{01}	surface shear stress before a change (Pa)
τ_{02}	surface shear stress after a step change (Pa)
Ψ	stability corrections term (-)
Ψ_E	stability correction term for humidity (-)
Ψ_H	stability correction term for heat (-)
Ψ_M	stability correction term for momentum (-)
Ψ_S	stability correction term for a passive scalar (-)
θ_0	potential surface temperature (K)
θ	virtual potential temperature (K)
ϕ	angular direction, incidence angle (°)

Abbreviations

AIRS	Advanced Infrared Radiometer Sounder
ALMAZ	Russian radar satellite
APAR	absorbed photosynthetic active radiation
ATSR	Along Track Scanning Radiometer
AVHRR	Advanced Very High Resolution Radiometer
BATS	Biosphere-Atmosphere Transfer Scheme
BOREAS	BOReal Ecosystem-Atmosphere Study (Canada 1991)
SIR	Shuttle Imaging Radar
CASI	Compact Airborne Spectrographic Imager
CBL	convective boundary layer
DANMAC	DANish Multisensor Airborne Campaign (Denmark 1994-1996)
DEM	digital elevation model
D-PAF	Deutschland-Processing and Archiving Facilities
DN	digital number
ECHIVAL	European project on Climate and Hydrological Interactions between Vegetation, Atmosphere and Land surfaces
EFEDA	ECHIVAL First field Experiment in Deserfication threatened Area (Spain 1991)
EMI	Electro Magnetics Institute
EMISAR	Electro Magnetics Institute Synthetic Aperture Radar
EOS	Earth Observing System
ENL	equivalent number of looks
ERS-1	European Research Satellite
EUROTRAC	EUROpean experiment on TRAnsport and transformation of environmentally relevant trace Constituents in the troposphere over Europe
FFT	fast fourier transform
FIFE	First ISLSCP Field Experiment (Kansas 1987 & 1989, USA)
GMT	Greenwich Mean Time
GCM	Global Circulation Model
GHIS	GOES High-Resolution Interferometer Sounder
GOES	Geostationary Operational Environmental Satellite
HAPEX	Hydrological and Atmospheric Pilot Experiment
MOBILHY	HAPEX-Modelization de BILan HYdrique (France 1986)

HAPEX-Sahel	HAPEX in Niger (1992)
HIRS	High-resolution Infrared Radiation Sounder
HIS	High-resolution Interferometer Sounder
IBL	Internal Boundary Layer
IRS	Indian Remote sensing Satellite
ISLSCP	International Satellite Land Surface Climatology Project
JERS	Japanese Earth Resources Satellite
KAMM	KArlsruhe Mesoscale Model
LAI	leaf area index (m^2 leaf m^{-2} ground) (-)
LAI_e	effective leaf area index (m^2 m^{-2}) (-)
LANDSAT	LAND remote sensing SATellite
LASA	Laser Atmospheric Sounder and Altimeter
METEOSAT	METEOrological SATellite
MONSOON 90	"monsoon" in arid area (Arizona, USA 1990)
NDVI	Normalized Difference Vegetation Index (-)
$NDVI^*$	scaled NDVI (-)
$NDVI_0$	NDVI for bare soil (-)
$NDVI_s$	NDVI for 100% vegetation cover (-)
NIR	near infrared band
NOAA	National Oceanic and Atmospheric Administration
NOPEX	NOrthern hemisphere climate Processes land-surface EXperiment (Sweden 1994)
PBL	planetary boundary layer
pixel	picture element
Radarsat	RADAR SATellite
RESURS	Russian Earth ressources satellite
Seasat	SEA SATellite
SAR	Synthetic Aperture Radar
SiB	Simple Biosphere model
SIR	Shuttle Imaging Radar
SIBL	Stable Internal Boundary Layer
SLIMM	Surface Layer Integration Measurement and Modelling project (The Netherlands 1997)
SMMR	Scanning Multichannel Microwave Radiometer
SSM/I	Special Sensor Microwave Imager
SST	sea surface temperature
SVAT	Soil-Vegetation-Atmospheric-Transfer
TIBL	Thermal Internal Boundary Layer
TM	Thematic Mapper
TOVS	TIROS-N Operational Vertical Sounder
TIROS	Television and Infrared Observational Satellite
TRACT	Transport of Pollutants over Complex Terrain (Germany, Switzerland, France 1992)
UK-PAF	United Kingdom-Processing and Archiving Facilities
UTM	Universal Transversal Mercator

1 Introduction

The fluxes between the earth's surface and the atmosphere are usually called surface fluxes. Many processes are involved such as evaporation from land and sea, warming and cooling of the earth, emission and deposition of gases and particles. These processes are vital to life and are being investigated in various scientific fields such as agriculture, bioclimatology, hydrology and meteorology.

Surface fluxes determine the mean profiles of wind, temperature and humidity in the surface layer and therefore play an important role in short-range forecasts of wind and temperature. Surface fluxes also enter models as varied as air pollution models, ocean wave models, plant stress models, wind energy prediction and global circulation models (GCM).

Exchange of water vapour, trace gases, pollutants, momentum and energy between the surface and the atmosphere is a continuous process which takes place on all scales in space and time. These range from the microscopic level, for example, the transfer of water through the stomata of leaves, to global level systems such as planetary warming due to the green house effects. Relating microscopic processes to global effects is not straightforward. An idealized link between the two is the so-called "nesting methodology".

Nesting here means describing a very small piece of the global system with a detailed parametrization. The system can be a single plant with roots and the adjacent air and soil. This small-scale phenomenon is subsequently nested into a local scale model. However new important parameters enter on the local scale and therefore the fine scale parameters will have to be reduced to "bulk" parameters. "Bulk" parameters are of a conceptual nature, contrary to the deterministic small-scale parameters. Often "bulk" parameters are area-integrated, as opposed to time-integrated values.

Local scale processes can be nested into regional-scale (mesoscale) processes, and these again nested into global-scale processes. At all scale steps new parameters enter, and a reduction of the finer scale parameters will be needed.

A simple and sensible way of proceeding from point to domain (upscaling) is to choose systems as homogeneous and large as physically possible. This forms the conceptual basis of a number of large-scale field experiments which typically encompass one to three large-scale terrain types.

In 1992 a highly heterogeneous mid-latitude area was investigated with respect to atmospheric flow and surface fluxes within the project TRACT. TRACT is an acronym for Transport of Pollutants over Complex Terrain. The pronounced heterogeneity made upscaling a very important issue. The present study addresses the issue of scaling surface fluxes from local scale to mesoscale. A physically based microscale flux aggregation method is the principle theme in the present report.

In practice spatial surface data are only available from satellite sensors. In the

present project remote data are linked to values measured in the field and used as boundary conditions in the microscale flux aggregation model. The increasing amount of accessible satellite data make estimation of more bio-geophysical parameters possible. This trend is described with regard to surface flux calculation. Optical and radar satellite data from the TRACT area in the Upper Rhine Valley provide a basis for the formation of regional roughness maps.

The microscale flux aggregation model is based on a physical description of turbulent flow and constitutes an alternative to the heuristic blending height method. The flow equations are linearized and only the diffusion term is modelled. A Fast Fourier Transform is used to solve the equations. The microscale model predicts area-integrated (effective) roughness values representative for mesoscale grid cells. It also predicts local values of friction velocity and land surface momentum flux. Maps of momentum flux in the Rhine Valley are produced with a resolution of 25 m * 25 m and 30 m * 30 m based on respectively, ERS-1 SAR and Landsat TM satellite data.

A future version of the microscale flux model aims at the prediction of heat and passive scalar fluxes. Prediction of land surface deposition of pollutants will be possible by inverting the model. Such downscaling require grid mean concentrations of the pollutant as input.

Momentum flux results from the microscale model compared reasonably to field data from a site. A further validation of the spatial land surface momentum flux map awaits adequate data. Airborne eddy correlation data seem ideal for this purpose.

In brief summary, the present project has focused on surface flux retrieval in a highly heterogeneous landscape. For all surface fluxes the surface roughness is important because of significant nonlinear effects. The more heterogeneous the landscape, the more pronounced the nonlinearity. A prerequisite therefore, for surface flux calculation, is spatial data of surface roughness. This boundary condition is only obtainable from high-resolution remote data. Satellite-based roughness maps were input in a microscale flux aggregation model. The outputs were detailed maps of area-integrated roughness values, effective local friction velocity maps and local land surface momentum flux maps. The highly detailed land surface momentum flux maps seem to be the first of their kind.

2 Surface fluxes in homogeneous terrain

Calculation of surface fluxes can be done by different methods. The measured values necessary to calculate surface fluxes are subject to variation. So are the assumptions. Surface fluxes in heterogeneous terrain are calculated with modifications to the methods valid for homogeneous terrain. The latter are briefly described in chapter 2: the gradient method, the eddy correlation method and the resistance approach.

2.1 Homogeneous terrain

Field measurements of, say, wind, temperature, radiation balance and humidity take place at a given point in space but are usually assumed to represent a given area in space. The surrounding area is horizontally homogeneous in respect to the values measured.

The classic equations for calculating the surface fluxes apply only to areas where the assumptions of horizontal homogeneity and stationarity hold. The stationarity assumption secures that the statistical properties of the flow do not change with time. In this case the time averages represents the properties of the process and not those of the averaging time.

If a variable is both stationary and horizontally homogeneous, the mean time average (averaging a time series) and the mean area average (averaging in space) are identical values. In such cases we actually have an ensemble value. Ensemble averages consist of the sum over an infinite number of identical experiments (Stull 1991, Wyngaard 1991). Ensemble values do exist only in numerical computer models or in laboratories but not in the field.

2.2 Gradient method

Calculation of fluxes of momentum (τ) (kg m^{-1} s^{-2}), sensible heat (H) (J m^{-2} s^{-1}), latent heat (E) (kg H_2O m^{-2} s^{-1}) and scalar fluxes (S) (kg m^{-2} s^{-1}) can be done by use of the gradient method. The method is based on the concept that the turbulent transport in the atmosphere is analogous to molecular diffusion. Flux is defined as the transfer of a quantity per unit area per unit time. When we know the vertical gradients of the mean virtual potential temperature ($\overline{\theta}$) (K), the mean specific humidity ($\overline{q}$) (g H_2O g^{-1} air), the mean streamwise wind component ($\overline{u}$) (m s^{-1}) and the mean concentration of a scalar ($\overline{c}$) (kg m^{-3}), the surface fluxes can be calculated by the following expressions

$$\tau = K_m \rho \frac{\partial \bar{u}}{\partial z} \quad (1)$$

$$H = -K_h \rho c_p \frac{\partial \bar{\theta}}{\partial z} \quad (2)$$

$$E = -K_e \rho \frac{\partial \bar{q}}{\partial z} \quad (3)$$

$$S = -K_s \frac{\partial \bar{c}}{\partial z} \quad (4)$$

The turbulent exchange coefficients (or so-called eddy diffusivities) are for momentum, K_m ($m^2\ s^{-1}$), heat, K_h ($m^2\ s^{-1}$), moisture, K_e ($m^2\ s^{-1}$) and passive scalars, K_s ($m^2\ s^{-1}$), respectively. ρ (kg m^{-3} ~ 1.2) is the density of air. c_p ($m^2\ s^{-2}\ K^{-1}$ ~ 1004) is the specific heat capacity at constant pressure for moist air. The exchange coefficients may be thought of as conductivity. The K's give name to K-theory which is just another name for the gradient method. An overbar denotes the time average.

In cases where the classic logarithmic wind profile is assumed to be valid, the turbulent exchange coefficients can be parametrized for momentum. On the assumption that $K_m=K_h=K_e=K_s$ and the scalar quantities obey logarithmic profiles, all of the surface fluxes can be calculated by the gradient method.

With the friction velocity, u_* (m s^{-1}), the aerodynamic roughness length for momentum, z_0 (m), and the von Karman constant (κ ~ 0.4) the logarithmic wind profile is

$$\bar{u}(z) = \frac{u_*}{\kappa} \ln\left(\frac{z}{z_0}\right) \quad (5)$$

In cases with tall canopy or built-up areas it is necessary to include a displacement height to take into account decoupling of the boundary layer wind field from say the bottom of the forest. Only treetops directly experience the boundary layer wind actions. For simplicity the displacement height is omitted.

The friction velocity represents the downward flux of momentum to the ground; this is the effect of wind stress, τ_0:

$$\tau_0 = \rho u_*^2 \quad (6)$$

A differentiation eq 5 with regard to z yields

$$\frac{d\bar{u}}{dz} = \frac{u_*}{\kappa z} \quad (7)$$

and when combining eqs 1 and 7 we obtain an expression for K_m

$$K_m = \kappa u_* z \tag{8}$$

The logarithmic profile occurs only under neutral conditions, that means cases with an adiabatic lapse rate. Neutral conditions are rare. Unstable conditions typically prevail during daytime and stable conditions during nighttime. Stability correction is important whenever non-neutral conditions occurs. Stability correction based on the Businger-Dyer method (Kaimal & Finnigan 1994) is widely accepted, although other methods are in current use as pointed out by Bougeault (1991).

When we substitute expressions for heat and scalars analogous to eqs 7 and 8 into eqs 1-4, and add stability corrections terms, Ψ (-), we obtain the following flux gradient equations for non-neutral conditions

$$\tau = \rho\kappa^2 \frac{(\overline{u_2}-\overline{u_1})^2}{\ln(z_2/z_1)-\Delta\psi_M(z/L)} \tag{9}$$

$$H = -\rho c_p \kappa^2 \frac{\overline{u_2} - \overline{u_1}}{\ln(z_2/z_1)-\Delta\psi_M(z/L)} * \frac{\overline{\theta_2} - \overline{\theta_1}}{\ln(z_2/z_1)-\Delta\psi_H(z/L)} \tag{10}$$

$$E = -\rho\kappa^2 \frac{\overline{u_2} - \overline{u_1}}{\ln(z_2/z_1)-\Delta\psi_M(z/L)} * \frac{\overline{q_2}-\overline{q_1}}{\ln(z_2/z_1)-\Delta\psi_E(z/L)} \tag{11}$$

$$S = -\rho\kappa^2 \frac{\overline{u_2}-\overline{u_1}}{\ln(z_2/z_1)-\Delta\psi_M(z/L)} * \frac{\overline{c_2}-\overline{c_1}}{\ln(z_2/z_1)-\Delta\psi_S(z/L)} \tag{12}$$

Subscripts 1 and 2 refer to the lower and upper level above ground, respectively. The stability correction terms Ψ with subscripts for the respective fluxes are functions of the Obukhov length scale, L (m). At a height proportional to L the buoyant forces dominate over the shear stress (Stull 1991). L is defined as:

$$L = \frac{-\overline{\theta} u_*^3}{\kappa g \, \overline{w'\theta'_0}} \tag{13}$$

where g is the acceleration of gravity (m s^{-2} ~9.82) and $\overline{w'\theta_0'}$ the kinematic surface heat flux. Eqs 9-12 basically show that only the vertical gradients of wind speed, temperature, humidity and scalar concentration need to be measured in order to calculate the surface fluxes.

L is a key variable used in the so-called Monin-Obukhov similarity scaling valid in the constant flux layer. Similarity theory (Buckingham Pi theory) is based on empirical fitting of variables put into dimensionless groups. By Monin-Obukhov

similarity scaling it is found that z/L is a universal function of u_*.

In analogy to the velocity scale u_*, a temperature scale, θ_* (K) and a humidity scale, q_* (g H_2O g^{-1} air) can be written:

$$\theta_* = \frac{-\overline{w'\theta'}_0}{u_*} \tag{14}$$

$$q_* = \frac{-\overline{w'q'}_0}{u_*} \tag{15}$$

Here the heat fluxes are expressed as covariance terms. These are obtained by decomposing wind speed, temperature, humidity and scalar concentration into mean and fluctuating (turbulent) parts and after Reynolds averaging, the following flux equations appear:

$$\frac{\tau}{\rho} = -\overline{u'w'} = u_*^2 \tag{16}$$

$$\frac{H}{\rho c_p} = \overline{w'\theta'} = -u_*\theta_* \tag{17}$$

$$\frac{E}{\rho} = \overline{w'q'} = -u_*q_* \tag{18}$$

$$\frac{S}{\rho} = \overline{w'c'} \tag{19}$$

In eqs 6-9 all of the fluxes are normalized with ρ and for latent heat also by c_p. Hence the so-called kinematic flux forms are obtained.

The mean parts are $\overline{\theta}$, $\overline{q}$, $\overline{u}$, $\overline{c}$. The turbulent parts are θ', q', u' and c'. w' (m s^{-1}) is vertical wind speed fluctuation. $\overline{w}$ is assumed to be 0.

At 10 m the scalar flux will be within 1% of the surface flux for a one kilometer deep horizontally homogeneous boundary layer (Wyngaard 1991). Therefore it is usual to measure the flux at some distance above the surface as the equations are not valid very close to the ground. On the other hand the gradients of wind, temperature and scalar constituents are larger close to the surface than far above. In general though the Monin Obukhov similarity scaling, which forms the basis of the various methods, is only known within 20% accuracy (Wyngaard 1991).The assumption of horizontal homogeneity will be treated in detail later on.

2.3 Eddy correlation method

The turbulent mixing is the process that governs the vertical fluxes. Eddies carry momentum, humidity, heat and passive scalars up and down by eddy movements. The vertical and horizontal movements can be recorded by fast-response sensors, so the fluxes can be calculated directly from the correlation terms. The covariances between w', u', q' and θ' give direct measures of the surface fluxes.

$$\tau = -\rho\overline{u'w'} \tag{20}$$

$$H = \rho c_p \overline{w'\theta'} \tag{21}$$

$$E = \rho\overline{w'q'} \tag{22}$$

$$S = \rho\overline{w'c'} \tag{23}$$

The assumption is that there is no vertical convergence or divergence present ($\bar{w}=0$) and u is the streamwise wind. No assumptions are made concerning the mixing properties of turbulence.

2.4 Aerodynamic resistance method

The aerodynamic resistance method treats the parameter governing the vertical transfer as a resistance. Here resistance has to be understood as the resistance to diffusion *between the surface and a reference level*, z. Resistance is the inverse of the conductance. Conductance is the conductivity times the length divided by the cross-section area of the media (here the turbulent air). The difference in temperature, humidity or passive scalar concentration between the two levels is the potential voltage difference. The flux is the current. So simply stated

$$Flux = \frac{Conc.difference}{Resistance} = Conc.difference * Conductance. \tag{24}$$

First the *surface* has to be defined. This is the boundary condition. It is done by integrating the logarithmic profile equations. Thus the mean potential surface temperature, θ_0, and the mean specific surface humidity, $\bar{q}_0$, are obtained by extrapolating the logarithmic profiles to the so-called *surfaces*. Integration of the potential temperature profile

$$\frac{d\bar{\theta}}{dz} = \frac{\theta_*}{\kappa z} \tag{25}$$

yields

$$\overline{\theta}(z) - \overline{\theta_0} = \frac{\theta_*}{\kappa}\ln(\frac{z}{z_{0t}}) \tag{26}$$

and integration of the humidity profile yields

$$\overline{q}(z) - \overline{q_0} = \frac{q_*}{\kappa}\ln(\frac{z}{z_{0q}}). \tag{27}$$

$\overline{\theta}_0$ and $\overline{q}_0$ are non-zero at the heights z_{0t} (m) and z_{0q} (m) respectively. This is contrary to the wind speed. Integration of the wind profile (eq 7) yields $\overline{u}_0=0$ (eq 5) at z_0.

The aerodynamic resistances to transfer of momentum, heat and water vapour are r_a, r_h and r_q (s m^{-1}), respectively. So the surface fluxes can be written as

$$\tau = \rho\frac{\overline{u}(z)}{r_a(z)} \tag{28}$$

$$H = -\rho c_p\frac{\overline{\theta}(z)-\overline{\theta_0}}{r_h(z)} \tag{29}$$

$$E = -\rho\frac{\overline{q}(z)-\overline{q_0}}{r_q(z)}. \tag{30}$$

By definition the flux is constant over a unit area per unit time and therefore a height dependence is found in the resistances. As the resistance concept is just another way of writing the turbulent transfer equations, the resistances r_a, r_h and r_q may be expressed as

$$r_a(z) = \frac{1}{\kappa u_*}(\ln(\frac{z}{z_0})-\psi_M(\frac{z}{L})) = \frac{1}{\kappa^2\,\overline{u}(z)}(\ln(\frac{z}{z_0})-\psi_M(\frac{z}{L}))^2 \tag{31}$$

$$r_h(z)=\frac{1}{\kappa u_*}(\ln(\frac{z}{z_{0t}})-\psi_H(\frac{z}{L}))=\frac{1}{\kappa^2\overline{u}(z)}(\ln(\frac{z}{z_0})-\psi_M(\frac{z}{L}))*(\ln(\frac{z}{z_{0t}})-\psi_H(\frac{z}{L})) \tag{32}$$

$$r_q(z)=\frac{1}{\kappa u_*}(\ln(\frac{z}{z_{0q}})-\psi_E(\frac{z}{L}))=\frac{1}{\kappa^2\overline{u}(z)}*(\ln(\frac{z}{z_0})-\psi_M(\frac{z}{L}))*(\ln(\frac{z}{z_{0q}})-\psi_E(\frac{z}{L})) \tag{33}$$

Tabulated values of the relation between z_0 and r_a are presented in Rowntree (1991). There is considerable evidence that z_0, z_{0t}, and z_{0q} are not equal. This means that the boundary condition surfaces are located at different heights above the physical surface. Inherent in this is the question of obtaining $\overline{u}$ at heights z_{0t} and z_{0q}. Elaborate forms of eq 31 are found in eg Shuttleworth (1991a). Note that when the scalar fluxes are *countergradient*, then z_{0t} and z_{0q} are undefined.

2.4.1 Excess resistance

There is a basic difference between the drag forces responsible for the transfer of momentum, heat and scalar fluxes. For heat and scalar fluxes molecular diffusion (skin drag) is giving rise to the transfer through the viscous layers on the physical surfaces. But for momentum the dynamic pressure differential caused by deceleration of the wind (form drag) is an important additional factor. The more obstacles the wind encounters, the stronger the pressure differential and the greater the transfer coefficient (bluff body effect). This means that the transfer coefficients for momentum usually are larger than for active and passive scalar fluxes.

The difference in the transfer coefficients of momentum and heat flux expressed in terms of resistances is often described as follows. In situations with many obstacles the heat resistance, r_h, is larger than that of momentum, r_a, such that an additional resistance has to be added

$$r_h(z) = r_a(z) + r_b. \tag{34}$$

r_b is a theoretical supplementary resistance to heat. Some people name it excess resistance (Stewart et al. 1993). The excess resistance can be expressed in the form of a non-dimensional parameter κB^{-1} (Chamberlain 1968, Brutsaert 1982, Prevot et al. 1993a)

$$\kappa B^{-1} = \kappa u_* r_b = \ln\frac{z_0}{z_{0t}} \tag{35}$$

This is the classic description. For surfaces with vegetation cover (porous or fibrous roughness elements) the logarithmic ratio

$$\ln(\frac{z_0}{z_{0t}})=\ln(\frac{z_0}{z_{0q}})=2.3 \tag{36}$$

is often assumed to be valid (hence $z_0=10z_{0t}=10z_{0q}$). Larger values have been observed and for (slightly) inhomogeneous cases the ratio may be very much larger (Beljaars and Viterbo 1994), eg 8.76 at flat grassland at Cabouw, The Netherlands (Beljaars and Holtslag 1991). Prior to this Garratt (1978) reported the ratio to be 7 ± 3.5 for a mixture of grassland, forest and soil in Australia.

Other researchers report a similar trend. Kohsiek et al. (1993) found $\kappa B^{-1}=3.68$ in semi-arid land in La Crau, France whereas Brutsaert et al. (1993) reported a value of 10 in the forest of Les Landes, France. Both areas are within the HAPEX-MOBILHY field site in southwestern France. HAPEX-MOBILHY is an acronym for Hydrological and Atmospheric Pilot Experiment-Modelization de BILan HYdrique. The experiment was conducted in southwestern France 1986. Stewart et al. (1993) report regional values of κB^{-1} ranging between 4 and 12.4 on various field sites. Sun and Mahrt (1995) cite values of z_{0t} in the ranges 10^{-7}-10^{-10} m from various experiments. All of this confirms that z_{0t} is several orders of magnitude smaller than z_0. These results are from sites that are not strictly homogeneous.

According to Beljaars and Viterbo (1994) long-term climatic data clearly indicate that the ratio of z_0/z_{0t} is much larger than 10 in slightly heterogeneous terrain. Likewise Mahrt et Ek (1993) report z_0/z_{0t} to be orders of magnitude larger in HAPEX-MOBILHY based on airborne data. Over forest $z_0=1$m but $z_{0t}=10^{-4}$m and over agricultural area z_{0t} was even smaller.

It is of great interest to parametrize the excess resistance. Prevot et al. (1993a) suggested an empirical relation from a radiative vegetation model (see eq 50). This includes LAI and a radiative temperature difference to predict κB^{-1} within values of -2 and +11. Negative values imply $z_0 < z_{0t}$. This has not been reported so far (Carlson et al. 1993).

Excess resistance, r_b, is assumed not to be height dependent (eq 34). r_b refers to the viscous sublayer. Jensen and Hummelshøj (1995, 1997) have developed a parametrization of r_b based on the growth of the viscous sublayer as a function of the geometry of the individual roughness elements as regards forests. The relation is

$$r_b = \frac{c_1}{u_*}\frac{\nu}{D}\left(\frac{l\,u_*}{\nu}\right)^{1/3} LAI_e^{-2/3} \qquad (37)$$

ν is the kinematic viscosity of air ($m^2\ s^{-1}\ \sim 15*10^{-6}$), D is the diffusion coefficient of gas ($m^2\ s^{-1}\ \sim 14*10^{-6}$ for O_3 and NO_2), l is the leaf dimension (m spruce ~ 0.005, deciduous ~ 0.01), LAI_e (m^2 leaf m^{-2} ground) is an effective LAI depending on the chemical substance being considered and c_1 is a parameter ($\sim$ 100 (-)). Results from Danish spruce and beech forest measurements reported in Pilegaard et al. (1995) show daytime r_a and r_b typically around 10 s m^{-1} for various gases.

Many parametrizations of r_b exist (eg Shuttleworth 1991a). A simple parametrization, $B^{-1}=6u_*^{1/3}$, was originally suggested by Thom (1972 *in* Shuttleworth 1991a). Later on more elaborate forms have been suggested. For (non-homogeneous) surfaces with bluff body roughness elements the friction velocity, u_*, the molecular Prandtl number (Pr=0.71) for heat (or Schmidt number (Sc=0.6) for water vapour have to be taken into account (Brutsaert 1979, Hicks 1985 both cited *in* Claussen 1990)

$$r_b = \frac{7.3}{u_*}\left(\left(\frac{u_* z_0}{\nu}\right)^{1/4} Pr^{1/2} - 5\right) \qquad (38)$$

An important difference between the two elaborate parametrizations of r_b (eq 37 and 38) is that the first is based on scaling with physically meaningful length scales, namely the length of leaves and effective leaf area, the other is not.

Geostrophic drag laws.

The completion of this short description of differences between r_a, r_h and r_b is done by a detour to the *geostrophic resistance law*, also called the drag laws (Jensen et al. 1984, Stull 1991). The assumption is that there is a near-geostrophic balance of the free flow. For stationary, homogeneous flow the

linking between u_*, z_0, the stability and the geostrophic wind speed, G (m s^{-1}), is known. A simple approximation for neutral conditions was proposed by Jensen (1978) as $u_* = \frac{1}{2}G/\ln(Ro)$ with Ro (-), the Rossby number equal to $G/(f_c z_0)$. f_c is the Coriolis parameter (s^{-1}).

By use of the geostrophic drag laws (Seguin & Itier 1983, Stull 1991 p. 262, Kaimal & Finnigan 1994 p. 70) analytically show that the bulk transfer coefficients for momentum, C_M (often called the drag coefficient), and heat, C_H, (the Stanton number) differ very much with canopy density and roughness length. The two bulk transfer coefficients both increase with increasing surface roughness but for high surface roughness values C_M is very much larger than C_H. This means that assuming C_M and C_H equal will introduce only a minor error in sensible heat flux calculation for smooth terrain, but large error for rough terrain.

The equations for the bulk transfer coefficients for momentum, temperature and humidity are

$$C_M(z) = \frac{\tau}{\rho \bar{u}(z)^2} = \frac{u_*^2}{\bar{u}(z)^2} = \frac{\kappa^2}{(\ln\frac{z}{z_0} + \psi_M(\frac{z}{L}))^2} \tag{39}$$

$$C_H(z) = \frac{-\rho\overline{w'\theta_0'}}{\bar{u}(z)(\bar{\theta}(z) - \bar{\theta}_0)} = \frac{\kappa^2}{(\ln\frac{z}{z_0} + \psi_M(\frac{z}{L}))(\ln\frac{z}{z_{0t}} + \psi_H(\frac{z}{L}))} \tag{40}$$

$$C_Q(z) = \frac{-\rho\overline{w'q_0'}}{\bar{u}(z)(\bar{q}(z) - \bar{q}_0)} = \frac{\kappa^2}{(\ln\frac{z}{z_0} + \psi_M(\frac{z}{L}))(\ln\frac{z}{z_{0q}} + \psi_Q(\frac{z}{L}))} \tag{41}$$

The drag coefficient really measures the strength of the turbulence. Here the drag laws are mentioned to emphasize the inherent 'roughness' problem on a large scale (eqs 39-41) as well as on a fine scale (eqs 31-34) calculations.

2.4.2 Stomatal resistance

Parametrization of resistance for water vapour in vegetated areas may be described as a sum of the aerodynamic resistance, excess resistance and canopy resistances, r_c

$$r_q(z) = r_a(z) + r_b + r_c \tag{42}$$

When the vegetation is wet $r_c = 0$ but when the available water for transpiration is scarce r_c may have a pronounced influence on E (Rowntree 1991, Beljaars and Viterbo 1994). The evapotranspiration passes mainly through the open

stomata, so some people name r_c stomata resistance. A lot of suggestions on how to estimate r_c are published (eg Bougeault (1991) and Noilhan et al. (1991). Blyth et al. (1993) rather call it surface resistance, r_s, defined as

$$r_s = \rho \frac{\bar{q} - \overline{q_{sat}(T_s)}}{E} \tag{43}$$

where $\bar{q}$ is the mean specific humidity inside the canopy. The mean specific surface humidity $\bar{q}_0$ is approximated by the saturated value at temperature T_s. As soil dries out a fraction of the potential evaporation, α (-), $\alpha\bar{q}_{sat}(T_s)$ will be evaporated. This simplistic approach is typical in GCM-modelling.

In complex models many kinds of resistances are defined (Shuttleworth 1991a). Baldocchi et al. (1991) stress that *canopy stomatal* conductance relates to biotic processes only. The canopy stomatal conductance is defined as the serially integrated single leaf conductance, weighted by leaf area. Stomata react to radiation, temperature and humidity through complex nonlinear plant processes. On the other hand *canopy surface* conductance relates only to abiotic processes. Again radiation, humidity and temperature but now they drive the aerodynamic transport between the canopy air column and the leaf surfaces and soil (through the excessive resistance r_b).

Just one method of how to estimate r_c will be mentioned here. It is based on the suggestions in Jensen and Hummelshøj (1995). Measurements of $r_a = \bar{u}/u_*^2$, r_b (in eq 37), the fluxes and the concentration gradients should be carried out in the field. Hence r_c can be found as the residual in eq 44:

$$\frac{Flux}{Conc.\ gradient} = \frac{1}{r_a + r_b + r_c} \tag{44}$$

2.5 Summary of fluxes in homogeneous terrain

In the surface boundary layer for statistically homogeneous terrain the Monin-Obukhov similarity theory is valid. A local balance (equilibrium) of the turbulent air flow is assumed. Hence the surface fluxes can be described by the diffusivity concept (K-theory), by the turbulent exchange coefficients and the gradients. The transfer coefficients can be viewed as conductances. Expressions of the inverse of the conductance give the aerodynamic resistance approach. The two methods rely on the same basic concepts. The data type needed is averaged time series of parameters measured on various levels above the surface.

The eddy correlation method is different because there is no assumptions on the mixing properties of the turbulent flow, and the data are from fast-response sensors with the covariances averaged in time.

3 Surface fluxes by remote sensing methods

Remote sensing data are spatial by nature. This is in contrast to the time series data used for the gradient method, the eddy correlation method and the aerodynamic resistance method. It is a challenge to make use of the spatial data for surface flux estimation. So far the remote sensing methods for surface flux estimation heavily rely on the time series methods. This means that the assumptions of stationarity and homogeneity are upheld. As the remote sensing data are instantaneous spatial values that do not map (all of) the requested input values, several modifications to the equations have been necessary.

Verification of remote sensing results of surface fluxes is difficult. The surface fluxes primarily used for verification are point measurements from one or more locations, not spatial averages. So if the assumptions of stationarity and homogeneity are not fulfilled, it is simply different fluxes that are compared. Airborne eddy correlation measurements may be an attractive alternative for verification purposes but some discrepancies in ground and airborne surface flux results remain unaccounted for (Shuttleworth 1991a, Hildebrand 1991, Bougeault et al. 1991, Desjardins and MacPherson 1991, Jochum 1993, Mahrt and Ek 1993, Moore et al. 1993).

The simplified relationship is the remote sensing method for spatial surface flux estimation that is most widely used. Sensible heat flux is estimated directly, and latent heat is estimated as a residual (section 3.1-3.3). Inclusion of vegetation and soil moisture parameters from space (section 3.4) and a planetary boundary layer model driven with remote sensing data (section 3.5) are described. Momentum flux estimation over ocean from satellite data is briefly mentioned (section 3.5), whereas land surface momentum flux from satellite data is described in detail (chapter 7). Conclusive remarks on satellite based flux retrievals are given in section 3.7.

3.1 Simplified relationship

In 1972 the first earth observing satellite was sent into orbit. It was equipped with sensors recording various bands of the electromagnetic spectrum. The digital information obtained from this and many later satellites have been studied with regard to estimation of surface fluxes.

In 1977 Jackson et al. proposed a method for estimating the daily evaporation from a single midday surface temperature. The surface temperature was measured by thermal infrared radiation with remote sensors. The equation suggested (Jackson et al. 1977) has later on been called the simplified relationship by many people (Riou et al. 1988, Vidal & Perrier 1989, Carlson et al. 95). It follows here:

$$Rn_d - ET_d = c_3(T_s - T_a) + c_2 \quad (45)$$

ET_d is the daily evaporation (mm), Rn_d is the daily net radiation (mm), T_s is the surface radiant temperature near midday, T_a is the maximum temperature at screen level height, c_2 (mm) is the intercept and c_3 (mm K^{-1}) the slope of a linear regression. The concept is that the instantaneous value of the midday temperature difference predicts the daily sensible heat flux (Seguin & Itier 1983). The validity of this seems to be justified in sunny weather both for humid (eg HAPEX-MOBILHY, FIFE) and for semi-arid areas (MONSOON 90) according to Crago (1996). FIFE is an acronym for First ISLSCP Field Experiment. ISLSCP is International Satellite Land Surface Climatology Project conducted in Kansas 1987 & 1989, USA (Shuttleworth 1991a). MONSOON 90 is a project conducted in an arid area in Arizona, USA 1990 during the rainy season "Moonson" (Kustas et al. 1991).

The simplified relationship is based on the surface energy balance integrated over 24 hours.

$$Rn_d = ET_d + QH_d + QG_d \quad (46)$$

The terms in the energy balance (W m^{-2}) are re-calculated to daily mm water column with dividing by the vaporization heat for water (2.45 10^6 J kg^{-1}) and multiplying by 86400 seconds.

Rn_d may by obtained from direct measurements by a net radiometer, calculated by empirical formulas for a given time and location or retrieved from radiation budget models by remote sensing methods.

The ground heat flux integrated over a day is $QG_d \sim 0$ (mm). In the regression it shows up as the intercept, usually a value near zero (Vidal & Perrier 1989). In fact it is the diurnal sensible heat flux, QH_d, that is parametrized in terms of measured surface radiant temperature and air temperature in eq 45. When eq 45 is rewritten this gives ET_d as a residual term.

$$ET_d = Rn_d - QH_d = Rn_d - c_3(T_s - T_a) - c_2 \quad (47)$$

The simplified method has been widely used to quantify the spatial daily evaporation. Values of c_2 and c_3 are listed in table 1 for a variety of regions and types of ground cover.

As the values of c_2 and especially c_3 are subset to a great variation in time and space, an operational use of the simplified method for evaporation estimation has not been viable. One reason is the very simple parametrization of QH_d. When we rewrite eq 45 in terms of eq 29 and 32 we get

$$c_3 = \frac{\rho c_p}{r_h(z)} = \frac{\rho\, c_p\, \kappa^2\, \bar{u}}{[\ln(\frac{z}{z_0}) - \psi_m(\frac{z}{L})][\ln(\frac{z}{z_{0t}}) - \psi_h(\frac{z}{L})]} \quad (48)$$

This implies $T_s - T_a \sim \bar{\theta}_0 - \bar{\theta}(z)$. It is obvious that c_3 is proportional to $u_*/\ln(z/z_{0t})$.

Thus the wind gradient, roughness length and stability have profound influence on c_3. The effects are described in section 3.1.2 and have been studied by many scientists so far (Seguin & Itier 1983, Rambal et al. 1985, Riou et al. 1988, Søgaard 1988, Carlson & Buffum 1989, Vidal & Perrier 1989, Lagouarde 1991, Brutsaert et al. 1993, Sandholt and Andersen 1993, Stewart 1993, Stewart et al. 1993, Hurtado et al. 1994, Sugita and Kubota 1994, Kubota and Sugita 1994, Carlson et al. 1995).

c_3 (mm/K)	c_2 mm	surface type	reference
0.64	0	wheat	Jackson et al. 1977
0.25	1.1	irrigated pasture dry-land short grass	Seguin & Itier 1983
0.30 0.25	0 0	irrigated wheat irrigated sugar cane	Vidal & Perrier 1989
0.51	0	maize	Hurtado et al 1994
0.32	0	bare soil (short) vegetation	Carlson & Buffum 1989
0.76 0.57 0.21	0 0 0	maize barley fallow	Caselles 1993
0.27	0.3	savanna	Søgaard 1988
0.50	1.18	savanna	Sandholt and Andersen 1993
0.51 0.22	0 0	wheat grass	Lagouarde & McAneney 1992
0.24 0.62	0 0	barley (May) barley (July)	Søgaard 1992

Table 1. Simplified relationship for flux estimation. The constants c_2 and c_3 are empirical values (eq 45).

In summary the basic assumptions implicit in the simplified relation are

1) $T_s \sim \bar{\theta}_0$

2) $r_h(z)$ is a constant.

The key parameter, T_s, a truly spatial value obtained from remote sensors, is first treated. Secondly $r_h(z)$ is treated (section 3.1.2).

3.1.1 Surface temperatures

In the simplified relationship is T_s the low-level temperature (eq 45). T_s is related to the thermal infrared radiance emitted from vegetation and substrates through Plancks law (Prevot et al. 1993a, Becker & Li 1993). In the turbulent heat flux equation (eq 29) the low-level temperature is the mean potential temperature, θ_0, at the integration height, z_{0t}. T_s and θ_0 may differ considerably introducing error into the sensible heat estimation if not corrected for (Prevot et al. 1993a, Stewart et al. 1993, Brutsaert et al. 1993).

Physically the discrepancy between T_s and $\bar{\theta}_0$ relates to the viscous sublayer surrounding all surface elements. Imagine the temperature of a single leaf. T_s is the temperature of the leaf itself, whereas θ_0 is the air temperature close to the leaf. A remote sensor "sees" a canopy rather than a single leaf. Thus the recorded signal is an aggregated value of temperatures from leaves, stems, branches and trunks, sunlit and shaded. On the other hand θ_0 is the air temperature wellmixed by turbulent eddies in the (upper) canopy.

If we revert to the heat-resistance equation, the effect of the viscous sublayer is here proposed to be related to r_b (eqs 34 and 37). H is by definition constant through the vertical layers. Thus a first-order approximation is that r_a accounts for the difference θ_0-θ, and that r_b accounts for the difference T_s-θ_0.

The viscous sublayer is adding a resistance to the transfer (eq 34). During the day it results in a negative temperature gradient with $T_s > \theta_0$. If values are inserted into eq 29 that are typical for Danish forests with H of the order 400 W m^{-2}, and r_a and $r_b \sim 10$ m s^{-1} (Pilegaard et al. 1995), this yields a result of a temperature gradient of the order 7 K. Bearing in mind a general temperature gradient of -0.5 K per 100 m, the result shows that T_s-θ_0 is significant. Similar results up to 6 K of temperature difference from tower data have been reported by Beljaars and Holtslag (1991).

Based on regional-scale remote sensing studies Hall et al. (1992) report the difference to be up to 3 K, while Norman et al. (1995) report up to 5 K.

It seems tempting to adjust (approximate) T_s to $\bar{\theta}_0$ but as z_{0t} is usually not well-known the equation cannot be solved. The excess resistance (eq 34) can be locally determined however with great difficulty. Often z_{0t} is assumed to be a constant fraction of z_0. According to Thom (1975 *in* Kaimal and Finnigan 1991) $z_0/z_{0t} \sim 5$. Over vegetation $z_0/z_{0t} \sim 10$ is more likely (Garratt and Hicks 1973 cited *in* Wood and Mason 1991).

z_{0t} is rarely obtained in field experiments. Therefore empirical expressions have emerged like (Kustas et al. 1989, Kustas et al 1994a, 1994b):

$$\kappa B^{-1} = c_4 \bar{u}(T_s - T_a). \tag{49}$$

c_4 (s m^{-1} K^{-1}) is determined empirically. Unfortunately the coefficient changes on a day-to-day basis. This makes the method useless for operational purposes.

According to Stewart (1993) inclusion of an appropriate (global) value of excess resistance in flux estimation may reduce the error considerably. He reported an average correction of 62% on r_a, which changed the error on QH from +141 W m^{-2} to -21 W m^{-2} on average in FIFE. "Global" excess resistance has an assumption of some kind of non-homogeneity. The name 'global' stresses that it is not a "local" (homogeneous local balance) situation.

Another way of getting around the problem is by defining a *radiometric* roughness length for temperature, $z_{0t,r}$ (m) by substituting θ_0 with T_s in eq 29. It is handy as T_s is measurable (and equals the temperature solved in a surface heat balance budget).

Sugita and Brutsaert (1990) "backed out" $z_{0t,r}$ from airborne data of T_s combined with flux data from FIFE. The variability of $z_{0t,r}$ was shown to be very large, several orders of magnitude. From multiple regression statistics it was found that $z_{0t,r}$ is dependent on solar elevation, canopy height and LAI. However the correlation coefficients were low.

Prevot et al. (1993a) suggest a parametrization of κB^{-1} from a radiative vegetation model and simulated data to be

$$\kappa B^{-1} = 0.655(T_s(nadir) - T_s(80° zenith)) + 3.82\exp(-LAI) - 1.34 \qquad (50)$$

The temperature distribution within a canopy is carefully modelled from leaf distribution and LAI. T_s-T_a is shown to vary with LAI (cool shaded soil, warm sunny canopy top). T_s varies with zenith and azimuth angles such that T_s(nadir)-T_s(off-nadir) partly models the contribution from the (shaded) soil. The method also discriminates water stressed and unstressed situations. The modelled heat flux results are inverted such that κB^{-1} "fits" to the original heat flux.

The approach by Prevot et al. (1993a) is interesting. However T_s far off-nadir is not generally available. Even NOAA AVHRR is not useful with the broad 55° scan angle (effectively ~65° due to the curvature of the globe). Other data problems would be a coarse resolution far off-nadir, and a less reliable atmospheric correction. NDVI probably would map LAI reasonably well as κB^{-1} seems most sensitive to LAI<3. The parametrization does not include u_*, so changes in roughness could introduce significant error (eq 35). Negative values of κB^{-1} does not seem to be physically realistic.

Sugita and Kubota (1994) measured z_{0t} and $z_{0t,r}$ over a pasture in Japan during the growing season. It was no surprise that the results showed that z_{0t} does not equal $z_{0t,r}$. $z_{0t,r}$ ranged between 10^{-1} and 10^{-7} m diurnally and seasonally. The mean canopy height developed from 0.13 m to 0.71 m (Kubota and Sugita 1994). The result suggests that it is no straightforward task to improve the simplified relationship by including $z_{0t,r}$.

Brutsaert and Sugita (1992) measured T_s with ground-based remote sensing in FIFE. Sensible heat was also measured. They then combined the data and retrieved $z_{0t,r}$. Subsequently $z_{0t,r}$ was used with a satellite-based T_s and they obtained very reasonable estimates of QH. As far as I know no such good results have been reported since then.

Brutsaert et al. (1993) carefully measured z_{0q} and z_0 over forest. Assuming $z_{0t}=z_{0q}$ they evaluated the excess resistance and concluded that z_{0q} should be very carefully calibrated. The standard error was ~ 30 W/m^2 ($\sim 10\%$ of QH). The assumption is questionable as the transfer of water vapour is strongly controlled by the canopy (stomata) resistance (eq 42). Only in the case of $r_c \sim 0$ (well-watered conditions) the assumption holds true. It is probably that this has introduced part of the error found.

Mahrt (1996) mentions that T_s may reach 80°C in some places on earth. For such hot surfaces the integration constant, $z_{0t,r}$, has to be extremely small in order to give a transfer coefficient small enough. Generally it is not attractive that models depend on small numerical values. Kohsiek et al. (1993) have shown QH to be very sensitive to kB^{-1} and recommend z_{0t} to be estimated from simple micro-meteorological observations.

Returning to the homogeneous resistance description of heat transfer (eq 34) we find that the error on $r_h(z)$ obviously is reduced when $r_a(z)$ is relatively large compared to r_b (our problem). As regards forests T_s and T_a may never diverge substantially. This is because of a high turbulent mixing compared to a relatively small scale of leaves. Hence the mean potential temperature gradient can be very small (McAneney & Lagouarde 1994). To improve the simplified method Carlson and Buffum (189) suggested the air temperature to be measured 50 m above ground and not at screen height (2 m above ground). Later suggestions are use of the temperature at the outer region of the unstable atmospheric boundary layer (Brutsaert and Sugita 1992, Brutsaert et al. 1993, Lagouarde et al. 1993, Menenti and Choudhury 1993). Kustas et al. (1994a) applied the potential temperature with a bulk resistance expression for the convective mixed layer.

If T_a is decreased relative to T_s this yields a larger temperature difference. A similar change can be obtained by use of T_a from the cross-over time instead of T_a maximum as originally proposed (eq 45). T_s typically is measured around 14.00 local time with NOAA AVHRR (and 1000 local time with Landsat TM). Meteorological networks often record only T_a maximum. The temperature curve is flat in the middle of the day so the error introduced is probably rather small.

3.1.2 Stability, wind speed and roughness effects

The two assumptions implicit in the simplified relationship namely that $\bar{\theta}_0$ equals T_s and that $r_h(z)$ is a constant both may corrupt the method. In the previous section problems related to the first assumption were described. Here follow comments on the second assumption.

It is readily seen that z_0, z_{0t}, $\bar{u}$ and L effect c_3 (eqs 45 and 48). These values are not constant even for a limited period of time (eg 10 days) in a homogeneous area. Therefore plots of Rn_d-ET_d as a function of T_s-T_a usually show considerable scatter and the linear regression correlation coefficients are low. Physically the variations are related to the surface soil moisture, the vegetation type and density as well as the state of the atmosphere (Jackson et al. 1977, Seguin & Itier 1983, Søgaard 1988, Lagouarde and McAneney 1992, Hasager

1993, Hurtado et al. 1994).

Neutral static stability is rare over land surfaces at sunny midday. In case of warm advection stable conditions may occur ($T_s < T_a$), but usually unstable conditions prevail. Cloudless optical remote sensing data therefore usually are from unstable conditions. Unstable conditions cause higher turbulent mixing rates. Analytical results show the importance of stability effects on the c_3-coefficient in the simplified method (eq 45) (Lagouarde & McAneney 1992).

A modified equation of the simplified relationship with a regression coefficient c_5 (mm $K^{-3/2}$)

$$QH_d = c_5(T_s - T_a)^{3/2} \tag{51}$$

was suggested by Seguin and Itier (1983) and some results are reported by Rambal et al. (1985). Strongly unstable stratification is likely to occur around noon on sunny days, and the power 3/2 is in accordance with dimensional analysis.

In the free convection situation the non-dimensional product is

$$(\overline{\theta' w'})^2 \propto \frac{g}{\theta_0}\left(\frac{d\bar{\theta}}{dz}\right)^3 z^4 \tag{52}$$

(Jensen and Busch 1982). From this it is found that H relates to the temperature gradient as

$$H \propto -\rho c_p z^2 \sqrt{\frac{g}{\theta_0}\left(\frac{d\bar{\theta}}{dz}\right)^{3/2}} \tag{53}$$

The analysis shows that eq 51 is a reasonable approximation but that the c_5 is not a constant parameter because the buoyancy parameter g/θ_0 as well as z affect it.

In regard to validation of stability effects work by Carlson and Buffum (1989) have given some insight into this field. By running a Soil-Vegetation-Atmospheric-Transfer (SVAT) model some results were obtained. These showed that stability effect are present but not dramatic. The results by Carlson and Buffum (1989) showed that c_3 is sensitive to wind speed changes especially for high surface roughness values. It was shown that the error in c_3 generally is less than 1 mm K^{-1} for a range of wind speeds and roughness lengths.

Empirical relations between c_3 and z_0 have been found. Riou et al. (1988) have shown that stability and roughness lengths may change c_3 from 0.24 to 0.7 mm K^{-1}. These results encompass a large range of stability and roughness lengths. The c_3-values listed in table 1 show a similar range [0.21,0.76].

In a recent study again based on SVAT model results, Carlson et al. (1995), conclude that c_3 depends more sensitively on percentage vegetation cover compared to full (homogeneous) vegetation cover than on $\bar{u}$ and z_0 (within limits). The study addresses intra-regional vegetation and soil variability, not

homogeneous conditions. Some assumptions were included on the dependence of vegetation amount and the hydrological state on the resulting T_s.

In summary modifications to the simplified method are demanded when regional-scale heterogeneity is present. Land surface heterogeneities causes a spatial variation of T_s and $r_h(z)$, so the empirical "constants" cannot be assumed valid. Mapping of the heterogeneities are important. However models that are capable of aggregating the surface values into reliable spatial quantities are just as important.

3.2 Retrieval of surface radiant temperature

Thermal emission data received by remote sensors are converted into radiant temperature through Planck's law (eq 54). Assuming the target to be an ideal radiator of thermal radiant energy, we relate the radiant exitance, E_λ, (W m^{-2} μm) to the absolute radiant temperature, T_s as

$$E_\lambda = \frac{\epsilon c_6}{\lambda^5 \left(e^{c_7/\lambda T_s} - 1\right)} \tag{54}$$

ϵ is the emissivity (dimensionless), λ is the radiation wave length (μm), c_6 (W μm^4 m^{-2} $=3.7413*10^8$) and c_7 (μm K $= 1.4388*10^4$) are radiation constants. Rewriting eq 54 to frequency form and integrating over all frequencies we obtain the Stefan-Boltzmann radiation law

$$E_{SB} = \epsilon \sigma_{SB} T_s^4 \tag{55}$$

with σ_{SB} (W m^{-2} K^{-4} $=5.6693*10^{-8}$) the Stefan-Boltzmann radiation constant (Silva 1978). E_{SB} is the radiant exitance integrated over all wave lengths (W m^{-2}).

Inversion of eq 55 shows T_s to be dependent on the fourth root of E_{SB} and ϵ. Emissivity has some importance. The emissivity of targets is known from laboratory experiments:a black body has $\epsilon=1$, a perfect reflector $\epsilon=0$, a grey body ϵ in the range]0,1[, whereas some targets have a wave length-dependent emissivity of $\epsilon=f(\lambda)$.

Emissivity of field-scale targets are not well-known. For simplicity they often are assumed to act as black bodies and the error assumed to be of second order. Coll et al. (1994) point out that the retrieved land surface temperature may be wrong with an error of the order of 0.4 K to 0.8 K resulting from an unknown ϵ. This error estimate corresponds roughly to a 1% variation in ϵ (Schmugge and Becker 1991).

A spaceborne radiometer "sees" the target from a certain viewing angle and with a certain instantaneous field of view. Thus the recorded radiant exitance is only a part of the energy emitted from the target. Hence the temperature derived is a directional temperature. Tacitly assumed in remote sensing techniques are hence Lambertian characteristics of the target.

From a physical point of view it can be argued (Becker and Li 1993, Norman et al. 1995) that a proper definition of T_s including viewing angle and viewed area is needed. Empirical results indicate that T_s varies considerably with viewing angle. Some scientists conclude that it is necessary to be concerned with directional T_s, when applying T_s in the simplified method. The sensible heat flux results are shown to be severely biased (Vining & Blad 1992, Prevot et al. 1993a).

Satellite remote sensing data obviously can be corrected for viewing angle effects such as the sensor position relative to the target and the sun (eg Antoine et al. 1992). The situation is more complex though as microclimatic effects caused by orography and ground cover can be important. In forests the effects of sunlit and shaded leaves can introduce uncertainty of how to physically relate T_s to the canopy temperature. A suggestion of a correction to this problem is proposed by Sun and Mahrt (1995).

Retrieval of radiant surface temperature is a well-documented discipline and only briefly described here. In regard to thermal satellite radiometers there is a trade-off between temporal and spatial resolution. Some thermal remote sensors in orbit, their spatial and temporal resolutions are listed in table 2.

Satellite	pixel (nadir)	temporal
IRS	70 m * 70 m	24 days
Landsat TM	120 m *120 m	16 days
RESURS	600 m * 600 m	4 days
ERS ATSR	1 km * 1 km	variable (~ 3 days)
NOAA AVHRR	1 km * 1 km	3 times daily
Meteosat	5 km * 5 km	30 minutes
GOES	5 km * 5 km	30 minutes

Table 2. Thermal satellite sensors in orbit, spatial and temporal resolutions. For acronyms please refer to the list of acronyms at page 7.

There are initiatives to develop a high-resolution thermal sensor and bring it into orbit so part of France is mapped daily. The new sensor should have a 40 m * 40 m spatial resolution with two thermal channels and scan around 10 am local time every day (Seguin 1996). One advantage of morning scans is that some areas are less cloudy early in the day. Dual-angle viewing as by ATSR is most attractive in regard to atmospheric correction.

One could imagine a suite of thermal high-resolution satellites for a global coverage. The amount of data would be large. However for improved land surface flux calculation it seems necessary especially in heterogeneous terrain.

Spatial temperature variations do exist and their effect on T_s can be quantified in terms of how much T_s deviates from $(\overline{T_s^4})^{1/4}$. This matter is dealt with in

detail in section 5.2. Now follows a brief view on the correction of atmospheric effects.

3.2.1 Atmospheric correction

Since the launching of the first satellites a major research topic has been atmospheric correction of optical data. The radiant exitance recorded originates from the earth and atmosphere. So correction for the atmospheric effect is vital.

The single window method is based on knowledge of the water vapour content of the air measured by radiosoundings and numerical solving of radiative transfer algorithms. Single window may of course be used for all kinds of thermal infrared data. Water vapour data from space ie High-resolution Infrared Radiation Sounder (HIRS) data within TIROS-N Operational Vertical Sounder (TOVS), has a rather low vertical and horizontal ($\sim$40 km) resolution.

The split window method is based on different absorption coefficients in two thermal wave bands. Generally a linear relation is assumed valid for local sea surface temperature (SST) estimation. Land surface temperatures have been estimated in the same way but nonlinear relations may perform better. Some split window equations also take into account emissivity or viewing angle effects explicitly into account (Antoine et al. 1992, Becker and Li 1993, Coll et al. 1994).

The triple window method is based on different absorption coefficients in three wave bands. But so far the addition of a third (middle infrared) channel does not tend to improve the results (Hansen et al. 1993). Split window and triple window apply to NOAA with the radiometer Advanced Very High Resolution Radiometer (AVHRR).

The dual-angle method is so far applicable only to the Along Track Scanning Radiometer (ATSR) on board ERS. The dual-angle method is based on one thermal channel sequentially viewing through the same atmosphere at two different angles. Evaluation of which method may be the best is at issue (Hansen et al. 1993, Brutsaert et al. 1993, Becker & Li 1993, Gu & Seguin 1993, Reutter et al. 1994, Coll et al. 1994, Gilabert et al. 1994).

The precision of T_s corrected for atmospheric effects and emissivity is of the order of $\pm$2 K (Hall et al. 1992, Stewart et al. 1993). This is true for NOAA AVHRR and airborne thermal data. Kohsiek et al. (1993) reports land surface T_s to be estimated within 1 K from satellite, the atmospheric correction done very carefully. The sensor accuracy is high eg AVHRR $\sim$0.1 K.

Meteosat data has an uncertainty as high as 5 K (Seguin et al. 1994). Landsat TM up to 10 K including atmospheric effects according to Wukelic et al. (1989) and Vidal et al. (1993) although some new results indicate the error to be less (Hurtado et al. 1996). A general problem is that the atmosphere is not homogeneous in time and space, so extrapolation of radiosounding data introduces significant errors.

3.3 Homogeneity and sensitivity

The spatial resolution of remotely sensed data determines the scale that can be mapped and hence be parametrized. High-resolution satellite data of T_s from Landsat TM (channel 6) have a resolution of 120 m * 120 m. This scale can be related to meteorological variables measured 1-3 m above the surface. On this level the atmosphere is strongly affected by surface conditions owing to local interactions over upwind distances of the order of 100 m.

GOES, Meteosat and AVHRR are appropriate only for regional and global studies of fluxes as the pixels are equal to or larger than 1 km * 1 km. The horizontal and vertical length scales are related and therefore it is important to secure that the horizontal and vertical scales are consistent when utilizing remote sensing data (Menenti and Choudhury 1993, Choudhury 1994). An example is that a screen height air temperature is likely not to represent an area comparable to AVHRR pixels.

Niewenhuis et al. (1985) suggested to use T_s of vegetation with *potential* evaporation (in a wet area of the region) instead of T_a. But as pointed out by Gash (1987) the assumptions of homogeneous aerodynamic resistance, temperature and surface temperature are needed to obtain a constant regression coefficient. In a terrain with contrasting wetness (as is actually needed to apply the Niewenhuis method) these assumptions are not fulfilled. In such heterogeneous terrain a site specific adjustment is suggested by Carlson et al. (1990) and further developed (Carlson et al. 1995), see section 3.4.

If an acceptable accuracy in QH is $\pm 50\%$, the gradient T_s-T_a has to be of the order of 5 to 10 K. Such large differences occur regularly only in dry areas like semi-arid and arid climatic zones (Stewart et al. 1993). Stated in another way a 1 K error may result in QH errors ranging between 8 and 87 W m^{-2} K^{-1} depending on canopy height, stability and wind speed (Norman et al. 1995). A sensitivity study by Brutsaert et al. (1993) showed that an error in T_s of 0.5 K would introduce errors in QH of the order of 10% (for constant $r_h(z)$).

Generally a validation of estimates of H and E on the local scale up to the 10 km scale are reported to be in the range 10-25 % (Eymard & Taconet 1995). The basis of validation here is field mast data. Spatial flux data would be preferable.

According to Seguin et al. (1994) ET_d ranging between 0 and 8 mm day^{-1} has an error of ± 1 mm day^{-1} on estimates by the simplified method. This may be acceptable estimates for some purposes like accumulated ten days values (stress degree day for agricultural use). However not satisfactory as an input to the water-energy-carbon models as proposed within International Satellite Land Surface Climatology Project (ISLSCP). Here the input of E is suggested to be ~ 0.3 mm day^{-1} for grid cells of 250 km * 250 km (Sellers et al. 1995).

3.4 Vegetation

In order to improve surface flux estimation but at the same time minimize the required number of input *field* data, several investigations have concentrated on the use of ancillary remote sensing data. In the following section these ideas and results are shortly described.

Surface sensible heat flux is closely linked with vegetation and soil water available for evaporation. A wet bare soil surface will be relatively cool and the difference T_s-T_a small or even negative (oasis effect, warm advection). Therefore sensible heat flux is low compared to latent heat flux. In cases of dry soils the situation can be reversed so that latent heat is negligible and sensible heat large.

Transpiring plants tend to lower the surface temperature even in relative dry (water stressed) conditions. The vegetation amount, type, phenological stage and leaf water potential influence the plant resistance. In areas with partly vegetated surfaces the variability in T_s can be large (Sun and Mahrt 1995). The relation between T_s and H (or E) is more complex than assumed in the simplified relationship. Plants have some ability to control their own environment in respect to water use. In slightly water stressed situations T_s may increase only little, but E has a notable decrease. This effect is called "the hat" in Carlson (1991).

Plants respond to temperature and available moisture. Mapping of the amount of vegetation and (near-surface) soil moisture is important. T_s alone does not predict how much water vapour will be emitted by a canopy. In analogy to human beings Carlson (pers.com.)

"You cannot tell if a person is thirsty just by measuring his radiative temperature".

One way to estimate the amount and the spatial distribution of vegetation is by use of spectral reflectance data obtained by radiometers on board satellites. Very widespread is the use of the Normalized Difference Vegetation Index, NDVI (-), to estimate vegetation spatially. VIS is the surface reflectance of visible radiation and NIR is the surface reflectance of near-infrared radiation. NDVI then is

$$NDVI = \frac{NIR-VIS}{NIR+VIS} \qquad (56)$$

NDVI is near linearly related with green LAI up to LAI ~3. Then NDVI saturates for agricultural crops. For the savanna in Senegal a linear relation between NDVI and QH was found to be reasonable. LAI was very low (Sandholt and Andersen 1993). In a coniferous pine forest in Montana, USA, NDVI was found to be logarithmical related to LAI 3-12 and that NDVI did not "saturate" for the high LAI-values (Running 1991).

Generally LAI and z_0 are not related eg a beech forest may have the same NDVI as a lawn but very different roughness lengths. In physiological terms NDVI is near linearly related with absorbed photosynthetic active radiation (APAR) (Sellers 1989) and APAR is linked with transpiration rates. To some extent NDVI quantify canopy resistance or excess resistance (eqs 37 and 50).

This suggests that there is a potential in mapping NDVI and T_s for inferring surface fluxes. Empirical relations between T_s and NDVI have been studied (Nemani & Running 1989, Carlson et al. 1990, Hasager 1993, Carlson et al. 1994, Moran et al. 1995). Running (1991) suggests a simple linear fit between T_s and NDVI. The slope of the relation was found to represent canopy resistance in conifer forest in Montana, USA.

Often NDVI does not have a linear relation with fractional vegetation cover, therefore a scaled NDVI, NDVI* (-), was proposed by Carlson et al. (1995)

$$NDVI^* = \frac{NDVI-NDVI_0}{NDVI_s-NDVI_0} \tag{57}$$

$NDVI_0$ describes bare soil and $NDVI_s$ describes full vegetation cover. The values are determined in image data for a given region. For full vegetation cover NDVI* equals one and for bare soil zero. A linear relation between NDVI* and the fractional vegetation cover is hypothesized. Based on this assumption SVAT model results show that c_3 in eq 45 relates to NDVI* as

$$c_3 = 0.109+0.51NDVI^* \tag{58}$$

c_3 ranges between [0.1,0.6] for NDVI* ranging from [0,1]. The standard deviation is ± 0.03.The range in c_3 compares well with the data in table 1.

Plots of T_s and NDVI* often show up with a triangular or trapezoid cluster shape. With T_s along the x-axis and NDVI* up the y-axis, a triangle forms with a broad basis. The base encompasses bare soils: cool-wet up to warm-dry. The triangle top is a cool-wet vegetation. Different plant species may have (slightly) different temperatures even under well-watered conditions because of variations in plant physiology. In some cases therefore the top of the triangle are dilated to a trapezoid (Carlson et al. 1994,1995, Moran et al. 1994).

The methods developed by Carlson (1994, 1995) and Moran (1995) focus first of all on mapping fractional vegetation cover and soil moisture conditions based on T_s and NDVI*. Next hypothesized curves of moisture availability as functions of vegetation fraction and surface soil moisture determine the actual evapotranspiration. T_s-T_a still is the driving force (not $\overline{q}_0$-$\overline{q}(z)$), so ET is as usual estimated from the energy balance residual.

As pointed out in Shuttleworth (1991a) the simplest type of "evaporative" models used in hydrology, that may be of interest in a meteorological sense, is an energy balance model. This in fact is what the simplified relation is. If remote sensing data are used in a more complex type of hydrological model like a two-layer model ("big-leaf") SVAT model, better estimates of surface fluxes may be obtained. Shuttleworth (1991b) has called these models "single source".

Simulation models with many layers and very detailed physical and physiological parametrizations are only useful for validation purposes because of the many computations. In fact the idea of initializing a multi-layer hydrological model with remote sensing data at irregular intervals (dependent on available satellite remote sensing data) has been investigated by Capehart and Carlson (1994) and Camillo et al. (1991). The latter study is based on airborne remote sensing data.

A different approach to include vegetation parameters into the simplified method is from empirical fitting by regression analysis. Kubota and Sugita (1994) and Sugita and Kubota (1994) found from a stepwise multiple regression analysis, including variables such as solar illumination, cloudiness, vegetation parameters and wind speed, that QH could be estimated with results just as good as those of the classic profile equations (~ 20 W m^{-2}). The data were from ground-based remote sensors. Independent eddy correlation data were used for validation. The method demands quantification of LAI, incoming and outgoing shortwave radiation among others. The multiple regression method is not generally attractive as the "constants" may not be robust. Most likely they will be site and time dependent.

Various deterministic approaches exist among which a thermal inertia approach (Schmugge and Becker 1991). The small-scale models can be deterministic, but large-scale models are of a conceptual nature. Some processes have to be "bulk" parametrized (or ignored) for simplicity.

3.5 Remote sensing data in a planetary boundary layer model

A large-scale method for surface flux estimation based on thermal remote sensing was proposed and applied by Diak and Stewart (1989) and Diak (1990). T_s was retrieved from GOES (30 minutes) and in combination with radiosounding data of the diurnal rise of the PBL height used as input in a PBL model.

The assumptions of the model are that subsynoptic features like advection and mesoscale circulation are not present. As the spatial scale of pixels (> 25 km^2) are much larger than a typical homogeneous patch, the method is not supposed to describe homogeneous areas.

In the PBL model a roughness length, $<z_0>$, representative for large grid cells was found empirically. Brackets denote a spatial average (as opposed to an overbar that denotes a time average). The method used was to solve for two unknowns, namely $<z_0>$ and β, the Bowen ratio (-), as functions of the rise of mixed layer height (time change of PBL height measured by radiosoundings) and the time change in T_s (measured by GOES). An ensemble of forecast model predictions was used to establish the relation between the four parameters: PBL height, T_s, $<z_0>$ and β. Empirical values of albedo and emissivity were used. With input of synoptic weather data the PBL model can predict temperature, moisture, winds and height of the PBL.

When the PBL model is established and run with input of new values of T_s, large-scale surface fluxes are estimated spatially. The results were only approximate to sets of values for dry or wet conditions over the United States. The method was evaluated to be rather sensitive to errors on T_s and the estimated $<z_0>$. Upper boundary conditions were evaluated to have much less effect on the surface flux estimation.

However McNaughton and Raupach (1996) modelled the entrainment rate over a comparable heterogenous large-scale domain and concluded that the entrainment was significant. On land surface evaporation Kaimal and Finnigan (1994) state in general that evaporation:

in agricultural areas is controlled by entrainment processes,

in natural ecosystems is controlled partly by meteorological feedback processes,

in very dry areas is controlled by the surface moisture availability.

As regards vegetation the partitioning between sensible and latent heat is dependent on the stomatal resistance.

3.6 Momentum flux

Momentum flux has been retrieved successfully only over ocean from remote sensing data. The passive microwave radiometer (SMMR and SSM/I) brightness temperature has provided empirical estimates of wind stress for years. SMMR is the acronym for Scanning Multichannel Microwave Radiometer and SSM/I for Special Sensor Microwave Imager (Kidder and Haar 1995).

More recently the ERS-1 scatterometer data have given estimates of wind stress and wind direction (Eymard and Taconet 1995). The retrieval method is based on inverting the roughness of the water surface to wind stress by empirical fitting. This is possible as the water surface characteristics such as capillary waves and foam are induced by the wind field.

The aerodynamic roughness of water is a function of wind speed and can be calculated from the Charnock equation

$$z_0=0.015\frac{u_*^2}{g} \tag{59}$$

(Charnock 1955 *in* Stull 1991). The backscattered signal (C-band VV) is affected by small-scale features like capillary waves. To predict the wind stress and direction at least three looks from different angles are necessary.

Over land surfaces the wind field does not modify the surface into such predictable patterns generally. Attempts to retrieve effective roughness lengths

from SEASAT scatterometer data (Menenti and Ritchie 1992, Menenti et al. 1996) have been reported but unfortunately the results are rather unclear. However bare soil roughness relate with SAR backscatter coefficients (Greeley et al. 1991, Greeley et al. 1995a and 1995b, Greeley and Blumberg 1995) (chapter 4).

Land surface momentum flux maps are calculated within the present project based on satellite-based roughness maps (see chapter 7). The detailed momentum flux maps seem to be the first of their kind.

3.7 Conclusive remarks on remote sensing methods

Spatial mapping of surface fluxes for homogeneous land surfaces have been studied for 20 years. So far estimates of sensible and latent heat flux at a regional scale have been obtained primarily by use of the simplified method. Appliance of the simplified method is straightforward and the flux results are most promising in semi-arid to arid regions. The concept of the simplified method is to circumvent use of data not readily available but unfortunately the method has inherent problems.

The performance of the simplified method in general is rather poor so modifications that require more field data have therefore received attention. Suggestions range from use of values of potential temperature and wind speed from the lowest level in climatic models or from radiosoundings to inclusion of vegetation and soil moisture information. It can be stated that near-surface values of temperature and wind speed should not be used for large-scale analysis in a heterogeneous terrain.

Operational mapping of evaporation with say 10 % accuracy would be of great interest. But so far it is not possible, primarily because present thermal remote sensors do not map the radiant surface temperature well enough in time (ie hourly) and on a horizontal scale (ie ~100-500 m). New remote sensors may overcome these problems.

However improved surface temperature maps alone do not provide us improved surface flux maps if surface heterogeneity is not taken care of. All current parametrizations break down because of nonlinear effects in heterogeneous terrain. Suggestion on developments on a physically based model presented in chapter 7 may overcome this problem.

For some years sea surface momentum flux has been retrieved operationally from satellite scatterometer data. Land surface momentum flux on the other hand has not been retrieved until within the present work (chapter 7).

4 Remote sensing mapping

Surface fluxes of momentum and heat are partly driven by the surface values of roughness, humidity and temperature. Retrievals of land surface roughness and humidity from remote sensors are described in chapter 4. Spatial temperature retrieval is described in chapter 3.

4.1 Roughness retrieval

Surface roughness as "felt" by atmospheric flow is a function of land cover and orography. Land cover is divided into a number of classes such as vegetation types, soil types, built-up areas and snow. Usually orographic roughness is not parameterized in terms of z_0. Methods for retrieval of digital elevation models (DEM) from satellite data are not described in the present project.

Satellite-based information is a necessary supplement to micrometeorological observations for production of regional- scale roughness maps. Field observations place a large demand on human resources. Therefore satellite-based roughness estimation in a stand-alone mode is desirable. Ideally satellite data should provide us the temporal variation in z_0. Temporal fluctuations of z_0 can be caused by crop height variation through a growing season and also by temporary ice and snow cover. Dobson et al. (1995) state that the actual, not the potential, ground cover should be used in climate models. Potential ground cover is for example global vegetation zones calculated from climatic data.

Roughness estimation from satellite data can be based either on direct or indirect retrieval methods. Direct retrieval are for example soil roughness estimated empirically from SAR backscatter coefficients (Greeley et al. 1995a). It also encompasses estimation of canopy height and density from airborne laser altimeter or windbreak tree height and porosity from airborne SLAR data. The data are input to empirical equations on z_0 (Menenti and Ritchie 1994, Vries 1996). Indirect retrieval on the other hand, here is used for the process of satellite image classification, then assignment of z_0 to each cover class (Dobson et al. 1995, Hasager and Jensen 1996a and 1996b).

Two questions can be posed on spatial roughness mapping

1) which details are needed

2) which details are possible

Sellers et al. (1995) advocate that an accuracy of $\pm 300\%$ on $<z_0>$ is thought to be adequate in large-scale water-energy-carbon models with a grid size on 250 km * 250 km. Furthermore they suggest that z_0 of the "dominant" cover type to be representative. This roughness assumption is currently used in some atmospheric models eg BATS (Dickenson 1995).

A GCM sensitivity test performed by Henderson-Sellers and Pitman (1992) showed profound implications on spring snow melt, albedo, wetness and surface energy balance owing to the grid roughness used. Their conclusion was that the roughness of a "dominant" cover type is far from ideal because $<z_0>$ is very sensitive to small amounts of rough area within a grid cell. The latter is relevant as large homogeneous areas (comparable to GCM grid cells) only describe minor parts of the globe and especially not the land surfaces. Therefore the roughness of a "dominant" cover type is too crude an assumption. Noilhan and Lacarrere (1995) also conclude that the "dominant" roughness is not satisfactory for the GCM scale evaporation modelling. They suggest using a logarithmic average (eq 98). Their requirement is an accuracy on $<z_0>$ lower than a factor of 10.

Studies of aggregation of roughness lengths indicate that the local ("dominant") z_0 and $<z_0>$ are very different (Mason 1988, Klaassen and Claussen 1995, Schmid and Bunzli 1995). Roughness data obtained from airborne eddy correlation momentum flux data support this too (Mahrt and Ek 1984, Moore et al. 1993). Similarly the microscale model results derived in the present work are consistent with this hypothesis (chapter 7). High nonlinearity exists in spatial roughness aggregation for heterogeneous terrain. Simple (logarithmic) averaging does not work well in some cases. This fact implies that small-scale roughness information are required here.

Roughness values for momentum vary five orders of magnitude (Stull 1991). The very rough areas such as cities are quasi-constant in position and time. Other very rough areas are forests. For deciduous forest roughness varies with season. The roughness of orchards, vineyards, maize, sorghum, sugarcane and other medium tall vegetation types varies greatly with season. Agricultural crops like grain, rice, beet and grass vary less but still significantly. These crops take up very large areas. The roughness of bare soils is small and with snow and ice cover even smaller. It is important to mention that natural ecosystems tend to have a less homogeneous vegetation cover and that there is strong evidence that isolated features such as scattered trees, bushes, windbreaks and buildings significantly influence the fluxes (Kohsiek et al. 1993, Beljaars and Viterbo 1994).

In summary very detailed roughness data are necessary in heterogeneous terrain because high nonlinearity exists. However calculation of a spatial mean is not trivial. A sound aggregation procedure is very important.

As the demand for roughness detail is high, the available data clearly set the limits. For some time to come we have to rely at least partly, on indirect retrieval methods.

4.2 Vegetation roughness

Vegetation consists of elements such as leaves and stems that relate physically to z_0. Oversimplified estimates are $z_0=0.2*h_c$ (Kaimal and Finnigan 1994) and $z_0=0.058*h_c^{1.19}$ (Lettau 1969), where h_c (m) is the canopy height. The oversimplification is because plant density is also important. Strong nonlinearity in the ratio z_0/h_c as a function of LAI is reported by Raupach (1994).

Lettau (1969) analysed data from an outdoor experiment where large "lego" blocks were placed on ice. The purpose was to determine z_0 in its natural environment. The similarity to vegetation is not overwhelming. Lettau (1969) points out that the validity of his suggested equation, $z_0=0.5*h_c^* \text{ æ}/Æ$, is limited. It has, however, been applied for homogeneous canopies due to lack of better parametrizations. æ (m^2) is the vertical silhouette area "seen" by the wind and Æ (m^2) is the lot size per element. h_c^* is an effective canopy height.

Recently Raupach (1994) derived a parametrization on z_0 for homogeneous canopies analytically from form and drag partitioning theory. The input parameters are vegetation height and LAI. The function is nonlinear. A global maximum of the ratio of z_0/h_c is found for LAI~0.3. As LAI increases, a shelter effect results in a smoother surface and z_0 approaches to $0.07*h_c$. Field and laboratory data were used to judge the parametrization. Forest roughness data from a Danish beech forest show z_0 to be higher before the forest came into leaf than after (Jensen pers.com.). The explanation probably again is that the leaves act smoother than naked twigs due to a sheltering effect. In forests the displacement height gains importance. Simple estimates like $d=0.66*h_c$ (Oke 1987) or $d=0.75*h_c$ (Kaimal and Finnigan 1994) are usually sufficiently accurate. Also Raupach (1994) shows d/h_c to depend only weakly on LAI.

Raupach (1994) further found that $z_0 \sim 0.01*h_c$ (or $\sim 0.001*h_c$) when LAI approaches zero. The plants stop exerting control and the momentum is absorbed primarily by the soil roughness. Therefore a determination of the soil roughness instead would probably be more useful.

Sellers et al. (1995) suggest obtaining local roughness values from LAI values. It is not clear how LAI should be measured globally. Unfortunately LAI and NDVI correlate only for sparse vegetation up to LAI~3. For larger LAI values NDVI tends to saturate and then diagnose senescence. NDVI does not correlate with z_0. The obvious reason that NDVI and z_0 do not generally correlate is that they relate to different vegetation characteristics. z_0 "measures" the geometry (height and density). NDVI "measures" the red light absorption by chlorophyll (the absorped photosynthetic active radiation, APAR) (Sellers 1989).

Since optical satellite data in a stand-alone mode have not provided us with direct estimates of z_0, recent investigations on radar data have been carried out (Dobson et al. 1995, Greeley et al. 1995a, Menenti et al. 1996, Søgaard et al. 1996). One possible way could be a mapping of LAI from SAR data. As shown by Raupach (1994) LAI and z_0 are related. A field based study by Prevot et al. (1993b) indicates that LAI can be obtained by an inversion technique. C- and X-band co-polarized scatterometer data were used. It was noted that a 1 dB precision was needed to estimate LAI by 1 (m^2 leaf m^{-2} ground).

Ulaby et al. (1984) investigated groundbased scatterometer data in regard to LAI in wheat, sorghum and maize. Four bands ranging from $\lambda=3.5$ cm down to 0.8 cm all at ϕ of 50° were used. The vegetation was modelled as a lossy volume of scattering elements and with soil scattering. In one version the vegetation was modelled as two-layer. The small wave length SAR signals were rather sensitive to heading in wheat. The conclusions were that for LAI > 0.5 the plant contribution was significant compared to the soil contribution, and that for LAI > 2 σ^0 did not change in maize and sorghum. In wheat σ^0 increased

with increasing LAI up to 9.

Investigations of a direct relation between σ^0 and z_0 for vegetation are scarce (Dobson et al. 1995, Søgaard et al. 1996). For bare soils Greeley et al. (1991,1995a,b) and Greeley and Blumberg (1995) have reported promising results. For water surfaces the relation is well-documented and used operationally (Offiler 1994, Kidder and Haar 1995, Eymard and Taconet 1995, Rufenach 1995).

A general section on SAR data follows. Subsequently comes on analysis of roughness retrieval on SAR data from Foulum in Denmark and the Rhine Valley in Germany.

4.3 On SAR data

Electromagnetic waves in the wave length range 0,3-100 cm are called microwaves (frequency range 0,3-100 GHz). Within radar technology typical "band names" are used and here listed in table 3.

Band	P	L	S	C	X
Wave length (cm)	70	23	10	5.6	3
Frequency (GHz)	0.3	1.0	3.0	5.3	10.0

Table 3. Microwave bands, wave length and frequency.

The relation between wave length, λ (m), and frequency, f (Hz) is

$$f = \frac{c_s}{\lambda} \tag{60}$$

c_s is the speed of light ($3*10^8$ m s^{-1}).

SAR data are polarimetric. This means that the received and transmitted signal matrix can be described from coordinates horizontal and vertical to the incidence angle, ϕ (°), relative to nadir for a plane surface. By way of example HV means horizontally received and vertically transmitted. HH and VV are co-polarized and HV and VH cross-polarized signals. The amount of SAR data has increased recently. Satellite and shuttle imaging radar (SIR) data are listed in table 4.

In addition to satellite and shuttle missions, a number of airborne SAR data have been recorded during field campaigns in various countries. Lee et al. (1994) mention some of these. Data from the so-called EMISAR scanner developed in Denmark is described in section 4.4.

Name	Period	Band	Polarization	ϕ (°)
SEASAT	July-Sep. 1978	L	HH	22
SIR 1 (A)*	Nov. 1981	L	HH	50
SIR 2 (B)	Oct. 1984	L	HH	20-50
ALMAZ 1	1987-	S	HH	25-50
ALMAZ 2	May 91-Oct. 92	S	HH	25-50
ERS-1	July 1991-	C	VV	23
JERS-1	Feb. 1992-	L	HH	38.5
SIR 3(C)	Dec. 1993	L,C	HH VV HV VH	variable
		X	HH	variable
ERS-2	April 1995-	C	VV	23
RADARSAT	Nov. 1995-	C	HH	20-50

*Table 4. SAR data available from satellites and shuttle missions. * means optically processed. All other scenes are digitally processed. Please refer to list of acronyms page 7.*

The radar antenna transmits microwaves with a controlled (known) strength, frequency and polarization. It is the backscattered signal of this electromagnetic radiation that is measured and calculated into a SAR image. SAR recording is independent of sunlight. Atmospheric damping of microwaves is very small at wave lengths larger than 3 cm (< 10 GHz). This means that the energy is transmitted practically undisturbed through the atmosphere. Clouds and precipitation do not effect the recording.

Microwaves are not only backscattered from the surface of the elements on the ground as is the case for optical (visual and infrared) data. In addition to backscattering from the surface of the ground elements, microwaves also slightly penetrate. The extent of penetration depends on wave length, view angle, water content and material. This means that SAR scenes do not only map the surface of elements, but in some cases the near subsurface characteristics. Therefore SAR data are complementary to optical data as they map different properties.

A SAR image contains digitally measured backscattered signals, that from a time- and space-dependent algorithm are projected into a grid of resolution cells. For image processing it can be considered as a grid of pixels. The value in each pixel usually is the signal strength squared. The unit is $Volt^2$ per pixel.

The mean value of energy received per pixel is given by the radar equation (FAO 1993)

$$\langle P_R \rangle = \frac{c_9 \, G^2(\phi) \Delta x \, \Delta y \, \sigma^0}{Ra^3 \sin(\phi)} \qquad (61)$$

with notation

P_R mean received amplitude per pixel (Volt^2)
c_9 system constant (a function of transmitted amplitude, wave length, various gains and losses)
$G(\Phi)$ one-way gain of antenna amplitude (Volt)
Δx pixel distance in azimuth range (m)
Δy pixel distance in slant range (m)
σ^0 mean reflection in the scene per unit area (-)
Ra range (distance) between antenna and reflecting terrain
ϕ incidence angle relative to nadir (°)

The mean reflection in a calibrated SAR image is called the *backscatter coefficient*, σ^0. It is dimensionless. It is proportional to the effect. σ^0 is defined as a measure of the expected return signal from randomly distributed scattering elements in an area of 1 m^2 in the horizontal plane. Hence it is a parameter related to the surface (the scattering media).

σ^0 at the same time is a function of surface parameters such as roughness, geometry and dielectric properties. Furthermore it is a function of radar observation parameter such as frequency, polarisation and incidence angle.

σ^0 has a very large dynamic range, roughly $1*10^5$, and therefore the values are recalculated with the logarithm (with base 10) as follows

$$\sigma^0_{dB} = 10 \log_{10}(\sigma^0) \qquad (62)$$

dB is decibel.

Calibration

The reflected radar signal from a geometric object in the scene with properties of a conductive sphere can be used for absolute calibration. Usually the return signal from several corner reflectors placed in homogeneous areas are used. A trihedral corner reflector is specular and the signal is called σ. It expresses the power of the reflection measured in area units (the radar cross-section of a sphere). This measure is defined from the size of a hypothetic uniform scattering sphere, that would give the same backscatter as is actually observed (FAO 1993).

As we know the gain and bias from a radar system the correction on the digital numbers is according to Skriver (pers.comm. 1992).

$$\sigma^0 = (gain * DN + bias)^2. \qquad (63)$$

Multi-looking

For technical reasons a chirp technique, ie a long pulse with modulations on the frequency, is emitted and after reception transformed into a short pulse value. The emitted pulses from the radar hit the objects in the resolution cell at the theoretically homogeneous scattering surface at different angles and times. Backscatter and surface penetration vary sligthly according to the scattering media. The result is that the backscattered contribution from the various places within the resolution cell changed to a different phase, power and polarization. Phase shift cause constructive or destructive interference to occur.

The SAR image constructed from a linear combination of all the individual scatters illuminated by the radar will vary around a mean value. When the amplitude is squared, the phase information is eliminated, but the brightness (intensity) differences are preserved. The standard deviation on brightness is given by (FAO 1993)

$$\sigma_{\sigma^0} = \frac{\sigma^0}{\sqrt{N_L}} \tag{64}$$

N_L is the number of looks.

Number of looks means uncorrelated radar recordings of the same element under ideally the same conditions. To eliminate the unwanted scatter in σ_0, the radar system is constructed so that it "sees" the object several times and the signals (effect values) are averaged. Hence the variance of the intensity is reduced. It is a non-coherent averaging. Averaging four scenes is called a four-look image. As an example it can be mentioned that the range between the 95% and 5% percentiles in a one-look image will be 17,7 dB, but summing into a four-look image the scatter decreases to 7.54 dB (Thomsen 1992).

To calculate the mean backscatter from N effective (independent) looks with inclusion of absolute calibration, the following operation is assumed to be valid

$$\overline{\sigma^0} = \frac{1}{N} * \sum_{i=1}^{N} (gain * DN + bias)^2 \tag{65}$$

As the number of effective looks are not determined by the user of SAR data, other tools have to be used to get rid of unwanted variance around the mean. This leads to the inevitable theme: speckle filtering. But first, what is speckle?

SAR speckles

Speckle is a statistic fluctuation or uncertainty associated with the brightness in each pixel. Speckle noise is multiplicative. This means that the higher the mean reflection, the larger the spread around the value. So in an area mapped with dark grey tones (low σ^0), the speckle will generally be less than in brighter areas.

Speckle (in a one-look image) consists of phase-independent complex contributions from many small scatterers where none of them dominates in regard to amplitude and where phase and amplitude are uncorrelated. Speckle is complex signals, so the signal is

$$amplitude = \sqrt{intensity} = \sqrt{\Re^2+\Im^2} \quad (66)$$

The amplitude follows a Rayleigh distribution and the intensity a gamma distribution (Thomsen 1992). Filtering is performed on intensity data.

Scene texture, which we want to map and analyse in a geographical image context, relates to space variations in the surface properties. The SAR image texture relates to scene texture multiplied with speckle variation, mathematically described as

*image intensity = signal intensity * speckle noise.*

The mean of speckle noise is 1 (Schumann 1990).

Reducing speckle noise can be performed in two ways:

1) Multi-looking

The process is performed in raw signal data, ie by dividing the antenna into more "seeing segments" thereby obtaining a larger number of uncorrelated recordings of the same resolution cell. The more looks, the less speckle noise. The end-user does not perform or decide on the multi-looking.

2) Filtering

The filtering is performed in image data by averaging a number of pixels in a moving window and assigning the centre pixels new (estimated) values based on the local statistics appearing within the window. An alternative is block-averaging, but in this case the spatial resolution is drastically decreased.

4.3.1 SAR filtering

Speckle filtering is performed to get rid of the speckle noise, but to maintain the scene information as much as possible. Scene information may be used for various purposes. The specific purpose should be considered before filtering. Some examples of typical image analysis are:

landuse classification where a good separation between each cover class is most important;

structure analysis where clear boundaries between macro- elements are most important,

texture analysis where the pattern is most important. Pattern includes density, dimension (scale) and spatial distribution (ie orientation, shadow effects and contextual relations).

Filtering is usually performed on intensity data where speckle noise is an independent complex multiplicative noise. (In amplitude data the speckle noise is additive owing to phase).

Filtering based on the local statistics in homogeneous areas is straightforward. A lowpass filter is sufficient. In a heterogeneous area this will not work for the obvious reason that the local information (within the window) encompasses truly different information. If a lowpass filter is applied, the result is a blurred image where separation among classes is impossible and (tiny) line elements are eliminated. The possible solution to filtering is hence use of an adaptive filter. These will analyse in an intelligent (mathematically controlled) way the image information of the surrounding pixels before any averaging takes place.

In many geophysical applications it is preferable to use unfiltered data. The advantage is that bias caused by filtering is avoided.

Simple filters

Low-pass filters assign for example the mean (mean-filter), the median (median) or variance (variance-filter) to the centre pixel based on simple statistics in the window. The variance-filter is useful when multiplicative noise is removed.

High-pass filters conserve the information that strongly deviate from the window mean. The information are usually called high-frequency. In land surface images this typically are single objects eg buildings, farms, poles, roads, coastlines.

However high-pass filters with much more relevance for SAR data are the so-called edge-detection or edge-enhancement filters. These typically work such that a more or less complicated algorithm investigates the intensity between pixels within the window and calculates the gradients and orientation. From this an appropriate value will be assigned to the centre pixel. This can be based on the gradient (gradient-filters) or relative to the gradient (ratio-filters). The latter is suited for multiplicative noise.

A relatively simple combination of low- and high-pass filters can be used as an edge-preserving smoothing-filter. The variance in a (large) window is calculated. Based on the mean of the subarea with the lowest variance, the centre pixel is assigned to a new value. The process is performed on the whole image. The process is run iteratively until no change is detected. The filtering technique sharpens edges and smoothens homogeneous areas (Schumann 1990).

Local-statistics filters

Local-statistic filters are based on image statistics within a window. Some local-statistics filters include texture in the filtering process. Frostfilter, Sigmafilter, Leefilter and Kuanfilter belong to this group (Schuman 1990, Lee et al. 1994).

Local-statistic filters observe that homogeneous areas have a low variance and heterogeneous areas a larger. A decision on smoothing or preservation of the information is then taken and applied. Stated differently, homogeneous areas will be smoothed whereas heterogeneous (high contrast) areas will conserve the information.

Frost-filter consists of an exponential weighting function between variance and mean intensity (Schumann 1990). The weighting function goes to zero in homogeneous areas and filtering is here performed with a low-pass filter. The weighting function goes to a large value in heterogeneous areas. The filtering is performed with a high-pass filter that quickly decrease away from the centre pixel. Frostfiltering is based on neighbouring values.

Sigma-filter masks out pixels with a standard deviation larger than two before estimating the mean for the centre pixel. In heterogeneous areas only few pixels may be used. A block mean can be used if point scatters have to be removed. Sigmafilter weights on non-masked neighbouring pixels.

Lee-filter and *Kuan-filter* are also based on local statistics and weight the estimate from a so-called coefficient of the variation. When the coefficient is low, all pixels are included in the average. When the coefficient is large (thresholds have to be defined) the pixel values are preserved. The coefficient of variation describes the heterogeneity well for isotropic texture and the filters are good in the case of Gaussian noise (Lopes et al. 1993). The filters preserve some of the texture. Close to edges and point scatters, some noise may persist because the coefficient of variation may be high inside the window. The two filters weight from the coefficient of variance in neighbouring pixels (Lee et al. 1994).

Adaptive filters

These filters are called adaptive filters because they adapt to the scene and to modelled speckle statistics. Adapting to the scene here has to be understood as follows. First the edges and point scatterers are located from gradient- or ratiofilters; then the averaging algorithms are based on a texture measure similar to the coefficient of variation in the local statistics filters. Anisotropic texture will be found and treated. One of the adaptive filters is the Gamma MAP-filter. It is especially developed for SAR image speckle noise removal (Lopes et al. 1993, Nezry et al. 1991). As the name implies the intensity values follow a gamma distribution, and MAP relates to Maximum A Posteriori.

Speckle filtering algorithms are developed along with the increased use of SAR data. A recent example is within the large classification project "Radarkarte Deutschland" where 150 ERS-1 SAR scenes were analysed (Hagg and Szies

1994, Markwitz et al. 1995).

Finally it should be mentioned that a correction of orographic effects requires a digital elevation model.

4.4 SAR analysis from Foulum

A number of airborne SAR scenes were recorded in 1993, 1994 and 1995 at Research Centre Foulum in Jutland, Denmark. All scenes were from the EMISAR scanner built and operated by Electro Magnetics Institute (EMI) at Denmarks Technical University. The SAR scenes recorded are fully polarimetric C-band and since 1995 L-band. Ground field data collection and subsequent analysis were and are done within the DANish Multisensor Airborne Campaign (DANMAC) project (Thomsen et al. 1994).

Micrometeorological data were sampled in a large field located south of Research Centre Foulum. A sketch of the area is shown in figure 1. There was a long fetch in two directions, namely in a sector from 40-155° (easterly winds) and 170-275° (south westerly winds). Wind speed and temperature were measured on three levels. Data on crop height, precipitation and wind direction were provided by Research Centre Foulum.

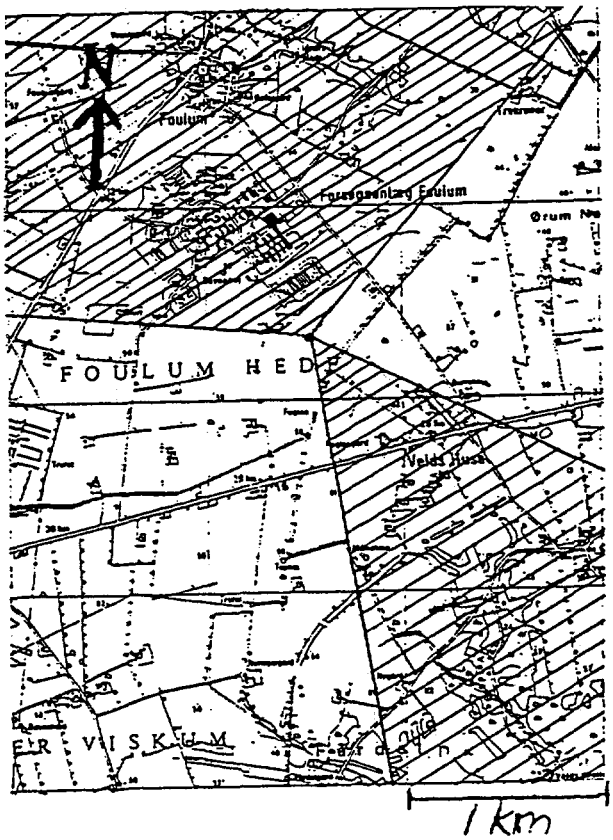

Figure 1. Foulum site with meteorological mast, April to August 1994. Denmark. Sectors with good fetch are clear, the others hatched.

Winter wheat was sown in the field in the autumn of 1993. In the beginning of April 1994 it was 8 cm tall and in July 81 cm. The field was harvested on August 11. The roughness, z_0, increased from 0.58 cm in April to 10 cm by the end of July. z_0 was calculated in situations of neutral stability and strong winds from the long-fetch sectors. In 1995 barley was grown in the field and a similar data set was collected by Søgaard et al. (1996).

In 1994 the EMISAR scanner recorded on April 28, June 23, July 29 and August 27. The latter is after harvesting. However the micrometeorological mast was removed prior to harvesting. Therefore only an estimate on z_0 is given for this date. Mean σ^0_{dB} values of the wheat field were in 1994
-12.5, -9.2, -9.2 and -14.1 dB for HH,
-11.5, -14.0, -12.9 and -13.7 dB for VV,
respectively. Søgaard et al. (1996) report the 1995 data of σ^0 and z_0. There is a total number of six data points from wheat and barley of (z_0,σ^0) at the Foulum site in 1994 and 1995. Before presenting the data in more detail, the preceding image processing is briefly described.

To reduce speckle the images were multi-looked at EMI with a 3*3 window. So the spatial resolution was decreased from the original 1.5 m * 1.5 m resolution cells to 4.5 m * 4.5 m. However speckle is still significant and geometrical correction not easy. Reliable ground control points were rather scarce owing to speckle. In ERS-1 SAR scenes the problem seemed even worse. An analysis on the effect of speckle filtering was performed on the 1994 EMISAR scenes.

An example of raw data, Leefiltered data and speckle noise alone are shown in figure 2. The salt-and-pepper image is the removed speckles. For the present purpose it is most important to consider bias on the mean value in homogeneous areas. The analysis showed no bias. This indicates that Lee filtering removes speckle noise in an acceptable way. Very recently van Oevelen et al. (1996) reported that a Gaussian "speckle" noise added to a SAR image (Monte Carlo simulation) did not bias the mean σ^0 of large homogeneous areas.

It is known that C-band SAR signals interact with vegetation and soil in complex ways. Wetness of soil influence the return signals significantly. Investigations of soil moisture in EMISAR data show this (Ji et al. 1995 a,b). It is well-known that the dielectric constant changes rapidly with soil moisture (eg Engman and Gurney 1991). However SAR data are also functions of soil structure, soil surface micro-topography and vegetation components.

The present analysis of the EMISAR data has focused on direct retrieval of aerodynamic roughness in wheat and barley fields. It was hypothesized that σ^0 is a function of z_0 in grain. This has been shown to be valid for soils (Greeley et al. 1991, 1995a,b) and water (see section 3.6 and 4.2)

Roughness of soils

The studies by Greeley et al. (1991,1995a,b) show promising results of estimating bare soil roughness from co-polarized data. However they conclude that cross-polarization is even more effective. Greeley et al. (1991) reported on

the assessment of z_0 by σ^0 from airborne SAR scenes. Their data set included seven data points from different bare soil areas. The log-log linear regression root mean square error ranged between 0.36 (C-band VV) to 0.84 (P-band HH and HV).

Subsequently further results by Greeley et al. (1995a) were included and new regression lines (with higher confidence levels) were obtained. Their data points encompass bare soil and very sparse vegetation in sand, gravel, playa and Hawaiian lava formations. Very recently their regression lines have been compared to new data from different bare soil sites throughout the world, among these a sparsely vegetated agricultural soil in Stauning, Denmark (Greeley et al.1995b).

A comparison with the Greeley et al. (1995a,b) regression "soil lines" is shown in figures 3 and 4. Micrometeorological observations of z_0 and values of σ^0 from EMISAR and ERS-1 SAR C-band data from Foulum in 1994 and 1995 are included.

Figure 3 shows that all C-band HH σ^0 data fall below the "Greeley soil line". To a first approximation on a 5 dB lower level regardless of grain species. Figure 4 shows that also C-band VV data from EMISAR and ERS-1 fall below the "Greeley soil line". Only for low values of z_0 do the data approach the "Greeley soil line". This finding seems physically justified as our low z_0 values occurred for sparse canopy cover. In this case the soil effect is dominant. Note that the filled square in figure 4 is a guess for z_0 since only σ^0 was measured after the harvest.

Figure 4 indicate that to a limited extent ERS-1 data agree with EMISAR. However it is not clear why this is so since their incidence angles are very different. In the case of EMISAR data ϕ ranges between 43.6 and 45.0° whereas in our ERS-1 SAR data ϕ ranges between 20.3 and 24.3°. The airborne SAR data reported by Greeley et al. (1995a,b) had a ϕ of around 40°.

σ^0 is very dependent on ϕ for different idealized surface roughnesses (measured as height and distance of the soil micro-topography). The roughness and radar backscatter intensity will be positively correlated only for $\phi > 30°$ (Ulaby et al. 1982 *in* Greeley et al. 1991). For $\phi < 12°$ there is a negative correlation whereas there is no correlation in 20-25° range.

At this point it is interesting to consider whether the small-scale structures made by the wind such as ripples on a sandy beach, capillary waves at water surfaces, aeolian gravel deposits and other similar features, could have a basic similarity between the horizontal and vertical length scales determined by u_* and gravity. The Charnock equation (eq 59) applies to sand surfaces within certain wind speeds but with an adjusted coefficient (Larsen 1993, Vugts and Cannemeijer 1981). This indicates that there may be a physical explanation as to why the empirical soil lines between z_0 and σ^0 fit so well (soil lines in figures 3 and 4). However at the same time it may indicate non-validity ranges eg dense canopy.

Soil moisture and vegetation moisture influence the backscatter coefficients. The moisture effects are not investigated in the present project but studied by others in regard to the EMISAR data set (Ji et al. 1995a,b, Søgaard et al. 1996).

*Figure 2. EMISAR airborne C-band SAR (HH) data from Foulum 1994. Upper panel raw data, middle panel Lee-filtered and lower panel the removed speckle noise. Pixel size 4.5 m * 4.5 m. The subset is from a field.*

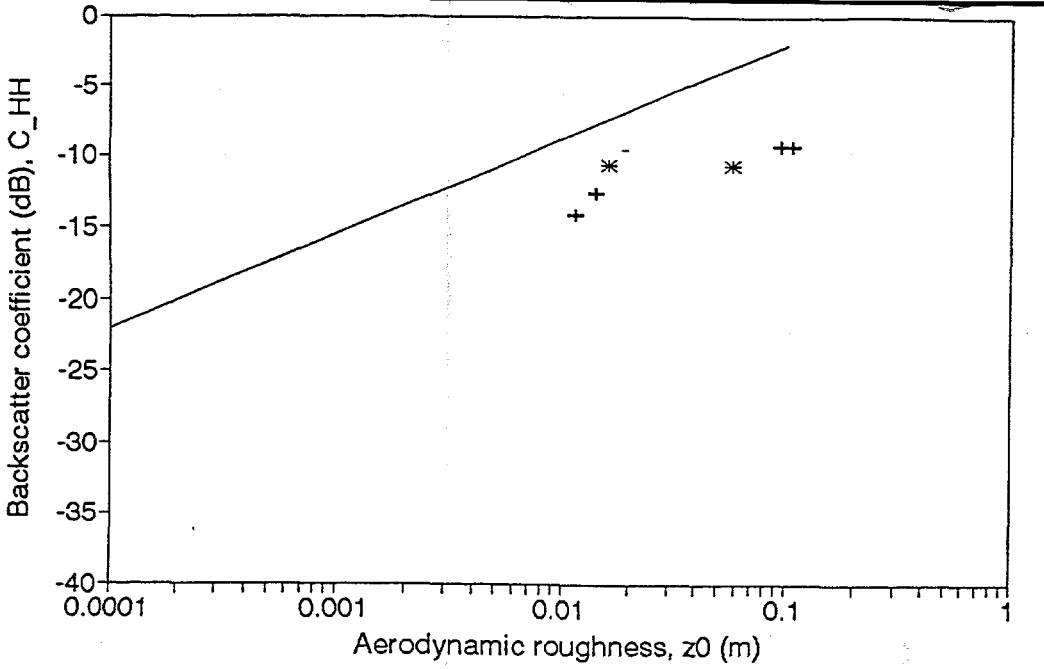

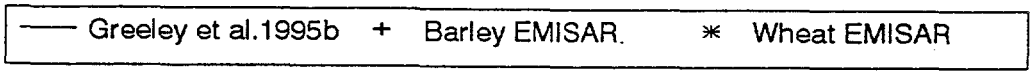

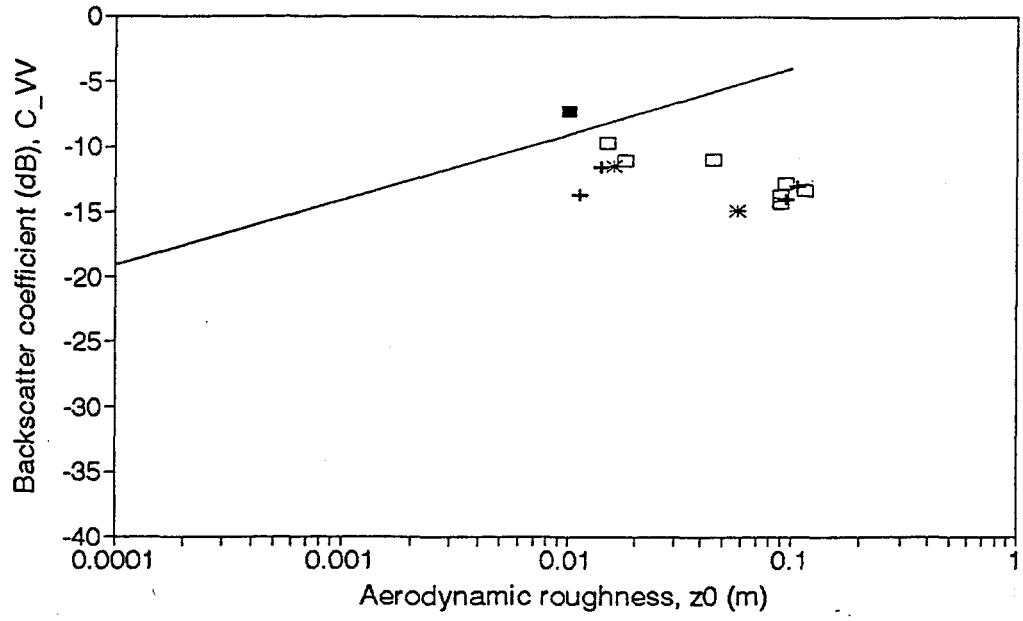

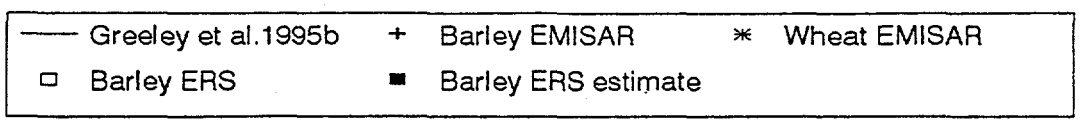

Figure 3 (above). C-band HH SAR data from EMISAR as a function of aerodynamic roughness length measured in Foulum, Denmark 1994 and 1995 in barley and wheat. The full line is from Greeley et al. (1995b) for bare soils.

Figure 4 (below). As figure 3 but C-band VV SAR and ERS-1 SAR data. The filled square indicate that σ^0 was measured and z_0 estimated after harvesting.

Roughness of grains

Vegetation can be discriminated from bare soil on the basis of the backscatter coefficient because vegetation has a more diffuse scattering (Oevelen 1996). Dubois et al. (1995a) used a ratio between cross- and co-polarized σ^0 to discriminate soil and vegetation. In the case of vegetation they found the cross-polarized SAR data to be the most useful discrimanators. Dobson et al. (1995) present a detailed description of vegetation components, leaf shape and plant structure. These features are argued to respond in certain (deterministic) ways with SAR signals so that SAR signal analysis facilitates separation of the plant groups into spatial cover classes. It was concluded that multi-angle or multi-frequency information are needed.

Cross-polarized signals are an order of magnitude weaker than co-polarized, hence only the latter are available from current satellites. Therefore the study of z_0 in vegetation was focused on co-polarized data (Søgaard et al. 1996). All of the present SAR satellites are single band, but it is now possible to combine eg ERS-1 and -2 (C-band VV), Radarsat (C-band HH) and JERS (L-band HH). Their spatial resolutions are comparable.

No simple relation between either z_0 and σ^0 VV, or z_0 and σ^0 HH in wheat and barley was found in the Foulum data set. Therefore combinations of HH and VV signals were investigated. The data indicate that VV is partly absorbed in vegetation whereas HH is less affected by vegetation. The analysis reported in Søgaard et al. (1996) used an empirical procedure between radar backscatter, incidence angle, dielectric constant and vegetation roughness. A semi-empirical equation developed by Dubois et al. (1995a,1995b) for non-vegetated soils was modified. An extinction of the radar signal was hypothezid in vegetation and was modelled with an exponential decay coefficient similar to Beer's law. The data set analysed by Søgaard et al. (1996) also included data from Sweden 1994 (within NOPEX). So far the results are only indicative and a larger (independent) data set is needed to validate the results. At all times the soil water content seemed to be important whereas the plant water content showed less significance.

Additional comments on the Foulum data

Water is easily recognised in the EMISAR scenes. Water has a very low σ^0. Markwitz et al. (1995) report from production of "Radarkarte Deutschland" by use of 150 ERS-1 SAR scenes that flowing water (ie the Rhine) is very sensitive to local winds and often mis-classified into grass/prairie. This does not appear to be a problem in the airborne data (but in an ERS scene shown in figure 8).

Snow is very smooth in an aerodynamic sense with a roughness length of the order of 10^{-4} m (Stull 1991). One C-band EMISAR scene was recorded in a situation with a three cm deep frozen snow cover in Foulum. The microwaves penetrated the frozen snow and σ^0 responded to the soil/vegetation state beneath the snow. It is not feasible to map the presence of snow with SAR. Optical data are ideal for this purpose.

In an attempt to produce a roughness map, a discrimination of rough areas is important. Urban areas have large z_0 and d values. Empirical methods of estimating $<z_0>$ based on obstacle height and density have been suggested (Kondo and Yamazawa 1986, Stull 1991) (section 6.3.1). SAR signals interact with buildings and similar objects. The SAR interactions may be described by means of multiple bounce. Atmospheric flow in urban areas is complex, and the empirical relations on $<z_0>$ not fully validated. At present it is therefore suggested to assign empirical values to classified urban areas.

Finally we will touch on the roughness of forests. Much research has been directed towards biomass estimation in forests from SAR data. This has importance in forestry. Results of z_0 as a function of σ^0 have not been reported. Woodhouse and Hoekman (1996) report that the backscatter from stems, branches and twigs exceed the leaf contribution in forests. Their approach was to link a physical (geometric) tree description to backscattering theory. Oevelen et al. (1996) point out the tremendous problem associated with forward and inverse backscatter modelling of very complex surfaces. Dobson et al. (1995) report various forest types in Michigan to be classified with high accuracy from multi-band satellite (ERS and JERS) data. They suggest an assignment of empirical roughness values to classified maps.

Windbreak and forest height

Windbreaks extract a large amount of momentum. For accurate wind energy prediction, knowledge of obstacle height and porosity is needed (Troen and Petersen 1989, Mortensen and Said 1996). Porosity is defined as open area to total area. Vries (1996) have presented interesting results of height and porosity estimates based on airborne Side Looking Aperture Radar (SLAR).

Derivation of the tree height from SLAR data is a simple algebraic calculation. The "shadows" cast behind tall obstacles have a size equal to obstacle height multiplied by the tangent of the sensor viewing angle. Owing to the large viewing angle of SLAR, the method is applicable. Porosity is estimated empirically from the "darkness" of the "shadow", ie the grey scale in the pixels (Vries 1996).

In principle the same method is applicable in other data types such as panchromatic aerial photographs. The sun and sensor position should then be known. However in regard to optical satellite data for example IRS panchromatic (6 m * 6 m pixels) or SPOT panchromatic (10 m * 10 m pixels), the number of shadow pixels will be too few.

It could be that airborne SAR data can be used to map windbreaks based on the same principle as de Vries (1996) used for SLAR. Large incidence angles are preferable. At some angles to the slant range windbreaks sill cast "shadows". Ground truth data on hedges and windbreaks were not collected at Foulum. From visual inspection of the Foulum scenes no clear "shadows" appear.

4.5 SAR analysis in Rhine Valley

In the international field experiment TRACT a large number of data were collected in the Upper Rhine Valley during two weeks in September 1992 (Fiedler 1991). The area included southwest Germany, part of Switzerland and part of France. The total area is of the order of 100 km * 100 km. z_0 was calculated from micrometeorological observations performed in most land cover types by Fiedler et al. (1994). Among many other parameters they also collected LAI.

Landsat TM scenes are an additional data source from the TRACT project. A land cover map from the Upper Rhine Valley was produced from a supervised multi-temporal classification by Konrad et al. (1994). In the year of 1992 there was no cloudless Landsat TM scenes available. Hence the land cover mapping was performed on scenes from 1993. The classified area is roughly of the size of 100 km * 100 km. A subset of the classified scene is shown in figure 5. It illustates the 19 cover types, the roughness of each cover type and the areal extent in the subset. The subset is roughly 15 km * 15 km and located 20 km northeast of Strassburg. A micrometeorological mast was located in the subset image centre that is in field site of Scherzheim in 1992 (Barthelmie and Jensen 1995) (section 7.5).

In the present project roughness values were assigned to the classified Landsat TM scene. Figure 6 shows a subset of the roughness map. From Fourier analysis the "typical" horizontal length scales in the roughness map were found to be of the order of 650 m. However patches with many other length scales are present. It is clear that the area is strongly heterogeneous.

An ERS-1 SAR scene from 20.9.92 was retrieved, with the aim of generating a roughness map valid for September 1992. A 15 km * 15 km subset of the SAR scene is presented in figure 7 covering the same area as shown in figures 5 and 6. The SAR scene was geometrically corrected to the Landsat scene (image to image) and speckle filtered with a Lee filter (threshold 3). Speckle filtering reduced the σ^0 range but do not change the mean from a homogeneous area (section 4.4). In the case of the Rhine Valley no homogeneous areas seemed to be present. All fields are small. Only very few pixels map a given patch.

In order to produce a roughness map it was attempted to classify the scene. Homogeneous subareas were deliminated and used as input for the classification. It was only possible to extract three cover types (water, vegetation and forest). However even these few classes were not clearly separated. It may be concluded that a single SAR scene is not sufficient to classify the land cover in the Rhine Valley. As the classification was poor, it was not possible to obtain a reliable roughness map from one SAR scene.

Another three ERS-1 SAR scenes were retrieved. They were close in time to the Landsat TM scenes. Information on all Landsat and ERS satellite scenes from the Rhine Valley are presented in table 5.

Rhine Valley, Germany

Landsat TM 1993

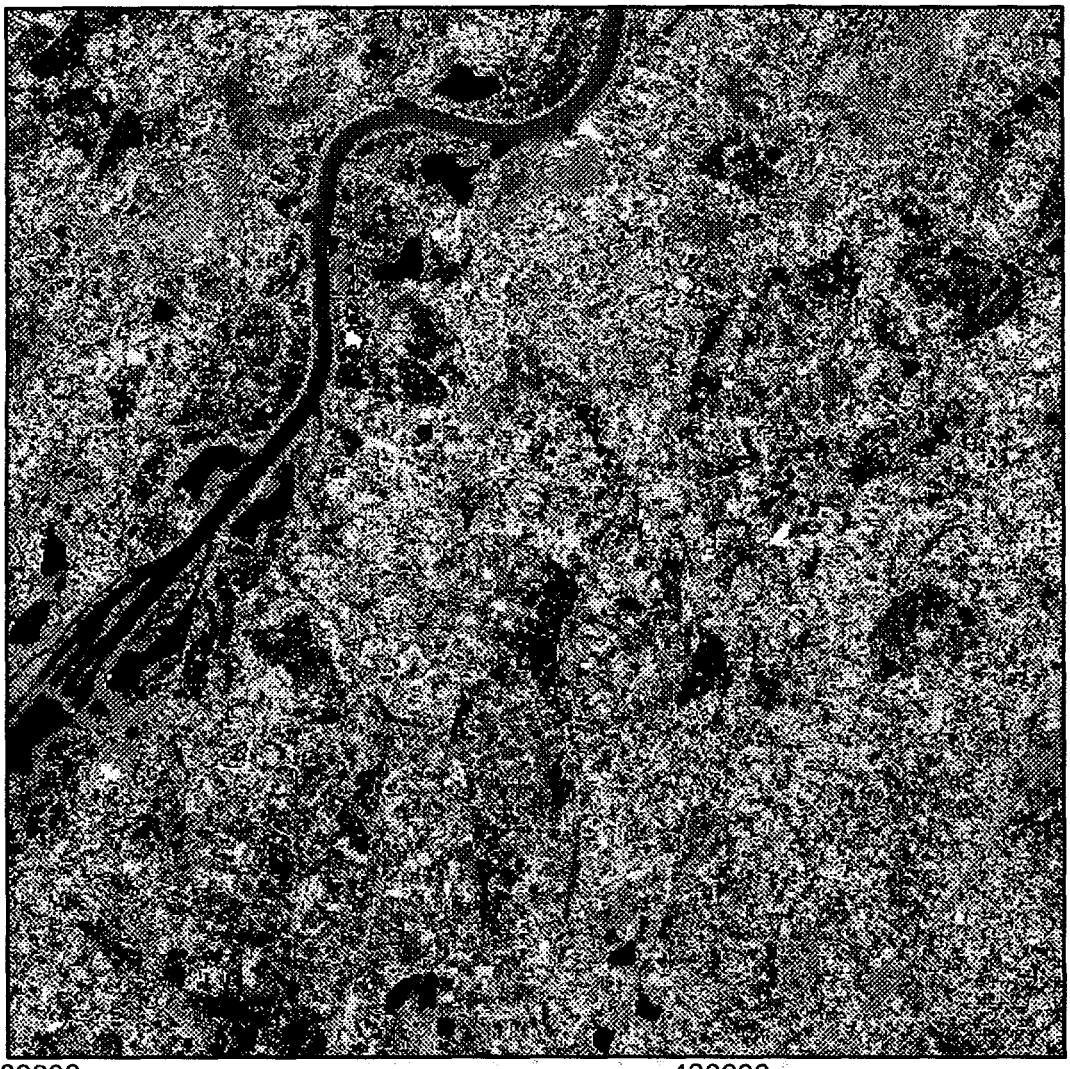

Cover type	Roughness	Area (km*km)	Cover type	Roughness	Area (km*km)
Reject	0.1	0	Vine	0.2	30
Lake	0.001	5	Suburban	0.5	14
Others	0.1	3	Conifer	0.9	0
River	0.001	4	Scatter trees	0.3	24
Decidous	1.2	24	Grain	0.09	21
Orchard	0.1	7	Pasture	0.08	23
Bog	0.03	10	Sunflower	0.18	1
Clearcut	0.004	11	Rootcrop	0.02	6
Industry	0.5	12	Corn	0.12	19
Urban	1	5	Mixforest	1	6

Figure 5.

Rhine Valley, Germany

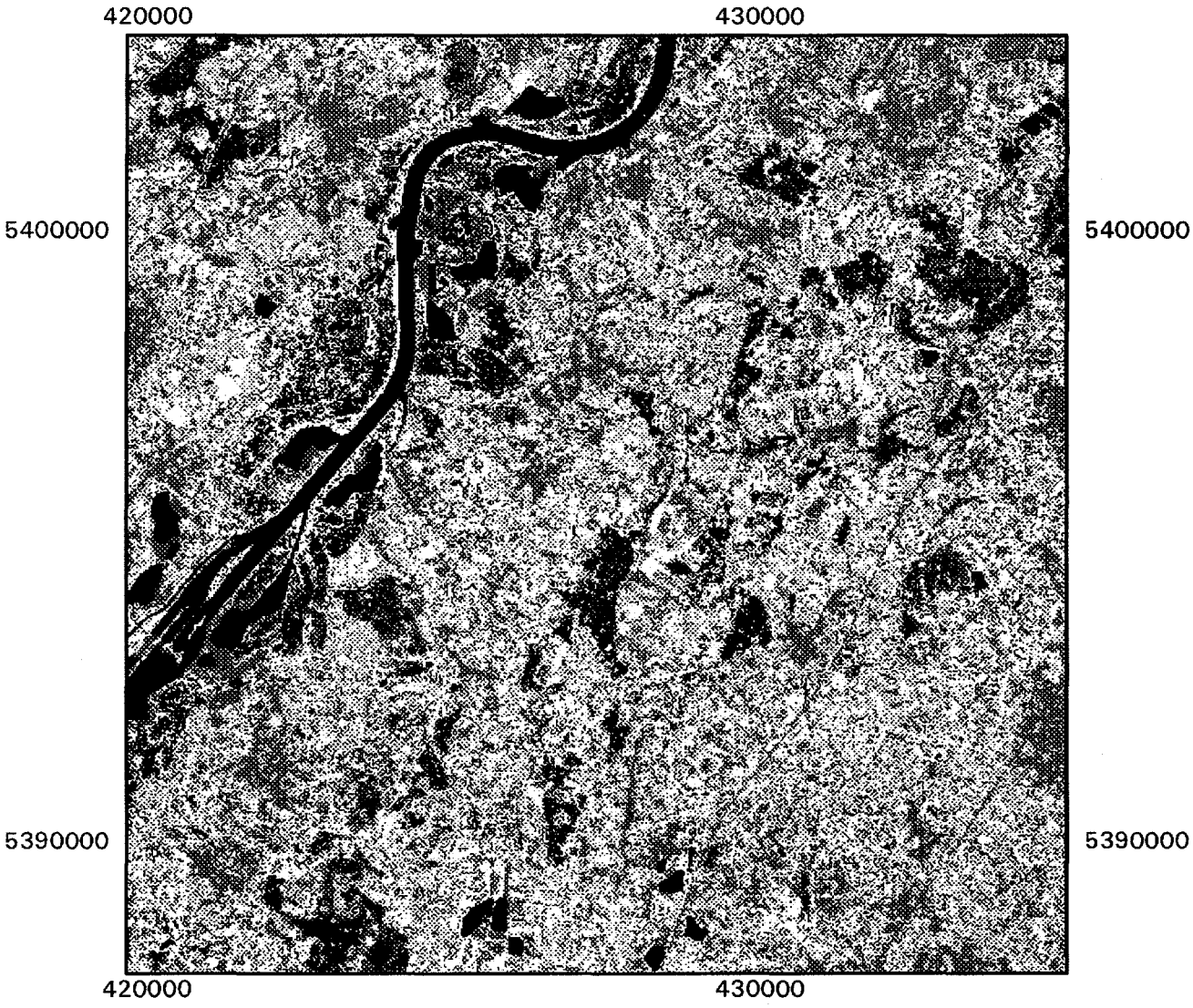

Roughness (m)	Area (km*km)
>= 0.001	26
>0.01	40
>0.1	52
>0.2	52
>0.9	20
= 1.2	24

Scale

2 0 Kilometers

Landsat TM 1993

Figure 6.

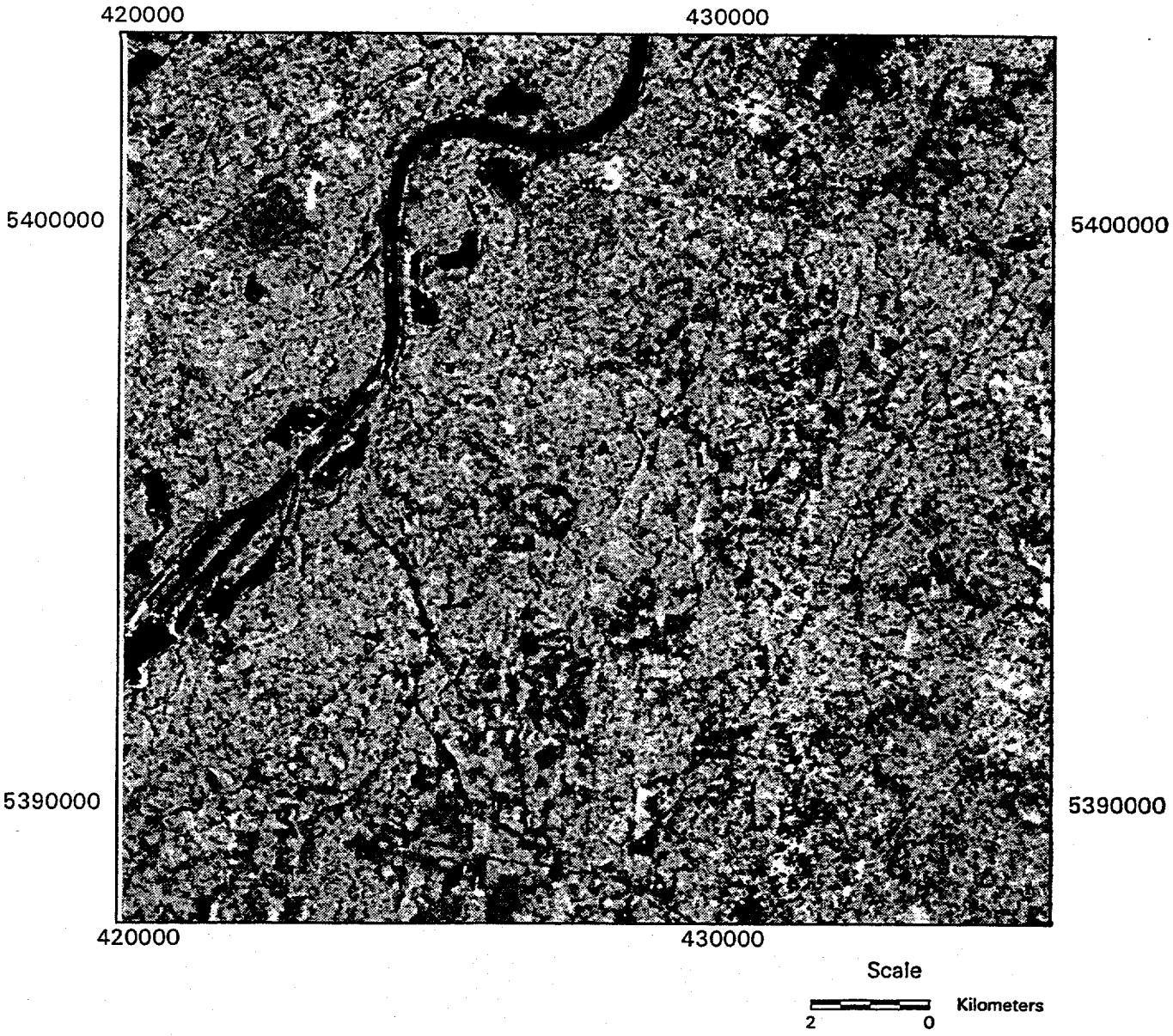

Figure 7. ERS-1 SAR backscatter coefficients in dB.

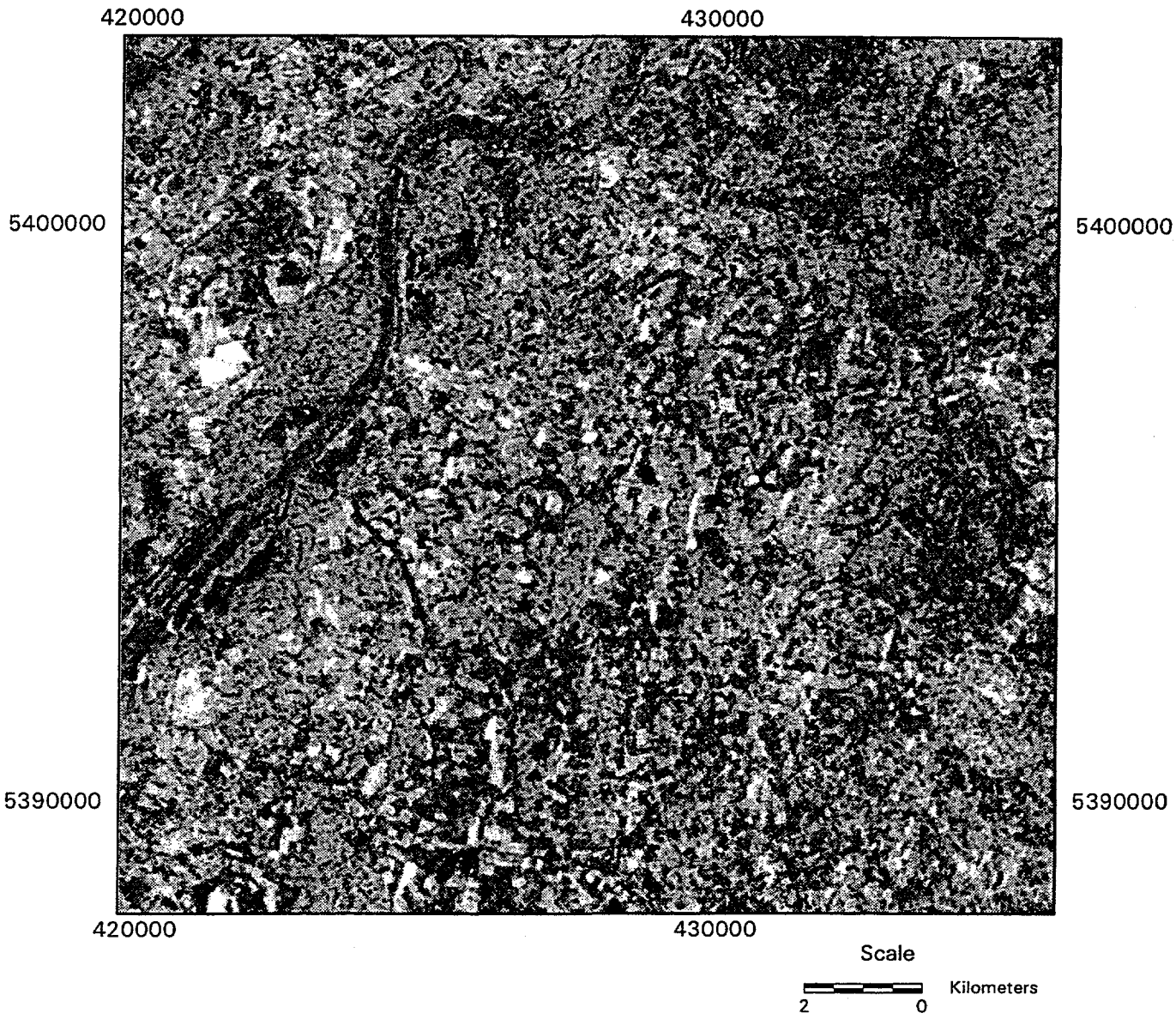

Figure 8. ERS-1 SAR backscatter coefficients in dB.

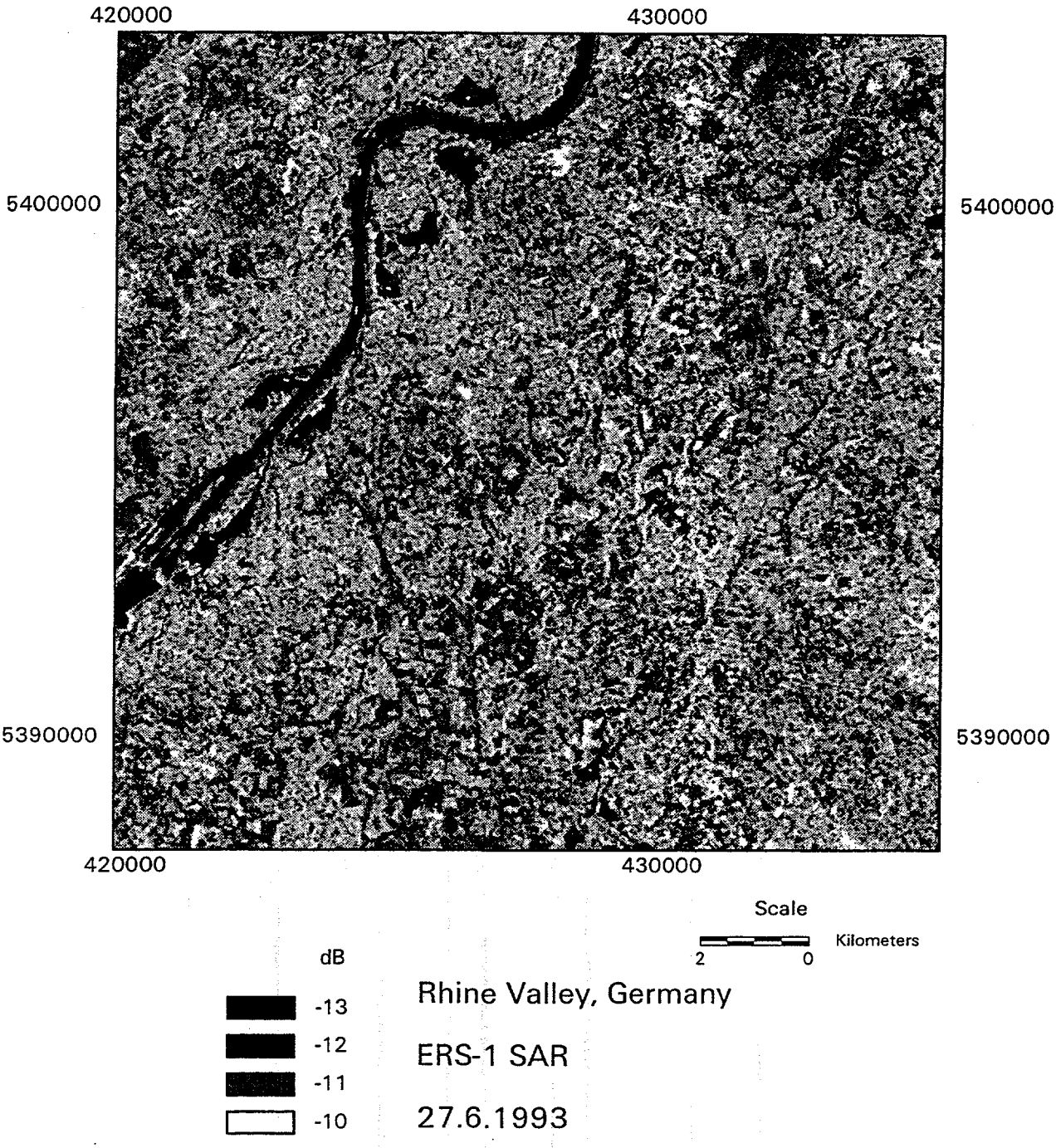

Figure 9. ERS-1 SAR backscatter coefficients in dB.

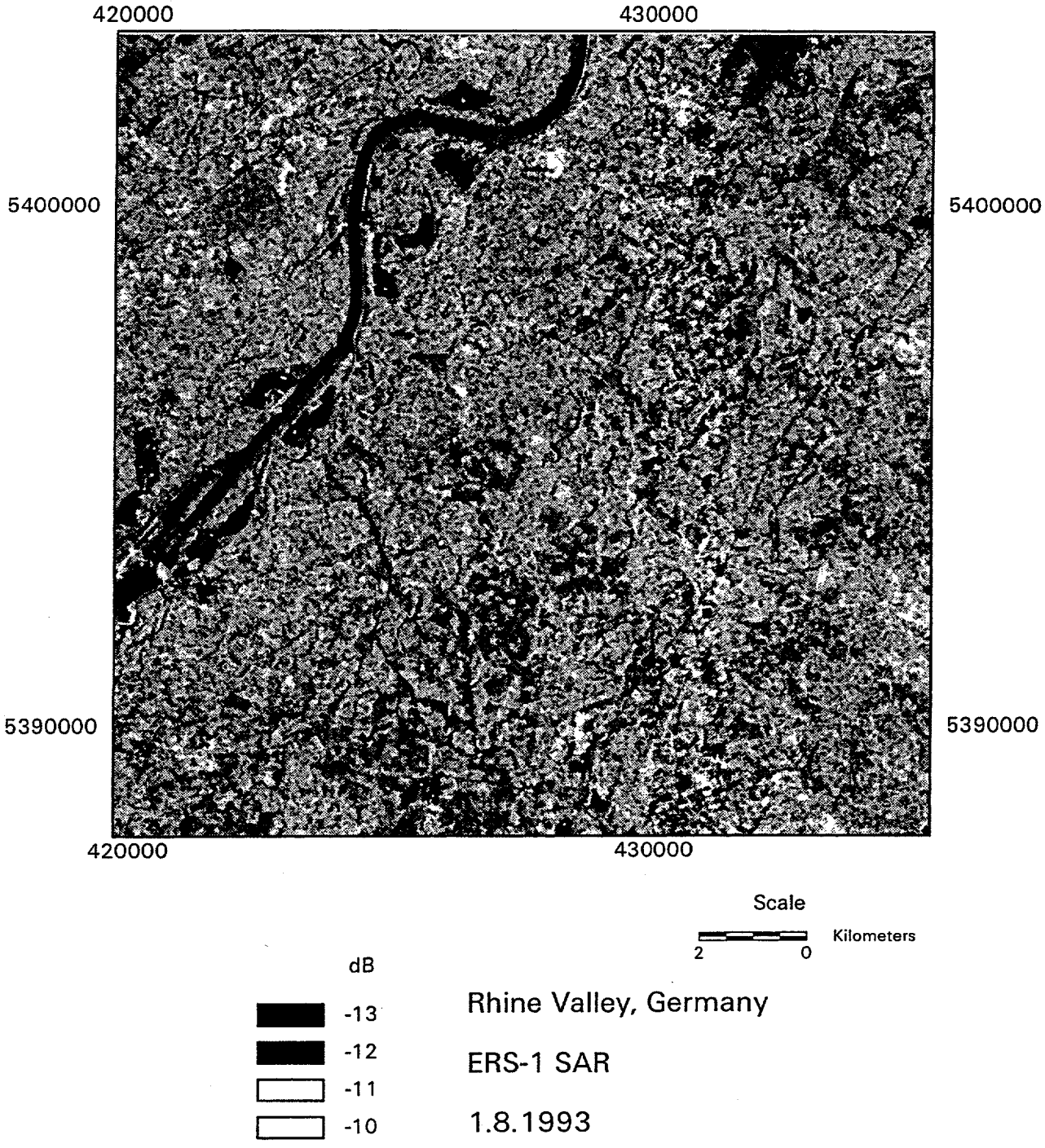

Figure 10. ERS-1 SAR backscatter coefficients in dB.

Satellite	Sensor	Date	Band	pixel (m^2)	orbit
Landsat-5	TM	27.4.93	3,4,5	30*30	195/26
Landsat-5	TM	30.6.93	3,4,5	30*30	
Landsat-5	TM	1.8.93	3,4,5	30*30	
ERS-1	SAR	20.9.92	5.3GHz/VV	25*25	6169
ERS-1	SAR	7.5.93	5.3GHz/VV	25*25	9457
ERS-1	SAR	27.6.93	5.3GHz/VV	25*25	10187
ERS-1	SAR	1.8.93	5.3GHz/VV	25*25	10688

Table 5. Information on the satellite scenes from the Rhine Valley.

The Landsat scenes and the ERS scenes were all recorded at approximately 10.00 am local time. The ERS scene from May was processed at the UK-PAF, the other three at the D-PAF and all were received at Kiruna. PAF is Processing and Archiving Facilities of the European Space Agency in respectively, United Kingdom and Germany.

The SAR scenes from 1993 are presented in figures 8 to 10. They were geometrically corrected image to image and speckle filtered with a Leefilter. No DEM was available. Only data from the valley have been used in the subsequent analysis. Data from the mountains are corrupted by local incidence angle effects. The ERS scenes were analysed in respect to correlations between σ_0, z_0, NDVI and LAI.

Figure 11 shows data of ERS-1 SAR C-band VV σ^0 on four dates along a four km transect through agricultural areas. In the August image, relative small values occurred. In the May image relative large values occurred with a small range. This is visible in figure 8 of May 1993 (a blurred appearance).

Figure 12 shows z_0 from Landsat in 1993 and σ^0 from ERS in September 1992 and August 93. The transect is in the same position as to those in figure 11, 13 and 14. There seems to be no correspondence between the curves of z_0 and σ^0 in figure 12. The area is very heterogeneous. No large homogeneous areas are found along this transect (nor anywhere else in the vegetated areas see figure 5 to 10).

Figure 13 and 14 show NDVI and σ^0 for June and August 1993 respectively. NDVI was calculated from Landsat TM channel 3 and 4 without atmospheric correction as this usually only shifts NDVI slightly. For the present comparison this has no significance. The transects of NDVI and σ^0 do not show any regular correspondence. However the analysis was extended to a pixel-by-pixel analysis in the spatial domain. Plots of z_0, σ^0, NDVI and LAI were produced but all these only confirmed that none of the parameters correlate. All vegetation types were included. The NDVI maps from June and August 1993 of the Rhine Valley are shown in figure 15 and 16.

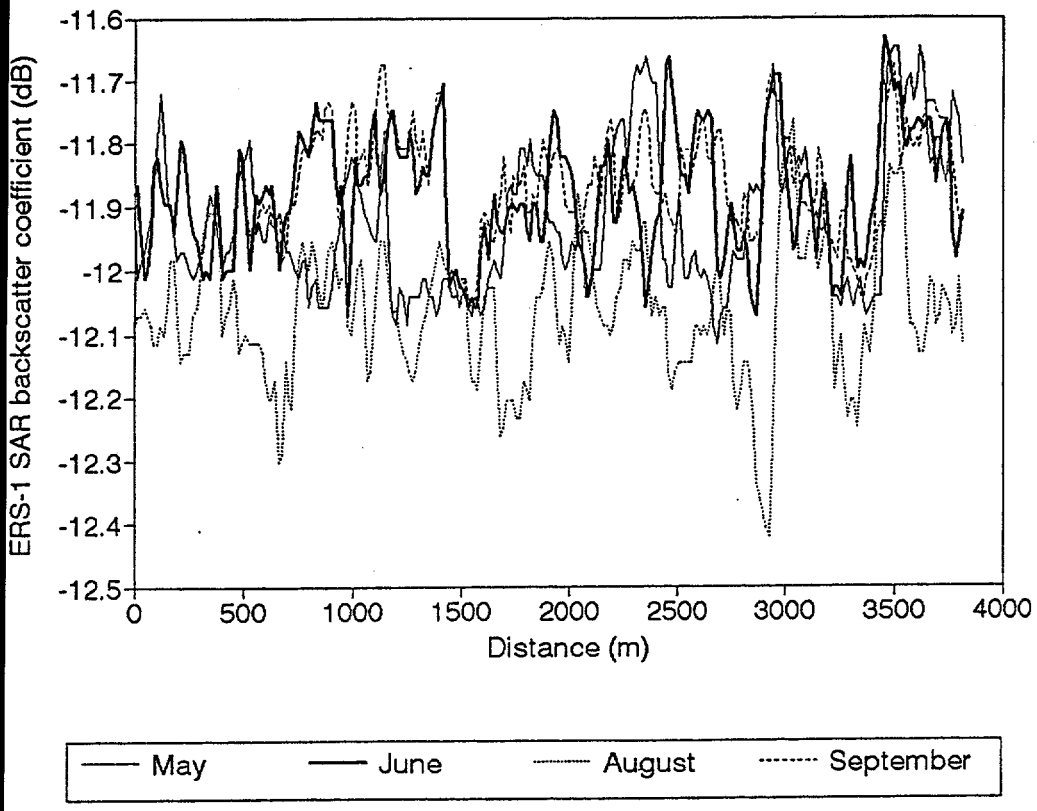

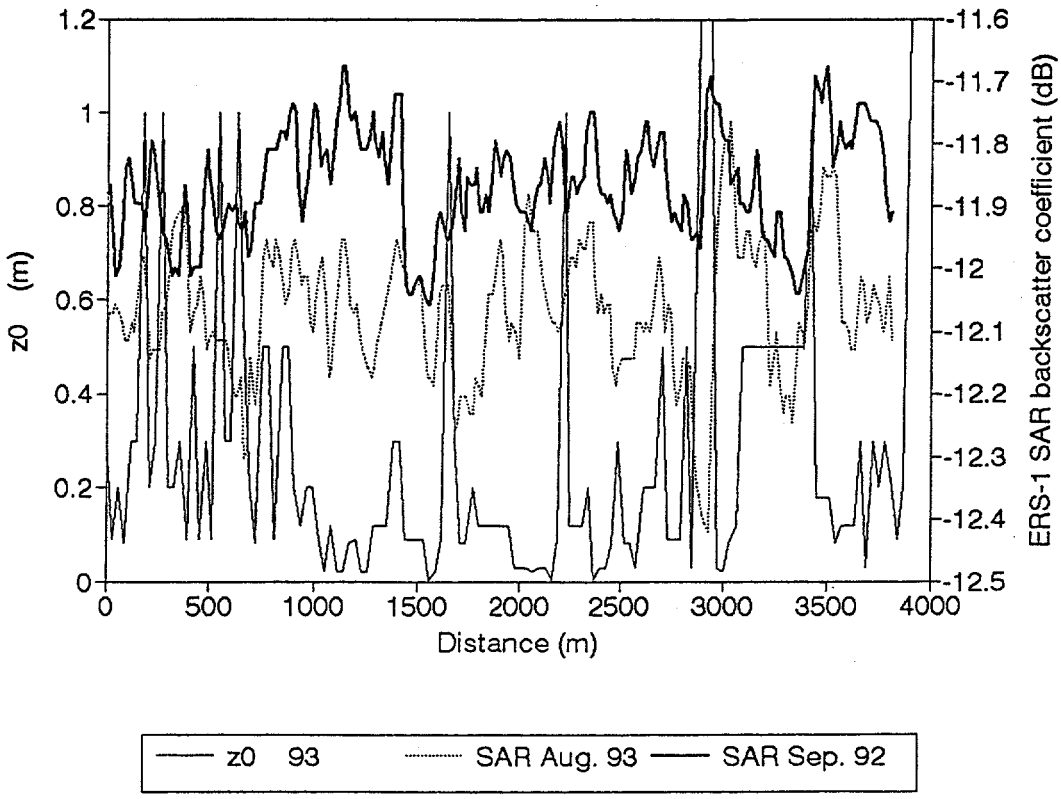

Figure 11 (above). ERS-1 SAR backscatter coefficient from four Lee-filtered scenes in the Rhine Valley, Germany from September 1992 and May, June and August 1993.

Figure 12 (below). As figure 11 but with aerodynamic roughness based on Landsat TM for 1993.

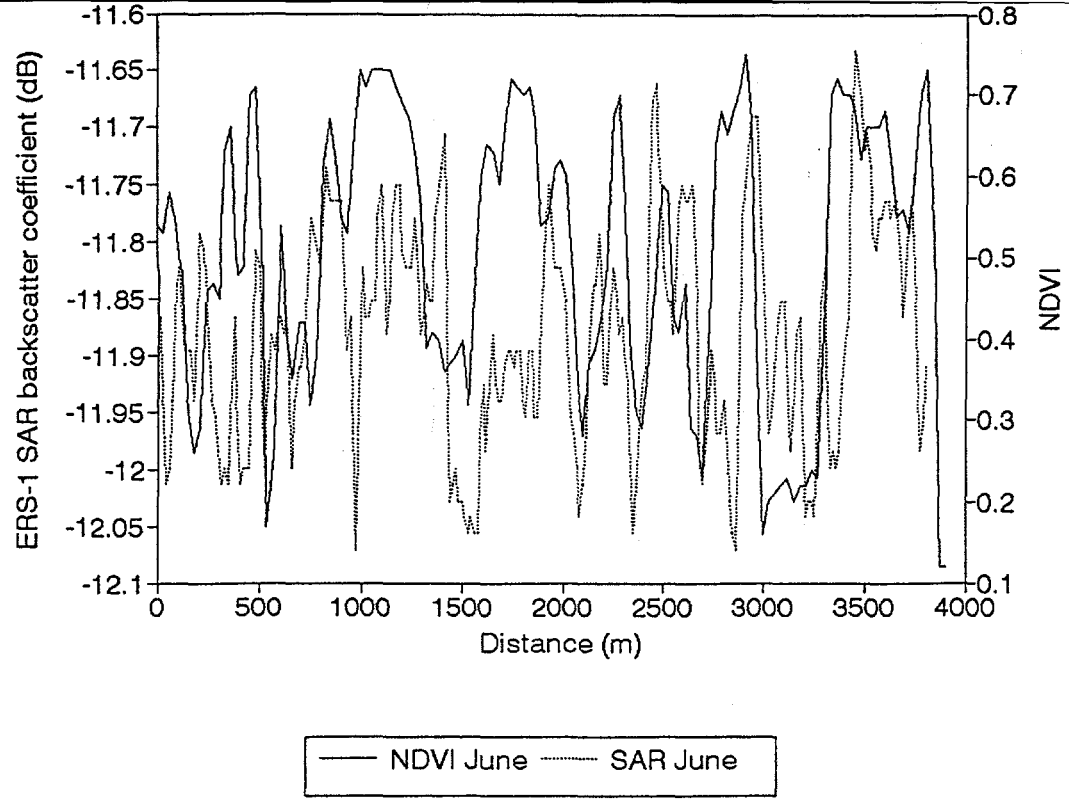

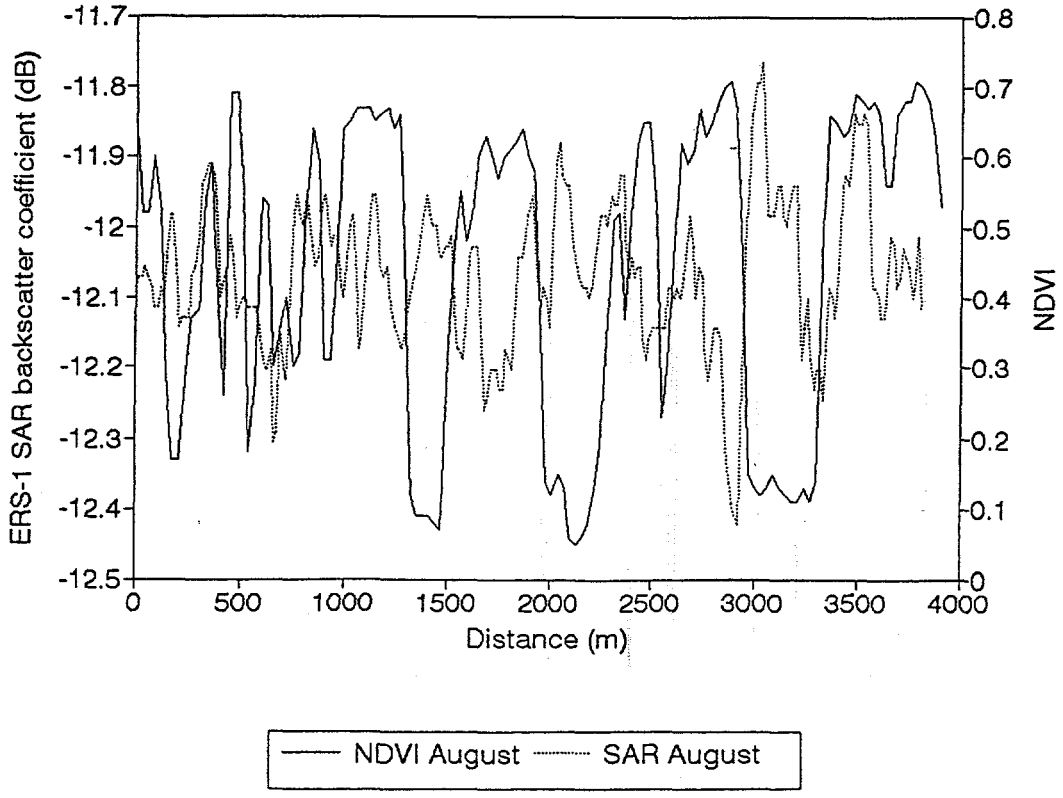

Figure 13 (above). As figure 11 but with Normalized Difference Vegetation Index based on Landsat TM in June 1993.

Figure 14 (below). As figure 11 but with Normalized Difference Vegetation Index based on Landsat TM in August 1993.

Figure 15. Normalized difference vegetation index map.

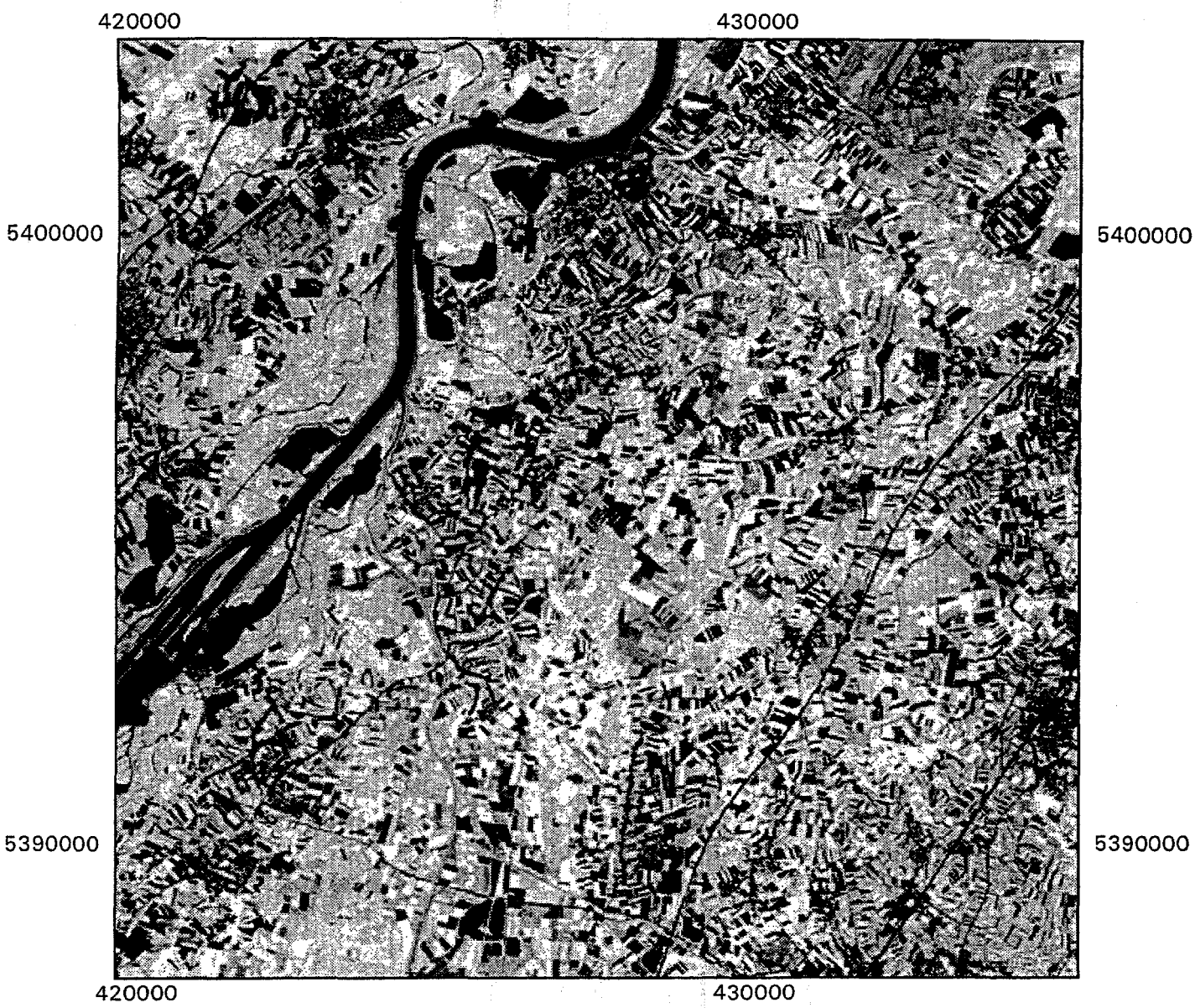

Figure 16. Normalized difference vegetation map.

One explanation to the complete lack of correlation between the parameters is thought to be owing to speckle noise. The scenes were filtered with a Lee filter but this local statistics filter cannot efficiently eliminate speckle noise in highly heterogeneous areas (nor can other filters). A *pixelwise* correlation procedure cannot be recommended. The indication is that a *mean* σ^0 of a considerably number of pixels should be used because the speckle noise is not efficiently removed. Oevelen et al. (1996) also point this out.

Work on large homogeneous areas in the Rhine Valley is not possible because of the small fields. The problems are partly owing to subpixel effects, partly owing to speckle noise that is not efficiently removed. In highly heterogeneous terrain with small fields, the retrieval of bio-geophysical parameters is not to be recommended. The conclusion is that the aerodynamic roughness in relatively large areas to some extent is mapped by SAR (chapter 4), but that the relation cannot be found in the Rhine Valley data set because of the landscape structure of microscale heterogeneity (chapter 6).

Recently a German research group investigated multi-temporal land cover classification based on ERS-1 SAR scenes only. They successfully produced a map of Germany on the basis of 150 scenes from 1992. The final product is the so-called "Radarkarte Deutschland" containing 13 classes (Markwitz et al. 1995). A subset of the "Radarkarte Deutschland" was kindly made available for the current project (in September 1996). Figure 17 shows a subset of the classified scene. The image was assigned appropriate roughness values from Fiedler et al. (1994) in order to obtain a summer and winter roughness map for 1992. These roughness maps were used as input in the flux-aggregation microscale model presented in chapter 7.

Typical patch sizes

Landscapes consist of more or less welldefined patches. Spatial aggregation of surface fluxes is related to the patch size distribution (chapters 5, 6 and 7). The "typical" size of patches may be quantified by the semi-variogram technique (kriging), autocorrelation lag and from Fourier spectra. The extraction of such information does have some relevance to surface flux estimation. Smaller patches induce a larger effective roughness than do larger patches, all things being equal. However from a physical point of view, the parameter information *in* the patches is most import. Schmid and Bünzli (1995) for example calls the "surface texture" (or pattern) for "second-order roughness" in their atmospheric flow modelling work.

The semi-variogram methodology was described by Curran (1987) and applied to (raw) Landsat TM data from an agricultural area in The Netherlands (Vries et al. 1996). In an arid natural ecosystem the typical length scale of vegetation (bushes) was quantified from Fourier spectra analysis of optical airborne data (Hipps and Neale 1996). The mapping of the amount and distribution of the soil and vegetation components allowed the surface heat fluxes to be calculated separately (with a Penman-Monteith approach).

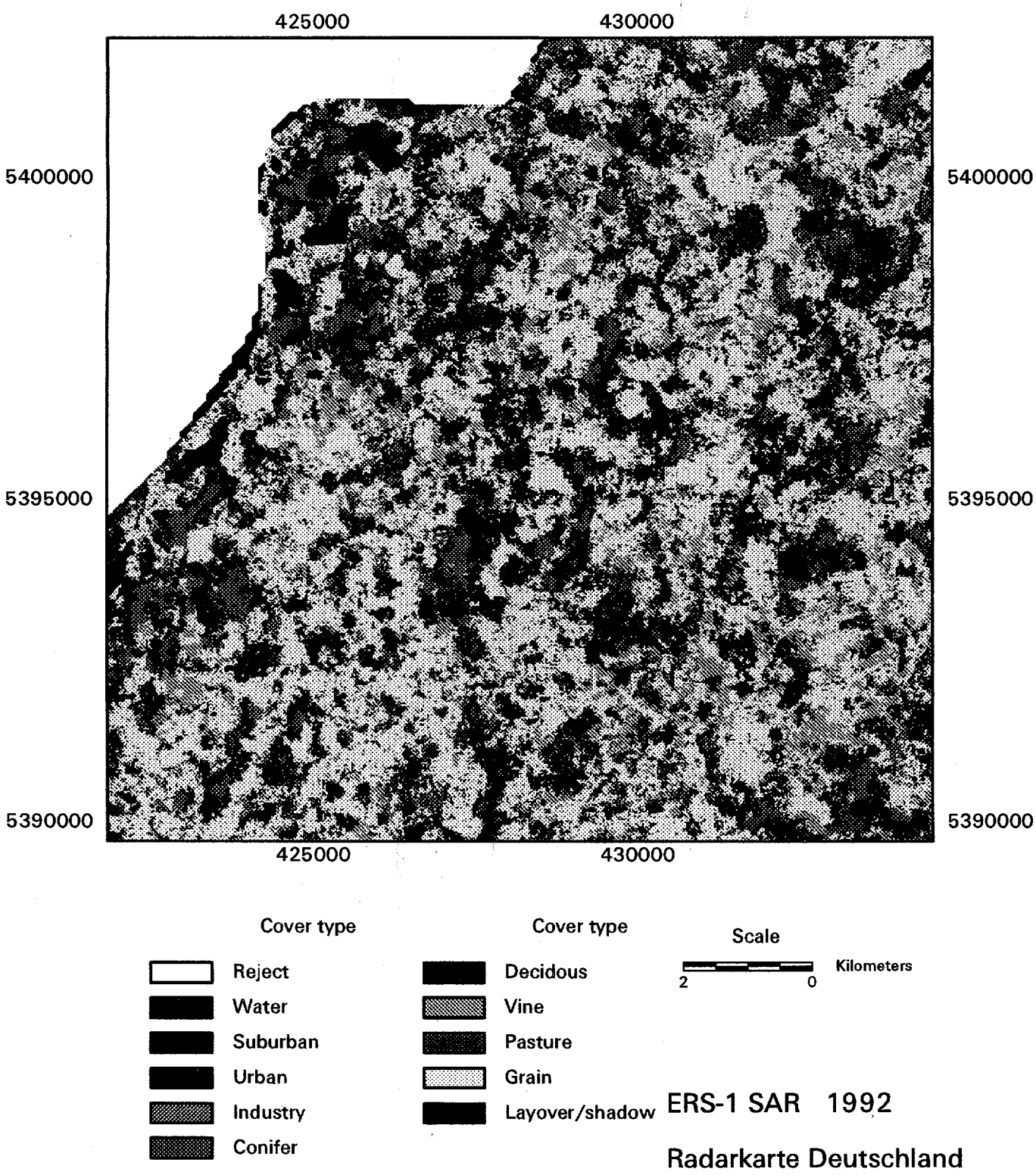

Figure 17. Land cover map.

In the present project the mean horizontal length scales of variation were determined from Fourier spectra of a roughness map and found to be 650 m in figure 6. This information was used to guide test runs on the length scales of interest (section 7.3).

4.6 Laser altimeter

Airborne laser altimeter data have been collected by Ritchie et al. (1993). Using a laser beam with a wavelength of 904 nm the land surface was measured at intervals of the order of 0.0125-0.025 m. The vertical recording accuracy was 0.05 m and the standard deviation typically 0.1 m. Data of this kind maps the physical distribution of vegetation and other landscape features along the flight lines. The laser beam penetrates all the way to the surface even in tall vegetation (eg pine). In very dense vegetation interpolation is necessary to obtain the ground level. Orography is also quantified.

Menenti and Ritchie (1992,1994) have reported in detail how estimation of $<z_0>$ can be performed from the laser altimeter data using an empirical method. The canopy mean height and the horizontal spacing (standard deviation in sections of less than one meter) were used as input. The horizontal and vertical length scales were assumed to be logarithmically dependent. The results are promising.

Results of z_0 from Niger, calculated from SEASAT radar altimeter data have been reported (Menenti and Ritchie 1992, Menenti et al. 1996). Unfortunately it is not clear how the large footprint of SEASAT relates to roughness.

4.7 Mapping soil moisture

Soil moisture retrieval have primarily been investigated from microwave remote sensing. Engman (1995) reports good progress during the last decade at the research level. However operational soil moisture mapping is still not viable.

Various airborne and spaceborne microwave investigations show that passive microwaves map the soil moisture content in the upper soil layer most accurately (Ferrazzoli et al. 1992). Soil moisture retrieval in bare fields is most straightforward. However also with vegetation the soil contribution can be estimated with the help of nonlinear models. The soil contribution then provides the soil moisture (Schmugge and Jackson 1992).

Passive L-band data from HAPEX-SAHEL, FIFE and MONSOON have been used to estimate soil moisture (Schmugge et al. 1992). In 1996 Schmugge and Jackson (1996) concluded the microwave brightness temperature to robustly predict soil moisture in slightly vegetated areas. They validated the relation from several airborne campaigns and numerous soil moisture samplings. In the MONSOON 90 experiment a 850 km^2 region (Little Washita, Oklahoma) was

mapped with a 200 m resolution (Schmugge and Jackson 1996). Unfortunatley satellite footprints of passive microwaves are rather coarse (25 km for SSM/I and 150 km for SMMR Engman (1995)).

Future passive microwave radiometers may have spatial resolutions as high as 5-60 km eg a Multi-frequency Imaging Microwave Radiometer (MIMR) with six frequencies ranging between 6.8 to 90 Ghz with ϕ 50°. This is planned from EOS for after year 2000. Due to the low spatial resolution of passive data intensive research on radar data is going on. Radar data have a much higher spatial resolution.

In basic research multi-band fully polarimetric SAR data are of interest. However satellite SAR are all single band and single co-polarized. Unfortunately such data seem inadequate for robust soil moisture retrieval in stand-alone mode, especially when vegetation is present. A combination of data from ERS and Radarsat seems attractive because models based on C-band VV and HH data combined are more promising (Dubois et al. 1995a,b,c).

Dubois et al. (1995a,b,c) have developed an empirical backscatter model. The input is σ^0 VV and HH from C-band SAR. The soil moisture result is obtained from the dielectric constant retrieved in the image. The empirical relation between the dielectric constant and soil moisture found by Hallikainen et al. (1985) is then used. Dubois et al. (1995c) conclude that a 4% soil moisture accuracy requires 2 dB absolute calibration and 0.5 relative calibration and that such criteria are met by eg SIR C data. Other bands for soil moisture retrievals are investigated and L-band seems to be promising (eg O'Neill et al. 1995, Schmullius 1995, Ji et al. 1995a,b). Some models are rather complex.

Robust high-resolution soil moisture mapping would be a turning-point and useful for many applications. In regard to atmospheric research it would help quantifying the water vapour flux. In the moisture flux equation (eq 30) the surface humidity, q_0, is in units of g H_20 per g air measured at the height of z_{0q} above the physical surface (very close to the physical surface). Soil moisture data on the other hand are in units of percentage water to dry soil weight. The soil moisture estimate from a passive microwave radiometer is the amount of soil water in a $\sim$5 cm near-surface soil slab. Some assumption is necessary in order to relate this soil moisture to q_0 (by inclusion of T_s). A direct calculation of the latent heat flux spatially would be possible in the microscale aggregation scheme (chapter 7).

4.8 Future data

EOS and SPOT platforms mounted with future high-resolution thermal infrared sensors may be used for sensible heat and, as a heat balance residual, evaporation mapping. The new sensors are scheduled to record before noon local time. In many regions cloud cover is less of a problem in the morning than later in the day (NOAA ~ 200 pm). Algorithms similar to the simplified relationship have been developed for T_s measured at 1000 am local time (Lagouarde 1993).

A future sensor is the High-Resolution Interferometer Sounder (HIS) to be mounted on a geostationary platform. This will give a much improved data set of the vertical temperature structure of the lower atmosphere and the surface itself (Diak 1993, Xie 1990 *in* Norman 1993, Diak et al. 1994). The time difference between subsequent images (30 minutes) will make possible surface energy balance estimation without knowledge of the surface itself. To establish (calibrate) the model radiosounding data, surface emissivity and albedo are needed. When run later the model is *not* dependent on these ancillary data (Norman 1993).

In future a precise spatial mapping of the mixed layer height may be obtained from a proposed Laser Atmospheric Sounder and Altimeter (LASA) on board EOS satellites (Engman and Gurney 1991). Such data can be used as input to estimate the sensible heat flux with a high accuracy from PBL models (eg Diak and Stewart 1989). According to Diak (1993) however there is doubt as to whether LASA will come into orbit. Other instruments such as Advanced Infrared Radiometer Sounder (AIRS) or GOES High-Resolution Interferometer Sounder (GHIS) may become operational and able to provide data to estimate the PBL height (Norman 1993, Norman et al 95).

Regarding future data multi-channel optical airborne data (so-called spectroradiometer data) may become available. In Denmark there are initiatives to buy and fly a Compact Airborne Spectrographic Imager (CASI). This system still at a research level, but slowly becoming a tool in environmental surveying in some countries.

4.9 Summary on remote sensing mapping

To improve land surface flux estimation different kinds of remote data are in need because only remote data are truly spatial. The more heterogeneous the landscape, the more urgent spatial data are.

Land surface temperature retrieval in strongly heterogeneous terrain is problematic because of the lack of reliable high-resolution data. At large-scales AVHRR and ATSR provide us good thermal data and even better data may become available from HIS. Thermal data from the Russian satellite, Resurs, are now available and could prove useful.

Soil moisture is very unevenly distributed spatially due to precipitation patterns, drainage conditions and soil types. Drying-out processes can be rapid, especially in the upper soil layer. Therefore frequent moisture maps are desirable. Unfortunately passive microwave data have very large footprints but at the same time are the most robust data in regard to soil moisture mapping.

Much research focuses on soil moisture retrieval from SAR data. ERS, JERS and Radarsat are in orbit and provide us high-resolution data now and in the future according to space agency plans. However soil moisture retrieval algorithms still need a further validation especially for cases of vegetation cover. Soil moisture retrieval from space SAR is at a research level still.

Only to some extent vegetation parameters such as LAI, biomass, fractional coverage, photosynthesis activity level, canopy height and canopy density can be mapped from remote sensors. For aerodynamic roughness mapping an ideal spatial resolution is of the order of five meters because scattered trees, buildings and hedges have a significant impact on the atmospheric flow. Only airborne scanners provide us these very high resolutions.

Much of the current research is based on high-resolution airborne data. If airborne multichannel optical scanners are flown at regular intervals high-resolution roughness maps can be produced. Panchromatic airborne data are well-known for cartographic updating. Airborne laser altimeter data seem very promising. SLAR and polarimetric SAR data are alternatives. However these are far from fully understood in a modelling sense.

Land-cover classification is traditionally based on multi-temporal optical data. Good classification results have been obtained from multi-temporal SAR data scuh as used for the so-called "Radarkarte Deutschland". Knowledge-based hierarchal classification on SAR also seems to be promising at discerning vegetation types but currently do only work for multiband or multipolarization. The future classification trend is most likely data merging of optical and SAR scenes. Improvements of classification accuracy and update rate could provide us a solid basis for roughness maps. This indeed would be useful in surface flux calculation locally, regionally and globally.

Direct retrieval of ocean roughness from satellite SAR data are well-documented. For bare soils and especially for aeolian deposits, linear relations between the aerodynamic roughness and the backscatter coefficients of C- and L-band co- and cross-polarized data have been demonstrated by Greeley et al.

(1995a) with a remarkable succes. The physical reason for the high log-log-linearity is speculated to relate to a slightly modified form of the Charnock equation.

Direct retrieval of aerodynamic roughness from SAR in grains have not shown such promising results. Inverse backscatter modelling is complicated because of the nature of SAR signal interactions with leaves, heads, stalks, soil and moisture. Analysing SAR data with a pixel-by-pixel approach is not feasible. A large number of pixels in a homogeneous area are needed to investige bio-geophysical relations. Based on the analysis of airborne SAR data from Foulum and the ERS-1 SAR scenes from the Rhine Valley it cannot be concluded whether the roughness in grains is directly related to the backscatter coefficients. Both data sets are too limited.

Future remote sensors will provide us with even more data types. Two of them are relevant for large-scale flux estimation. The first interest is mapping of the thermal structure of the surface *and* the lowest part of the atmosphere from a geostationary platform. The other is mapping of the diurnal PBL height. PBL heat flux budget methods may then gain some attention. Let us consider a conclusive remark from Shuttleworth (1991a)

"Could it be that enhanced remote sensing of atmospheric structure is almost as valuable to the proposed Earth Observation System as remote sensing land surface characteristics ?".

This may be true in regard to large-scale surface heat flux estimation. However highly nonlinear effects caused by local- and regional scale land surface heterogeneity are significant for microscale and mesoscale flux retrieval. Therefore the statement is only valid for homogeneous large-scale modelling.

5 Heterogeneous terrain

Homogeneous means that in a statistic sense a variable is the same at each point in space (section 2.1). It is obvious that the homogeneity assumption is not fulfilled in some landscapes. A typical land surface is heterogeneous. It can consist of patches (tiles) with differences in soil, vegetation, buildings, moisture, snow and ice. Orography may add to the complexity.

A definition of heterogeneity (Pocket Webster Dictionary 1990) is

"The word heterogeneous originating from Greek heter (more) and genos (kind) is an adjective with the meaning "opposite or dissimilar in character, quality, structure, etc.", "consisting of miscellaneous parts"".

How many is "more"? Just *one* more than the first kind makes two kinds. Then a landscape can be described as heterogeneous with only two kinds and one discontinuity between them. It is common though in atmospheric science to call it a step change or an inhomogeneity. With repeated discontinuities between two kinds a pattern develops. The pattern is characterized by shape, size and fractional coverage. Based on the typical patch size (horizontal length scale of variation) five groups of heterogeneous terrain are described.

Terrain with patches of the order of 10-100 m is called "finely grained system" (Dickenson 1995) or "mosaic" (Koster and Suarez 1992). It is assumed that homogeneity assumptions are valid for these heterogeneous surfaces above a shallow height, namely above the roughness sublayer (Oke 1987). Similarity scaling methods are appropriate.

Terrain with patches of the order of 100-1000 m is called "microscale" (Raupach 1993), "more coarsely grained system" (Dickenson 1995), "mixture" (Koster and Suarez 1992) and "disordered" heterogeneity ("type A") (Shuttleworth 1988). The assumption is that each patch interacts with the atmosphere up to a certain level in the PBL. Local advection between the patches is large and adds considerably to the total grid flux. It has been suggested to calculate effective roughness lengths by averaging the drag coefficients at the blending height (Wieringa 1986, Mason 1988).

Terrain with patches of the order of 1-10 km is partly covered by the microscale blending height description, partly covered by high-resolution mesoscale models (eg KArlsruhe Atmospheric Mesoscale Model (KAMM) with a grid size of 5 km * 5 km (Adrian and Fiedler 1991)). Flow over patches of this length scale has so far gained relatively less attention than flow over other terrain groups. The prognostic microscale flow model developed by Jensen (1995) bridges the gap. It is described in detail in chapter 7.

Terrain with patches of the order of 10-100 km is called "mesoscale" (Raupach 1993), "yet coarser scale" (Dickenson 1995) and "ordered" heterogeneity ("type B") (Shuttleworth 1988). Here the individual patch interacts so strongly with the atmosphere that the whole PBL is affected. It is assumed that the internal

boundary layer height equals the PBL height before a new discontinuity is encountered. Hence the upper boundary conditions are important. Mesoscale processes related with such large patches are likely to occur. Shuttleworth (1991b) concludes that surface fluxes have to be obtained from mesoscale models. High-resolution mesoscale models probably are the best tool for obtaining grid-averaged surface fluxes. However the lower boundary conditions in the mesoscale models are simple and physically unrealistic because of lack of data and the aggregation methods applied.

Terrain with patches of the order of > 100 km is called "large-scale" heterogeneity by Raupach (1993). In such terrain the advection between the patches is negligible in regard to mean grid values. The patches can be seen as energetically independent. The convective boundary layer is fully developed (since dawn). So the homogeneous assumptions are fully valid, similarity scaling and 1D-SVAT models are describing the vertical processes well. Simple area weighted averages of surface fluxes yield correct results. The large-scale patch size corresponds to the resolution of GCMs. However since extensive regions of the globe cannot be described by such large patches, GCM results may be biased owing to unrealistic surface boundary conditions among other things.

Band (1991) points out that in certain cases sophisticated 1D models may be less reliable than simple 2D-models. This will especially be true when advection effects from one patch to the other are not negligible. Also whenever the co-occurrence of various patch types are important for the aggregation, 1D-models may show a less reliable performance. If not done carefully scaling between raster information from various scale levels can cause significant biased error. Therefore the appropriate scale for a specific problem must be specified in order to optimize computation demands and to avoid scaling errors.

Scaling is the process of considering how parameters and algorithms have to be modified to be valid from a point in space to a spatial scale. Sometimes the word upscaling is used to emphasize this kind of scaling as opposed to downscaling. Downscaling describes the process of distributing a grid mean non-evenly to an area. One example is the modelling of a convective precipitation distribution.

Aggregated (upscaled) values often are called *effective* values to separate them from local balance values (Wieringa 1986, Shuttleworth 1988, Claussen 1990, Mason 1988, Blyth et al. 1993, Lhomme et al. 1994, Mahrt and Sun 1995). In the present work spatial (effective) mean values are given in brackets: $<z_0>$ is the spatial mean as opposed to z_0 a local (patch) roughness (section 6.3).

5.1 Surface flux estimation in heterogeneous terrain

Estimation of surface fluxes from a conglomerate of dissimilar patches is not straightforward. Simple cases have been investigated. The changes in surface fluxes have been studied when the turbulent flow passes from one infinite patch type to another infinite patch type with just one variable changing abruptly (T_s,

z_0 or q_0) (Kaimal & Finnigan 1994). Such cases are described as cases with an inhomogeneity.

Slightly more realistically we can picture a heterogeneous terrain as follows. Let us assume that the terrain is flat and consists of a number of different patches. Each patch is distinctive from one another by abrupt changes between all of them. Let us assume that the local balance surface flux from each individual surface type of the patches is known as well as the areal extent of each patch type in the given landscape. Finally let us assume that the patches do *not* interact with each other. Such a case has been investigated by Seth et al. (1994).

In the study by Seth et al. (1994) a vectorized version of the Biosphere-Atmosphere Transfer Scheme (BATS) with a grid size of 3.0° (latitude, longitude) was split into 36 subgrid patches (each patch approx. 50km*50 km) (Rowntree 1991). The method has not been used with satellite information as surface boundary conditions. Yet it would be possible because the patches are distributed explicitly even allowing for orography.

The local (subgrid) air temperature, T_{ai}, is parametrized as

$$T_{ai} = <T_a> + w_{temp}(T_{si} - <T_s>) \tag{67}$$

The spatial (grid) mean air temperature $<T_a>$ equals the sum of area-weighted local air temperatures, T_{ai}. Likewise the grid surface temperature, $<T_s>$, equals the area-weighted sum of T_{si}. In this way it is assumed that T_{ai} is a linear function of the model simulated local surface temperature. w_{temp} (-) is a weighting coefficient

Furthermore Seth et al. (1994) assume that local air specific humidity, q_i, relates to the model simulated local surface soil moisture content, W_i (%, g H_2O g^{-1} dry soil volume) as

$$q_i = <q>\left(1 + w_q \frac{W_i - <W>}{<W>}\right) \tag{68}$$

Here $<q>$ is the area-weighted mean of q_i and $<W>$ is the area-weighted mean of W_i. The moisture weighting coefficient, w_q (-), was assigned to a value of 0.25 and w_{temp} to a value of 0.8.

The model results rely on the weighting coefficients. The ones chosen were assumed to be valid for a constant wind of 3 m s^{-1}. The nonlinear dynamics between z_0, z_{0t}, z_{0q}, u and $\psi(z/L)$ are neglected. This is likely to cause bias in terrain with microscale patches.

The conclusion of the analysis by Seth et al. (1994) is that the effect of subgrid heterogeneity is significant. The area-weighted means of H and E deviated ~20 W/m^2 (20-30%) and momentum 140 N m^{-2} (68%) from assuming a *homogeneous (dominant)* ground cover. The results are mentioned as an order-of-magnitude example.

In BATS the individual patches are not regrouped into larger patches as in the

mosaic approach (Avissar 1991, Koster & Suarez 1992). However no horizontal dynamics are considered, ie neglecting advective effects. The underlying assumption of the 50 km * 50 km scale homogeneity is unrealistic in many areas of the world.

5.2 Aggregation of flux parameters

In a heterogeneous landscape the statistics (mean, variance, etc.) of parameters vary with the spatial scale. Ideally these variations should be quantified. It would help asserting the degree of scale dependency, ie how much a spatial mean vary as a function of area.

Scale invariance simply means that the area-average does not vary with the spatial scale over which the averaging takes place. With a notation partly from Hall et al. (1992) the area averaging can be expressed as follows:

R is an element (eg a mesoscale resolution element) that can be decomposed into n homogeneous patches numbered from i=1,2,..,n. Each patch consists of a multivariate parameter set eg $\{T_a, T_s, z_0, z_{0t}, L, \epsilon, u\}_i$. The parameter set is notified $\{p_j\}_i$. Hence there are j local patch values relevant to each patch.

Values from the *i*th patch are related as a function of the local parameter set $f(p_j)_i)$. When the true value from the mesoscale element is F_R, then f is scale invariant only in case

$$F_R = f(\Pi_{Rj}) \tag{69}$$

Π_{Rj} is a set of (effective) mesoscale parameters characterizing R.

Let w_i represent the area of patch i relative to the area of R, then F_R, the true mesoscale value, is related to the area-weighted sum of patch level values as:

$$F_R = f(\Pi_{Rj}) = \sum_{i=1}^{n} w_i f(p_j)_i) = f(\sum_{i=1}^{n} w_i (p_j)_i) \tag{70}$$

Two conditions must hold to fulfil eq 70.

Condition 1: *f* is linear
Condition 2: Π_{Rj} is the simple area-weighted average of the patch level parameters.

Only when the two conditions are both fulfilled, the value of the function or parameter is scale invariant.

A good example of a nonlinear parameter function of local patch values, is the conversion from radiant exitance to the radiant surface temperature (eq 54). Subgrid surface temperature variations affect the grid mean. To quantify how much T_s deviates from $(T_s^4)^{1/4}$ a Taylor expansion of eq 55 is performed.

A Taylor expansion with

$$f(x) = f(\bar{x}) + f(x-\bar{x})f'(\bar{x}) + \tfrac{1}{2}(x-\bar{x})^2 f''(\bar{x}) + \ldots. \quad (71)$$

and the mean and variance

$$\textit{Mean} \quad \overline{f(x)} = f(\bar{x}) + \tfrac{1}{2}\,\sigma^2 f''(\bar{x})$$

$$\textit{Variance} \quad \sigma^2 = \overline{(x-\bar{x})^2} \quad (72)$$

Applying a Taylor expansion on T_s in eq 55

$$f(T_s) = T_s^4$$

$$f(T_s)'' = 12T_s^2 \quad (73)$$

we obtain

$$\overline{T_s^4} = \overline{T}_s^4 + \tfrac{1}{2}\,\sigma_T^2\,12\,\overline{T}_s^2 = \overline{T}_s^4\left(1+6\frac{\sigma_T^2}{\overline{T}_s^2}\right) \quad (74)$$

and

$$(\overline{T_s^4})^{1/4} = \overline{T}_s\left(1+6\frac{\sigma_T^2}{\overline{T}_s^2}\right)^{1/4} \approx \overline{T}_s\left(1+\frac{6}{4}\frac{\sigma_T^2}{\overline{T}_s^2}\right) \quad (75)$$

where the variance of T_s is

$$\sigma_T^2 = \overline{(T_s-\overline{T}_s)^2} \quad (76)$$

and then finally that

$$\frac{(\overline{T_s^4})^{1/4}-\overline{T}_s}{\overline{T}_s} = \frac{3}{2}\frac{\sigma_T^2}{\overline{T}_s^2} \quad (77)$$

This result shows that the variance in T_s affects the mean $\overline{T}_s$. Please note that averaging in time and space are mathematically identical. Some findings based on remote sensing data are reported in the following.

Hall et al. (1992) investigated how temperatures at a prairie site in Kansas (FIFE) were influenced by the calibration procedure on T_s for Landsat TM (channel 6).

First the values of T_s per pixel were aggregated into a simple area weighted average value of T_s for a 1 km^2 area ($n \sim 69$). Next radiant exitance was aggregated into the 1 km^2 area and then converted into T_s. The conversion function from Markham and Barker (1985,1987) was applied. The case study

result yielded a difference of 0.25-0.5 K. The Kansas prairie site basically was described as homogeneous and therefore chosen for the FIFE experiment (Strebel et al. 1991). Hence heterogeneous effects are likely to be insignificant.

A similar study by Kustas et al. (1991) showed differences up to 8 K from Arizona (MONSOON 90). The difference depends on the absolute temperature as well as the contrasts (the variance). Emissivity was assumed spatially constant.

Based on theory and data it is concluded that upscaling T_s have to be done with care because condition 1 in eq 70 is not fulfilled.

When condition 2 in eq 70 is not fulfilled then the general case is that

$$F_R = \sum_{i=1}^{n} w_i f(\sum_{i=1}^{n} (p_j)_i) \tag{78}$$

This implies that when the value of patch i is calculated, not only the j *local* variables from patch i has to be taken into account but also the local j variables from other patches.

A classic example of such nonlinearity is the (u $\partial u/\partial z$) term (advective term) in the Navier-Stokes equation.

Spatial averaging is mathematically identical to time averaging of variables split into mean and turbulent parts (Reynolds decomposition). For time averaging $x=\bar{x}+x'$ and $y=\bar{y}+y'$. For the average of a product of x and y (Stull 1991) we can write

$$\overline{xy} = \overline{(\bar{x}+x')(\bar{y}+y')} = \bar{x}\,\bar{y}+\overline{x'y'} \tag{79}$$

The mean of each of the perturbation parts, x' and y', equals zero by definition. The mean of the product of x' and y' is

$$\overline{x'y'} = cov(x,y) = \rho_{corr}\sigma_x\sigma_y \tag{80}$$

ρ_{corr} is the correlation coefficient and σ_x and σ_y the standard deviations of x and y.

When spatial averages have to be calculated, it is therefore of interest to evaluate the covariance (or autocovariance) of parameters. The autocovariance is for a product as

$$\overline{xx} = \bar{x}^2 + \overline{x'^2} \tag{81}$$

5.3 Scale variance of surface flux algorithms

Some examples of surface flux scaling studies are reported. First is a weighting factor approach described (Hall et al. 1992, Lhomme et al. 1994). Secondly the covariance analysis by McAneney and Lagouarde (1994) is described.

Quantification of the scale variance of QH_d and QE_d was reported by Hall et al. (1992). QH_d was estimated at a prairie site in Kansas (FIFE) from a Landsat TM image. First it was done with a pixelwise calculation of QH_d summed into a spatial mean. Next it was done by area averaging the parameters entering the remote sensing flux algorithm followed by calculation of QH_d from *effective* parameters. The two results showed a very small difference. The flux algorithm was more physically based than is the simplified relation. The aerodynamic resistance (eq 31) was parametrized to include effects of roughness, wind and stability.

Hall et al. (1992) also calculated QE_d from the Landsat TM image. The method used assumed saturated humidity in the canopy at the remotely sensed temperatures and a conductance between canopy and air (QE_d was not a residual term). The difference test on QE_d was done by use of the Simple Biosphere model (SiB) by Sellers et al. (1992), a detailed SVAT model. The two results of QE_d showed only a minor difference namely 10 W m^{-2} at the peak near 550 W m^{-2} between 30 m to 1 km scales.

As stated previously, the Kansas site was rather homogeneous hence aggregation effects are expected to be small. Nevertheless Hall et al. found NDVI (eq 56) to be very scale-dependent in the area.

Seguin et al. (1994) used AVHRR and Meteosat temperatures for evaporation prediction by use of the simplified relationship (eq 45). Their large-scale results compared reasonably with ground based values. This lead them to the conclusion that microscale surface heterogeneity is only causing a problem for surface flux prediction at scales < 10 km and not at larger scales. Their data were from France, Senegal and the Sahel. In a way the argument then is that nonlinearity cancel out at a large enough length scale.

The weighting factor approach was elaborated by Lhomme et al. (1994) who consider upscaling through weighting factors

"an easier way of predicting surface fluxes over large heterogeneous terrain (than reformulating the physics)".

Lhomme et al. (1994) used basically the same approach as Seth et al.(1994). However Lhomme et al. compared the flux results to a simple area average instead of the flux from the dominant cover type. Both studies are sensitivity studies.

Lhomme et al. (1994) based their analysis on eq 70 with a modification to it. They suggested to multiply w_i with a fitted coefficient (found from a matching analysis between local and mesoscale values of various parameters). The equations

$$f(\Pi_{Rj}) = \sum_{i=1}^{n} c_i w_i f(p_j)_i) \tag{82}$$

and

$$\Pi_{Rj} = \frac{\sum_{i=1}^{n} c_i w_i f((p_j)_i)}{\sum_{i=1}^{n} c_i w_i} \tag{83}$$

were suggested. c_i is a local (subgrid) coefficient. For simple area averaging the coefficient is 1.

In order to derive appropriate weighting coefficients Lhomme et al. (1994) considered the resistance equations for surface heat transfer (eqs 29 and 30) as well as a Penman-Monteith formulation. The latter linearized in respect to the saturated vapour pressure curve but this usually causes only a minor error (Milly 1991).

The controlling surface parameters like albedo, ϵ, T_s^4, QG_d, r_h, and r_q were derived on patch level and on mesoscale level. Then the weighting coefficients were obtained by matching the local balance equations to effective values. The resistance laws and the Penman-Monteith equation yielded different results. It turned out that the weighting coefficients are dependent on r_h, r_q and T_s but in rather different ways.

A disquieting result was that the surface energy balance is not closed if QH_d, QE_d and QH_d+QE_d were calculated separately by either method. The methods are not compatible amongst themselves! This problem most likely is caused by too crude a parametrization of nonlinearity in the surface processes. Assuming the simple area average as the 'truth' implies equilibrium flow to exist. That is debatable in heterogeneous landscape (chapter 6). Lhomme et al. (1994) suggest to evaluate one of the fluxes and close the energy balance as the residual (a flux conservation approach). This is not comforting since the energy balance is a scanty control of the heat terms.

Yet another study on scaling the heat fluxes was based on high-resolution airborne data from southwestern France in HAPEX-MOBILHY (see Goutorbe and Tarrieu (1991)) by McAneney & Lagouarde (1994). The study was based on a modified form of the simplified relationship

$$QH_d = (c_{10}+c_{11}z_0)(0.31+\bar{u})\Delta T \tag{84}$$

where QH_d is in mm, $\bar{u}$ is the streamwise mean daytime wind and ΔT (K) is the difference of T_s at 1400 hours and T_a maximum. The constants are c_{10} (kg s^{-2} m^{-1} K^{-1} (0.046)) and c_{11} (kg s^{-2} m^{-2} K^{-1} (1.791)).

Equation 84 was expanded and the covariance terms evaluated separately. Third moments were neglected. The complete expanded equation then was

$$
\begin{aligned}
\langle QH \rangle = {} & (c_{10}+c_{11}\langle z_0 \rangle)(0.31+\langle \bar{u} \rangle)\langle \Delta T \rangle \\
& +c_{10}(0.31+\langle \bar{u} \rangle)cov(z_0,\Delta T) \\
& +c_{11}\langle \Delta T \rangle cov(z_0,\bar{u}) \\
& +(c_{10}+c_{10}\langle z_0 \rangle)cov(\bar{u},\Delta T)
\end{aligned}
\tag{85}
$$

Note that the first term on the right hand side is identical to eq 84 except that the bracketed values are spatial means not patch level values as in eq 84. The second term of eq 85 was rewritten as

$$c_{11}(0.31+\langle \bar{u} \rangle)\rho_1 \sigma_{z_0} \sigma_{\Delta T} \tag{86}$$

the third term as

$$c_{11}\langle \Delta T \rangle \rho_2 \sigma_{z_0} \sigma_{\bar{u}} \tag{87}$$

and the last term as

$$(c_{10}+c_{11}\langle z_0 \rangle)\rho_3 \sigma_{\Delta T}\ \sigma_{\bar{u}} \tag{88}$$

ρ is the correlation coefficient and σ is the standard deviation. ρ and σ could not be evaluated directly as only T_s was measured. Based on estimates it was concluded that all three terms were an order of magnitude less than $\langle QH_d \rangle$ and hence could be neglected (McAneney and Lagouarde 1994). It was noted that for $\Delta T \sim 0$ (a typical situation in conifer forest) eq 84 is not applicable. Supposing a situation with transpiring forest interspersed with dry agricultural areas then z_0 and T_s would correlate (negatively) and eq 86 introduce error.

Most of the many studies on improvements to the simplified relation (sections 3.1-3.4) were based on assumptions of homogeneity. The covariance approach by McAneney and Lagouarde (1994) is interesting as spatial surface variability is considered explicitely. The empirical relation (eq 84) is a fitted function on the full sensible heat flux equation. The function may fit within limits but ideally it should behave correctly in the limits too. Otherwise a further mathematical analysis is not feasible.

To estimate the possible validity of the fitted form the first part of eq 84 is rewritten as

$$c_{12}=(c_{10}+c_{11}z_0)(0.31+\bar{u}) \tag{89}$$

Then from similarity theory c_{12} may be expressed as

$$c_{12}=\frac{\rho c_p \kappa u_*}{\ln(\frac{z}{z_{0t}})+\psi(\frac{z}{L})} \tag{90}$$

In free convection $\Psi(z/L)$ goes to $\ln(-z/L)+0.7$ (Jensen pers. comm.) and hence c_{10} approach $(\rho_a c_p \kappa u_*)/(\ln(-L/z_{0t})-0.7)$. However to fulfil this $z_0 \propto \ln(-L/z_{0t})$. This does not seem physical. In free convection $\bar{u} \sim 0$ so the value 0.31 in eq

84 gains importance. At neutral stability c_{12} should approximate to $(\rho_a c_p \kappa)/(\ln(z/z_0)$ meaning that $z_0 \propto z/1.5(0.046+1.791z_0)$. Finally it can be seen that for a large $\bar{u}$ then $(c_{10}+c_{11}z_0) \propto \kappa/(\ln(z/z_0)$. The above conditions are not generally met.

The approach of evaluating spatial covariance terms as suggested by McAneney and Lagouarde (1994) does provide insight into aggregation procedures. However a comprehensive analysis would demand the statistical properties related to spatial field data of T_s, z_0, $\bar{u}$ and $\Psi(z/L)$ to be quantified. Such data are not available at present.

5.4 Summary on surface flux scaling

Aggregation means area-averaging values from different patches within a grid cell to grid mean values. Aggregation is sometimes called upscaling to separate it from downscaling. Parameters with linear functions can be aggregated by simple area-weighted averaging. The parameters are scale invariant.

In nonlinear cases appropriate weighting factors are presently used. Another method is to quantify the nonlinear contribution by evaluation of the covariances terms from expanded equations.

Case studies on remotely sensed surface parameters like the surface radiant temperature and vegetation index (NDVI) have documented these to be significantly scale dependent in some landscape. Hence it is of importance to parametrize the nonlinear terms in the averaging process. The fine scale information are needed for this purpose.

In regard to surface fluxes neither the weighting factor, nor the covariance approach has so far produced ultimate conclusions. Scaling of surface flux parameters in heterogeneous terrain therefore need further investigation.

6 Dynamics of turbulent flow

The local balance equations are not readily applicable for turbulent flow in heterogeneous terrain as the spatial homogeneity assumption is not fulfilled. Flow over hills will not be considered here but only flow over heterogeneous flat terrain. Kaimal and Finnigan (1994) have summarized the state of art on parametrization of flow over a flat changing terrain.

An internal boundary layer develops when the surface air advects from one type of environment to another. The border is usually pictured as a step change in one or more parameters. The inhomogeneity can be rough to smooth, dry to wet, cold to warm or any possible combination. Common to all changes is that an internal boundary layer (IBL) or thermal internal boundary layer (TIBL) develops within the PBL. With a quotation from Kaimal and Finnigan (1994):

"An internal boundary layer develops over the new surface, growing in height with downwind distance. Profiles of wind, temperature and other scalars behind the change are not in equilibrium with the new surface. A complicated turbulent response to the change is observed with loss of the local-equilibrium character of homogeneous surface flow".

de Bruin et al. (1991) shows for example that the Monin Obukhov similarity scaling is not appropriate in a terrain with changing surface temperature and wetness. The surface fluxes obviously change when the profiles of wind, temperature, humidity and passive scalars change as the wind flows over a variety of surfaces in a heterogeneous terrain. In order to be able to treat the topic of the dynamic response to heterogeneity, it is necessary to simplify to one type of change at a time.

6.1 Flow response to a step change in roughness

The dynamic response when air flows from a smooth to a rough surface is a large increase in surface shear stress, τ, first followed by a rapid and then by a relatively slow attainment to a new equilibrium stress value. The equilibrium value is the stress in an infinite homogeneous area. When air flows from a rough to smooth surface the stress drops near the transition and then slowly recovers to the new equilibrium value.

The very different response curves of surface stress between a rough to smooth transition and a smooth to rough transition are owing to turbulence production and decay. In the smooth to rough situation the decaying upwind turbulence soon is controlled by the new turbulence due to a high turbulence production rate caused by a large shear stress at the rough surface (large momentum absorption). In the rough to smooth situation the upwind turbulence is decaying slowly caused by a low shear stress at the smooth surface. The vertical diffusion by turbulence dominates the downwind IBL growth. The pressure force usually causes a negligible velocity perturbation (Jensen 1981, Kaimal and Finnigan

1994). See also scetion 6.3 and figure 18.

The highly nonlinear stress response function is dependent on the size of the step change and on the static stability in each patch. In a heterogeneous terrain a new roughness step change may be encountered before the new equilibrium stress value is reached (Perrier and Tuzet 1991, Stull 1991, Kaimal and Finnigan 1994). In such cases also the patch length will influence the areal average of the surface stress.

The development of the surface stress in case of a single step change in roughness lengths has been modelled by elaborate turbulence models as well as by simpler models. The simple approach made by Jensen (1978) has produced good agreement with higher-order closure models (Peterson 1969, Rao et al. 1974) and with experimental data (Bradley 1968).

The surface stress model (Jensen 1978) relates the surface stress before the step change, τ_{01}, to the surface stress after the step change, τ_{02},

$$\frac{\tau_{02}}{\tau_{01}} = [1 - \frac{M}{\ln(\frac{\delta_i}{z_{02}})}]^2 \qquad (91)$$

The discontinuity is at the location x=0. Subscript 1 indicates upwind, $x<0$, and 2 downwind, $x>0$. M (-) is the magnitude of the step change in roughness lengths at the discontinuity

$$M = \ln(\frac{z_{01}}{z_{02}}) \qquad (92)$$

δ_i (m) is the internal boundary layer height described by a simple power law of the downwind distance, L_x (m), and the downwind roughness length

$$\delta_i = z_{02}(\frac{L_x}{z_{02}})^{4/5} \qquad (93)$$

The above model is valid for flow over *one* step change between two extensive areas. The model predicts the surface stress when the IBL fills the PBL height to be higher than from more elaborate models. The model predicts the equilibrium state to be reached only far downstream ie of the order of 20 km. Experimental data are not available to verify values far downstream (Kaimal and Finnigan 1994). In terms of the drag coefficient is $\delta_i \propto L_x\sqrt{C_M}$.

Consecutive step changes may occur and then the IBL may never develop fully into the new equilibrium state. In these cases flux calculation based on equilibrium assumptions may cause an error. In other words, the advective effect is significant.

6.2 Dynamic length scales

It is a matter of scale when advective effects become dominant. Terrain patch sizes are related to dynamic length scales.

Raupach (1993) defines microscale as patches of a dynamic length, X (m), where $X << \bar{u}t_*$. $\bar{u}$ is the mean wind speed in the convective boundary layer (CBL) and t_*=the convective eddy time scale needed for good mixing. t_* is dependent on the convective boundary layer height, h (m), and the turbulent velocity scale, w_*, in the CBL, ($t_*=h/w_*$). The velocity scale equals

$$w_*=(h\ \overline{w'\theta_v'}\frac{g}{T})^{1/3} \tag{94}$$

Hence for an air mass advected a distance of $X << \bar{u}t_*$, the mixing is poor and the adjustment process is at its maximum. This means that the local influence is significant. The strong advective effects are only dominant close to the surface. Above a certain height (blending height) the CBL properties have uniform, average values. If relevant values are inserted in eq 94 for h 1000 m, $\bar{u}$ 2-20 m s^{-1} and w_* 2 m s^{-1} we obtain X of the order of 1-10 km (Raupach 1991)

Under neutral conditions the patch size needed to approximately obtain a homogeneous (quasi-equilibrium) air column, L_x, roughly equals

$$L_x \approx \frac{z}{C_E\sqrt{C_M}} \tag{95}$$

(Mahrt 1996). C_E is the transfer coefficient in an equilibrium layer for heat (-) (eg Stull 1991). Inserting appropriate values in eq 95 of z=50 m, C_E=0.1 and $C_M=5*10^{-3}$ gives L_x ~7 km at which length scale quasi-epuilibrium is achieved. At smaller length scales $<C_M>$ is to some extent scale variant because of advective effects. The effect of non-neutral stability is that under stable conditions a larger patch scale is found and under unstable a shorter.

The mesoscale patch size is characterized by a flow where the turbulence is fully adjusted to the surface properties, however, not fully adjusted to the CBL flow (that basically develops since dawn). Hence "traditional" mesoscale advective effects are present, ie flow phenomena caused by differential heating, gravity waves or scattered clouds. A dynamic length for the mesoscale defined by Raupach (1993) is $\bar{u}t_* < X < \bar{u}T$, where T is time (since dawn) required for complete CBL equilibrium.

Homogeneous terrain is only found when the dynamic length scale of a patch is $X > \bar{u}T$ (T time since dawn). Advection will be negligible and the CBL fully developed (Raupach 1993). In such large-scale terrain a logarithmic averaging of z_0 (eq 98) is appropriate for grid mean flux prediction. The geostrophic drag laws (eqs 39-41 and 167) are truly valid.

The dynamic length scales are mentioned to stress that ensemble averaging actually is necessary (though not possible). Spatial mean values of gradients,

exchange coefficients and stability parameters do not predict the grid mean heat fluxes at all scales. In some cases the fluxes may even be countergradient.

6.3 Aggregation of roughness lengths for momentum

The spatial average of z_0 in heterogeneous terrain, $<z_0>$, is often called the effective roughness length for momentum. Obviously $<z_0>$ should give a correct spatial average surface stress rather than a correct spatial average of the velocity profile for momentum flux calculationas as well as for other flux calculations. Both things cannot be fulfilled at once owing to correlation terms on the time or space variations in u and z_0 (Mason 1988).

Calculation of $<z_0>$ is basically done by averaging drag coefficients at an appropriate height above the surface. One model for the determination of this height for alternating values of z_0 (ie z_{01} and z_{02}) would be to take a characteristic patch length scale in the mean flow direction and then estimate the height from $f(L_x/z_{02})$ (eq 93). In the homogeneous case it simplifies in averaging geostrophic drag coefficients and converting to $<z_0>$ through Rossby number similarity theory.

In the heterogeneous case with patches in the microscale range, the appropriate height has been called the blending height (Wieringa 1986,1993, Mason 1988, Claussen 1990,1991,1992, Wood and Mason 1991, Chehbouni et al. 1993, Schmid and Bünzli 1995). Wieringa (1986) suggested the blending height to equal 60 m without regard to horizontal length scales. The 60 m height was assumed to represent grid cells of the order of 5 * 5 km^2. All the others explicitely include a horizontal length scale to estimate a blending height. Wieringa introduced the blending height concept and Mason (1988) supported this by physical considerations.

A heuristic model was developed by Mason (1988) for calculation of an areal average of the roughness lengths at the blending height. Later Wood and Mason (1991) developed the model to include roughness lengths of temperature. The assumptions in the model are that the step changes occur arbitrarily on the horizontal domain. The distribution of roughness step changes is assumed to be statistically uniform within the area. Hence line elements are excluded ie areas with baroclinicity from, say, land-sea temperature gradients should be excluded as the homogeneity assumption is not fulfilled.

Based on a theory for the depth of the so-called inner layer provided by Jensen (1988) a method for estimating the blending height, l_b (m), takes the following form as a function of a characteristic horizontal length scale in the mean flow direction

$$l_b = 2\left(\frac{u_*}{\bar{u}(l_b)}\right)^2 L_x \qquad (96)$$

or rewritten to

$$l_b(\ln(\frac{l_b}{<z_0>}))^2 = 2\kappa^2 L_x \qquad (97)$$

The blending height is not a fixed height above the surface but rather an approximate height above the surface where certain things about the dynamics of the flow are estimated to be roughly fulfilled. Below l_b the surface layer is in *local balance* with the surface and the similarity scaling of Monin-Obukhov theory is valid for the flow. Above l_b a horizontally homogeneous (*area averaged*) mean flow is found that is expected to assume a logarithmic profile with a roughness length equal to $<z_0>$. At the blending height the flow is assumed to be independent of horizontal position. In terms of the drag coefficient $l_b \propto 2C_M L_x$.

A physical interpretation of the blending height concept is given in Mason (1988), where two different methods are described to estimate l_b as a function of a characteristic horizontal lengths scale, L_x. One method is balancing the two more important terms in the momentum equation, the horizontal advection term and the vertical stress divergence term. The other method is considering the vertical integral of the advective velocity perturbation advection. This is assumed to be balanced by the change in surface stress at height l_b. Roughly speaking is l_b found at height $\sim L_x/200$ (figure 23).

The blending height concept is rather abstract and figure 18 is shown to visualise the play between local surface roughness (z_0), IBL growth (δ_i), the stress response (u_*), the wind profile ($\partial u/\partial z$), the blending height (l_b) and the spatial roughness values (z_{0a} and $<z_0>$). The order of magnitude of the various terms are included.

The upper part of figure 18 shows the patches with a length scale of $L_x = 100$ m. The wind is advected from left to right. At each step change a new IBL starts to grow. The air column of each IBL is adjusting to the roughness of the new patch. The instruments mounted on the meteorological mast measure the turbulence statistics of the various IBLs advected past the sensors ("frozen turbulence assumption"). In the lower part of figure 18 are data of wind speed as a function of height shown. This give us the log-profiles of wind.

The logarithmic wind profile is only valid for equilibrium flow. If the terrain is assumed to be infinite and z_0 to equal 0.01 m, the matching log-profile will follow the lower dashed line, or if z_0 equals 1 m the upper dashed line. The area-weighted (geometric) mean of smooth and rough is z_{0a} (eq 98). This spatial average is valid for prediction of the flux in infinite patches. At smaller length scale is only the velocity profile predicted correct, not the stress profile.

Relatively strong wind advected from a smooth patch to a rough grows up against a slowly moving air mass. This causes a large shear most pronounced near the inhomogeneity but significant for a considerable downwind distance (as equilibrium is only reached at ~ 20 km). Momentum absorption at the rough surface is large and the turbulence production high. Figure 18 shows the quick growth and slow decline in u_* that would be measured on a constant level (by a horizontally moving sensor). Air traversing from a rough to a smooth patch

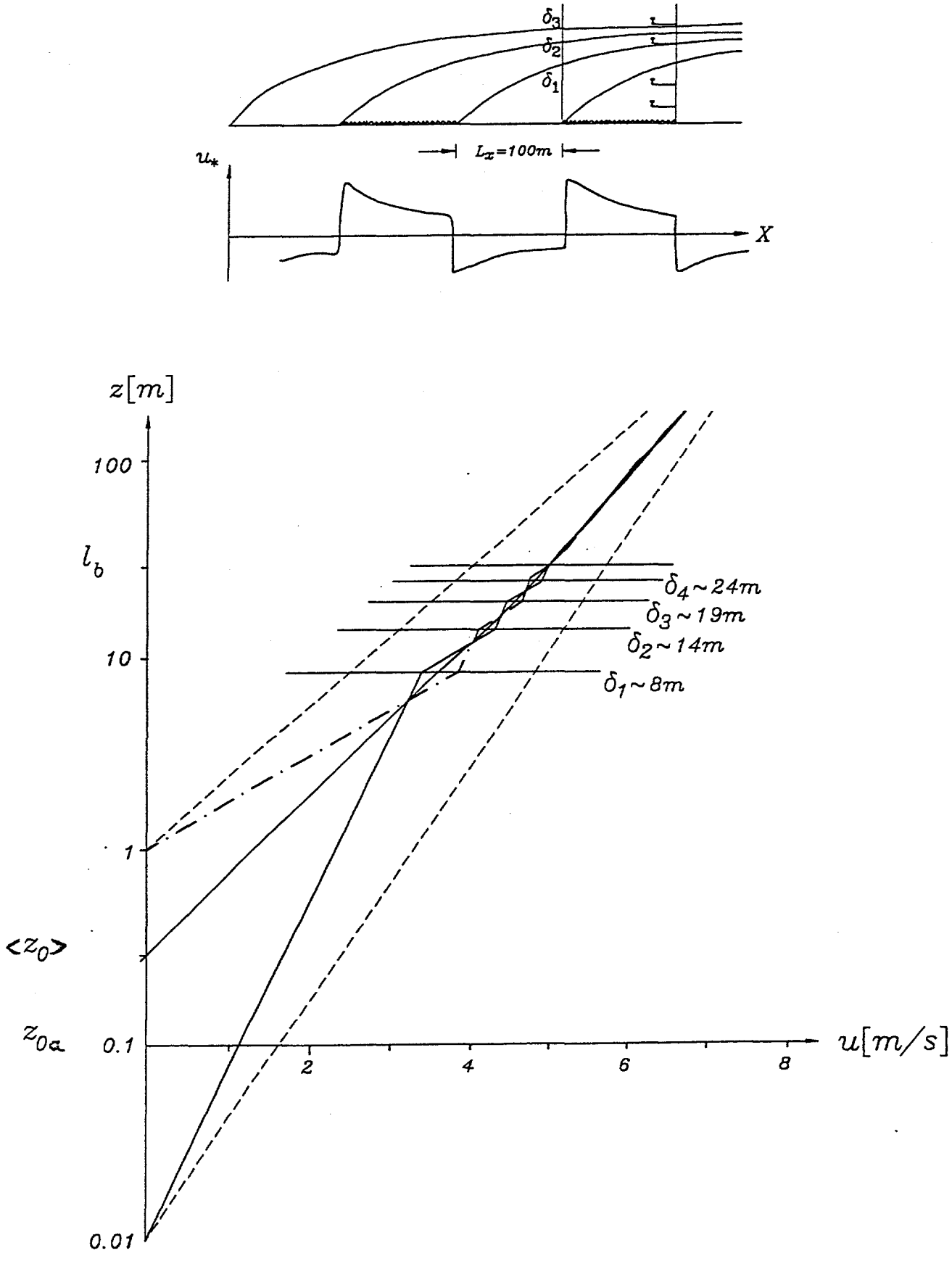

Figure 18. Response in friction velocity and wind speed to roughness step changes. The upper panel shows the landscape with a micrometeorological mast and the development of internal boundary layers. In the middle panel the shear stress response. In the lower panel the wind profiles above and below the blending height and area-averaged roughness lengths. See also text.

is relatively slow. The smooth terrain very gradually absorp the momentum. The stress response curve is seen to approach equilibrium very slowly.

The shear stress response primarily is a function of the wind profile "growing up" against a different air mass. The smooth to rough response is more vigorous than the rough to smooth response. This explains why the rough surface, so to speak, dominates the response. The result is that $<z_0>$ is always larger than z_{0a}. In the lower part of figure 18 the averaged wind profile is seen to be above z_{0a} and below maximum z_0. It should also be noted that $<z_0>$ is the roughness found when extrapolating the homogeneous log-profile above the blending height, l_b, to a zero wind speed in figure 18.

Mason (1988) calculated $<z_0>$ for various distributions of two roughnesses by use of two PBL models with different closure assumptions and by an analytic model. $<z_0>$ was found to be very much larger than that of local *equilibrium*. The spatial roughness for equilibrium flow is

$$z_{0a} = \exp(\sum_{i=1}^{n} \ln(z_0)) \qquad (98)$$

This classic equation is from (Taylor 1987 *in* Mason 1988). It is used by many scientists (eg Seth et al. 1994, Noilhan et al. 1991). Claussen (1991) states that this procedure can result in far too low estimates of the averaged momentum flux.

Two cases from Mason (1988) will be referred here. For a case of 70% rough area and 30% smooth area $<z_0>$ was 1.6 times z_{0a} whereas for a case with 30% rough area and 70% smooth area $<z_0>$ was three times z_{0a}. Claussen (1991) aggregated z_0 for an idealized terrain with four cover classes (water, sand, grass and forest) and obtained $z_{0a}=0.006$ m and $<z_0>=0.072$ m. Claussen's method (eq 107) of aggregation is somewhat different from that of Mason. Schmid and Bünzli (1995) report result of a similar order-of-magnitude with a so-called texture analysis with a full flow description. The results just have to be considered as order of magnitude examples because step change, patch size and stability varies.

Nonlinear dynamic effects are most notable when small patches of large roughness are present. It is worth stressing that averaging of drag coefficients at l_b gives extra weight to high values of z_0 occurring in small fractions of area. This in fact is a key to understand what happens dynamically in a very patchy (highly heterogeneous) terrain.

6.3.1 Estimation methods

Spatial roughness estimation has a long history. Some of the many methods are described shortly here. One is to use the wind statistics, ie atmospherically "integrated" quantities (Wieringa 1986, Beljaars 1987 *in* Beljaars and Holtslag 1991). Other methods are based on weighting functions of

1) horizontal length scales (dominant cover, fractional area, element spacing)

2) vertical length scales (roughness length, displacement height, element height)

(Lettau 1969, Arya 1975 *in* Menenti and Ritchie 1994, Kondo and Yamazawa 1986, Klaassen 1992, Vihma and Savijarvi 1991, Seth et al. 1994, Sellers et al. 1995).

Wieringa (1986) suggested a so-called gustiness-derived roughness estimate. The roughness was derived from knowledge of maximum and median gusts and the mean wind. It is based on the fact that the turbulence level $\sigma_u/\overline{u}$ increases with increasing roughness. The gustiness roughness is an area-integrated value as inhomogeneity within an upwind distance of roughly three kilometer will add to the turbulence level.

A different way of obtaining $<z_0>$ from wind statistics was proposed by Beljaars (1987 *in* Beljaars and Holtslag 1991). The atmospheric response to surface heterogeneity are mirrored in large eddy structures. The horizontal velocity components, streamwise and lateral, give a measure of upstream terrain heterogeneity. The relations suggested for obtaining $<z_0>$ are: $\sigma_u/u_*=2.2$, $\sigma_v/u_*=1.9$, $\sigma_v=u\sigma_\Phi$ and the logarithmic wind profile (eq 5). σ_Φ (°) is the standard deviation on wind speed direction. Results from the Cabouw tower in The Netherlands showed a good aggreement to the gustiness-derived (Wieringa 1986) and the σ_Φ-derived roughness according to Beljaars and Holtslag (1991).

Examples of weighting the dominant cover type(s) are found in Seth et al. (1994) and Vihma and Savijarvi (1991). Vihma and Savijarvi (1991) compared their "dominant-cover-types" weighting function model with several other weighting function models as well as with Mason's analytical model (eq 97). It is not easy to verify the validity of the models though. Simplification of weighting between two or three dominant roughness classes within each 15 km * 15 km grid cell do not provide a sound physical basis for the calculated $<z_0>$ map of Finland in 150 km * 150 km grid cells. Subgrid effects are not accounted for.

A simple equation to calculate $<z_0>$ from the height and spacing of large obstacles was shown by Kondo & Yamazawa (1986) to be useful in urban areas. Their idea is similar to Lettau's (1969) for small-scale elements. Both methods consider the vertical cross-wind area, element height (of building, box or plant) and density per horizontal area.

Klaassen (1992) proposed the mixing length similarity theory to describe the flow inside a multi-layer canopy (forest) with a modification to the mixing length. The modified mixing length is assumed to be a function of the drag exerted by leaves and stems on the airflow in a canopy. The modified mixing length and the advection term (resulting in grid values of r_a) was parametrized from LAI, canopy height, displacement height, leaf width and leaf shading. The degree of advection was "measured" from displacement height differences. Countergradient transfer was modelled and r_c were assumed to be a function of canopy height and net radiation penetrating the canopy.

The horizontal advection was parametrized by a smoothly fitted function between equilibrium in one patch to equilibrium in the adjacent patch. In order not to include regional advection but only to quantify local advection Klaassen (1992) ran the model iteratively over a sequence of identical regions until in- and outflowing air converged. The procedure is equivalent to Fourier analysis which is also based on an infinite extension of identical regions. The results were found to be very dependent on displacement height differences.

Two comments on the model follow. The model parametrizations are not physically based. The well-known mixing length (eg Stull 1991) gives a measure of the ability of turbulence to cause mixing. The turbulence has to be generated mechanically in a statically neutral surface layer with only log-linear gradients. These conditions are not met inside tall canopy. Secondly the nonlinear stress response is given from a smoothed (fitted) function based on equilibrium states in all patches. The equilibrium assumption is not fullfilled for terrain of microscale heterogeneity.

The modified mixing-length model results show $<z_0>$ to be larger than *maximum* z_0 in a terrain with forest fractions in the range between 40 and 100 % (Klaassen & Claussen 1995, their figure on p.184). This is remarkable. In general their $<z_0>$ results were much larger than that of most others. Klaassen and Claussen (1995) suggest to explain their results from drag partitioning, ie drag from a homogeneous surface with some drag added from single obstacles (pressure effects). It awaits validation from experiments such as Northern Hemisphere Climate Processes Land-surface Experiment (NOPEX) and SLIMM (Vugts 1996). SLIMM is the acronym for Surface Layer Integration Measurement and Modelling project that will be conducted in The Netherlands 1997.

6.3.2 Spatial roughness data

Wieringa (1993), who carefully reviewed current literature on roughness in *homogeneous* terrain, made clear that local z_0 tends to be underestimated. This effect rely on two matters

1) small inhomogeneity in a seemingly homogenous terrain introduce a negative bias owing to drag effects from scattered elements

2) measuring techniques tend to bias z_0 too low because of insufficient correction for stability and/or anemometer overspeeding

In inhomogeneous terrain z_{0a} is always smaller than the effective roughness and combined with the general information above lead us to expect relatively larger $<z_0>$ values than previously assumed. Findings based on airborne eddy correlation data support this.

Mahrt and Ek (1993) found from airborne momentum flux data by "inverting" similarity scaling (ie the similarity theory predicts the correct area-averaged flux) that $<z_0>$ was 1 m rather than 0.1 m in an agricultural area with few obstacles. Above forest the ratio between local and effective roughness was less. The flights were from HAPEX-MOBILHY in France.

In Alaska airborne momentum flux data from an area dominated by tundra interspersed with lakes of the order 500 m were analysed by Moore et al. (1993). Their results had a similar order-of-magnitude difference to those of Mahrt and Ek. Tower data gave a local z_0 of 0.5 cm, while the airborne data yielded $<z_0>$ of 6.7 cm over the land surface. The difference is an order of magnitude.

Compared to flat terrain topographic effects will cause $<z_0>$ measured by airborne sensors to be enlarged compared to flat terrain (Panofsky and Dutton 1984). Both sites cited here are flat.

6.4 Aggregation of roughness lengths for scalars

The roughness length for heat transfer, z_{0t}, is a key parameter for surface heat flux calculation. A definition of z_{0t} (Kaimal and Finnigan 1994, Wood and Mason 1991) could be

$$\bar{\theta}(z)-\bar{\theta}_0 = \frac{\theta_*}{\kappa}\left(\ln\left(\frac{z}{z_{0t}}\right)-\psi_H\left(\frac{z}{L}\right)\right) \qquad (99)$$

Calculation of z_{0t} is highly iterative. The Monin-Obukhov length, L, and the surface layer temperature scale, θ_*, are both functions of the surface heat flux (which is the flux we actually want to retrieve). Again we neglect the displacement height (that even may diverge from the one for momentum). Problems related to measuring θ_0, z_{0t}, T_s and $z_{t,r}$ in homogeneous situations were described in chapter 3. When it comes to heterogeneity the situation is just more complex.

A thermal internal boundary layer (TIBL) develops when an air mass is advected across a warm to cool or a cool to warm transition. Very often the transition is related to a humidity transition at the same time, and - just to complicate matters more - a roughness change in z_0. Land-sea breezes constitute a classic transition. These are between cool, smooth water to warm, rough land areas (or the opposite). Another classic transition is between warm, dry, smooth land to cool, humid, rough land (oasis, irrigation). The responses are different indeed. Offshore flow typically yields a stable IBL (SIBL) with a small growth rate whereas onshore flow typically yields a convective IBL (CIBL) with a high growth rate.

A starting point is to assume that z_{0t} (or z_{0q}) is a constant fraction (or function) of z_0, and that the turbulent response after a step change physically is similar to the shear stress response curve. If so an aggregation procedure valid for $<z_0>$ can be applied.

Empirical results indicate that the first condition is not met (section 2.4.1 and 3.1.1.) (Sugita and Brutsaert 1990, Beljaars and Holtslag 1991, Kohsiek et al. 1993, Mahrt and Ek 1993, Prevot et al. 1993a, Beljaars and Viterbo 1994, Sugita and Kubota 1994).

The second condition of dynamic response curves physically similar to the shear stress curves, obviously is not always fulfilled. Very different situations may occur (eg CIBL, SIBL). It is necessary though to simplify the problem. The blending height method has been applied to obtain estimates of $<z_{0t}>$.

Mason (1988) and Wood and Mason (1991) again used the blending height concept, however, now with a blending height for temperature l_{bh}. The balance considered was the advection of the perturbation temperature field that was assumed to balance the vertical gradient of the perturbation turbulent temperature flux at height l_{bh}. At this height the temperature field is independent of horizontal position. l_{bh} is smaller than l_b.

Wood and Mason (1991) assumed z_0/z_{0t} to be constant with a value of ten being realistic for vegetated areas for neutral stability. The model results of $<z_{0t}>$ were very different from logarithmic area averaged values, z_{0ta} (m) (analogous to eq 98). It was shown that $<z_{0t}>$ was *smaller* than z_{0ta} (reduced by a factor of about three). This is in contrast to $<z_0>$ that was *larger* (increased by a factor of two).

Wood and Mason (1991) also showed that $<z_{0t}>$ is highly sensitive to the distribution of the roughness elements. Small patches with large roughness elements have a more pronounced influence than relatively larger patches. It is therefore very important to map small patches with large roughness elements. Conversely, Mahrt and Ek (1993) concluded that $<z_{0t}>$ tend to be primarily determined by the surface type which occupies the largest area. However both studies agree that $<z_{0t}>$ is very much smaller than $<z_0>$.

It is interesting to note that $<z_{0t}>$ can attain a value *lower* than local balance z_{0t} values of the smoothest elements in a terrain. This occurs for smooth terrain where very small patches consisting of large roughness elements are present. The reason is that very large amounts of momentum can be extracted from the flow by a few large roughness elements. The surface temperature field is nearly constant. Thus it is the change in surface stress that influences $<z_{0t}>$. The horizontal distribution of z_{0t} naturally effects the area average too.

The bottomline is that the averaging effects are large indeed. z_{0t}, z_{0ta}, $<z_{0t}>$ and $<z_{0ta}>$ can deviate strongly. This may explain some of the scatter in field data on z_{0t}. (Non-neutral stability effects also may explain some of the scatter). Incorrect estimates of the thermal roughness length may cause significant bias on the surface heat flux results.

Recently a practical approach to aggregate z_{0t} was proposed by Jensen et al. (1996). The aggregation again takes place at a blending height. It was shown from analytical analysis that

$$\ln\frac{\langle z_{0t}\rangle}{z_{0ta}} \approx -2 \ln\frac{\langle z_0\rangle}{z_{0a}} \tag{100}$$

consistent with the power law description

$$\frac{\langle z_{0t}\rangle}{z_{0ta}} \approx \left(\frac{\langle z_0\rangle}{z_{0a}}\right)^{-2} \tag{101}$$

$\langle z_0\rangle$ is always larger than z_{0a}. Conversely $\langle z_{0t}\rangle$ is always smaller that z_{0ta}. The power of -2 reduces $\langle z_{0t}\rangle$ significantly.

Equation 101 is useful when z_{0a} and $\langle z_0\rangle$ is known on the subgrid scale, because then $\langle z_{0t}\rangle / z_{0ta}$ is predicted for the grid. It is a very attractive approach as z_{0t} is indeed difficult to obtain from measurements. Maps of z_{0a} and $\langle z_0\rangle$ are available (see chapter 7).

The analytic result in eq 101 was obtained by assuming

$$\frac{H}{\langle u_*\rangle}\ln\frac{l_{bh}}{\langle z_{0t}\rangle} = \left\langle \frac{H}{u_*(x)}\ln\frac{l_{bh}}{z_{0t}(x)} \right\rangle \tag{102}$$

where H is a constant fraction of the available energy. The variation of $u_*(x)$ and $z_{0t}(x)$ was assumed to be periodic and $z_0/z_{0t} = 10$. The last assumption is not important as the ratio cancelled out (Jensen et al. 1996).

Wood and Mason (1991) showed the magnitude of $\langle z_{0t}\rangle$ in a two-component landscape (rough and smooth patches) to relate to the fractional cover, f_i, in the following form

$$f_i = \frac{1}{3}\left(1 - \frac{2u_*^2(smooth)}{u_*^2(rough) - u_*^2(smooth)}\right) \tag{103}$$

Global minimum in $\ln(\langle z_{0t}\rangle / z_{0ta})$ is found for $f_i \sim 0.14$. It was also found that the smaller the patch size, the lower the minimum.

Data available to verify $\langle z_{0t}\rangle$ values are scarce. Recently Holtslag and Ek (1996) showed that $\langle z_0\rangle / \langle z_{0t}\rangle$ is of the order of $5*10^3$. Their sensitivity study was based on a PBL-model and a SVAT-scheme. The data used were representative for a pine forest interspersed with clearings. $\langle z_0\rangle$ was of the order of 1-2.3 m. Their model results compared well with airborne data and tower data.

Kustas et al. (1989) have analysed airborne T_s data. The study area was located in California with a local ground cover of 30% bush and 70% dry bare soil. The heat fluxes were measured in the field. From inverting similarity theory $\langle z_{0t,r}\rangle$ was calculated. The results showed very small values. κB^{-1} was reported to be up to 10. This gives $\langle z_0\rangle / \langle z_{0t}\rangle$ of the order of $2*10^4$.

Sugita and Brutsaert (1990) analysed airborne radiometric data over rather homogeneous grassland in Kansas (FIFE) in a similar fashion. Their result was assumed to be valid for a 10 * 10 km^2 area. The scatter in $<z_{0t,r}>$ was several orders of magnitude and $<z_{0t,r}>$ mean very small.

It should be borne in mind that z_{0t} is undefined in countergradient flux situations. In situations with two surface sources for example dry, hot pine tree tops and cool, shaded ground $<T_s>$ and hence $<z_{0t}>$ is not applicable in a (traditional) single source methodology sense. Hence dual-source or multiple-source temperature models seem necessary (Dolman 1993, Prevot et al. 1993a, Kustas et al. 1996, Blyth and Dolman 1995, Sun and Mahrt 1995).

On roughness lengths for humidity.

The roughness lenght for humidity z_{0q} has received less attention than z_{0t}. The reason is that z_{0q} is problematic from a measuring point of view. Humidity sensors are less accurate than temperature sensors. Therefore the log-profile extrapolation routine is less reliable.

On account of the lack of q_0 values it is common practice to substitute q_0 with $q_{sat}(T_s)$. This naturally only works well over saturated surfaces (Garratt 1978). Plants regulate humidity emission by bio-chemical processes. Soils dry up in nonlinear ways. Often a wetness coefficient, α (-) is multiplied to $q_{sat}(T_s)$. Typically α has a value of zero for dry conditions and one for saturated conditions.

Another approach is to calculate q_0 (kg H_20 per kg dry air) from soil moisture data in units of kg H_20 per kg dry soil. Menenti (1993) points out that we have to take account of the transition from liquid to vapour phase. Soil moisture data from airborne passive microwave radiometers estimate humidity in the upper five cm soil layer at a resolution of 200 * 200 m^2 (Schmugge and Jackson 1996). Brutsaert et al. (1993) reported results of $<z_{0q}>$ between 0.12 and 0.29 m based on airborne latent heat flux data in HAPEX-MOBILHY. These values were slightly smaller than their values of $<z_{0t}>$. Nevertheless the scalar roughness lengths continue to be assumed equal.

A pragmatic statement is that one can chose to assume $z_{0t}=z_{0q}$ as there is no experimental evidence against the assumption (Beljaars and Holtslag 1991).

The same statement is valid for the spatial means. Roughness lengths for passive scalars are not well-known.

6.5 Aggregation of exchange coefficients

So far turbulent flow over heterogeneous terrain has been described in terms of effective roughness lengths. The spatial averaging can also be cast in terms of effective exchange coefficients.

According to Mahrt and Sun (1995) effective exchange coefficients based on the bulk aerodynamic formulations may be parametrized for momentum, sensible heat and humidity, respectively,

$$<C_M(z)>=\frac{<u_*>^2}{<\bar{u}(z)>^2} \tag{104}$$

$$<C_H(z)>=\frac{\rho c_p<\overline{w'\theta'}>}{<\bar{u}(z)>(<\theta_0>-<\theta(z)>)} \tag{105}$$

$$<C_Q(z)>=\frac{\rho<\overline{w'q_0}>}{<\bar{u}(z)>(<q_0>)-<q(z)>)} \tag{106}$$

The usual bulk formulation is based on time averages in homogeneous terrain (eqs 39-41). Monin-Obukov similarity is not strictly valid in spatially varying environments and does not predict effective transfer coefficients. The fact is that the subgrid fluxes are not resolved. Therefore eqs 104-106 are merely estimates of exchange coefficients for a given grid space.

Claussen (1990) suggests to calculate effective exchange coefficients at the diffusion height, l_d (see also Mason 1988). l_d is an order of magnitude larger than l_b. The diffusion height method defines $<z_0>$ as

$$l_d \ln(\frac{l_d}{<z_0>})=\kappa L_x \tag{107}$$

or rewritten to

$$l_d=\frac{u_*}{\bar{u}(l_d)}L_x \tag{108}$$

Claussen (1990) approximates l_d with a power law expression.

$$l_d=0.7z_0(\frac{L_x}{z_{0a}})^{4/5} \tag{109}$$

The difference between eq 97 and eq 107 is the power. At height l_d the *local* mean profile is logarithmic. Not only the stress perturbation has decayed, but also the flow perturbations (Wood and Mason 1991). Claussen (1990) chose l_d

as a height where the deviation of the local profile and the horizontal velocity reach minimum values. In drag coefficient terms the diffusion height can be described as $l_d \propto \sqrt{(C_D L_x)}$.

Surface flux estimates tend to be rather independent of the exact value of the blending height. Therefore the diffusion height chosen seems to be of less importance. Claussen (1990) assumes that in a smooth case $<z_0>$ equals z_{0a}. However in a strongly heterogeneous terrain with large roughness changes and/or thermal differences the dependence between l_d, L_x and $<z_0>$ is of importance (Claussen 1990). L_x is quantified from the mean sizes of all land cover types. The method first demands a mapping of the fractions of area with each land cover type and the horizontal length scale of variation (statistical quantities). Then the surface fluxes from each surface type weighted by area are calculated. Finally the effective exchange coefficients are obtained for the area. The transfer coefficients are obtained by interpolation between smooth and rough situations. The suggested method was tested by a flow model and the surface fluxes found to be within $\pm 10\%$ for various hypothesized distributions.

A major difference between the heuristic model of Mason (1988) and the model of Claussen (1990) is that the latter suggests to evaluate the effective turbulent transfer diffusion coefficients $<C_M>$, $<C_H>$ and $<C_Q>$ rather than $<z_0>$, $<z_{0t}>$ and $<z_{0q}>$.

Mahrt and Sun (1995) linearized the bulk formulations to evaluate the Reynolds averaging covariance terms. The conclusion was that in cases of weak flow over strong heterogeneity the unresolved wind speed increase the effective exchange coefficients. So does spatial heterogeneity in T_s. In other situations the terms tend to cancel out. The scale dependence is only significant for $<C_M>$. The result is based on airborne eddy correlation data. $<C_M>$ decreases with increasing grid spacing caused by spatial stress variations. This means that the stress happens to reverse sign. Therefore $<u_*>$ decreases faster than $<u>$ on a larger grid scale causing $<C_M>$ to decrease. Results based on HAPEX-MOBILHY data from France showed a decrease in $<C_M>$ between $\sim 40*10^{-3}$ and $20*10^{-3}$ for scales of the order of 5-90 km. The result implies a larger effective roughness on larger length scale.

In cases of flow in opposite directions the averaged wind vector field $<u>$ may go to zero. In such cases all exchange coefficients are severely scale dependent when retrieved from the bulk aerodynamic formulation (Mahrt and Sun 1995). Generally the stress is more variant than the wind vector. Thence $<C_H>$ and $<C_Q>$ are less affected of the averaging scale than $<C_M>$.

6.6 Aggregation of resistances

Climate models resolve the mean values of grid averaged wind speed, humidity and temperature. Based on these mean values the surface heat fluxes have to be calculated. The resistance approach (section 2.4) needs to be modified to account for subgrid variability of roughness, moisture and temperature.

The effective resistances, analogous to eqs 31-33, are

$$<r_a(z)>=\rho\frac{<u(z)>}{<u_*>^2} \tag{110}$$

$$<r_h(z)>=\rho c_p\frac{<\theta_0>-<\theta(z)>}{<w'\theta'>} \tag{111}$$

$$<r_q(z)>=\rho\frac{<q_0>-<q(z)>}{<w'q'>} \tag{112}$$

To quantify the grid resistances spatial data of lower boundary conditions are in explicit need. T_s is available. Hence $<r_h>$ usually is "fit" to $<T_s>$ rather than to $<\theta_0>$. Discrepancy between the two is described for homogeneous (section 2.4.1) and for heterogeneous (section 6.4). Surface humidity is pragmatically taken to be $\alpha q_{sat}(<T_s>)$. Alternatively soil moisture data may be used (section 6.4).

A statistical approach to calculate the effective surface resistances was proposed by Avissar (1991). A Gaussian probability density function was assumed to be valid for stomatal resistance in each cover type. The mosaic approach with a regrouping of patches and no representation of local advection was used. If advection is disregarded and a simple averaging is performed we obtain an effective aerodynamic resistance $<r_a>$ as

$$\frac{1}{<r_a>}=\sum_{i=1}^{n}\frac{1}{r_a} \tag{113}$$

$\bar{u}$ is assumed to be constant at a (blending) height and zero at the ground. So in a homogenous case a parallel summing is performed, $r_a=\bar{u}/u_*^2$.

The sensible heat flux is not constant in heterogeneous terrain so series averaging $<r_h>$ as

$$<r_h>=\sum_{i=1}^{n}r_h \tag{114}$$

is not a good assumption although used in some climate models as pointed out by eg Blyth et al. (1993) and Beljaars and Viterbo (1994).

A general problem is that when the flux approaches zero, the resistance goes to infinity. When summing "zero-flux" sub-areas, however small they may be, the resulting $<r>$ has a positive bias. Mahrt and Sun (1995) analysed airborne flux data and found $<r_h>$ to be scale dependent. The explanation was that on smaller scales zero-flux subareas introduce significant bias.

Equations analog to eqs 113 and 114 may be written for humidity. However results from a PBL-model showed that a constant underestimation of $<r_q>$ in eq 113 whereas in eq 114 a constant overestimate of $<r_q>$ occurs. Therefore a mean of the two methods was proposed by Blyth et al. (1993) as a very simple improvement.

$$<r_q> = \frac{1}{2}\left(\sum_{i=1}^{n} r_q + 1/\sum_{i=1}^{n} \frac{1}{r_q}\right) \qquad (115)$$

Unfortunately neither $<r_h>$ nor $<r_q>$ can be estimated with a reasonably accuracy by such simple methods. Equations 113-115 cannot be applied in heterogeneous terrain with a pronounced subgrid variability (Blyth et al. 1993).

Therefore an iterative method to retrieve effective resistances based on the blending height concept was proposed by Blyth et al. (1993). Some iterative steps include evaluation of $<r_q>$ from a Penman-Monteith energy-combination equation and the effective surface resistance, $<r_s>$, to be evaluated from the surface conditions. Hence $<r_a> = <r_q> - <r_s>$. Through the iterative process the surface values of canopy humidity and temperatures are derived. $<r_a>$ is not evaluated directly but as a residual.

The iterative model demands information on the patch cover types, their proportional area and their characteristic length scale of variation. Based on this information the blending height can be determined and assigned to each heterogeneous grid cell in the climate model. Wind speed, temperature and humidity at the blending height will have to be determined at each time step. This has to be done by interpolation between the surface and the first grid point (Blyth et al 1993). The results from the suggested model were promising as H and E were always estimated within 25% of PBL-model results. This was in contrast to results from the simpler models (eqs 113-115) that tended to give results way off especially for H. The problem was most pronounced when strong surface humidity contrasts are involved. Recently humidity contrasts were studied by Blyth and Dolman (1995). They found the evaporation to be enhanced in a partly dry, partly wet terrain. The shorter the length scale of variation, the larger the enhancement.

Raupach (1993) suggested another aggregation method for resistances in terrain with microscale heterogeneity. It was assumed that the boundary layer height and the atmospheric saturation deficit at the top of the convective boundary layer are independent of the underlying (small) patches. On the other hand the near surface advection is large. The properties of each patch were specified by assigning typical resistances and roughness lengths. The aggregation was basically the Penman-Monteith equation obtained with a parallel summing of the resistances.

Raupach (1993) obtained E larger than that for simple area averaging. A maximum difference in E between simple (large-scale) area averaging and the microscale aggregation was seen for 50% of two contrasting surface cover types (Raupach 1993). The results were not validated by data or PBL-models. The results are different from other aggregation results (eg Mason 1988, Claussen 1990, 1992, Claussen and Klaassen 1992, Klaassen 1992) as well as aggregation results in the present project (chapter 7). It seems to be agreed upon that small patches of high roughness lengths have a relative greater effect than larger patches.

Yet another analysis on aggregating resistances was undertaken by Kustas et al. (1996). The Priestley-Taylor approximation was used to infer r_h. A dual-source model with a parallel addition of soil and canopy resistances was applied in two data sets. One was from MONSOON 90 in the Walnut Gulch, Arizona with a ground cover of shrubs and grass. T_s was obtained with by portable radiometer. The other data set was from FIFE, Kansas with a ground cover dominated by grass and some deciduous trees. A helicopter based system recorded T_s. Both areas are semi-arid. The fractions of soil and canopy were estimated from NDVI. The model results were concluded to be superior to single source results. It was also concluded that a finer surface partitioning was needed.

Mahrt (1996) pointed out that aggregating fractions (ratios) lead to statistical problems when the denominator goes to zero. Hence in a statistical sense aggregation of conductances is more sound than that of resistances.

6.7 Aggregation of conductances

Dolman (1992) assumed the surface conductance, g (m s^{-1}) to vary spatially (following a gamma distribution) and showed from model results that the largest error arose in $<g>$ for low values (ie $g < 5$ mm s^{-1}). The situation is identical to a large resistance (zero flux) and therefore consistent with findings from the resistance approach.

Spatial data from BOREAS showed a countergradient heat flux (Sun and Mahrt 1995). T_s was found to be lower than T_a, but the heat flux to be positive. This was explained by the fact that cool, shaded ground and canopy contributed more than 75% to the remotely sensed temperature and that the warm, sunny pine tree tops less than 25% . It was, however, the surface of the well-ventilated tree tops that dominated the heat flux.

To calculate an effective grid transfer parameter Sun and Mahrt suggested a parallel averaging of the conductances. The radiative temperature and the conductance were "fit" to give the heat flux (assuming $z_{0t}=z_0$). The conductances averaged in parallel were

$$H=\sum_{i=1}^{n} f_i g_i (T_{si}-T_a) \qquad (116)$$

f_i is the fraction of cover type i and the total area is $\sum f_i = 1$. The conductance

of each cover type is g_i and T_{si} is the subgrid radiant surface temperature. The bulk conductance hence is calculated as

$$<g>=\sum_{i=1}^{n} f_i g_i = C_H u \qquad (117)$$

The above methodology has some similarity with the one of Prevot et al. (1993a). The latter did not consider f_i explicitly and estimated an aggregated value of κB^{-1}.

6.8 Stability effects

It is well-known that in stable conditions sporadic turbulent episodes may cause a countergradient heat flux (Mahrt 1987, Claussen 1990, Stull 1991, Kaimal and Finnigan 1994). This is because the fluxes for short periods of time (or in small patches) are opposite to the mean fluxes (or background gradient). The static stability in those periods (or patches) is unstable despite that the *mean stability* is stable. In thin layers convection may exist in otherwise stable conditions. It is obvious in such cases that the vertical mean profiles and the turbulent fluxes have a nonlinear relation (which is also true but less obvious in other non-equilibrium situations).

Mahrt (1991) has described the intermittency of turbulence by structure functions. Airborne measurements above a pine forest interspersed with clearings were analysed. Intermittency caused by a large scale (compared to the scale of interest) was not found on the two (HAPEX) dates analysed. Microscale intermittency was most notable for temperature. It could be a result of thermals, low-level shear driven overturning or edges of large scale eddies (microfronts). The conclusion was that subgrid fluxes in high-resolution mesoscale models may need careful consideration of horizontal fluxes compared to the vertical fluxes, especially for momentum and moisture fluxes.

The choise of similarity parametrization can influence the predicted surface fluxes. Mahrt and Ek (1993) reported the similarity parametrization of Paulson (1970) to yield $<z_0>$ larger than that of Louis (1979) for airborne eddy correlation data from France (HAPEX). A difference was obvious for local values but not significant for regional values.

Mahrt (1987) assumed the stability effects to have a profound influence on grid averaged fluxes. The effects were investigated through a sensitivity study on spatially averaged exchange coefficients. Stability was quantified by the bulk Richardson number and assumed to obey a Gaussian frequency distribution in the spatial domain. It was concluded that in stable stratification cases a simple correction could account for the persistent underestimate of heat flux. For climate modelling an underestimate of downward heat flux will (typically) result in too low surface temperatures (rapid surface cooling) in the model results.

The suggested exchange coefficient correction for stable cases was

$$<C_H>(Ri) = <C_{HN}>\exp(<Ri>) \tag{118}$$

$<C_H>$ is the aggregated exchange coefficient. $<C_{HN}>$ is the value in neutral stability. The parametrization of Ri was based on the Louis formulation and written as

$$<Ri> = \frac{g}{T_0}(<\theta> - <\theta_0>)\frac{z}{<u>^2} \tag{119}$$

T_0 is a basic state temperature.

For unstable cases correction was not considered to be necessary as the various spatial correlation terms tended to cancel out (Mahrt 1987).

Passive scalar exchange coefficients also vary with stability (eq 12). Jensen et al. (1996) give a generic equation for the stability dependence of $<C_s>$, the bulk exchange coefficient for passive scalar transport. For a stable situation with Ri in the range [0;0.2] the function is

$$<C_s> = \frac{\kappa^2}{(\ln\frac{z}{z_{0s}})^2}(1-5<Ri>)^2 \tag{120}$$

From a Taylor expansion it was shown that nonlinearity between stability and the exchange coefficients depends on $<Ri>$ as well as on σ_{Ri} (standard deviation of the spatial Ri distribution). The relative error on the flux was found to be

$$\frac{<F(Ri)> - F(<Ri>)}{F(<Ri>)} = \frac{75<Ri> - 10}{(1-5<Ri>)^2<Ri>}\sigma_{Ri}^2 \tag{121}$$

F is the flux. Most interesting is it that the flux may increase, decrease or reverse depending on $<Ri>$ and σ_{Ri}. The effect is most important for large σ_{Ri}.

Claussen (1991) aggregated C_M at the diffusion height and found $<C_M>$ to be slightly increased for non-neutral stability. $<C_S>$ has a tendency similar to $<C_M>$. However inclusion of a varying surface resistance complicated matters. Claussen (1991) concluded that for a large variability in r_s it is essential to know u_* locally for the calculation of $<C_s>$.

Wood and Mason (1991) studied the influence of static stability on $<z_0>$ and $<z_{0t}>$. According to their results $<z_0>$ is, for all practical purposes, not affected by changes in stability. This is consistent with the fact that stability effects on C_M are less pronounced than on C_H.

In contrast $<z_{0t}>$ is very sensitive to changes in stability. For Monin-Obukhov lengths between -10 and -30 (unstable) there is some effect but for stable conditions (L=+400) there is a very large effect on $<z_{0t}>$ (Wood and Mason 1990). It has to be noted that it is the combined effect of roughness distribution

and stability that gives the very large range in $<z_{0t}>$. Maps of stability are not obtainable. Therefore estimates on stability effects on $<z_{0t}>$ are necessary.

Moore et al.(1993) performed a linear averaging of the bulk transfer coefficients and then inserted tower and airborne eddy correlation data into the equations. The measurements were from a lake and tundra system in Alaska with typical horizontal lengths scales of 500 m. Their conclusion on the effect of stability on the surface fluxes was that

"In this region surface type exerts its strongest control on surface fluxes through its influence on stability".

6.9 Summary on aggregation

Heterogeneous landscapes are in atmospheric aggregation models described in terms of step changes. Gradual changes are not modelled. The aggregation schemes predict either the boundary conditions by way of effective roughnesses or alternatively by way of effective transfer efficiency, ie exchange coefficients, conductances or resistances.

Effective roughness lengths of momentum have been modelled by many scientists. The area-weighted logarithmic mean is valid for large-scale heterogeneity. On the microscale level the dynamic response at each step change gains so much importance for the overall roughness that the nonlinear contribution has to be included in the aggregation process.

The nonlinear effect on the momentum roughness is always an increase compared to the logarithmic average. Conversely the temperature roughness is decreased. The roughnesses for humidity and passive scalars continue to be assumed equal to the temperature roughness.

Unfortunately do simple aggregation methods on resistances not provide adequate results for the prediction of the heat fluxes. The resistances are highly scale dependent partly because of the mathematical problem of zero division (dry conditions cause an infinite resistance), partly owing to non-neutral stability effects. The first problem may be overcome by aggregating conductances. The second can only be handled on assumptions of spatial variations in stability. Effective exchange coefficients are sensitive to spatial stability distributions but these are not known. Stability effects are only minor in regard to the prediction of momentum flux.

There is general agreement on the blending height as a useful vertical aggregation scale. The blending height varies with the patch size, roughness step change and stability. Below the blending height the local patch effect is dominant. Above the blending height the well-mixed air mass respond to the effective roughness of all patches.

None of the models referenced in the above are developed to take real terrain roughness distributions as input. Only solutions to specific simple landscapes are provided. Conceptual and computational problems seem to limit general

application. The next chapter describes and demonstrates the use of a microscale flux aggregation model capable of treating real terrain roughness distributions in highly heterogeneous landscapes.

7 Satellite data in microscale aggregation

Heterogeneous landscape with patches in the range between 100 m and 10 km is widespread. The atmospheric boundary layer responds significantly to the local heterogeneity of temperature, roughness and humidity. An objective method on how to aggregate the atmospheric response at each roughness step change is useful for upscaling and downscaling fluxes.

The goal of the microscale flux aggregation model by Jensen (1995) is to predict the surface fluxes of momentum and scalars pixel by pixel in heterogenous terrain. Spatial flux data are then sought for the purpose of validation.

The study area for the present project was the Upper Rhine Valley in Germany. An intensive data collection campaign took place in September 1992 within TRACT (Fiedler 1991, Fiedler et al. 1996).

Chapter 7 contains a presentation of the satellite data used. Then follows a mathematical description of the microscale aggregation model (section 7.2) and presentation of results on checkerboard and striped landscapes (section 7.3) and satellite data (section 7.4). The model results are compared to field mast data (section 7.5). Finally are comments on future use (section 7.6) and conclusions drawn (section 7.7).

7.1 Available satellite data

The satellite data available in relation to the TRACT project are 3 Landsat TM scenes recorded in 1993. No cloudless scenes where available in 1992. NOAA AVHRR and Meteosat scenes have a spatial resolution too coarse for the present purpose. Konrad et al. (1994) from a multi-temporal classification produced a classified image separated into 19 cover types with an overall classification accuracy of 81%. An image subset is presented in figure 5.

The ERS-1 satellite was operational during the 1992 field campaign. Four scenes recorded by the SAR scanner have been retrieved. Information on the satellite scenes are given in section 4.5 including table 5. Recently a classified image from 1992 based on ERS-1 SAR data was kindly made available for the present project. The image is a subset of the "Radarkarte Deutschland" produced by Markwitz et al.(1995) from a multi-temporal analysis. There are nine cover classes and the overall classification accuracy is 71%. It is presented in figure 17.

Field data were collected in many cover types by Fiedler et al. (1994). Especially important for the present work are the micrometeorological field data because these provide a good measure of the local roughness. When combining

Rhine Valley, Germany

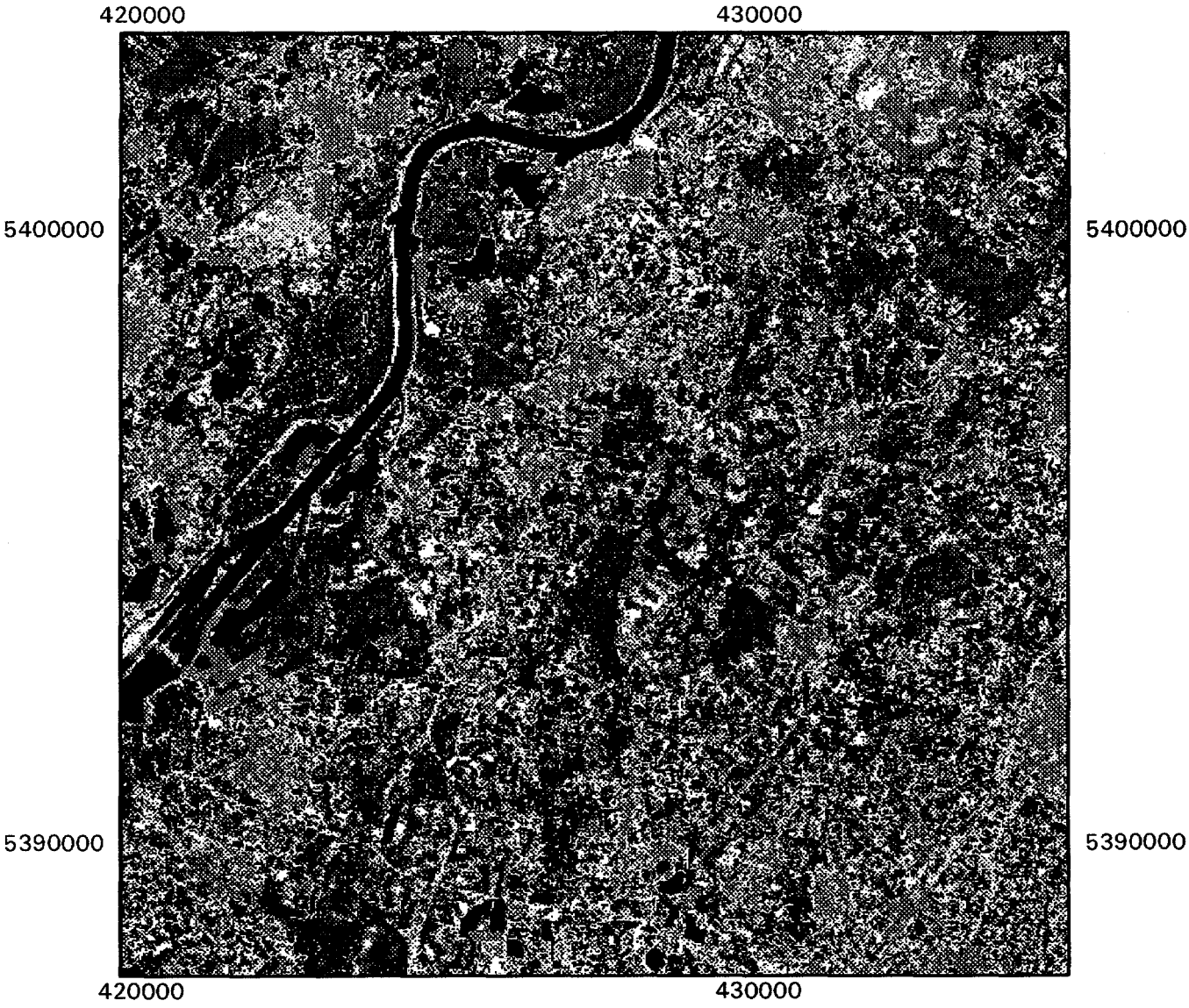

Rougness (m)	Area (km*km)
>= 0.001	94
> 0.01	22
> 0.1	31
> 0.2	53
> 0.9	12
= 1.2	24

Scale

2 0 Kilometers

Landsat TM 1993
Winter

Figure 19.

field and Landsat satellite information we obtain rather accurate roughness maps for a region roughly 100 km * 100 km with a 30 m * 30 m resolution. Based on ERS we obtain maps for a region of 15 km * 15 km with a 25 m * 25 m resolution.

The roughness values assigned to the classified scenes represent two cases, summer and winter conditions. The winter roughness maps were produced bearing in mind traditional crop practices in Germany. In total we obtained four roughness maps. They represent conditions of Summer 1992 (ERS), Winter 1992 (ERS), Summer 1993 (Landsat) and Winter 1993 (Landsat) in the Upper Rhine Valley. Subsets of the roughness maps are presented in figure 33, 34, 6 and 19, respectively. The maps are used as input in the microscale flux aggregation model decribed next.

7.2 The microscale aggregation model

The prognostic microscale aggregation model was developed by Jensen (1995). It was first presented orally (Jensen 1994).
The model has been tested and used by Jensen & Mann (1995), Jensen & Frank (1996), Astrup et al. (1996) and Jensen et al. (1996). Preliminary results with input of satellite data have been presented orally (Hasager & Jensen 1996a, Hasager & Jensen 1996b).

The aggregation model is useful for aggregating the surface fluxes from microscale up to mesoscale. So for larger regions a mesoscale model then should be run with input from the microscale model.

The atmospheric flow equations (equations of motion eg Stull 1991) are simplified such that only the advective term and the diffusive term persist. The equations solved are hence for the conservation of momentum (Newton's second law).

$$\bar{u}\frac{\partial u'}{\partial x}+\bar{v}\frac{\partial u'}{\partial y} = K_x\left(\frac{\partial^2 u'}{\partial x^2}+\frac{\partial^2 u'}{\partial y^2}\right)+K_z\frac{\partial^2 u'}{\partial z^2} \qquad (122)$$

$$\bar{u}\frac{\partial v'}{\partial x}+\bar{v}\frac{\partial v'}{\partial y} = K_x\left(\frac{\partial^2 v'}{\partial x^2}+\frac{\partial^2 v'}{\partial y^2}\right)+K_z\frac{\partial^2 v'}{\partial z^2} \qquad (123)$$

The flow equations are linearized in the advective term such that the nonlinearity originating from $u=\bar{u}+u'$ and $v=\bar{v}+v'$ are neglected. K_x and K_z are turbulent exchange coefficients in the horizontal and vertical.

The conservation of mass (the continuity equation) is approximated to incompressible flow. The mean flow is assumed to be uniform. There is no divergence. $\bar{w}=0$ at the surface and since the flow is uniform $\bar{w}=0$ everywhere. The continuity equation is only written for the turbulent fluctuations

$$\frac{\partial u'}{\partial x}+\frac{\partial v'}{\partial y}+\frac{\partial w'}{\partial x} = 0 \tag{124}$$

The Coriolis effect (rotation), the gravitational effect (vertical motion) and the pressure perturbation (pressure-gradient) are assumed to be very small in regard to surface roughness changes and are therefore neglected. Pressure perturbations caused by changing surface roughnesses are very small (second order) and buoyancy effects are small (Jensen 1981).

The flow is assumed to be stationary and neutrally stratified. The Fourier space representation for u´ is given as

$$u'(x,y,z) = \int_{-\infty}^{\infty}\int_{-\infty}^{\infty} \hat{u}(k,l,z)e^{i(kx+ly)}dkdl \tag{125}$$

where $\hat{u}$ is the Fourier transform of u´. Likewise $\hat{v}$ is the Fourier transform of v´ and $\hat{w}$ of w´. k and l are wavenumbers.

Before expressing eqs 122-124 in Fourier space u´, v´ and w´ have to be differentiated twice with respect to x, y and z. The formulas are written for u'

$$\frac{\partial u'}{\partial x} = \int_{-\infty}^{\infty}\int_{-\infty}^{\infty} ik\hat{u}e^{i(kx+ly)}dkdl \tag{126}$$

$$\frac{\partial u'}{\partial y} = \int_{-\infty}^{\infty}\int_{-\infty}^{\infty} il\hat{u}e^{i(kx+ly)}dkdl \tag{127}$$

$$\frac{\partial u'}{\partial z} = \int_{-\infty}^{\infty}\int_{-\infty}^{\infty} \frac{\partial}{\partial z}\hat{u}e^{i(kx+ly)}dkdl \tag{128}$$

$$\frac{\partial^2 u'}{\partial x^2} = -\int_{-\infty}^{\infty}\int_{-\infty}^{\infty} k^2\hat{u}e^{i(kx+ly)}dkdl \tag{129}$$

$$\frac{\partial^2 u'}{\partial y^2} = -\int_{-\infty}^{\infty}\int_{-\infty}^{\infty} l^2\hat{u}e^{i(kx+ly)}dkdl \tag{130}$$

$$\frac{\partial^2 u'}{\partial z^2} = \int_{-\infty}^{\infty}\int_{-\infty}^{\infty} \frac{\partial^2}{\partial z^2}\hat{u}e^{i(kx+ly)}dkdl \tag{131}$$

Equations for v´ and w´ are similar.

In Fourier space eqs 122 and 124 hence become

$$\int_{-\infty}^{\infty}\int_{-\infty}^{\infty}[\bar{u}ik\hat{u}+\bar{v}il\hat{u}-K_x(-k^2\hat{u}-l^2\hat{u})-K_z\partial^2\frac{\hat{u}}{\partial z^2}]e^{i(kx+ly)}dkdl = 0 \quad (132)$$

$$\int_{-\infty}^{\infty}\int_{-\infty}^{\infty}[\bar{u}ik\hat{v}+\bar{v}il\hat{v}-K_x(-k^2\hat{v}-l^2\hat{v})-K_z\partial^2\frac{\hat{v}}{\partial z^2}]e^{i(kx+ly)}dkdl = 0 \quad (133)$$

Eqs 132 and 133 have to be satisfied for arbitrary $\bar{u}$, $\bar{v}$, K_x, K_z and every wavenumber pair (k,l). Therefore the terms inside the square brackets have to be zero. When rewriting eqs 132 and 133 we obtain

$$K_z\frac{\partial^2\hat{u}}{\partial z^2}-(K_x(k^2+l^2)+(i(k\bar{u}+l\bar{v}))\hat{u} = 0 \quad (134)$$

$$K_z\frac{\partial^2\hat{v}}{\partial z^2}-(K_x(k^2+l^2)+(i(k\bar{u}+l\bar{v}))\hat{v} = 0 \quad (135)$$

Note the similarity for $\hat{u}$ and $\hat{v}$. With the notation from Jensen and Frank (1996) $k_h^2=k^2+l^2$. Hence $|k_h|$ is the magnitude of the wave, and $\vec{k}_h=\{k,l\}$ a wave vector. The wind vector is $\vec{U}=\{\bar{u},\bar{v}\}$. The angle between $\vec{k}_h$ and $\vec{U}$ is called γ. So from this

$$\vec{k}_h\vec{U} = |\vec{k}_h||\vec{U}|\cos(\gamma) = k\bar{u}+l\bar{v} \quad (136)$$

In figure 20 is a sketch of the situation in one pixel.

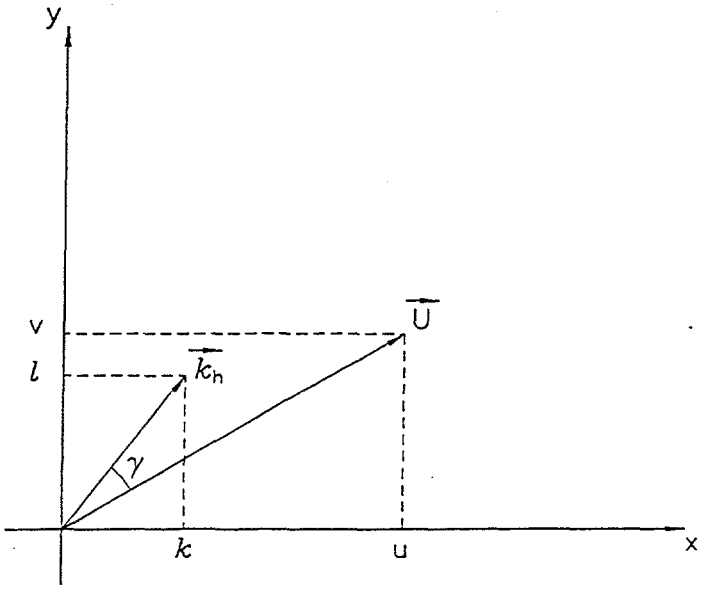

Figure 20. A display of the wind vector $\vec{U}$ and wavenumber vector $\vec{k}_h$ in one pixel. The angle between the vectors is γ. u and v are wind speeds. k and l are wavenumbers. Please refer to the text on the microscale model.

If eqs 134 and 135 are combined into one equation valid for the response in the direction of the mean flow we have

$$K_z \frac{\partial^2 \hat{u}}{\partial z^2} = (i\vec{k}_h \vec{U} + K_x k_h^2)\hat{u} \tag{137}$$

The general solution to a second-order differential equation with constant coefficients is of the form

$$\hat{u}(k,l,z) = C(k,l)e^{\alpha z} \tag{138}$$

α has two roots, a positive and a negative. The negative root is

$$\alpha = -\sqrt{((i\vec{k}_h \vec{U} + K_x k_h^2)/K_z)} \tag{139}$$

Only the negative root has physical meaning as perturbations decay exponentially through the atmosphere. It is assumed that the diffusivities K_x and K_z are independent of height. The boundary condition determines C(k,l).

It is a simplification to say K_z is independent of height but used as a working hypothesis. As will later be shown it seems to be acceptable from model results obtained.

7.2.1 Boundary condition and solution

The boundary condition for the microscale aggregation model is based on similarity theory for the surface boundary layer. Below the computational level, z_r, the flow is assumed to be in equilibrium with the local patch. The surface roughness is given as a digital map with values of $z_0(x,y)$.

The simple average of the roughness map, z_{0a}, valid only for equilibrium flow (no advective effects) is

$$\ln z_{0a} = \sum_{x=1}^{n_1} \sum_{y=1}^{n_2} \frac{\ln(z_0(x,y))}{n_1 * n_2} \tag{140}$$

where n_1 and n_2 are the numbers of rows and columns (see eq 98).

The roughness lengths may be expressed as perturbations, m(x,y) (-) from the logarithmic average in each pixel

$$\ln(z_0(x,y)) = \ln(z_{0a}) + m(x,y) \tag{141}$$

The roughness perturbation map is hence given as

$$m(x,y)=\ln(\frac{z_0(x,y)}{z_{0a}}) \tag{142}$$

The roughness perturbation map quantifies the friction generated by the numerous obstacles in the physical domain. The roughness changes are felt from heights of the order of $L_x/80$ up to $L_x/200$, where L_x is a typical horizontal patch size. So the computational level, z_r, has to be chosen within these limits. This means that for a mean patch size $\sim$100 m, z_r has to be $\sim$1-5 m, but for L_x $\sim$500 m, z_r has to be $\sim$6-25 m.

In a homogeneous landscape with a roughness of $z_0=z_{0a}$, a mean friction velocity, u_{*0}, will be found. In an inhomogeneous landscape with the same average roughness of z_{0a} but with spatial changes in $z_0(x,y)$, the roughness variations will generate spatial changes in $u_*(x,y)$. Owing to nonlinear effects the spatial mean of the friction velocity will *not* sum to u_{*0}.

Below z_r the logarithmic profile is assumed to be valid so

$$\bar{u}(x,y,z_r)+u'(x,y,z_r) = \frac{u_{*0}+\Delta u*(x,y,z_r)}{\kappa}\ln(\frac{z_r}{z_0(x,y)}) \tag{143}$$

Δu_* is the perturbation friction velocity. When the roughness perturbation map and the logarithmic profile for mean wind (eq 5) are included, eq 143 becomes

$$\frac{u_{*0}}{\kappa}\ln(\frac{z_r}{z_{0a}})+u'(x,y,z_r) = \frac{u_{*0}+\Delta u*(x,y,z_r)}{\kappa}[\ln(\frac{z_r}{z_{0a}})-m(x,y)] \tag{144}$$

As eq 144 holds a multiplicative term, the equation has to be linearized before a solution in Fourier space is available. If eq 144 is expanded and the small term $\Delta u_*(x,y,z_r)*m(x,y)$ is neglected, this will results in

$$u'(x,y,z_r) = \frac{\Delta u_*(x,y,z_r)}{\kappa}\ln(\frac{z_r}{z_{0a}})-\frac{u_{*0}}{\kappa}m(x,y) \tag{145}$$

In the effort to express $\Delta u_*(x,y,z_r)$ on linear form, the stress perturbation equation

$$\tau=\tau_0+\Delta\tau=\rho(u_{*0}+\Delta u_*)^2\approx u_{*a}^2+2u_{*0}\Delta u_* \tag{146}$$

is first approximated to a form where $\Delta\tau(x,y,z_r)\sim 2u_{*0}\Delta u_*(x,y,z_r)$ and from this linearized.

Hence in physical space eq 145 is

$$u'(x,y,z_r)=\frac{\Delta\tau(x,y,z_r)}{2u_{*0}\kappa}\ln(\frac{z_r}{z_{0a}})-\frac{u_{*0}}{\kappa}m(x,y) \tag{147}$$

and the equivalent in Fourier space is

$$\hat{u}(k,l,z_r)=\frac{\Delta\hat{\tau}(k,l,z_r)}{2u_{*0}\kappa}\ln(\frac{z_r}{z_0})-\frac{u_{*0}}{\kappa}\hat{m}(k,l). \tag{148}$$

Here the Fourier transform of the perturbation map, $\hat{m}(k,l)$, enters the model. $\hat{m}(k,l)$ is determined by

$$m(x,y)=\int_{-\infty}^{\infty}\int_{-\infty}^{\infty}\hat{m}(k,l)e^{i(kx+ly)}dkdl \tag{149}$$

$\Delta\hat{\tau}(k,l,z)$ is the Fourier transform of $\Delta\tau(x,y,z)$.

The stress is given by

$$\tau=\tau_0+\Delta\tau=K_z(\frac{\partial\overline{u}}{\partial z}+\frac{\partial u'}{\partial z}) \tag{150}$$

So $\Delta\tau$ equals

$$\Delta\tau=K_z\frac{\partial u'}{\partial z}. \tag{151}$$

which in Fourier space is

$$\Delta\hat{\tau}=K_z\frac{\partial\hat{u}}{\partial z}, \tag{152}$$

Then to determine the solution of eq 152 the differentiated form is needed.

A result is available. Differentiation of eq 138 once gives

$$\frac{\partial\hat{u}}{\partial z}=\alpha C(k,l)e^{\alpha z}. \tag{153}$$

So $\Delta\hat{\tau}$ equals

$$\Delta\hat{\tau}(k,l,z_r)=K_z\alpha C\ (k,l)e^{\alpha z_r} \tag{154}$$

When eq 154 is inserted into eq 148 and C(k,l) is isolated we obtain

$$C(k,l)=\frac{\hat{u}(k,l,z_r)+\frac{u_{*0}}{\kappa}\hat{m}(k,l)}{\ln(\frac{z_r}{z_{0a}})\frac{K_z}{2u_{*0}\kappa}\alpha\ e^{\alpha z_r}} \tag{155}$$

Next C(k,l) is inserted into eq 138

$$\hat{u}(k,l,z_r)=\frac{\hat{u}(k,l,z_r)+\frac{u_{*0}}{\kappa}\hat{m}(k,l)}{\ln(\frac{z_r}{z_0})\frac{K_z}{2u_{*0}\kappa}\ \alpha e^{\alpha z_r}}e^{\alpha z_r} \tag{156}$$

and when eq 156 is rearranged the explicit solution for $\hat{u}(k,l,z_r)$ is found to be

$$\hat{u}(k,l,z_r)=\frac{-\frac{u_{*0}}{\kappa}\hat{m}(k,l)}{1-\frac{\alpha K_z}{2\kappa u_{*0}}\ln(\frac{z_r}{z_{0a}})} \tag{157}$$

Now α is reintroduced from eq 139 and it is assumed that $K_z=\kappa u_{*0}z_r$. This gives a final equation of the Fourier mode of the velocity perturbation $\hat{u}(k,l,z_r)$ namely

$$\hat{u}(k,l,z_r)=-\frac{u_{*0}}{\kappa}\hat{m}(k,l)\frac{1}{\sqrt{(i\vec{k}_h\vec{U}+K_x k_h^2)/K_z}*\frac{z_r}{2}\ln\frac{z_r}{z_{0a}}} \tag{158}$$

The Fourier mode of the velocity perturbation is being calculated for each pixel.

The magnitude and horizontal pattern of the real velocity response, u'(x,y), owing to roughness inhomogeneity in the terrain is found by the inverse Fourier transform of $\hat{u}(k,l,z_r)$.

The inverse Fourier transform (back transform) is

$$u'(x,y,z_r)=\frac{1}{4\pi^2}\int_{-\infty}^{\infty}\int_{-\infty}^{\infty}\hat{u}(k,l,z_r)e^{-i(kx+ly)}dkdl \tag{159}$$

In the microscale aggregation model u_* is now calculated pixelwise from

$$u_*=\frac{\kappa(U+u'(x,y,z_r))}{\ln(\frac{z_r}{z_0(x,y)})} \tag{160}$$

and finally $<u_*>$ is calculated from

$$u_* = \sqrt{\frac{1}{n_1 n_2} \sum_{x=1}^{n_1} \sum_{y=1}^{n_2} u_*^2(x,y)} \qquad (161)$$

The mean momentum flux is obtained by simple averaging of $u_*^2(x,y)$ whereas $<u_*>$ is the square root of the summed $u_*^2(x,y)$.

7.3 Two-dimensional testing

Testing of the model is vital. In a one-dimensional mode this was done successfully by Jensen (1995) and Astrup et al. (1996). The tests were based on available field data of the response of the shear stress after a step change in roughness. The microscale model results fit very well to the data collected by Bradley (1968) and higher-order flow models (Peterson 1969, Rao et al. 1974).

Testing of the model in two-dimensions is not as straightforward since a good data set is not readily available. Therefore artificial surface types were calculated and used as input. The results are compared in qualitative terms.

Checkerboard and striped landscapes were produced. To obtain results of interest for the present project it was decided to use input data representative for the Rhine Valley area. The chosen parameter limits are given in list form in table 6.

Roughness length	$z_0(x,y)$	0.001 - 1 m
Turbulent exchange coefficient ratio	K_x/K_z	1.0 - 2.3
Patch size	L_p	30 - 3840 m
Domain length	L_d	1920 -7680 m
Grid resolution (pixels)		64^2 - 512^2
Wind direction		0 - 90°
Computational level	z_r	1.5 - 30.0 m

Table 6. Two-dimensional test run parameters for the microscale flux aggregation model.

Only square domains were used. This means that for a domain of 7680 m, the results are calculated for an area of 7680 m * 7680 m (~59 km^2). From Fourier analysis on real terrain data it was found that the mean (typical) length scale in the summer roughness map is 650 m (figure 6). However a large range of scales are present. L_p was varied from the resolution the Landsat TM data (ie 30 m) up to 3840 m.

The model results obtained are $<u_*>$ and $<z_0>$. The values are compared to

u_{*0} and z_{0a}. All test runs are on domains with a 50-50% cover distribution except in the investigation on fractional coverage where the domains were varied between zero and 100%.

Two-dimensional test results

First results from a checkerboard terrain with varying z_0 and L_p are presented. z_0 is varied is steps of 0.001, 0.01, 0.1 and 1 m. L_p is varied from 30 to 3840 m. The domain is 7680 m, z_r 10 m, K_x/K_z 1, U 5 m s^{-2} from the west and the resolution 256 pixels. The result of $<u_*>/u_{*0}$ is shown in figure 21. It is clear that the largest ratio of $<u_*>/u_{*0}$ arises in connection with the largest magnitude in roughness change, namely $M=\pm 6.9$ (eq 92). Also it is clear that the ratio $<u_*>/u_{*0}$ increases with decreasing size of the patches, L_p.

Figure 21a also shows that $<u_*>/u_{*0}$ is not only a function of M and L_p/L_d but also depends on z_{0a}. The results show that the rougher terrain yields a larger response for a constant M. In terrain with very large patches, $<u_*>/u_{*0}$ naturally goes to 1, but this is clearly not reached within a domain of the order of 4 km. The advective effect is significant.

Figure 21b presents the results of $<z_0>/z_{0a}$ for the same runs as in figure 21a. Large M, of course, yields the largest ratio. But note that the curves for $M=\pm 2.3$ are close. It here seems that M separates the responses rather than the absolute values of z_0. Simulations by Schmid and Bunzli (1995) of a mixing-length model yielded similar results. A calculation of z_{0a} for each checkerboard yields (top-down): 0.0316, 0.1, 0.01, 0.316, 0.0316, 0.00316 m, respectively.

The computational level was kept constant at $z_r=10$ m. The results in figure 21 need consideration of the ratio z_r/z_{0a}. The larger this ratio, the less affected is the flow. The ratio of z_r/z_{0a} was (top-down): 316, 100, 1000, 32, 316, 3165), respectively. Next the influence of varying z_r/z_a is investigated.

Results are shown in figure 22 from a checkerboard with $z_{0a}=0.0316$ m (z_0 0.001 and 1 m). L_p is taken as 240, 480 and 960 m, U=5 m s^{-1} from the west, $K_x/K_z=1$, $L_d=7680$ m and a resolution of 256 pixels. z_r is varied so that the dependence of $<u_*>/u_{*0}$ on z_r/z_{0a} became clear. The results are as expected. For z_r close to z_{0a} the ratio $<u_*>/u_{*0}$ achieves a maximum. A similar trend is found for the ratio $<z_0>/z_{0a}$ (not shown). Figure 22 also shows that the smaller patches have a larger response than larger patches for a given z_r/z_{0a}. However at z_r/z_{0a} around 500 the flow seems to be independent of the patch size. This leads to a consideration of the blending height, or rather the height below which the flow seems to respond to a given patch.

The blending height is determined as a height where the change in surface stress balances the advective velocity perturbation. An approximation to eq 97 is

$$l_b=0.3\ z_{0a}^{1/3} L_p^{2/3} \qquad (162)$$

(Jensen et al. 1984). Figure 23 shows curves of l_b calculated from eq 162. Naturally it grows downwind. For comparison a curve of the growth of the IBL is included in figure 23. δ_i is calculated from eq 164.

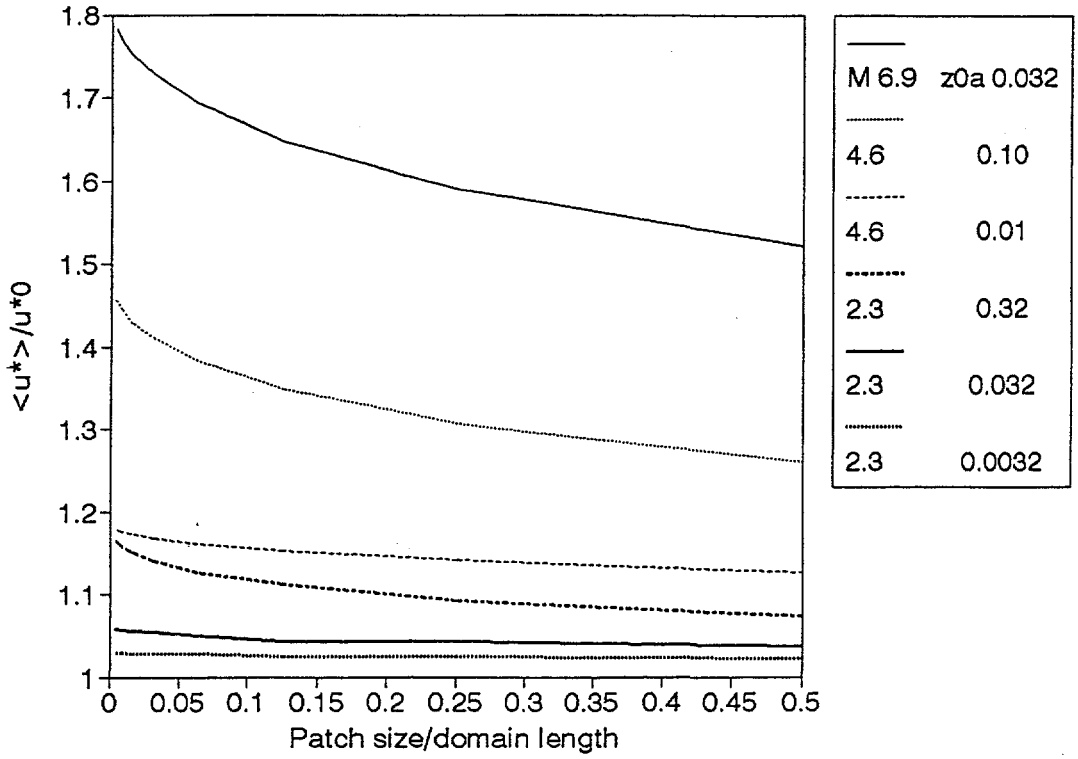

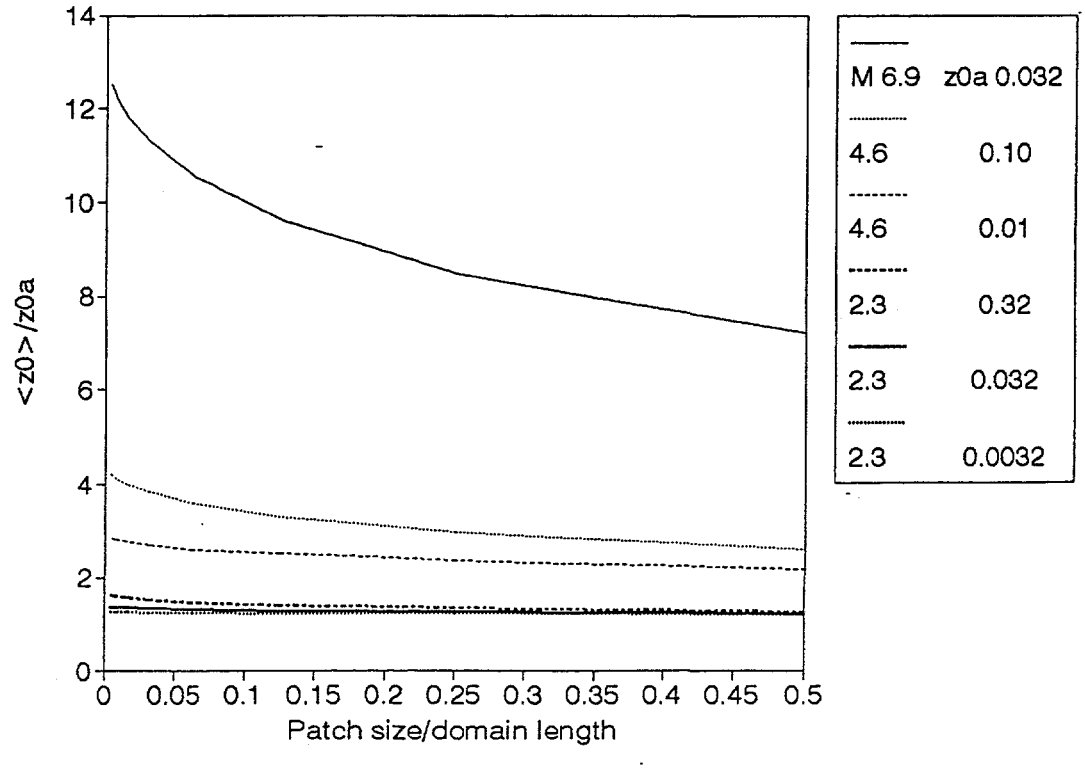

Figure 21 a) Microscale model results of normalized friction velocity as a function of step change frequency and magnitude of roughness step change M. L_d=7680 m, z_r=10 m, K_x/K_z=1, 256 pixels and U=5 m s^{-1}. b) as for a but normalized effective roughness.

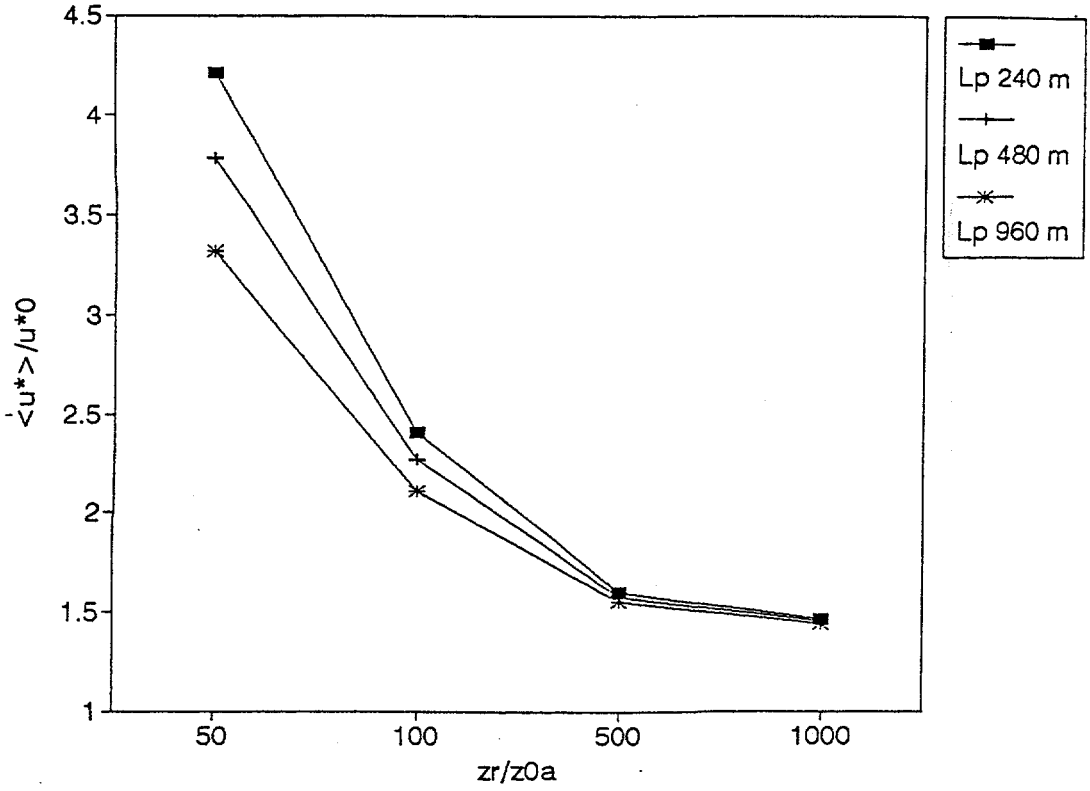

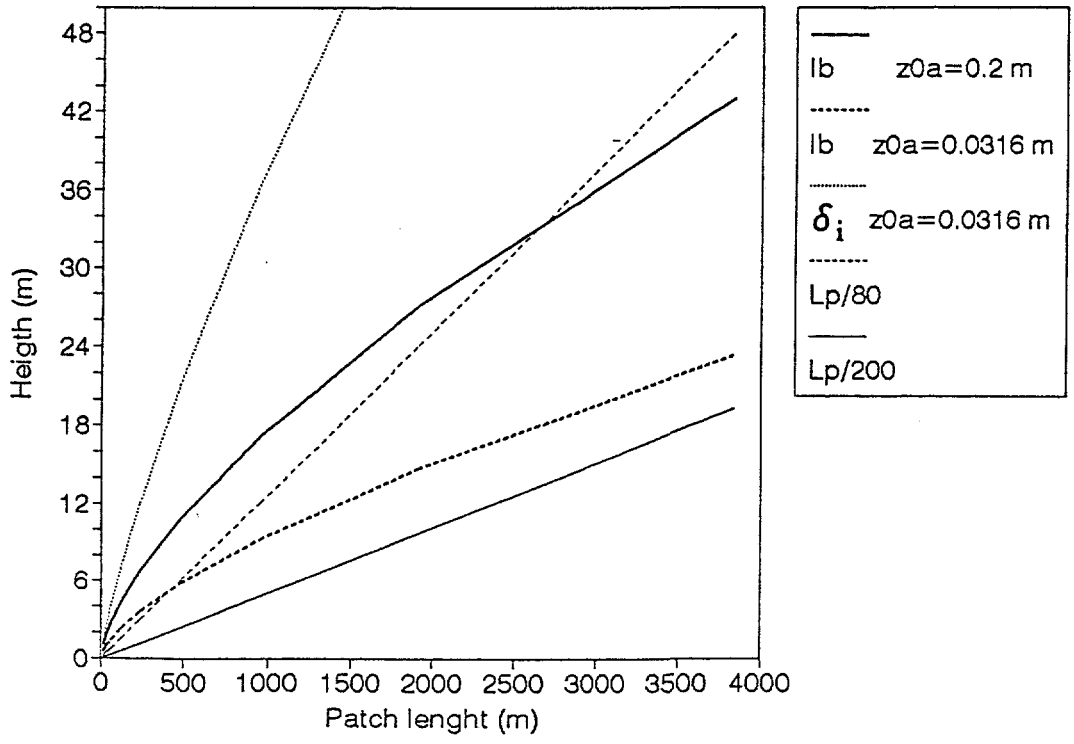

Figure 22. (above) Microscale model results of normalized friction velocity as a function of computational level and patch size, L_p for z_{0a}=0.0316 m (0.001 and 1 m), U=5m s^{-1}, K_x/K_z=1, L_d=7680 m and 256 pixels.

Figure 23. (below) Internal boundary layer growth (δ_i) and blending height (l_b) for two value of z_{0a}. Lines of Lp/80 and Lp/200. L_p is the patch size.

δ_i is the height above ground where a kink in the velocity profile is conceived. Jensen et al. (1984) suggest for IBL growth under neutral conditions

$$\delta_i \ln(\frac{\delta_i}{z_{0a}}) = 0.3 L_p \tag{163}$$

and approximate eq 163 with a power law

$$\delta_i = 0.3 z_{0a}^{1/5} L_p^{4/5} \tag{164}$$

The power law expressions are valid only for limited ranges. Obviously l_b is less than δ_i. l_b is seen to be well within the IBL in figure 23. Equation 109 from Claussen (1990) would follow δ_i closely.

Very simple estimates of l_b are $L_p/200$ (Mason 1988) and $L_p/80$ (Jensen 1995). These straight lines are included in figure 23. They are only crude guidelines. Generally spoken horizontal and vertical length scales are related, and the response at z_r is strongly dependent on the size of L_p. In their appendix Wood and Mason (1991) give the validity range of the heuristic blending height method as $z_0 << z_r << \delta_i$. The same is true in the present model.

A very different aspect of the model needs consideration. How is the model performance when the patch size resolution is close to the pixel resolution? Results from the test runs are shown in figure 24a. The runs are for a checkerboard with $z_{0a}=0.0316$ m (z_0 0.001 and 1 m), $U=5$ m s^{-1} from the west, $z_r=5$ m, $K_x/K_z=1$, $L_d=3840$ and L_p varies between 60 and 1920 m. The resolution varies between 64^2 and 512^2 pixels. In the "worst case" 1 pixel equals one patch and is compared to 8^2 pixels for the same patch of size 60 m * 60 m, whereas in the "best case" 32^2 pixels map one patch and is compared to 256^2 pixels for the same patch of size 1920 m * 1920 m.

Figure 24a shows $<u_*>/u_{*0}$ to be slightly smaller for the coarse resolutions. Hence the bias is negative. The relative error owing to resolution is calculated from

$$\frac{true-value}{true} * 100\% \tag{165}$$

on the assumption that the response results from the high (512) resolution are "true". Figure 24b shows that the relative error is less than 1% in all cases and of the order of 0.1% for the 256 resolution. Important is that satellite data with pixel resolutions of the same order as a typical patch is expected not to bias the flux results significantly.

Wind direction is important in natural landscapes as well as in checkerboard terrain. The surface roughness changes along checkerboard rows are different from those of angular tracks. The simple geometry of a checkerboard means that only a 45° sector needs investigation. Parallel to rows is 0 degrees and diagonal 45°. From figure 25 it is clear that $<u_*>/u_{*0}$ decreases as the wind approaches the diagonal. The reason is that near-diagonal flow traverses approximately homogeneous stripes (where corners meet). So relatively smooth

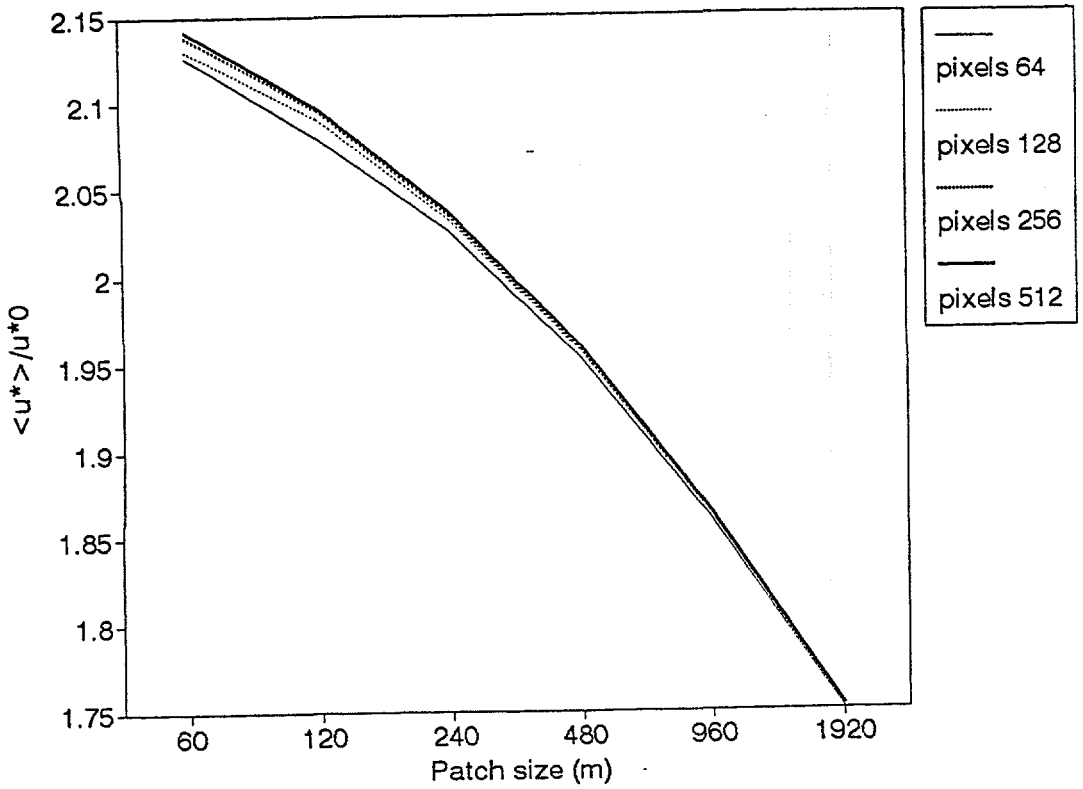

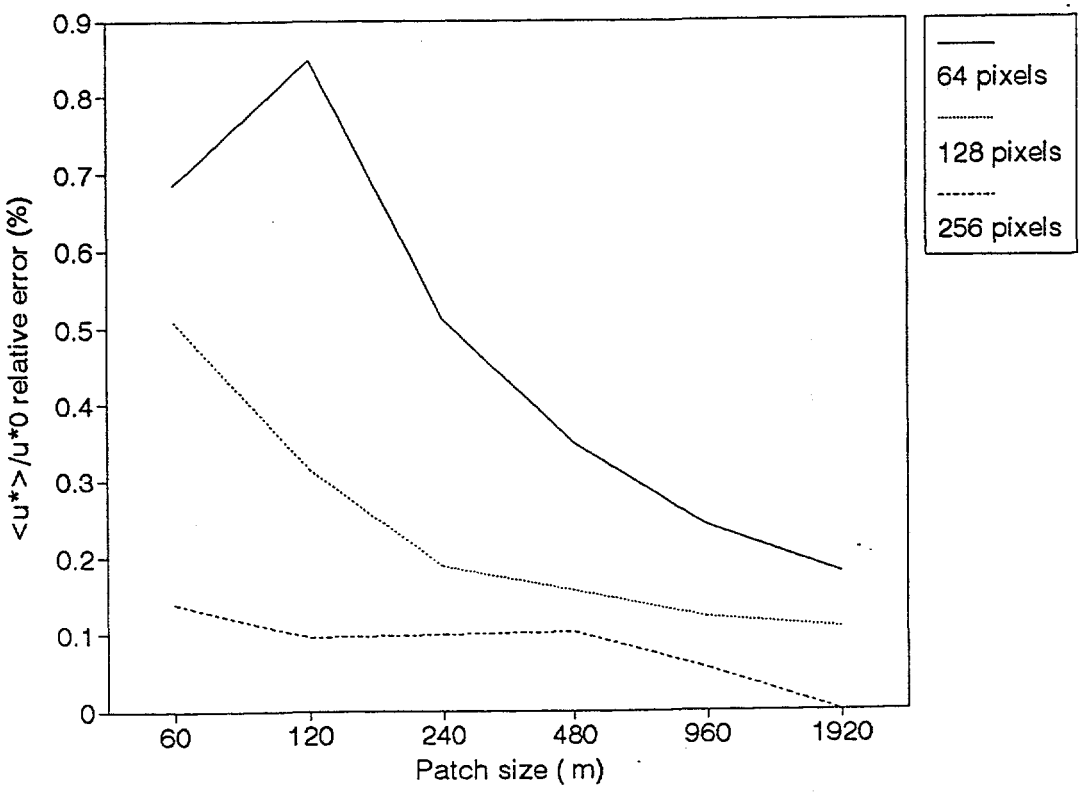

*Figure 24 a) (above) Microscale model results of normalized friction velocity as a function of patch size and pixel resolution. z_{0a}=0.0316 m (0.001 and 1 m), z_r=5 m, U=5m s^{-1}, K_x/K_z=1 and L_d=3840m. b) (below) as above but relative to the highest resolution 512*512*

tracks interchange with relatively rough tracks. The checkerboard has z_{0a}=0.0316 m (z_0 of 0.001 and 1 m), z_r=5 m, 256 pixels, L_d=3840 m and U=5 m s^{-1}. L_p is varied between 30 and 960 m, and K_x/K_z between 1 and 2. Model results for K_x/K_z= 1 and 2 are shown together in figure 25. For L_p=30 m it is clear that flow with K_x/K_z=1 is more sensitive to wind direction than flow with K_x/K_z=2. The ratio of K_x/K_z determines the width of lateral upwind area effectively traversed ("seen"). For L_p=480 m and 960 m no lateral diffusion effect is noted. In order to more fully appreciate the effect of horizontal diffusion and angular effects some striped terrain surfaces are generated.

Unfortunately the reported values of the ratio K_x/K_z are too low as eq 166 in corrected form gives K_x/K_z=23.

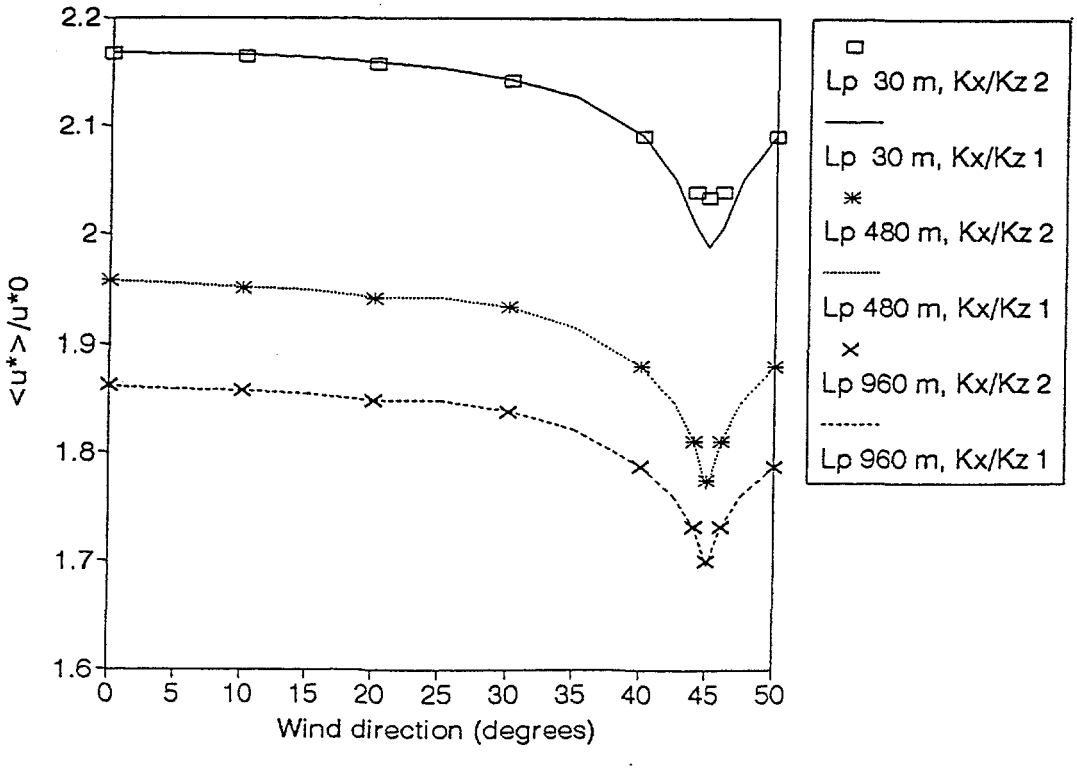

Figure 25. (above) Microscale model results of normalized friction velocity as a function of wind direction and diffusivity in a checkerboard terrain. z_{0a}=0.0316 m, 256 pixels, z_r=5 m, U=5m s^{-1} and L_d=3840 m.

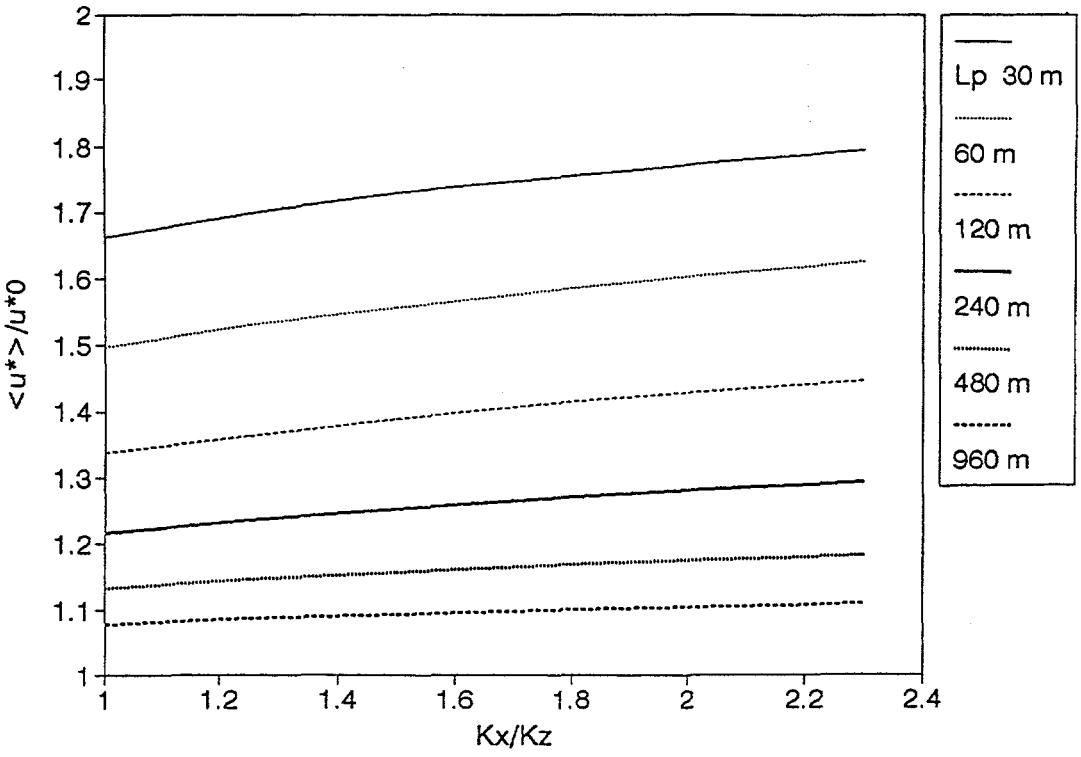

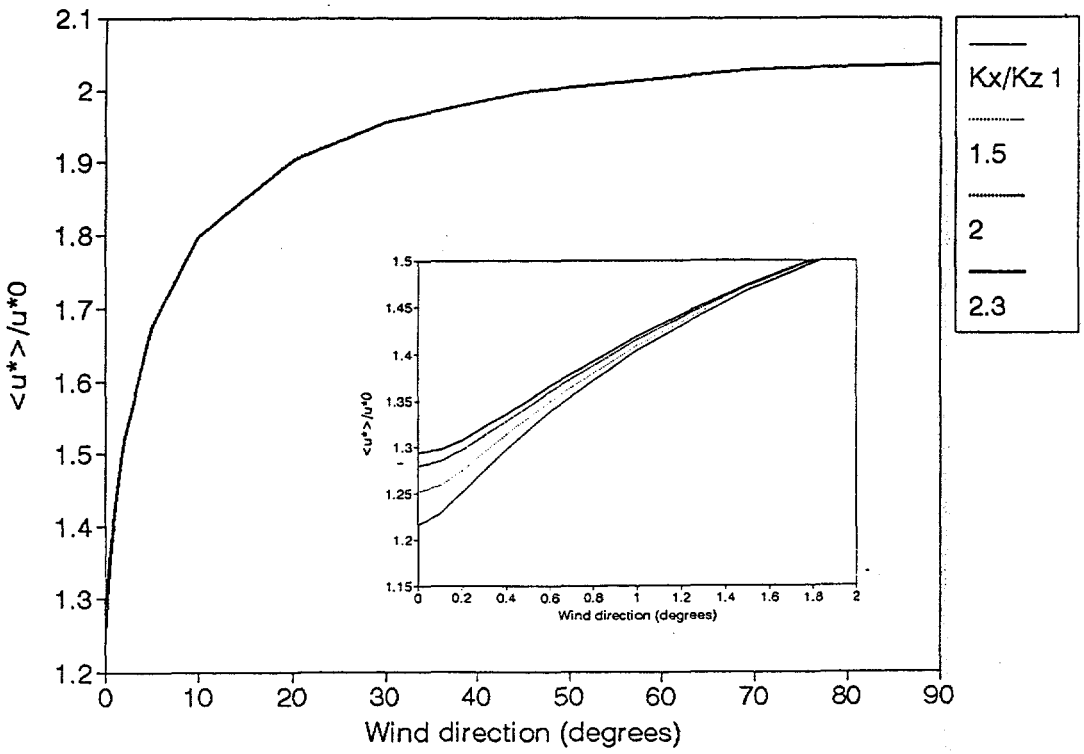

Figure 26. (above) Microscale model results of normalized friction velocity as a function of diffusivity and stripe width (L_p). z_r=5 m, U=5 m s^{-1}, 256 pixels, z_{0a}=0.0316 m and L_d=3840 m.

Figure 27. (below) Normalized friction velocity as a function of wind direction and with $L_{p=240\,m}$. The inner bow shows an enlargement of the 0-2° bin. Other conditions as figure 26.

The ratio K_x/K_z should be chosen from general wind statistics on horizontal and vertical flow that show (Busch 1973)

$$\frac{K_x}{K_z} \approx \frac{\sigma_u l_x}{\sigma_w l_z} \approx \frac{2.5 u_* 10 l_z}{1.2 u_* l_z} \tag{166}$$

Horizontal diffusion affects the effective shear stress. The vertical lenght scale l_z could be approximated to height z.

The striped terrain is given with z_{0a}=0.0316 m (z_0 of 0.001 and 1 m), z_r=5 m, 256 pixels, U=5 m s^{-1}, L_d=3840 m and variable L_p between 30 and 960 m. $<u_*>/u_{*0}$ is presented as a function of K_x/K_z for various values of L_p (here stripe width) in figure 26. The wind direction is parallel to the stripes. The largest effect is seen for narrow stripes, and most pronounced for flow with a large horizontal diffusion component. Narrow stripes effectively include more roughness changes than broader stripes, therefore the increase of $<u_*>$ is larger. For K_x=2.3*K_z more roughness changes are "seen" than for $K_x=K_z$. This explains why $<u_*>/u_{*0}$ is larger for a large horizontal turbulent exchange coefficient. A value of K_x=23*K_z would be a more natural choice according to the *corrected form of eq 166* but has not been used in this report (but will be in future work).

Another series of test runs on striped terrain is performed with L_p=240, variable K_x/K_z and variable wind direction within a 90 degree sector. Other parameters are set as in figure 26. The idea is to show the very pronounced effect on $<u_*>/u_{*0}$ for flow perpendicular compared to parallel. Figure 27 show that $<u_*>/u_{*0}$ is nearly constant within the 45-90° bin (note that perpendicular equals 90° and parallel to stripes 0°) whereas a large change is clear as the wind direction approaches zero (= parallel to stripes). $<u_*>/u_{*0}$ seems to asymptotically approach zero. However enlargement of the 0-2° bin (graphed in the inserted box) reveals as expected the minimum values to be slightly larger than one. The effect of varying K_x/K_z is similar to the results shown in figure 26.

Fractional cover

Finally are test runs with a variable fractional cover presented. (All the previous test runs were for 50-50% roughness distributions). The rough area is assigned a value of z_0 1 m (eg forest) and the smooth 0.01 m (eg grass) hence M=$\pm$4.6. The results are presented in figure 28. The maximum ratios of $<z_0>/z_{0a}$ are found for 25 % rough cover. It compares reasonably with the 17% reported by Mason and Wood (1991) and 25% reported by Schmid and Bunzli (1995). Schmid and Bunzli by a mixing-length model calculated the ratio, but they suspect their results to be biased towards too low fractions. They compared their results to k-ϵ model results that show a maximum in $<z_0>/z_{0a}$ around 40 % rough cover.

Schmid and Bünzli (1995) suspect their effective roughness results to be overpredicted. However our test run with L_d=500 m is directly comparable to their figure 2d and the correspondence is good indeed. It is comforting since the mixing-length model has the advantage of the full flow equations whereas the

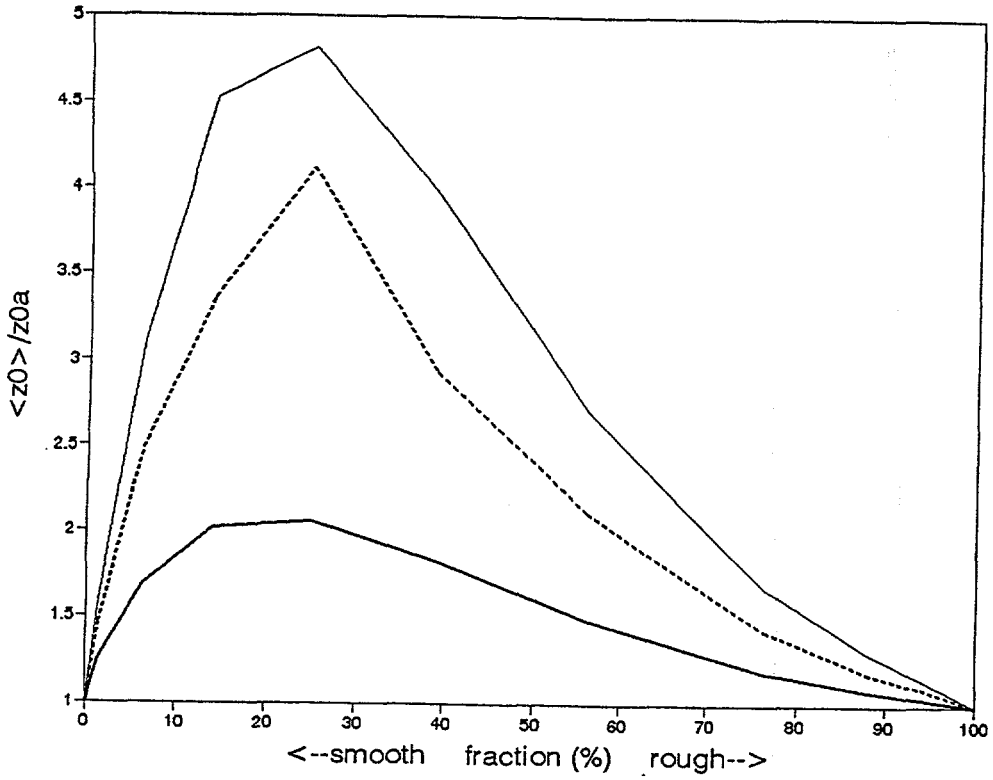

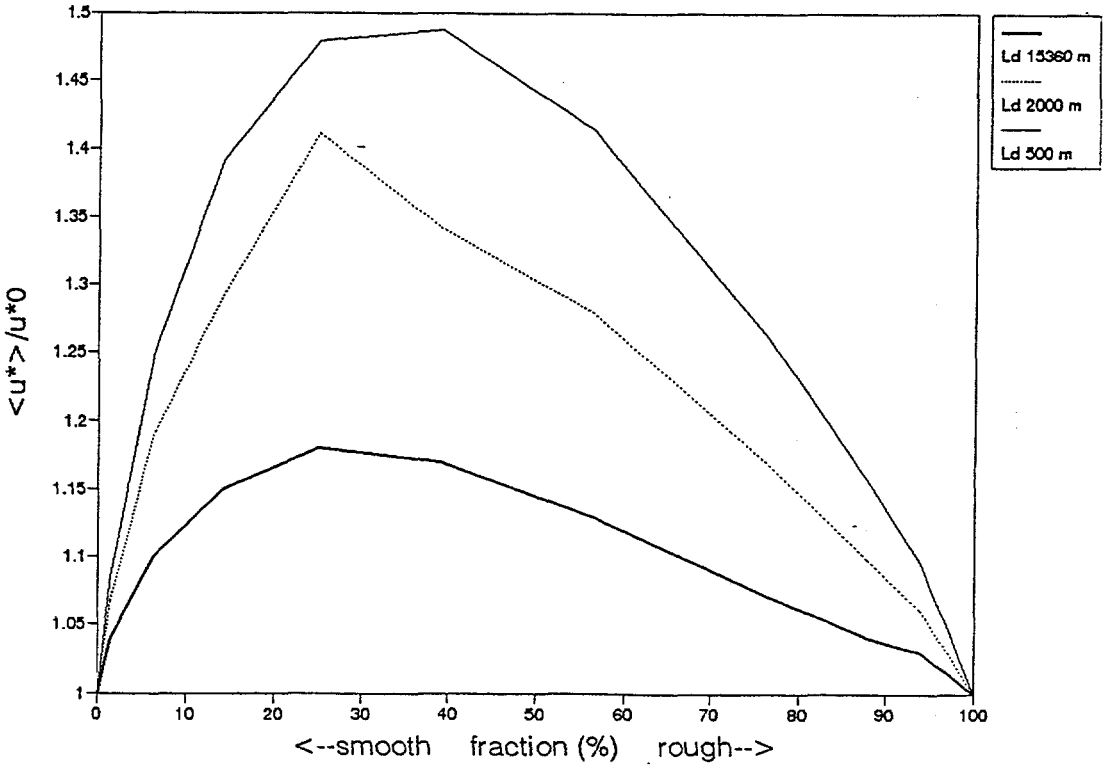

Figure 28 a) above. Normalized effective roughness as a function of fraction roughness cover. Minimum roughness is 0.01 m and maximum 1m. 0% means a smooth and 100% a rough case. b) below. As a) but normalized friction velocity. U=5 m s^{-1}, z_r=5 m, 256 pixels, K_x/K_z=2.

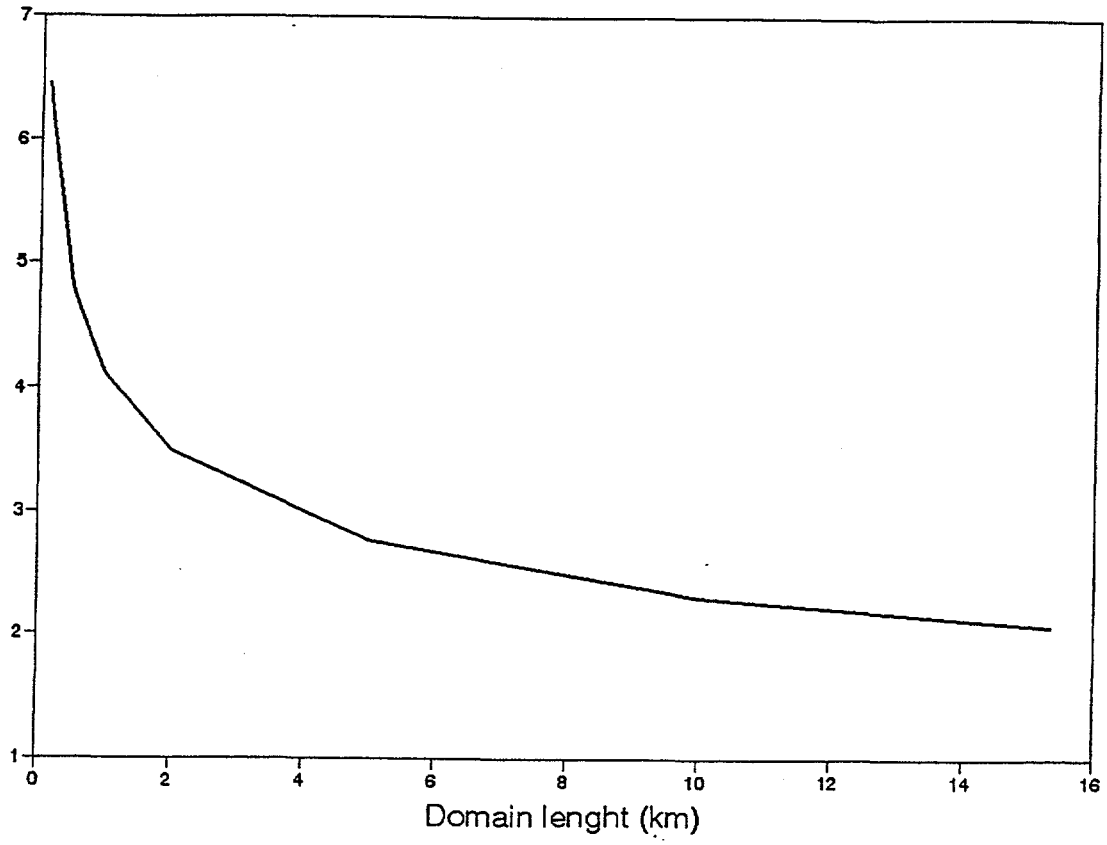

Figure 29. Microscale model results of normalized effective roughness for a 75% cover of 0.01 m and 25% of 1 m as a function of domain length. Other conditions as figure 28.

microscale model is a linearized model. Both models consider the roughness wave length variation. Schmid and Bünzli call it "texture" and quantify it as the frequency of roughness changes. In the microscale model it is quantified explicitely from Fourier spectra. A disadvantage of the Schmid and Bünzli model is that it only offers a solution to terrains of simple geometry of two roughness classes. Their model cannot be used with a real terrain roughness input.

Figure 28b shows the $<u_*>/u_{*0}$ response. Note that the maximum is shifted towards a 50% value compared to $<z_0>/z_{0a}$. The reason is ascribed to the normalization with u_{*0} and z_{0a} respectively. The final test run presentation is given in figure 29. For a 25% rough (z_0=1 m) and 75% smooth (z_0=0.01 m) the patch length is varied between 240m and 15.36 km for U = 5 m s^{-1}, z_r=5 m and K_x/K_z= 2. The results show that the ratio of $<z_0>/z_{0a}$ increases rapidly for domains smaller than 1 km.

Summary on test results

In summary the two-dimensional tests of the microscale model yield values of $<u_*>/u_{*0}$ and $<z_0>/z_{0a}$ within the expected range. Most important is the high sensitivity to patch size. The stress response to wind directional changes as well as to diffusivity changes are evaluated to be within reasonable limits. It is comforting that the microscale results compare well with those from the mixing-length model by Schmid and Bünzli (1995). The advantage of the microscalel model is the option of utilizing arbitrary real terrain roughness data sets.

It is also comforting that no severe bias or numerical problems seem to be present in the microscale model, not even when the pixel size just matches the patch size. This is important for requirements on the spatial resolution of satellite data. The landscape heterogeneity will determine the resolution in need.

7.4 Satellite data results

The classified satellite data from the Rhine Valley, Germany form the necessary basis for a successful application of the microscale flux aggregation model to real terrain. In the current work there is a strong focus on the Landsat TM data because the ERS SAR data were made available only recently. The multi-temporal classification on the Landsat data was performed by Konrad et al. (1994) and of the ERS data by Markwitz et al. (1995) all at the Institut für Photogrammetrie und Fernerkundung, University of Karlsruhe, Germany.

The ERS data are from 1992 and are a subset of the so-called "Radarkarte Deutschland". The Landsat data are from 1993. Field data from the TRACT experiment in September 1992 are analysed (Fiedler 1991, Fiedler et al. 1996). For use in the microscale model roughness values were assigned to all cover classes for summer and winter conditions. For the cover types called "rejected", "others" and "layover" a roughness value close to a logarithmic average of the other classes were used. Presentations of the data are given in figures 5, 6, 17, 19, 33 and 34.

The Rhine Valley area consists of a mixture of agricultural crops and forest interspersed with urban, suburban and industrial areas. Linear features are vaguely visible such as roads and rails between the densely populated areas in the Landsat data. The heterogeneity is very pronounced. The centre pixel is located in a field in Scherzheim. Here a meteorological mast with fast-response eddy-correlation sensors was operated in September 1992 (Barthelmie and Jensen 1995).

The Rhine Valley is bordered by forested mountains on both sides. These areas are not included in the analysis as the microscale model is only suited for flat terrain with surface changes. The subset areas in figures 5 and 17 are well within the valley floor.

The roughness maps (figures 6, 19, 33 and 34) show the minimum of z_0 to be 0.001 m and the maximum 1.2 m. In figure 5 the legend provide a key to the roughness of all cover types under summer conditions. Logarithmic mean roughness values of given areas for all four situations are given in table 8. It is clear from this and visual inspection of the figures that the terrain is smoother in winter than in summer. Crops like maize and grains are harvested and the fields are bare. In case of snow cover even smoother conditions would prevail.

A map of the momentum flux under summer conditions in 1993 is shown in figure 30. The momentum is calculated as $\tau=\rho_a u_*^2$ (Pa). The magnitude of wind (U) is assumed to be 5 m s^{-1} from the north at the computational level (z_r) 4 m above ground. Relatively small values of τ are found in the smooth areas, ie the water bodies and relatively high values in the rougher, ie forests. These results are as expected.

To appreciate graphically in more detail what effect a given real world z_0 distribution means for the momentum flux, a subset of z_0 and τ is shown in figure 31 (again centred on the Scherzheim climate mast). First we note that the momentum flux is maximum at the leading edge of all the forests and decreases downwind (the wind blows from the north). The forest edges stand out clearly

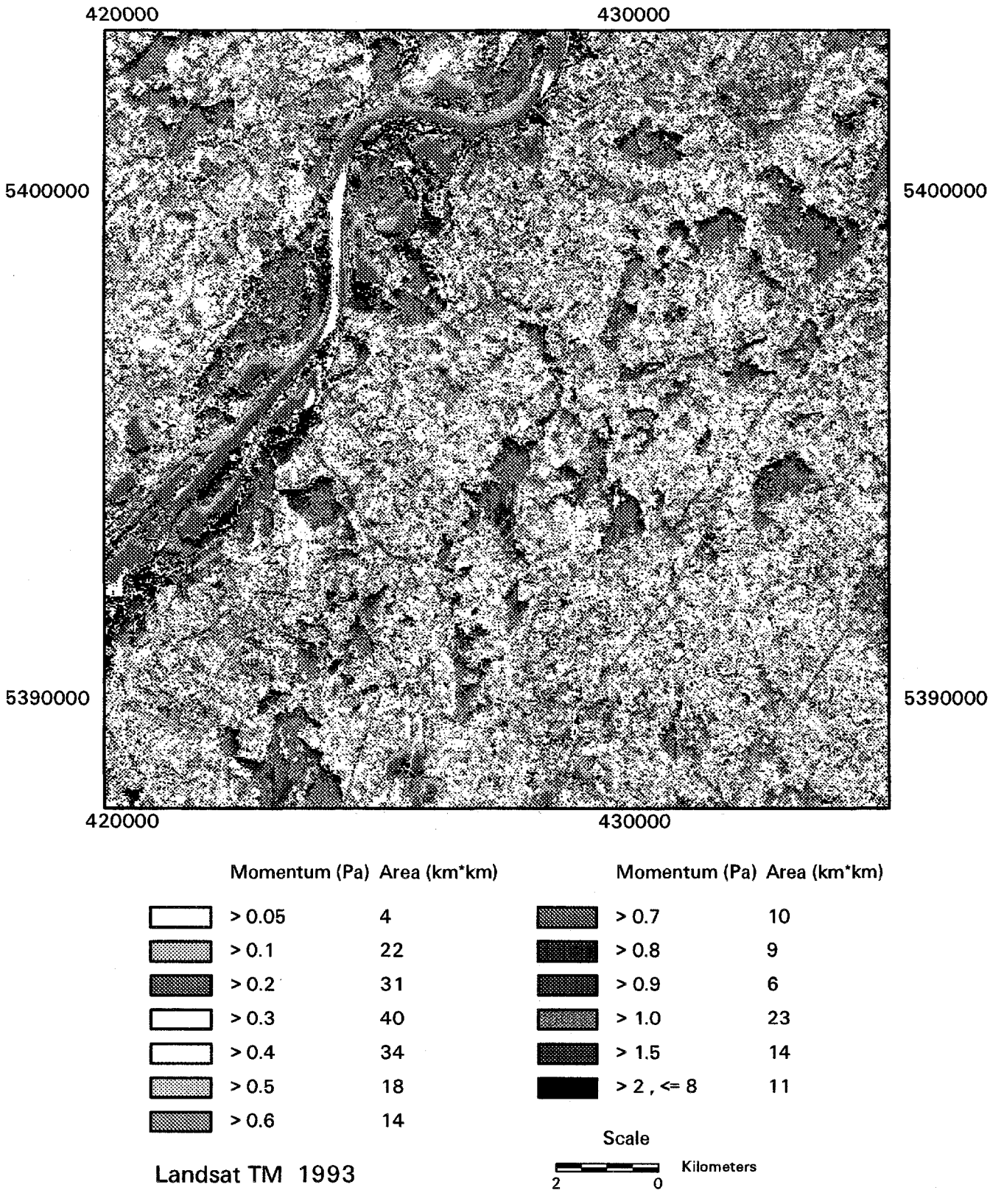

Figure 30. Momentum flux map for summer conditions with wind 5 m/s from North at 4 m height.

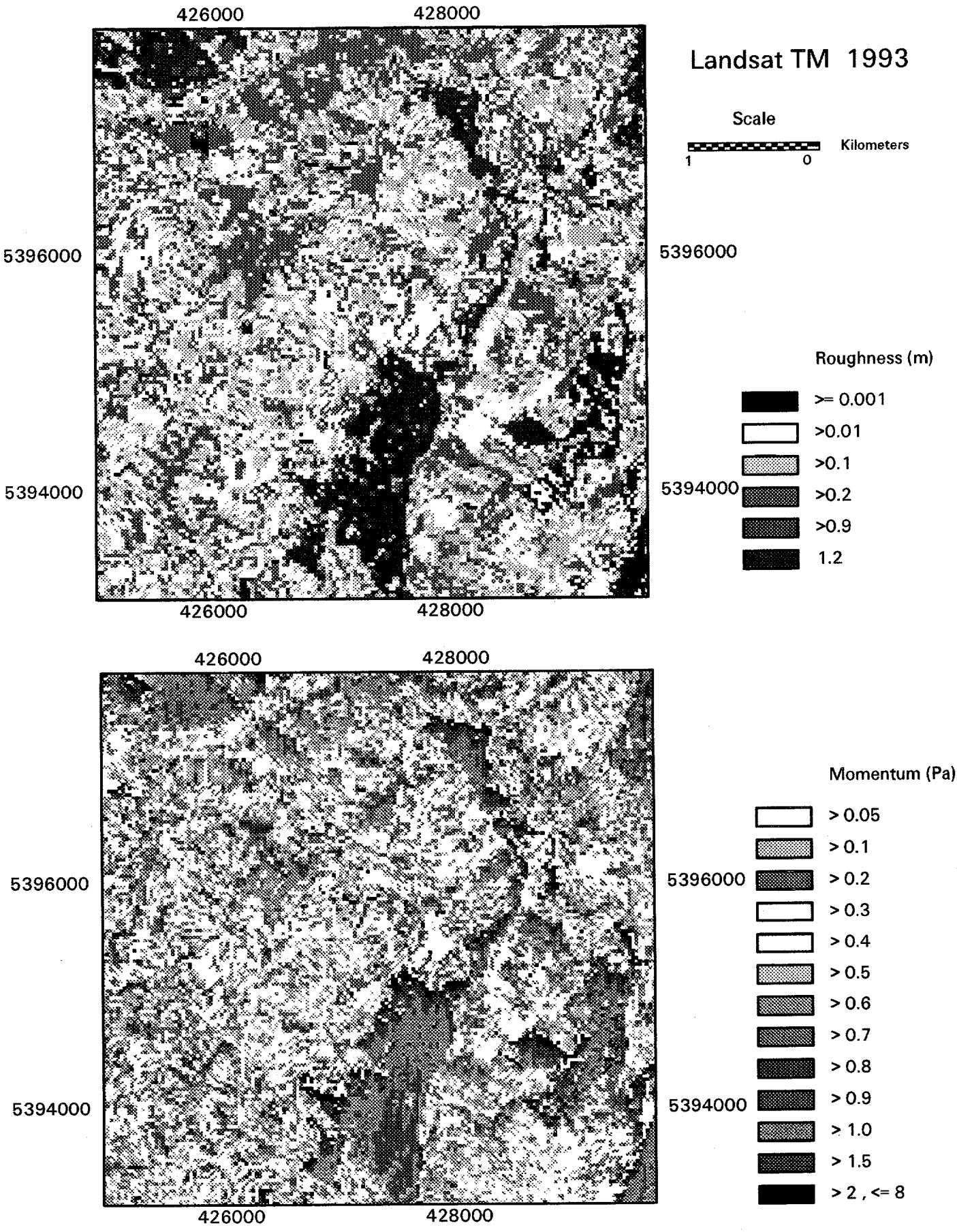

Figure 31. Roughness map for summer conditions 1993 and a momentum flux map for wind 5 m/s from North at 4 m height.

Rhine Valley, Germany

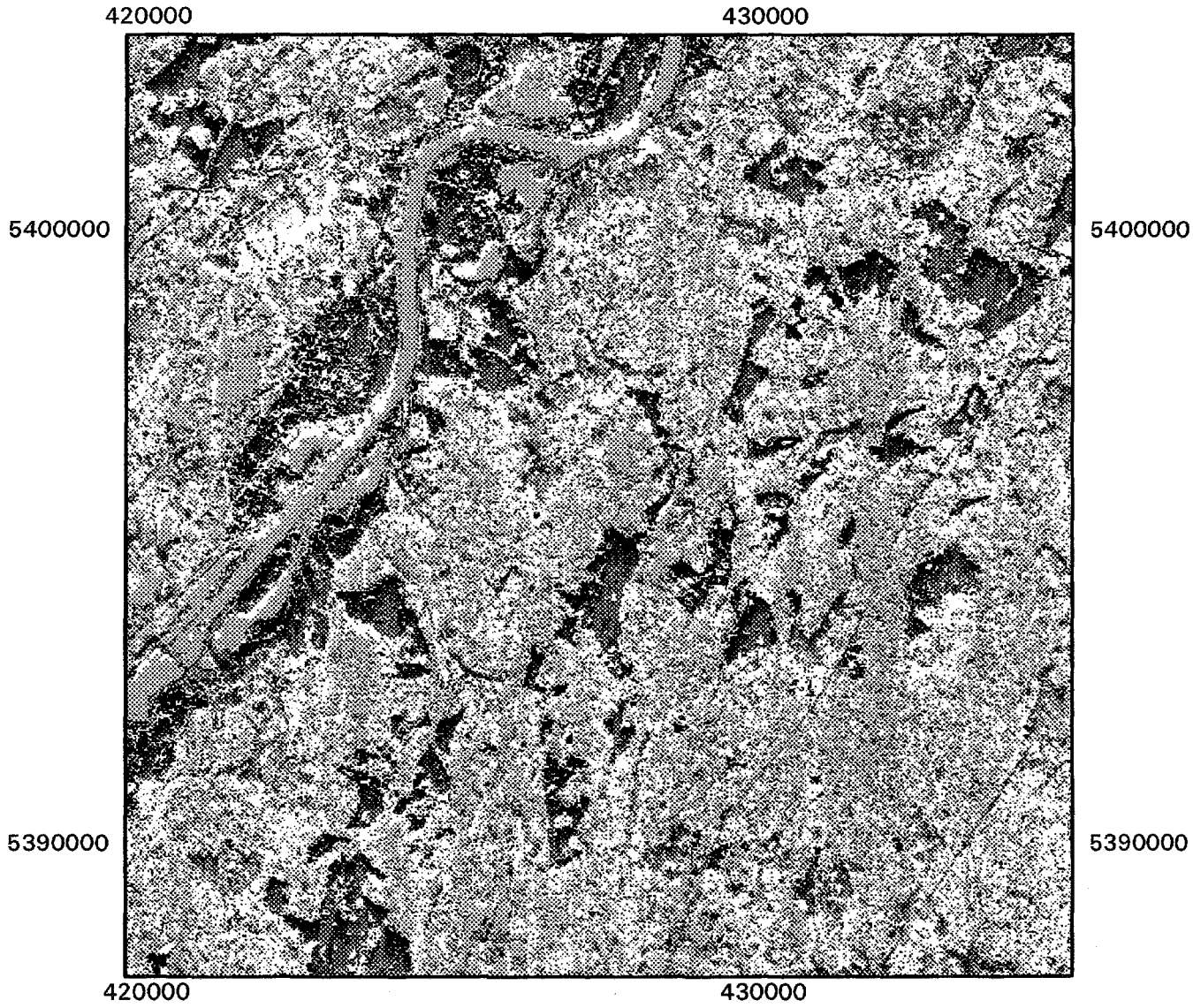

Momentum (Pa)	Area (km*km)
> 0.003	56
> 0.1	44
> 0.2	10
> 0.3	13
> 0.4	16
> 0.5	18
> 0.6	13

Momentum (Pa)	Area (km*km)
> 0.7	10
> 0.8	8
> 0.9	6
> 1.0	18
> 1.5	11
> 2.0, < 6.0	13

Scale

2 0 Kilometers

Figure 32. Momentum flux map for winter conditions with wind 5 m/s from North at 4 m height. Based on Landsat TM 1993.

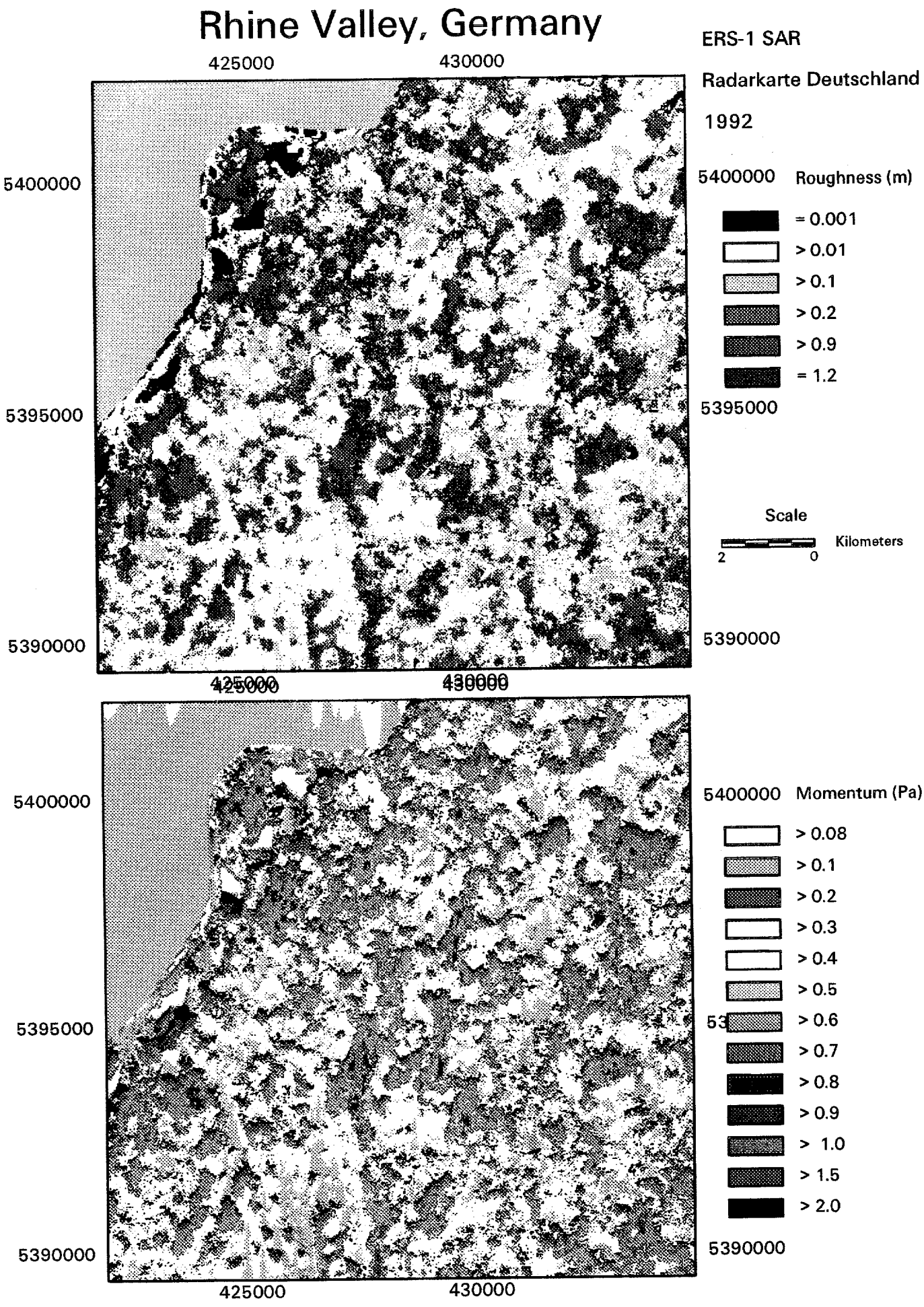

Figure 33. Roughness and momentum flux maps for summer conditions with wind 5 m/s from North at 4 m height.

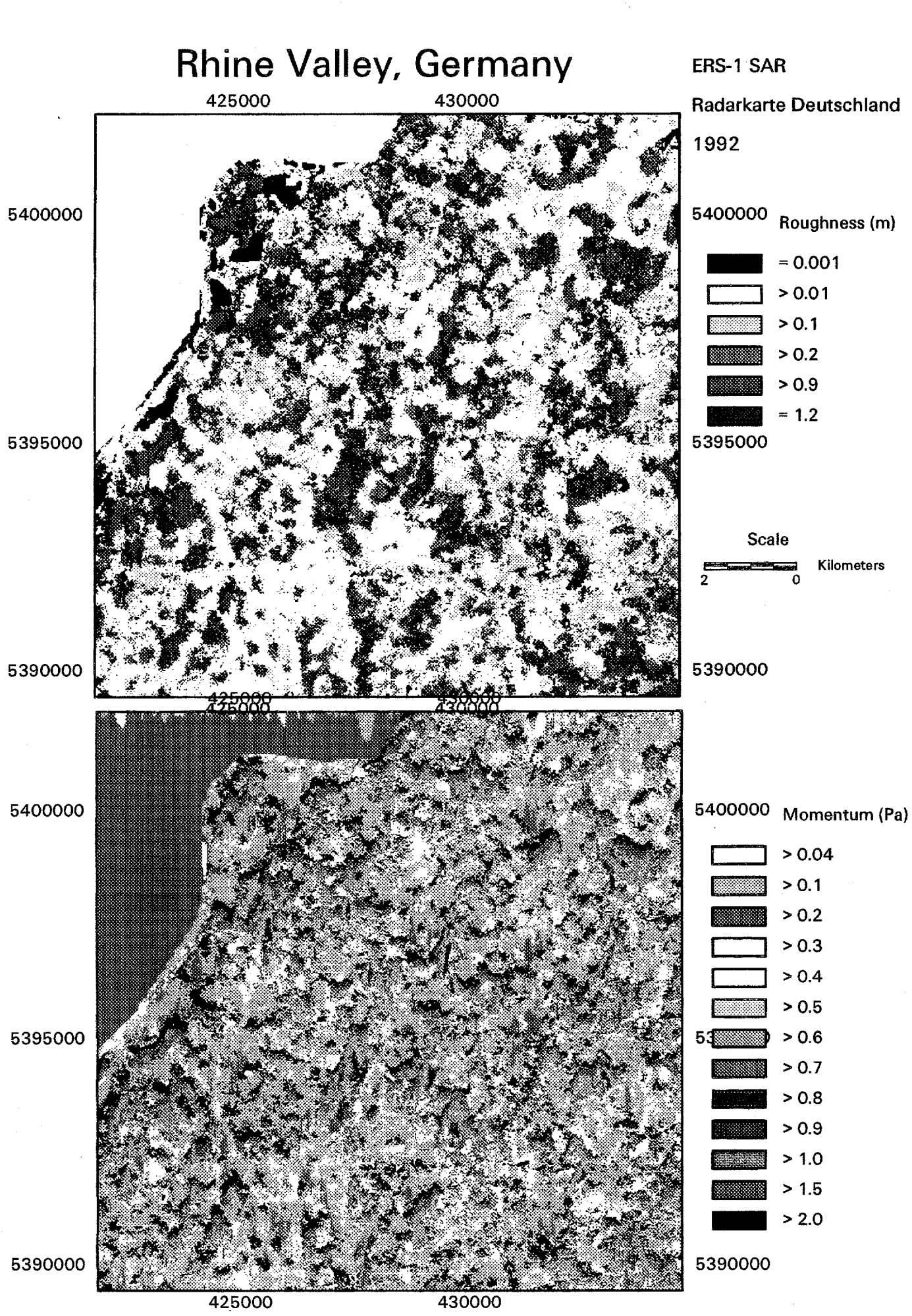

Figure 34. Roughness and momentum flux maps for winter conditions with wind 5 m/s from North at 4 m height.

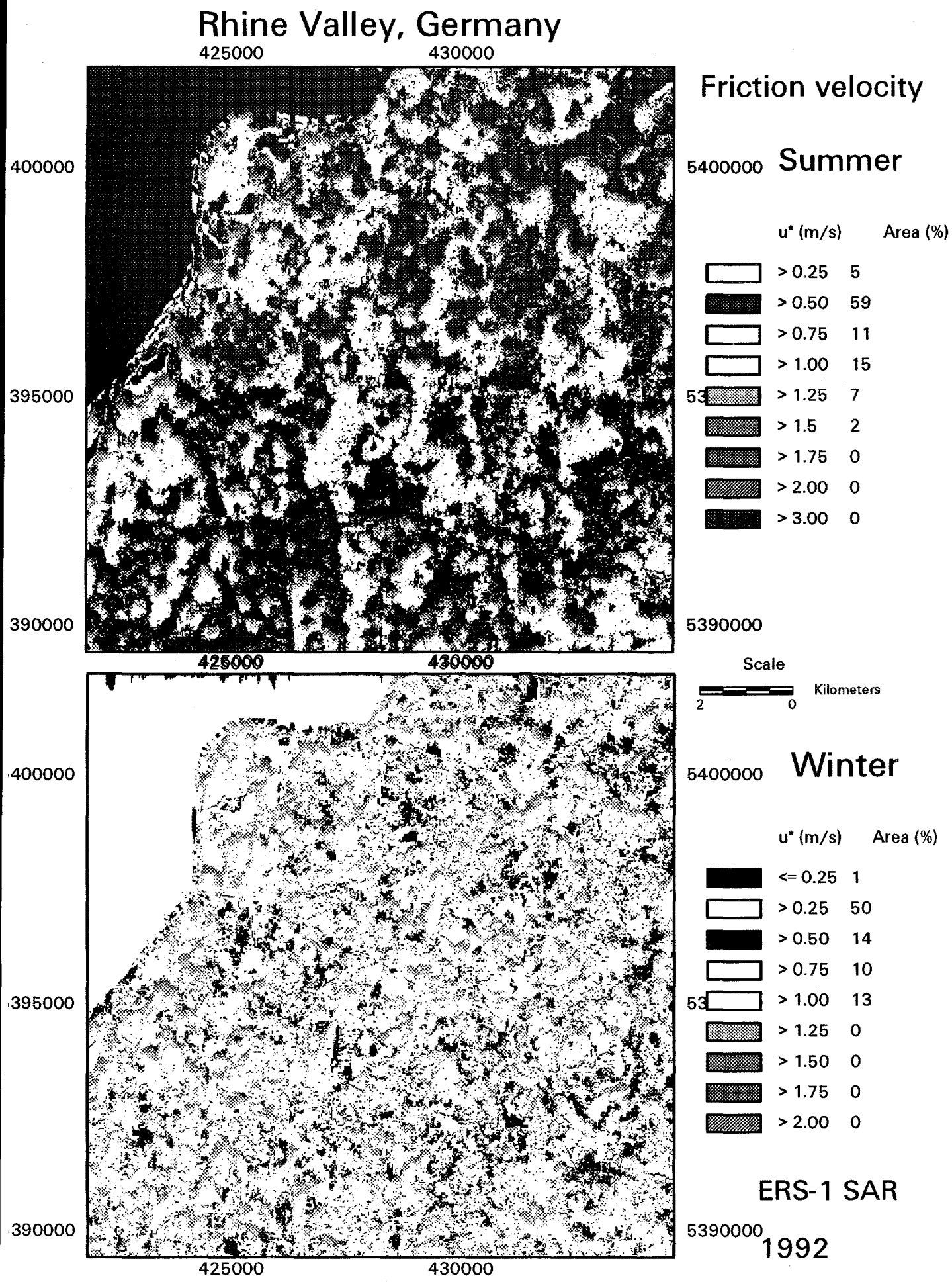

Figure 35. Friction velocity maps 1992 with wind 5 m/s from North at 4 m height.

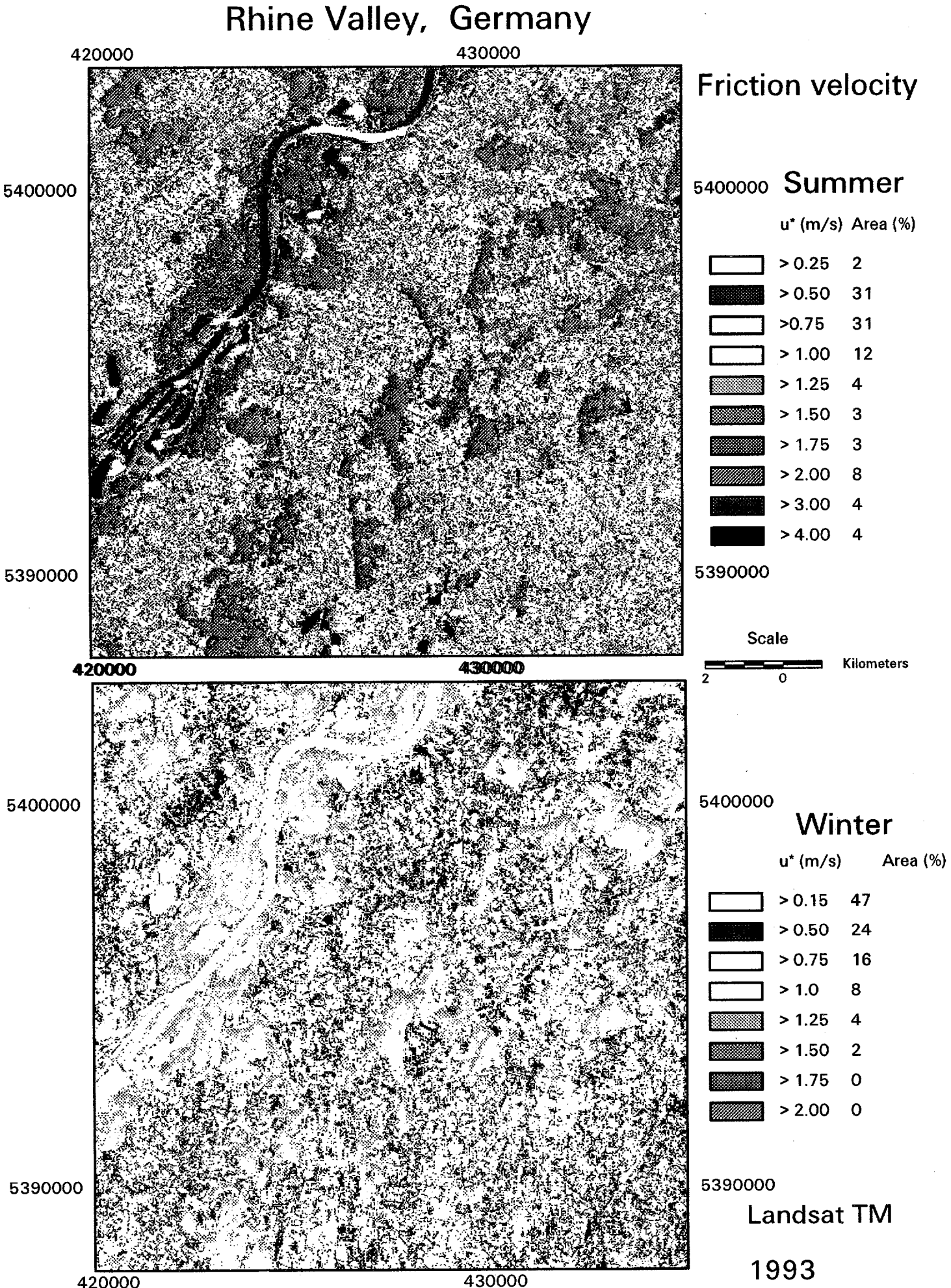

Figure 36. Friction velocity maps 1993 with wind 5 m/s from North at 4 m height.

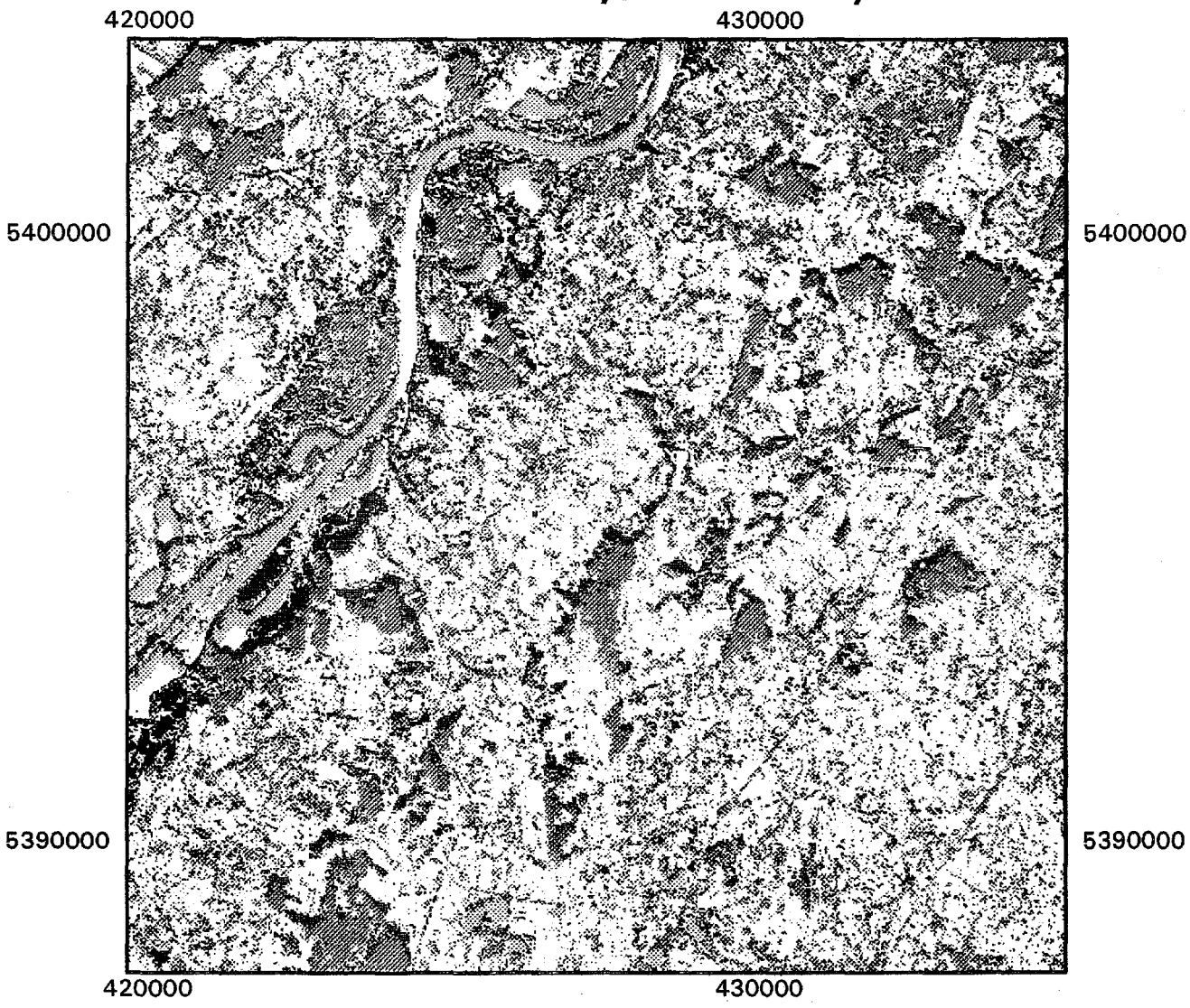

Figure 37. Relative error on friction velocity compared to equilibrium flow for summer conditions with a wind of 5 m/s from North at 4 m height.

in black colour for the very high flux rates.

In figure 31 it is not obvious how τ responds to a smooth surface because no extensive areas are present within the subset. However from figure 30 it is clear that the lowest flux rates are found from the smoothest surface, the Rhine river. If we have a very detailed look into the flux response from the river this reveals that at the windward side τ is very low, but is gradually increasing downwind. It is especially clear at the long north-south stretch of the river.

Figure 32 presents a map of τ for the winter situation. The same kind of features as in the summer map is visible. Worth noting is that in winter extensive areas (~ 100 km^2) have a momentum flux < 0.2 Pa compared to only 26 km^2 in the summer. On the other hand areas with a momentum flux > 1.5 Pa are nearly constant in winter and summer.

Values of roughness, momentum flux and friction velocity under summer and winter conditions in 1993 are listed in table 7. The mean values are from the area shown in figures 5, 6, 19, 30 and 32. The area totals 236 km^2. As input to the calculation the wind was set to 5 m s^{-1} from the north at 4 m above ground.

	z_{0a} (m)	$<z_0>$ (m)	$z_{0a}/<z_0>$	u_{*0} (m s^{-1})	$<u_*>$ (m s^{-1})	$u_{*0}/<u_*>$	u_* min (m s^{-1})	u_* max (m s^{-1})	τ (Pa)	τ_{mi} (Pa)	τ_{ma} (Pa)
Summer	0.13	0.29	2.18	0.59	0.76	1.30	0.23	2.71	0.70	0.06	8.80
Winter	0.03	0.23	6.60	0.42	0.70	1.66	0.17	2.09	0.59	0.03	5.23

Table 7. Values of roughness, friction velocity and momentum flux for a 236 km^2 area in the Rhine Valley, Germany for summer and winter conditions in 1993. Mean, minimum and maximum values are reported for a wind speed of 5 m s-1 from the north at 4 m height. The analysis is based on Landsat TM satellite data.

From table 7 it can be seen that the effective roughness in summer is more than twice the value of z_{0a} and in winter more than 6 times z_{0a}. Seen in absolute values $<z_0>$ does not vary much from summer to winter (from 0.29 m to 0.23 m). However z_{0a} varies an order of magnitude between the seasons. The effective roughness in winter is enlarged because of many *large* step changes. Under summer conditions the step changes are somewhat smaller than under winter conditions. The typical horizontal length scales calculated from the mean Fourier wave length are nearly identical in the two seasons.

The effect of the winter roughness distribution is that the mean friction velocity is 1.66 larger than the equilibrium value. The maximum value of u_* is 5 times larger than the friction velocity for equilibrium flow (u_{*0}). The same order of magnitude is found under summer conditions. Maps of friction velocity under summer and winter conditions 1993 are presented in figure 36.

To visualize the area-wise distribution of error by assuming u_{*0} to be representative over the whole area, a map of the relative error in percentage is calculated as $(<u_*>-u_{*0})/<u_*>*100\%$. The result is shown in figure 37. Approximately half of the area would have an absolute error larger than $\pm 25\%$.

Most noteworthy is that the large errors are scattered over the whole scene, encompassing both rough and smooth locations. Naturally the largest error is close to large step changes, ie land to water and agriculture to forest.

Figures 33 and 34 show roughness and momentum flux maps for 1992. These maps are based on a subset of "Radarkarte Deutschland". The same comments as for the 1993 data apply (figures 30 and 32). Please note that the area northwest of the Rhine river in the classification is so-called "rejected" area. To avoid including this area in a comparative analysis with the 1993 results, subsets are extracted. The subsets are only 36 km^2 (compared to the 236 km^2 reported before). A listing of roughness, friction velocity and momentum flux results is provided in table 8.

	z_{0a} (m)	$<z_0>$ (m)	$z_{0a}/<z_0>$	u_{*0}	$<u_*>$	$u_{*0}/<u_*>$	u_* min	u_* max	τ (Pa)	τ_{min} (Pa)	τ_{max} (Pa)
Summer 1992	0.29	0.47	1.62	0.76	0.93	1.22	0.31	2.52	1.04	0.11	7.63
Winter 1992	0.09	0.41	4.74	0.52	0.88	1.69	0.20	2.24	0.93	0.05	5.99
Summer 1993	0.15	0.30	1.93	0.61	0.77	1.25	0.26	2.34	0.71	0.08	6.57
Winter 1993	0.03	0.22	6.79	0.42	0.69	1.66	0.17	1.99	0.57	0.04	4.73

Table 8. Values of roughness, friction velocity and momentum flux for a 36 km^2 area in the Rhine Valley, Germany for summer and winter conditions in 1992 and 1993. Mean, minimum and maximum values are reported for a wind speed of 5 m s^{-1} from the north at 4 m height. The results are based on ERS-1 SAR data in 1992 and on Landsat TM in 1993.

The 1993 results in table 8 correspond well with those listed in table 7 despite a considerably smaller area is included. It can be noted that the ratios of roughness are larger in the 1993 data than in the 1992 data. This probably is explained by the more detailed classification (19 classes compared to 9) that allow smaller areas to be deliminated. In general this causes more step changes to be mapped. The 1992 values of z_{0a} are twice as large in 1993. A possible explanation is given below. Generally spoken the 1992 hold only three relatively smooth classes (water, pasture and grain) whereas the 1993 data in addition hold (bog, clearcut, scattered trees, sunflower, rootcrop and corn). Some of these relatively smooth classes then are likely to be included in the rougher cover types in the 1992 data set.

Friction velocity maps for the four cases are shown in figures 35 and 36. It is clear that u_* results are larger in the summer than the winter, and larger in 1993 than 1992. Histograms of the area-wise distribution of friction velocity are shown in figure 38. The histogram for the summer conditions show a bimodal

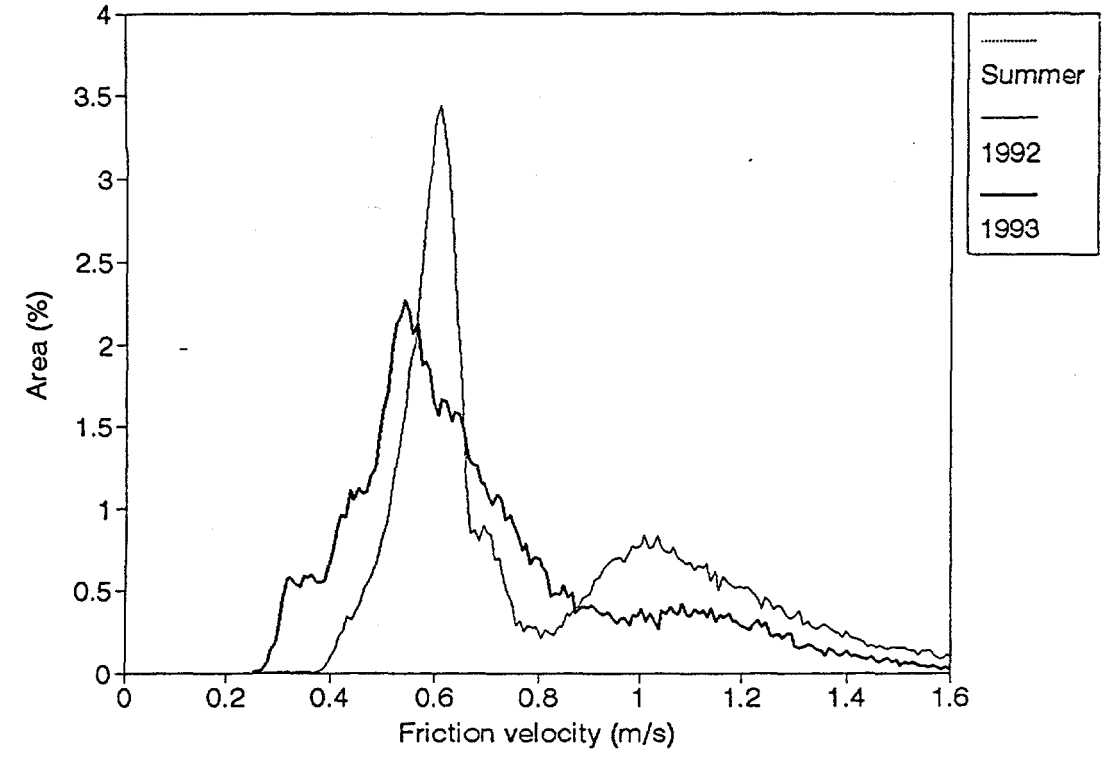

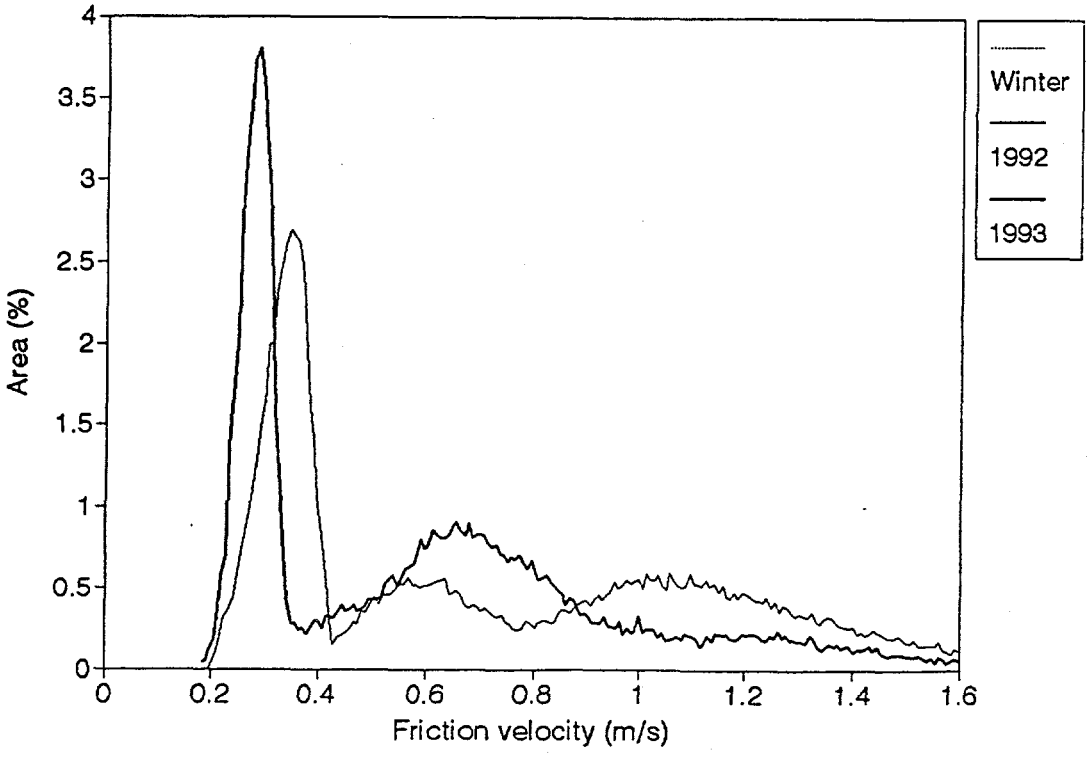

Figure 38. a) Histogram of the areal distribution of friction velocity in a 36 km² large landscape centered at Scherzheim in the Rhine Valley, Germany. The results are from ERS-1 SAR in 1992 and Landsat TM in 1993 with wind speeds of 5 m s⁻¹ 4 m above ground in the summer. b) in winter.

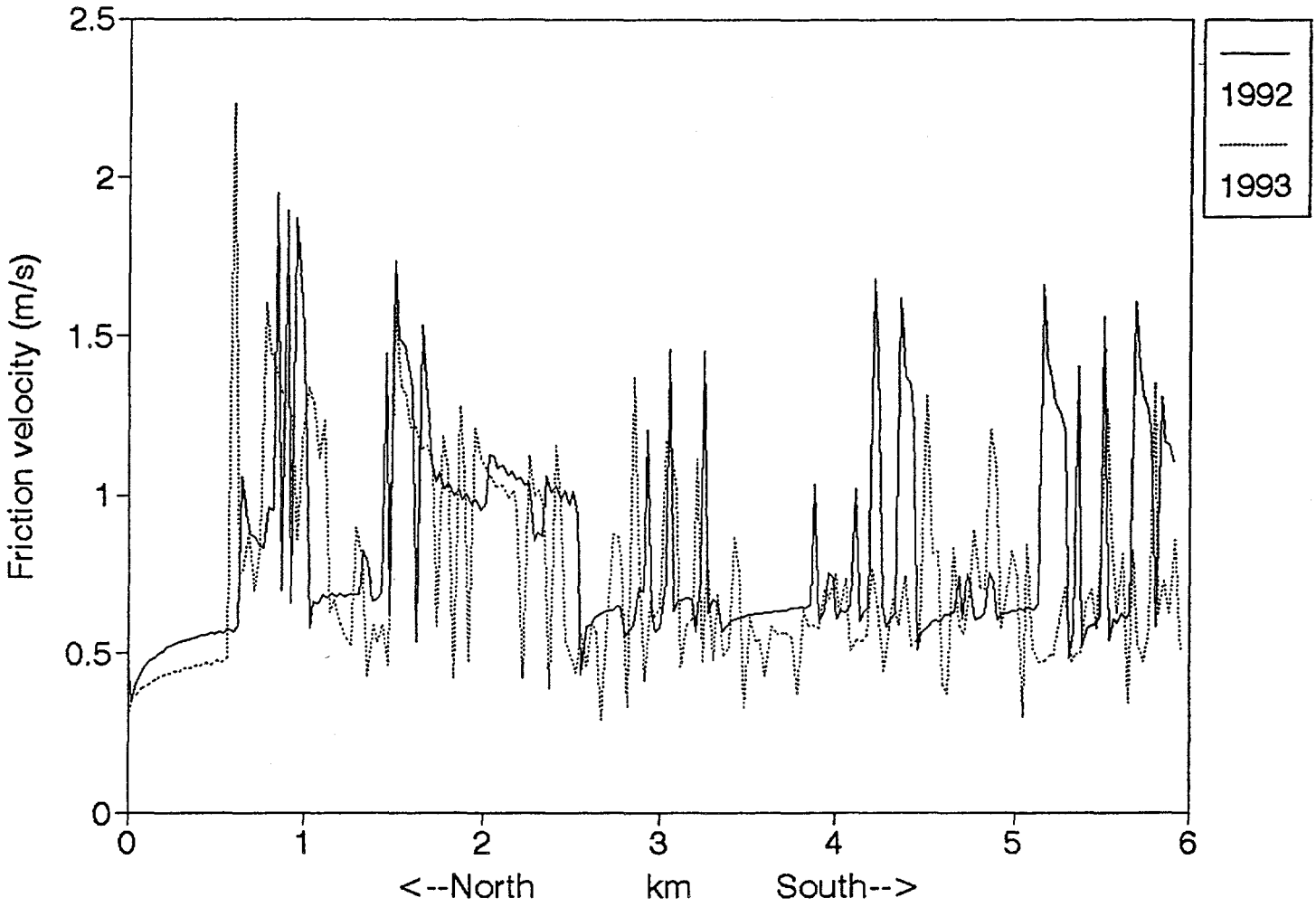

Figure 39. Profile of the friction velocity response at a six km long north to south transect in the Rhine Valley, Germany. The results are from the microscale model for a wind speed of 5 m s^{-1} 4 m above ground from north. ERS-1 SAR satellite data with a 25 m resolution was used for 1992 and Landsat TM with a 30 m resolution for 1993.

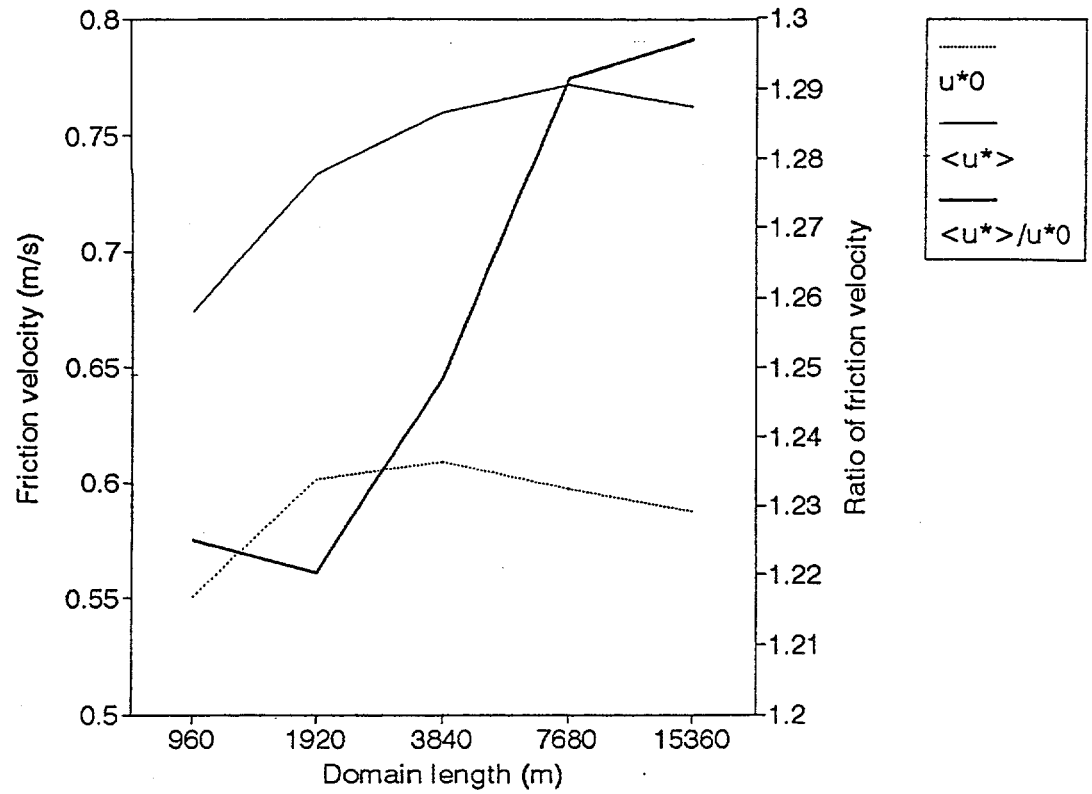

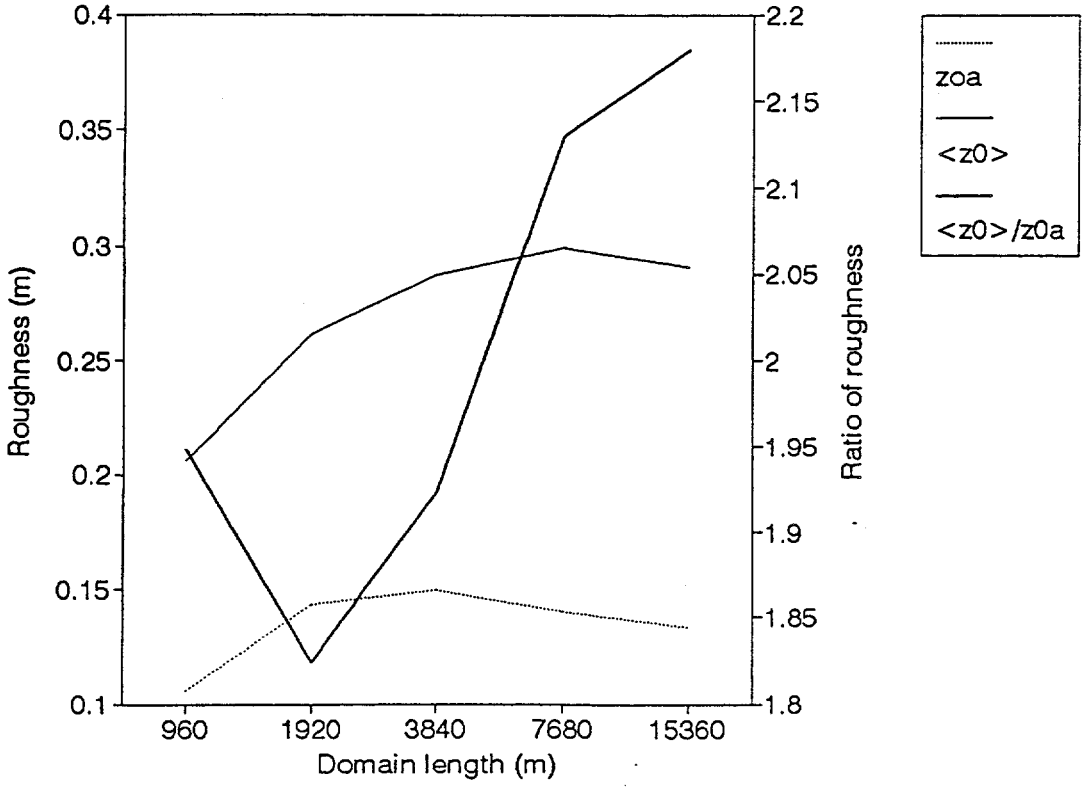

Figure 40 a). Microscale model results of friction velocity and b) roughness as a function of domain size in the Rhine Valley, Germany. A Landsat TM 1993 summer roughness map centered at Scherzheim was used for a wind speed of 5 m s^{-1} 4 m above ground.

distribution in 1992 with a global maximum of u_* 0.6 m s^{-1} and a local maximum of 1.0 m s^{-1}. The 1993 values show a Gaussian-like distribution. The maximum is 0.5 m s^{-1}, ie a shift toward a lower value compared to the 1992 data. (The total area is 100 %, ie the areas below the curves are identical in size).

Figure 38 show the area-wise histogram of u_* for winter conditions. The global maximum is found for 0.3 m s^{-1} in 1992. However in 1993 this maximum is shifted towards a lower value namely 0.2 m s^{-1}. Generally the spread in u_* is smaller in winter than in summer. The 1992 winter data have a trimodal distribution. The local maxima are found for 0.6 and 1.0 m s^{-1} whereas the 1993 winter show a local maximum of 0.6 m s^{-1} (bimodal).

In conclusion the histograms of the area-wise distribution of u_* under summer conditions show a reasonably correspondence between the two years. So do the histograms of the winter conditions. It is anticipated that the u_* variations between the two years cannot be ascribed to land cover changes, but primarily are an artifact of differences in the data sources. However both data sources are able to predict the differences between summer and winter conditions. It is concluded that the seasonal roughness effect is large.

A different comparison of u_* calculated from ERS and Landsat data is made. A six kilometer long transect from the north to the south is graphed in figure 39. The results are for a 4 m level above ground for a 5 m s^{-1} wind speed from the north. The transect starts over water, traverses mainly forested areas until the 2.5 km, then continues over mixed agricultural land interspersed with small wooded areas. There is a good correspondence between the ERS (1992) and the Landsat (1993) results. The Landsat results show larger u_* fluctuations. This owes to a more differentiated roughness mapping as mentioned before.

7.4.1 Scaling in real terrain

Real terrain mapped by remote sensors quantifies the spatial changes in surface characteristics. The satellite based roughness map from the Rhine Valley is an example of such a spatial distribution. An analysis on how roughness and friction velocity vary with scale has been performed. Here, it was chosen to maintain the centre of the image at the location of the micrometeorological mast in Scherzheim and then calculate values for domains with horizontal lengths ranging between 1 and 15 km.

Results from the scaling analysis are shown in figure 40. It is clear that the terrain is heterogenous as z_{0a}, $<z_0>$, u_{*0} and $<u_*>$ vary with scale. Also, the ratios of roughness lengths and friction velocities vary with scale. The wind was assumed to be 5 m s^{-1} from the north at z_r 4 m.

From the test results described in section 7.3.1 it appeared that the small-scale terrain variations influence the atmospheric response significantly close to the ground and only to a minor degree high above the ground. In the real terrain scaling analysis we also focus on this. The ratios of roughness and friction velocity as functions of domain length and computational level is presented in

figure 41. Close to the ground the differences reach a maximum. For the roughness ratio the difference is significant up to the 30 m level. In contrast the friction velocity ratio only show a major difference below z_r=3 m. These results are for the *mean values.*

The strong roughness heterogeneity in the Rhine Valley cause a large spatial variability in local values of u_*. In figure 42 the effective mean ($<u_*>$), equilibrium (u_{*0}) and minimum and maximum is shown for a 15 km^2 area. (z_{0a} is 0.13 m and u_{*0} constant of 0.55 m s^{-1}. This means that U varies as a function of height according to the logarithmic wind profile (eq 5), ie U varies from 3.35 m s^{-1} at z_r 1.5 m to 7.45 m s_1 at 30 m). Figure 42 mainly clarifies that the spatial roughness heterogeneity induce very large values of u_*. Even at a considerably height above ground, say 15 m, is the variability significant.

It is obvious that the real terrain scaling results would be different if the image centre was moved to any other place in the terrain because the terrain is very heterogeneous. The bottomline is that both the scale of interest and the location of interest have to be specified explicitly.

A matter of concern is the typical length scale of horizontal roughness variation. In the 236 km^2 area the mean length is 650 m west-east and 653 m north-south under summer conditions 1993. This was determined from the mean wave length weighted by the amplitude of roughness perturbations. It means that around 20 * 20 pixels map one typical "patch". The Fourier method "looks at" the real terrain as an infinite sequence of identical regions. In case there is a general trend in typical wave lengths spatially, the results could be biased.

To quantify the possible bias for the Rhine Valley a subarea of the scene is extracted. The subarea is a 1920 m * 1920 m domain centred at Scherzheim. The subarea (called "testarea=4 km^2) is padded with values of z_{0a} at all sides into domains of 3840 m * 3840 m, 7680 m * 7680 m and 15360 m * 15360 m (called "testarea=15 km^2" etc.) and graphed in figure 43. The results from the subarea alone and from the padded areas are practically identical. Hence the result of padding values around the subarea show absolutely no influence to the results. A comparison to "Scene-subarea=4 km" show slightly larger values. This means that the landscape surrounding the subarea is (slightly) different to the subarea itself. The explanation may be that the full scene has a slightly different length scale of variation than the subarea.

7.4.2 Downscaling

So far the results reported are concerned only with aggregating (upscaling) roughness values in order to obtain spatial mean values of roughness, friction velocity and momentum flux. This is interesting from the point of view of producing realistic boundary conditions for mesoscale and GCM models.

Downscaling on the other hand is of importance, when the question is how to predict the flux of a given location in a heterogenous terrain when only the grid mean values at larger scales are known. It is especially relevant when eg the amount of trace gases or (dry) particle deposition has to be measured and

calculated. The model can be used (in an inverted manner) to throw light on two questions of relevance to local deposition:

1) how representative are measurements taken at a given site compared to the regional values?

2) how large is the flux at a give location for a given grid mean value?

To choose a representative location for measurements demands the upwind area to encompass typical terrain types and patterns. Good local conditions can be identified roughly from the homogeneity in u_*. Therefore a map of u_* is a help in locating areas representative of a region. The microscale model sums up the effect of roughness changes (remembers the past) and hence is an alternative to the footprint methods (Gash 1986, Schmid and Oke 1990). The diffusion based footprint models give the maximum height of influence as $\kappa L_x \sqrt{C_M}$.

At a given location the flux is linearly proportional to u_* (eq 17-19) for a constant transfer coefficient. If chemical reactions are assumed to influence the concentration such that a logarithmic concentration profile is not present, a modification to the exchange coefficient is needed. However the spatial variability in u_*, and the local values of z_0, can be used to infer the deposition rate for given concentration gradients.

A simple but (very) unrealistic downscaling could be to calculate "u_*" pixelwise assuming U to be constant at z_r and then solve for "u_*" pixelwise for known local z_0 values. Such results are way off because of the too simplistic assumption of an undisturbed wind field at z_r. So a more natural choice is to use the geostrophic drag laws, calculate the geostrophic wind, and then redistribute the stress to the local areas. The same methodology as used in the Wind Atlas Analysis and Application Programme (WA^{S}P) (Troen and Petersen 1989, Mortensen and Said 1996).

Calculation by use of the drag law (eg Panofsky and Dutton 1984, Larsen 1993)

$$G=\frac{u_{*0}}{\kappa}\sqrt{(\ln(\frac{u_{*0}}{z_{0a} f_c})-A)^2+B^2} \qquad (167)$$

gives the geostrophic wind, G (m s^{-1}). f_c is the Coriolis parameter (s^{-1}, here:$1.1*10^{-4}$). A and B are non-dimensional stability dependent functions. For neutral conditions they are approximately 1.8 and 4.5, respectively. Back calculation to local values of u_* are made by the same equation through an iterative process, $u_*=f(G,z_0,f_c)$.

The drag law method is applied to the summer 1993 data. This means with values of $u_{*0}=0.59$ m s^{-1}, U=5 m^{-1} from the north, $z_r=4$ m and $z_{0a}=0.13$ m for a domain of the size of 236 km^2 (figure 6). To visualize the drag law result in comparison to that of the microscale model two transects in the north-south direction are given. The wind is from north. In figure 44a the 3-km transect starts over mixed agricultural crop and meets the large forest "Strüt" 1000 m downwind. The forest has a few clearings. (UTM profile coordinates are 427439, 5396174 at the northern end to 427439, 5393197 at the southern end).

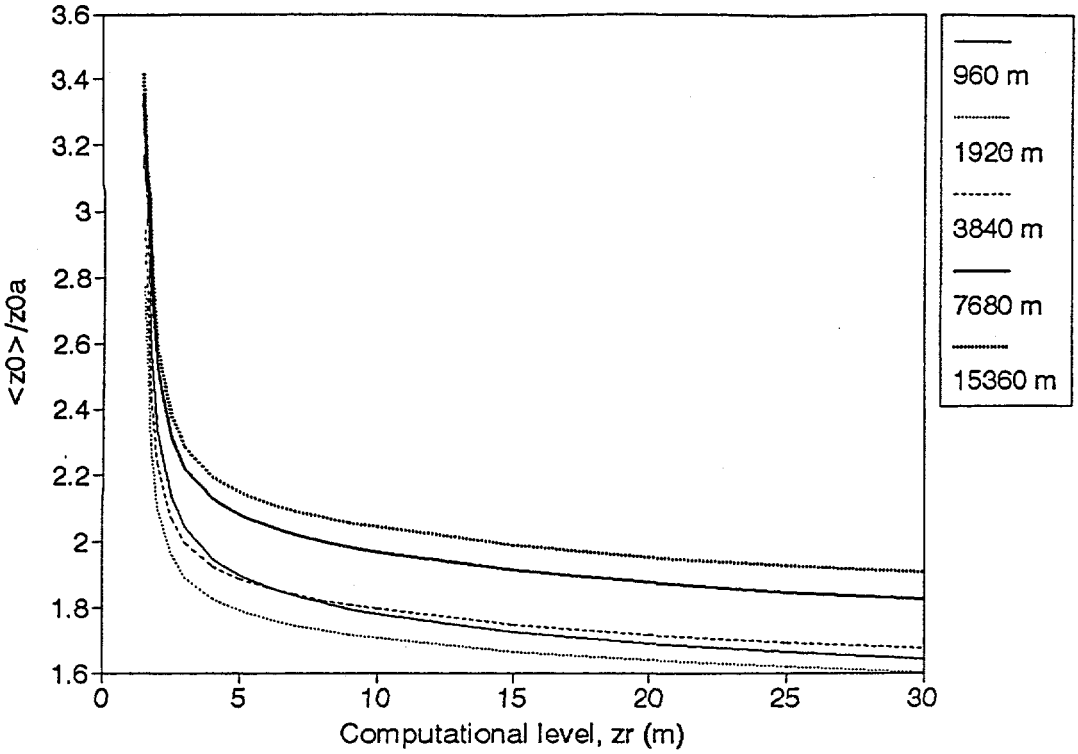

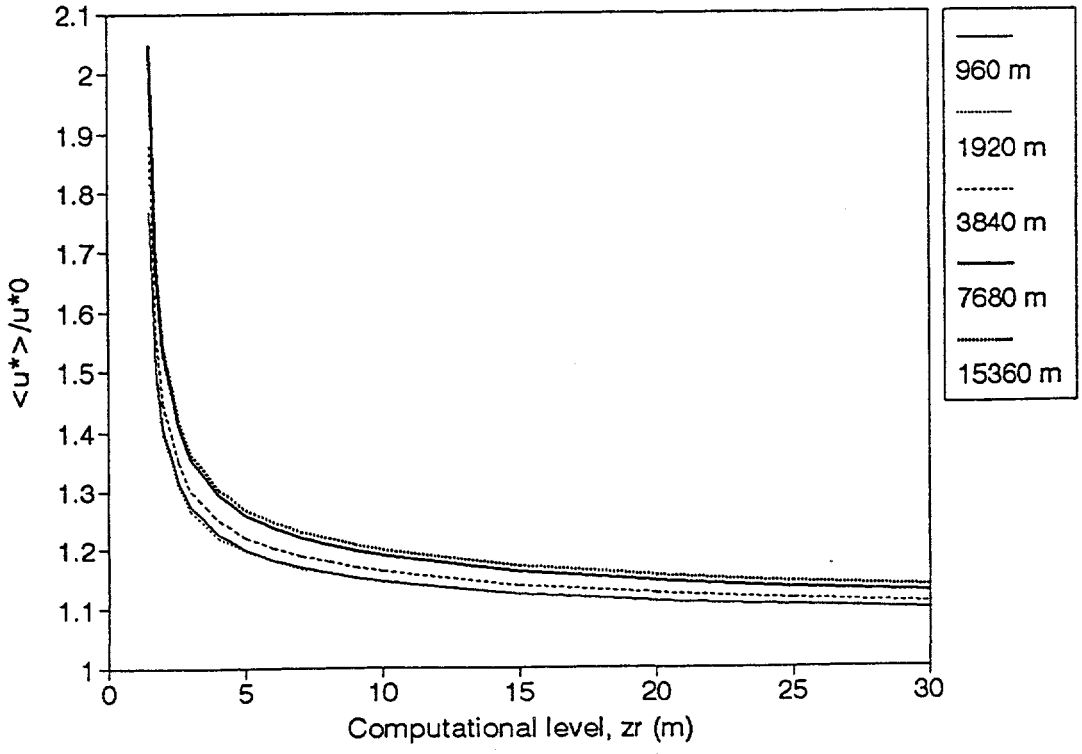

Figure 41. a) Normalized effective roughness as a function of computational level and domain size for the Rhine Valley, Germany in summer 1993 from Landsat TM satellite data. The microscale model results are for a wind speed of 5 m s^{-1} 4 m above ground with the area centered at Scherzheim. b) for normalized effective friction velocity.

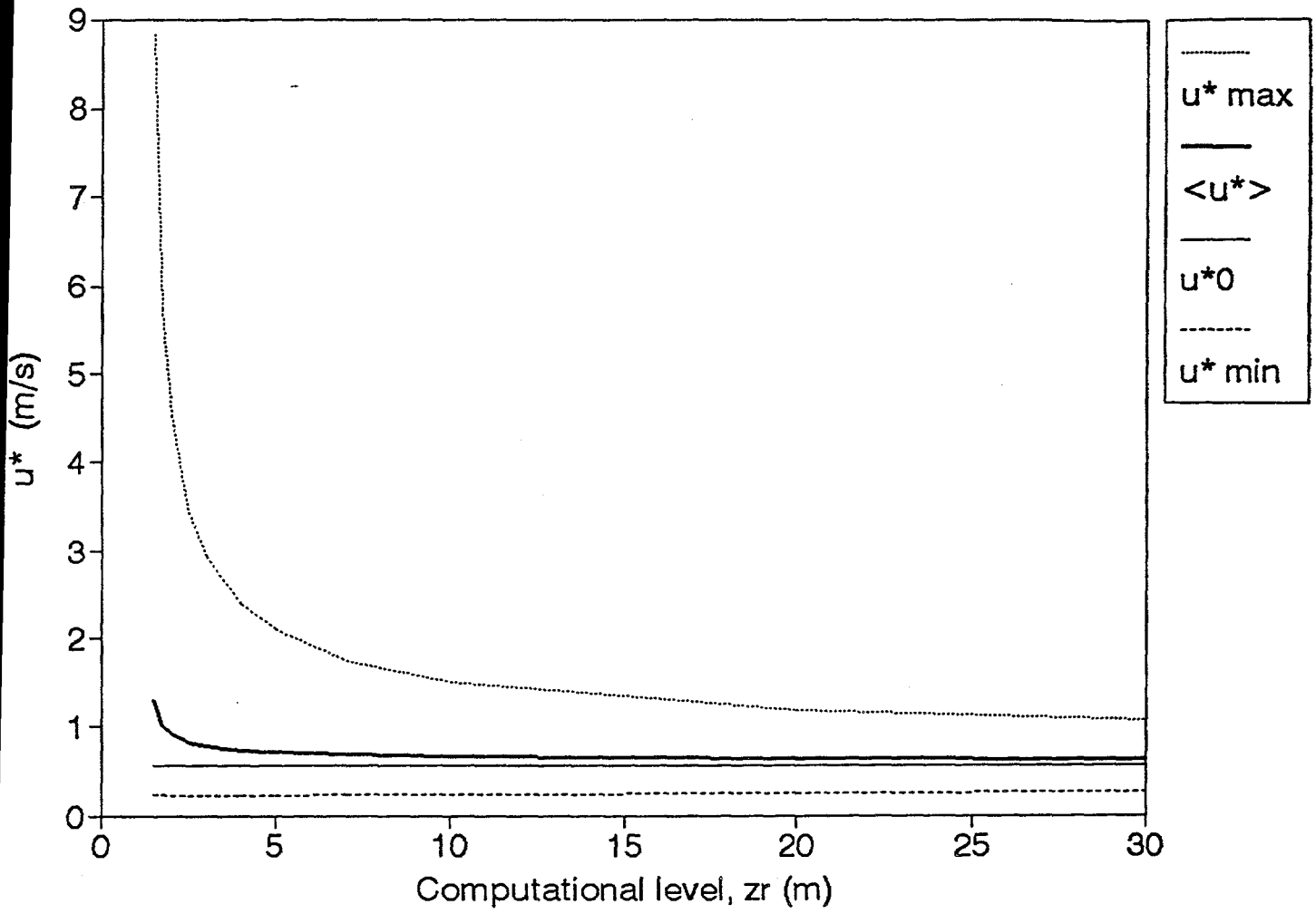

Figure 42. Microscale model results of friction velocity (minimum, maximum and means) as a function of computational level in a 236 km² area in the Rhine Valley, Germany for summer 1993 based on Landsat TM satellite data. For a wind speed of 5 m s⁻¹ 4 m above ground.

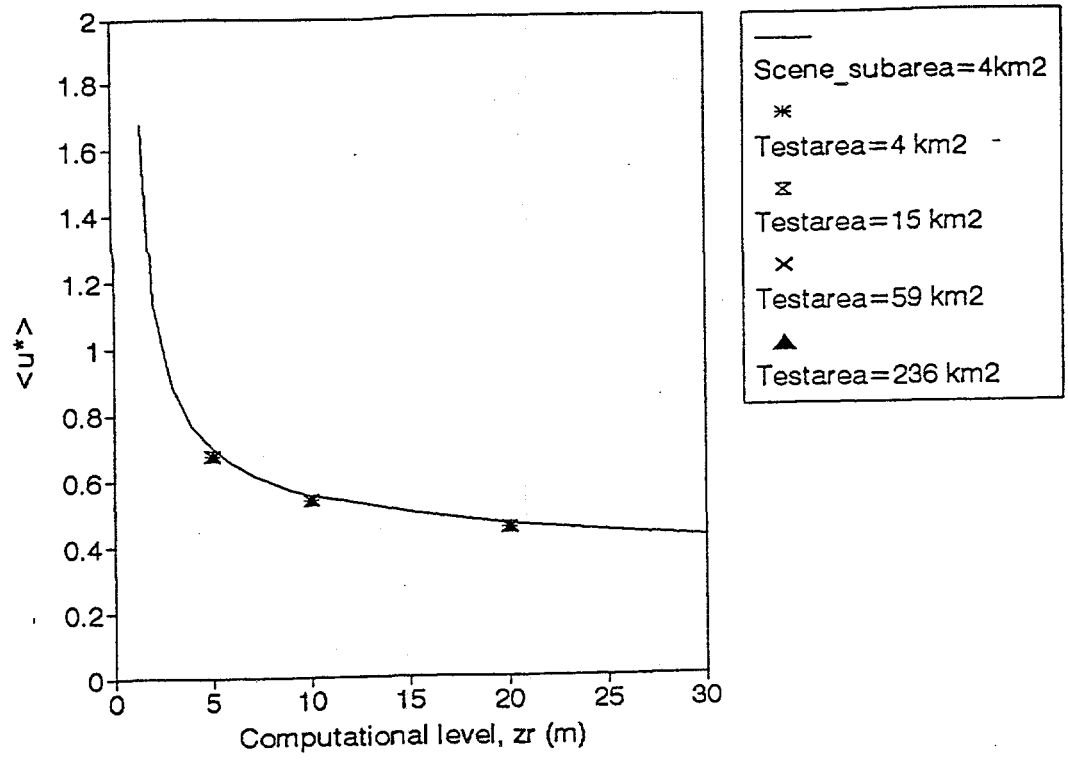

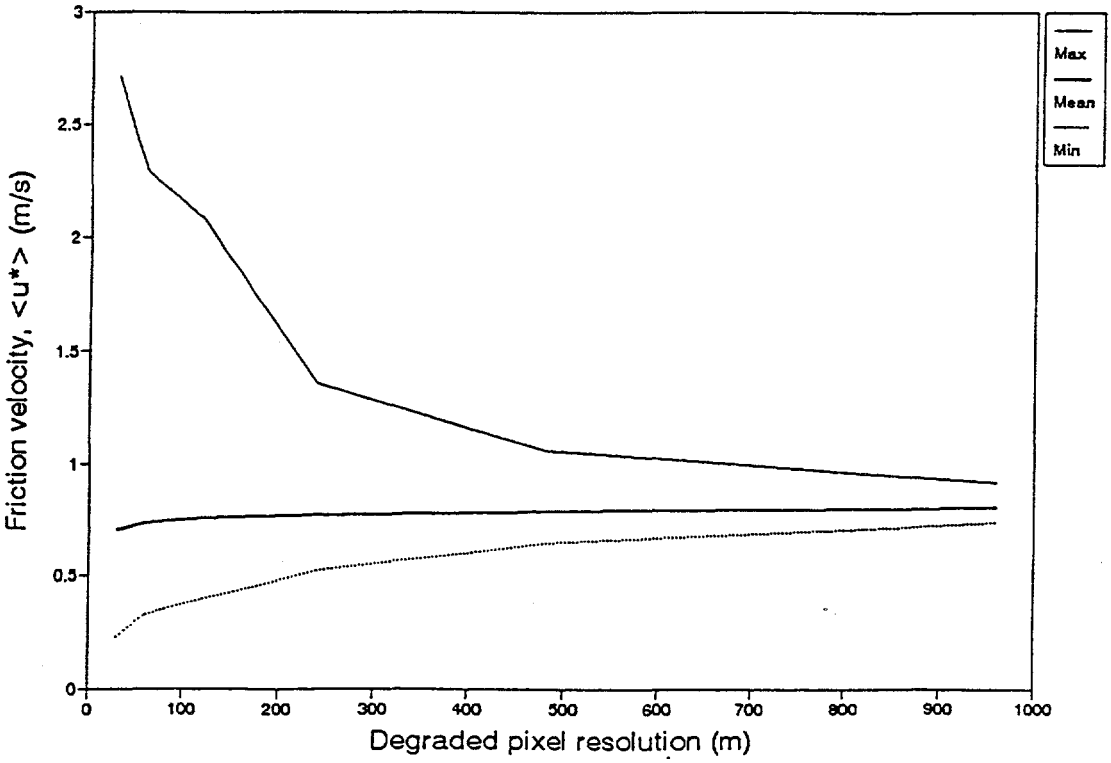

Figure 43. (above) Friction velocity results from the microscale model. A 4 km² scene_subarea (full line). Subsequently only the subarea was used (Testarea 4 km²) and finally this testarea was padded with values of z_{0a} up to image sizes of 15 km², 59 km² and 236 km².

*Figure 44. (below) Degradation of resolution. Microscale model results based on the 1993 summer roughness map from Landsat TM. The original resolution is 30 m * 30 m, then progressively degraded up to 960 m * 960 m pixels. Maximum, mean and minimum values of friction velocity are shown.*

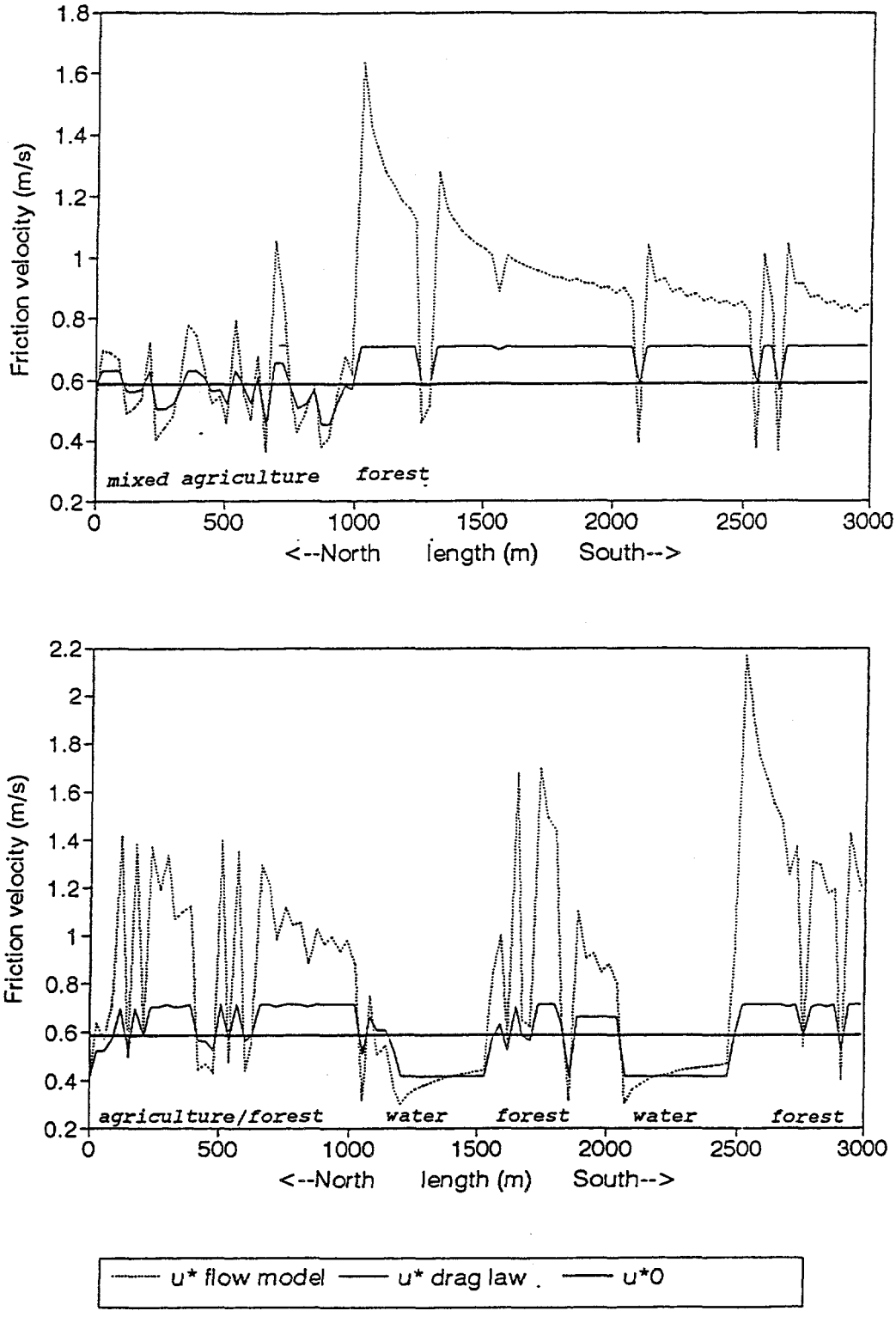

Figure 45. a) (above) Friction velocity calculated from the microscale flow model, from the geostrophic drag laws and the equilibrium area mean (u_{*0}). Wind from north at 5 m s^{-1} 4 m above ground was assumed. The transect shows from 0-1000 m a mixed agriculture area and along 1000-3000 m forest "Strüt" with clearings.

b) (below) as before. This transect crosses two water bodies namely at 1200-1500 m and again at 2100-2500 m. The land surface consist of mixed forest and agricultural crops.

The microscale model results of u_* show a larger variability than from the drag law method (figure 45). The microscale model is seen to have a large response in u_* at the forest edge and then a relaxation towards equilibrium downwind. However u_* far from reaches equilibrium before new step changes are encountered. In essence the drag law predicts u_* for equilibrium flow. Therefore the drag law results are not truly valid in terrain with microscale roughness heterogeneity. If we compare with the drag law results it is obvious that the drag law method does not include advection (the wind direction is irrelevant), so edge effects are ignored. Also notable is that the drag law results are very much smaller above forest than the microscale model results. The microscale model favours the rougher areas.

Figure 45b shows a north-south transect located partly along the Rhine river. (UTM coordinates 423569, 5398229 and 423569, 5395244). The transect starts in an area of mixed agriculture and traverses the Rhine river twice at 1200-1500 m and 2200-2700 m. The same comments as for figure 44a applies. In addition it can be seen that u_* is low after the transitions from land to river. This is expected. However it was expected that u_* would only slowly approach the drag law values from below. As mentioned before the drag law method is not applicable to microscale heterogeneity. It can be noted that the value of u_{*0} is far from reached over the Rhine.Results from the microscale model and the drag law method are summarized in table 9 for summer and winter conditions 1993 for a 236 km^2 area. These data confirm that the friction velocity is highly variable and much larger than in equilibrium flow.

1993	Summer		Winter	
	Model	Drag law	Model	Drag law
$<u_*>$	0.71	0.59	0.61	0.44
u_* minimum	0.23	0.41	0.17	0.33
u_* maximum	2.71	0.71	2.09	0.57

Table 9. Friction velocity calculated by the microscale model and the geostrophic drag law method for a 236 km^2 area under winter and summer conditions 1993 based on Landsat TM satellite data. The wind is 5 m s^{-1} from the north at 4 m height in the Rhine Valley, Germany.

Finally is a so-called degradation analysis reported. The roughness map (figure 6) is gradually degraded by summing a number of pixels. The original resolution is 30 m * 30 m. The lowest resolution tested is ~1000 m * 1000 m (comparable to NOAA AVHRR). Figure 44 shows the effective friction velocity for the 236 km^2 area calculated by the microscale model. It is seen that the u_* prediction deteriorates quickly. The mean is not much affected, but the minimum and maximum are very affected. Most of the response is lost with pixels larger than 200 m * 200 m. Concerning the microscale aggregation model, images with a horizontal resolution coarser than 500 m * 500 m are not useful.

7.5 Comparison to field data

At this point a validation of the satellite based flux results seems adequate. However available data are far from ideal. Field data of the momentum flux are available from a micro-meteorological mast located at a field in Scherzheim (Barthelmie and Jensen 1995). The ideal data would be spatial eddy correlation data.

The measurements of temperature, wind speed and wind direction from a two-week period in September 1992 are stored as 30 minute mean values. A total of 600 records from September 10 18.00 pm to September 23 8.00 am are available. Before presention of the relevant data a short description of the site is given.

Figure 46 show a sketch of the Scherzheim field site. The wheat stubble with regrown wheat had a roughness of 0.008 m. The mast was located at position "1". An auxiliary mast was moved around to positions "2", "3" and "4", and at position "H" a Hungarian group performed measurements. Only data from position "1" are reported here. The sector with the best fetch conditions was the 340°-70° sector. The mustard field upwind had a similar roughness, so the first major change in roughness was 200 m upwind where a mature maize field was located (0° is to the north, 90° is to the east) (Hummelshøj et al. 1994). A grouping into four sectors follows, see table 10.

Sector	Direction	Fetch conditions	u_*/U	number
North	340°-70°	~ 200 m fetch, then scattered trees	0.080	45
Southeast	70°-180°	~ 50 m fetch, then maize, then wood	0.117	12
Southwest	180°-250°	~ 35 m fetch, then maize, then farmhouse	0.159	54
West	250°-340°	~ 200 m fetch, then scattered trees and wood	0.098	16

Table 10. Field site Scherzheim in the Rhine Valley, Germany. Information on fetch conditions, field data on u_*/U and the number of data points used from September 1992.

Sector "North" has the best fetch. Sector "West" is less ideal, and sectors "Southeast" and "Southwest" are disturbed by very rough elements in close vicinity. The terrain is flat.

The position of the mast was chosen from the assumption that the prevailing wind in the Rhine Valley would be northerly in September. In figure 47 all 30 minute wind speeds measured at 4 m with the sonic anemometer are displayed, $U=\sqrt{(u^2+v^2)}$. Sometimes the wind blew from the north, though more frequently from the south. The mean wind speed was only 1.17 m s^{-1}.

The quantity of interest for a comparison with the satellite based results is u_*/U. When including stability in eq 5 we find that

$$\frac{u_*}{U}=\frac{\kappa}{\ln(\frac{z}{z_{0a}})-\psi_M(\frac{z}{L})} \qquad (168)$$

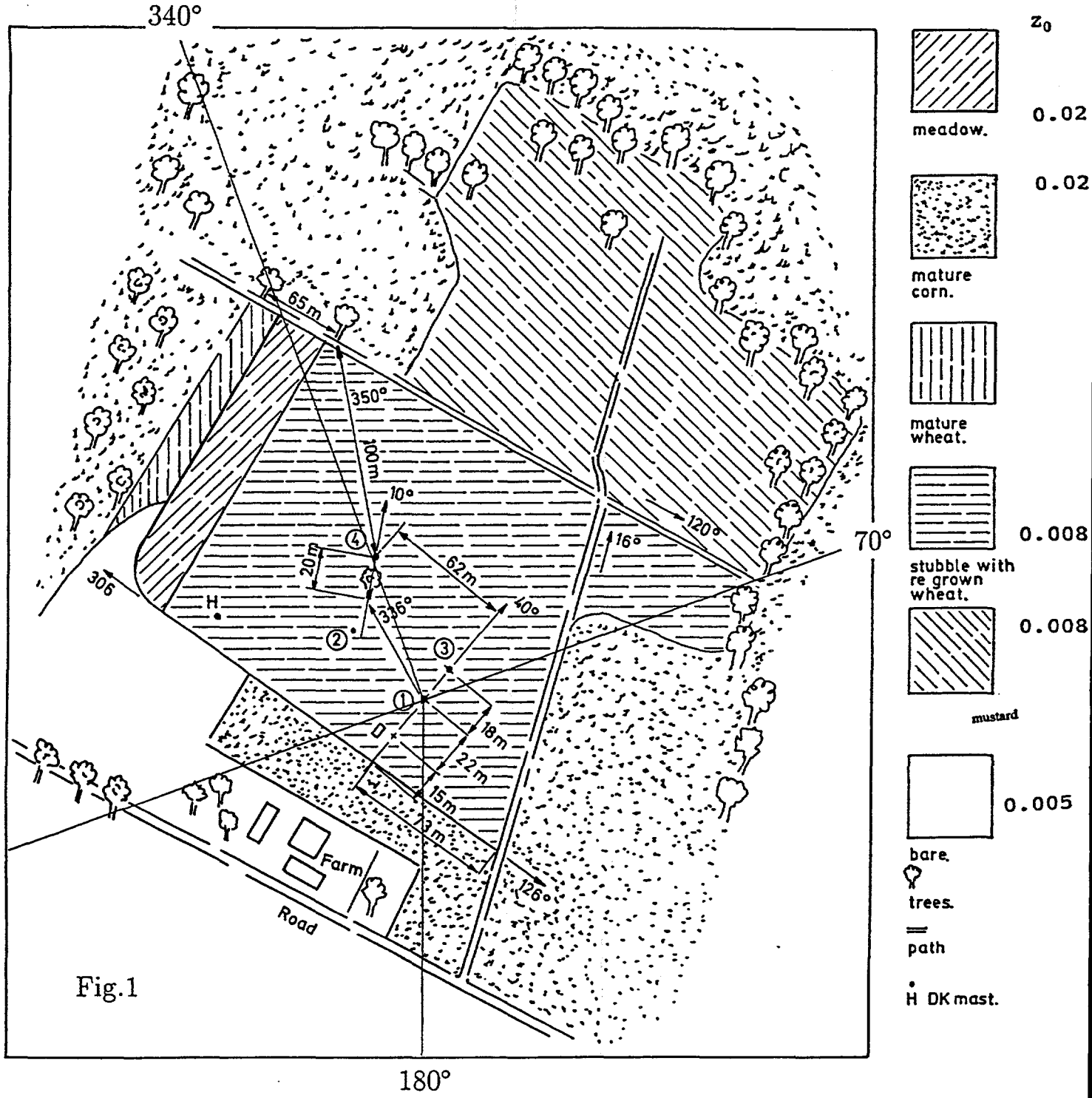

Fig.1

Figure 46. Scherzheim field site in Rhine Valley, Germany with a micrometeorological mast in September 1992 at location number 1. Land cover and roughness length are shown. Four sectors are delimited: NORTH with good fecth, SOUTHEAST with poor fetch, SOUTHWEST with very poor fetch and WEST with reasonably fetch.

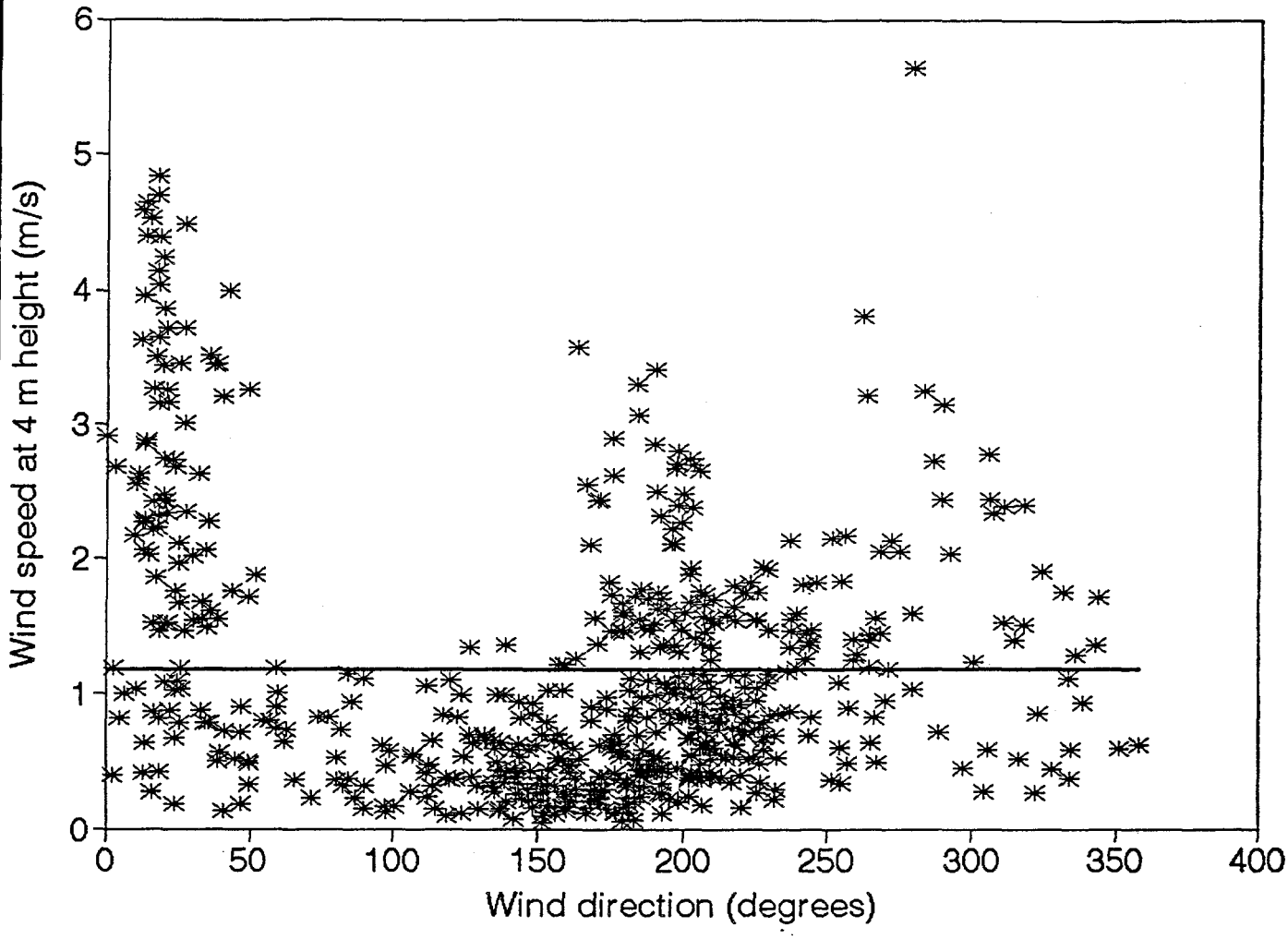

Figure 47. Wind speed measured at Scherzheim, Rhine Valley in September 1992. Half-hourly mean values from sonic anemometer
4 m above ground as a function of wind direction. The mean wind speed is 1.17 m s^{-1}.

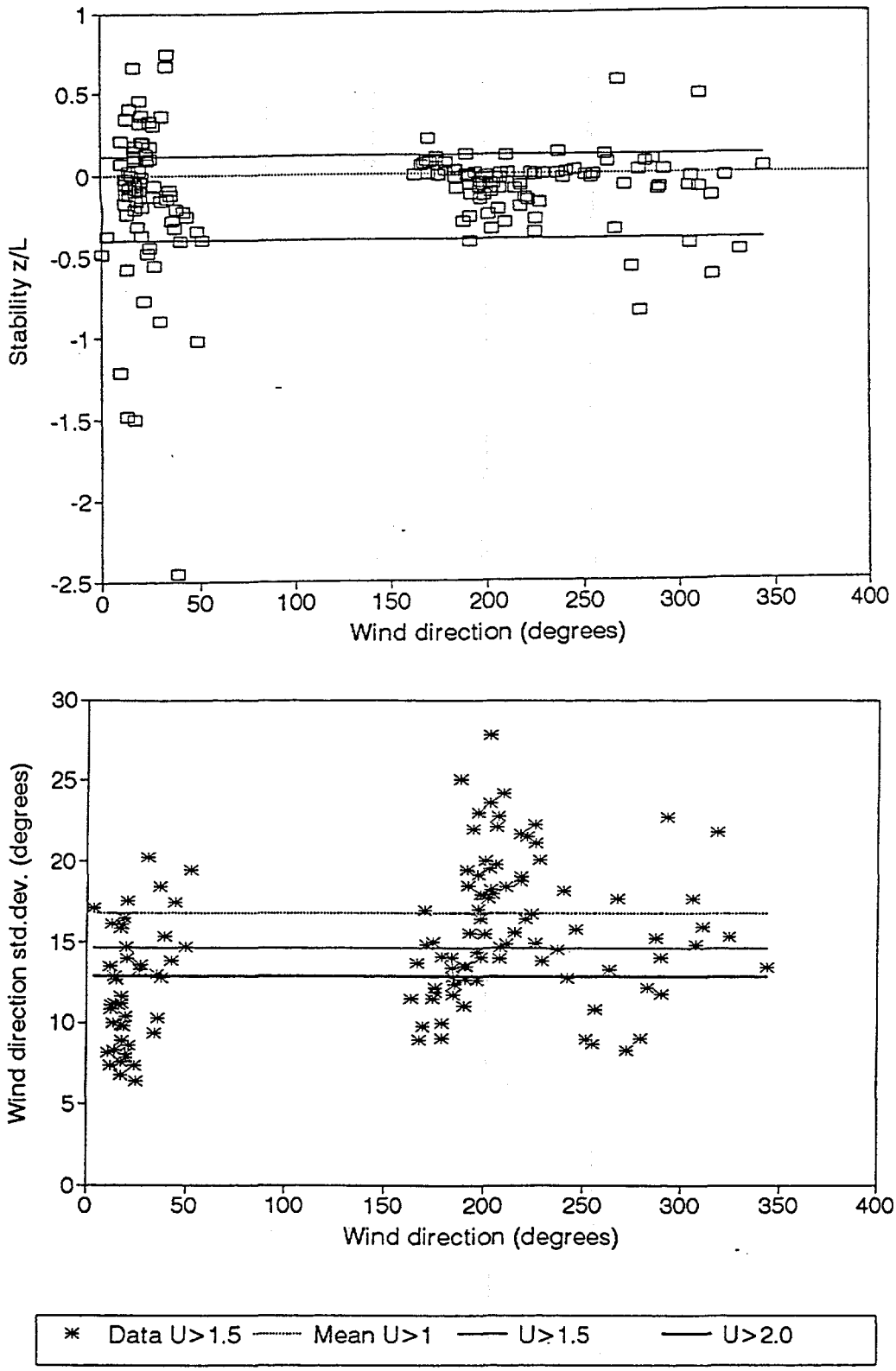

Figure 48. a) (above) Stability measured at Scherzheim, Rhine Valley in September 1992. Half-hourly mean values 4 m above ground as a function of wind direction. Outside the full lines stays u_*/U within ±10% compared to the neutral conditions values.

b) (below) Wind speed measured at Scherzheim, Rhine Valley in September 1992. Half-hourly mean values 4 m above ground as a function of wind direction deviations. Only data for U > 1.5 m s^{-1} are shown, and the mean for wind speeds of respectively, > 1.0, > 1.5 and > 2.0 m s^{-1}.

As we know that z_0 is 0.008 m, z is 4 m and the stability term zero for neutral conditions, u_*/U is 0.0643 m s^{-1} under windy adiabatic conditions. We should obtain a reliable value of u_*/U as a function of wind direction.

In general the wind speed was low. Although the sonic anemometer has a lower "starting velocity" as compared to the cup anemometers, a careful screening revealed u_*/U to be rather sensitive to low wind speeds. For U 1 m s^{-1} the scatter in u_*/U was significant. The methodology of the log-profile roughness derivation demands strong winds. Subsequently it was chosen to use data of U > 1.5 m s^{-1}.

The range in stability was as expected: very unstable by day, very stable at night and with only very few neutral conditions at sunrise and sunset. Figure 48a shows the ratio of z/L as a function of wind direction for $U > 1.5$ m s^{-1}.

It was decided to relax the criteria on "neutral stability" to encompass data where the quantity of interest, namely u_*/U, was affected less than $\pm 10\%$. The corresponding range in z/L is found from eq 168 and the tabulated values of z/L to ψ_M (Businger-Dyer) in Panofsky and Dutton (1984) for unstable conditions. For stable conditions $\psi_M = -5z/L$. Then the result is that "near-neutral" is, rather crudely, assumed for $z/L \in [-0.4;0.1129]$ (this equals L to be outside the range of [-10,35]).

The stability criteria included roughly 75% unstable and 25% stable situations. Stable stratification affects the wind profile to deviate relatively more from a logarithmic profile. u_*/U increases for unstable conditions and decreases for stable.

For the rest of the analysis *"all" data refer to values where $U > 1.5$ m s^{-1} and u_*/U stays within $\pm 10\%$ of the theoretical neutral stability value.*

The wind has "seen" surface elements that are different from the ones straight upwind, when the wind direction is highly variable. Hence to more precisely pinpoint the upwind surface roughness a wind direction criterion was applied. In figure 48b the standard deviation on wind direction is shown for "all" data. The spread is large.

The standard deviation becomes undefined at very low wind speeds, and experimental errors on low wind speeds will introduce errors in the calculation. From this point of view higher wind speeds are preferable. At the same time stronger winds usually have a more steady direction. The data support this general fact: a smaller directional spread is found at higher wind speeds. Mean values of the spread for wind speeds > 1.0, > 1.5 and 2.0 m s^{-1}, respectively are 16.8°, 14.6° and 12.9°.

Part of the directional problem is eliminated when data of $U > 1.5$ m s^{-1} are chosen. However in order to minimize the effect further, data with a directional change $< 15°$ are picked out and shown in figure 49a (with symbols of *. These are 76 records out of the original 600). The jagged line include "all" data (without a criterion on direction in total 131 records). It was decided to calculate mean values of u_*/U sector-wise from "all" data else very few points

were found in two sectors. The sector-wise mean values are shown as horizontal lines in figure 49a and as numbers in table 8.

The result of a careful applicance of criteria on wind speed, stability and wind direction, leaves us with a data set useful for mapping u_*/U as a function of wind direction. Figure 49a clearly shows u_*/U to be dependent on wind direction. The minimum mean value is 0.08 in sector "North". The maximum is 0.16 in sector "Southwest". Sector "Southeast" only experienced a gentle breeze (figure 47) and the mean is truly for the 160°-180° bin because no data meet all criteria in the 55°-160° bin.

The conclusion is that sector "North" has a minimum in u_*/U, sector "Southwest" has a maximum, and the other two sectors range in between. This fits well to what is expected due to the local fetch conditions described. The rougher the upwind surface, the larger u_*/U. The shorter the fetch, the larger u_*/U.

Microscale model results under summer conditions in 1992 and 1993 are calculated for every 10° and the information on u_*/U is extracted from one pixel and from a 3*3 centred window on the Scherzheim site. Data from one pixel is called "local" and from the window called "mean". These do not differ much. The values are shown in figure 49b as well as field data that meet all criteria. The microscale model results are of the right order in all cases. The relative error on the model results are within $\pm 50\%$ compared to the field data calculated from: (model data-field data)/field data*100%. The directional effect is not clear in figure 49b.

Comments on the result are three:

1) The field was covered with (sparse) regrown wheat in 1992. It was 5 cm tall and emerged after harrowing. The 1992 image data classify the area as grain and the 1993 image data as maize. The latter is more rough. A rougher ground cover will cause larger u_*/U, but this effect is not clear. Adjacent areas have different cover types in the two years and that may explain these results.

2) The second point is that elements smaller than 25 m * 25 m and 30 m * 30 m are not mapped. Subpixel information is problematic for two reasons. The first is that small elements are not mapped. These can be important. The other that mixed pixels have a tendency to be mis-classified. The problem is especially relevant in terrain with small-scale heterogeneity. In the Scherzheim site scattered trees were present (figure 46). This is far from ideal for the purpose of comparison to microscale model results.

3) The third comment is on the assignment of roughness values to correctly classified areas. Roughnesses vary in space and time in most vegetation types. Therefore the above roughness maps are only accurate to "first-order". They are, however, the best available. For surface flux calculation in heterogeneous terrain roughness map are absolutely necessary.

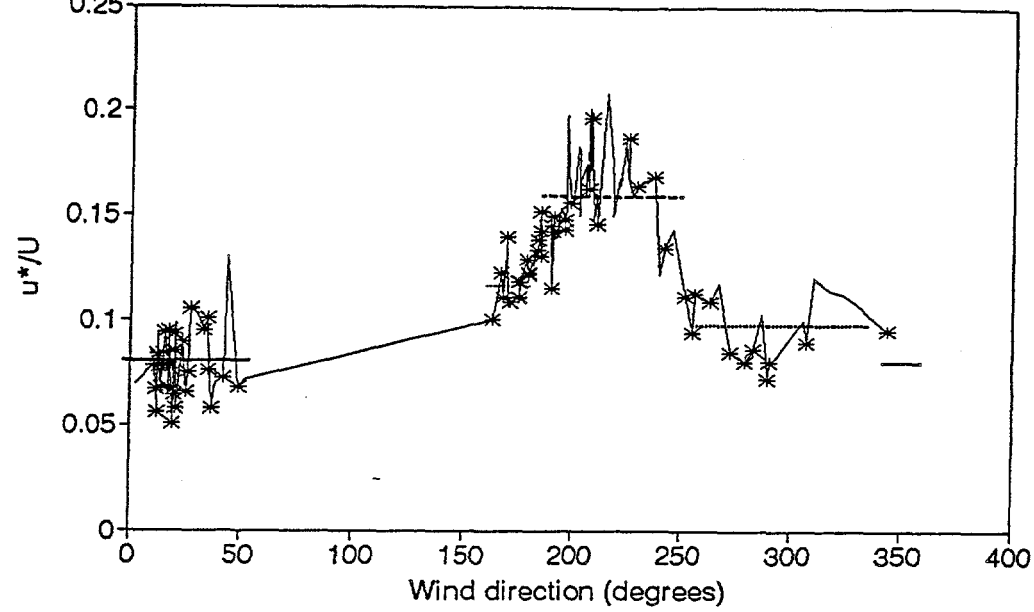

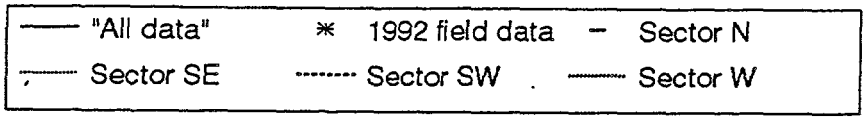

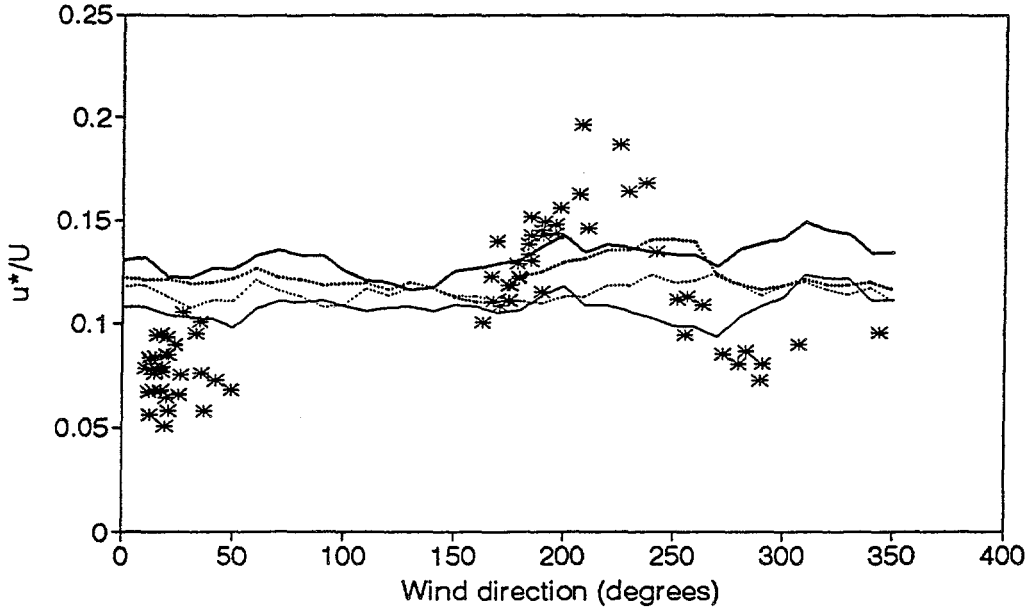

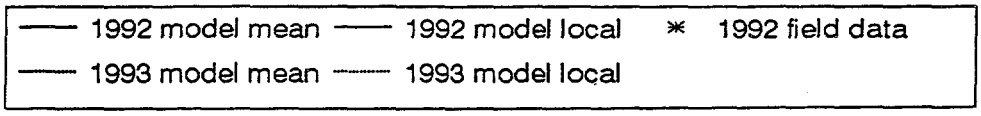

Figure 49. a) (above) Normalized friction velocity measured at Scherzheim, Rhine Valley in September 1992. Half-hourly mean values 4 m above ground as a function of wind direction. Only data affected less than ±10% owing to non-neutralality and U > 1.5 m s^{-1} are shown. The full curve is for wind direction deviations within 15°. The horizontal lines are the mean values for each sector.

b) (below) Normalized friction velocity at Scherzheim, Rhine Valley measured in September 1992, as well as microscale model results for 1 pixel and for a mean of 9 pixels at the field site. 1992 data are based on ERS-1 SAR satellite data and 1993 on Landsat TM data.

Comparison of single site fluxes to the modelled output is not ideal. However in case it will have to be performed again, it is recommended to site the mast in a relatively large field with a pronounced directional variation. The data sampling should have a duration time long enough to collect strong near-neutral winds from all directions.

The ideal validation method would be comparison between modelled fluxes and spatially sampled fluxes. In this case flux data collected by airborne eddy-correlation systems would be the best. Errors inherent in that kind of sampling should be considered. In the TRACT experiment the fluxes of sensible and latent heat were measured by airborne eddy correlation (Jochum et al. 1994). The number of repeat flights were too few and the data showed only small spatial gradients (Mahrt pers.com.). The momentum flux was not measured.

7.6 Future use of the microscale model

The microscale aggregation model can be developed to calculate scalar fluxes. Maps of the lower boundary conditions are hence in demand for real terrain application.

Sensible heat flux

For sensible heat flux the lower boundary conditions are maps of roughness *and* surface temperature. The latter is currently available from satellites. If we assume the air temperature to be homogeneous in the horizontal direction above a certain height we can calculate a heat flux map. The heat flux equation (eq 99) gives the heat flux from the temperature scale and the friction velocity, $H=-\rho c_p u_* \theta_*$ (eq 17). The calculation requires iteration as the stability term, ψ_H, is dependent on the sensible heat flux. The output will be a pixel-by-pixel heat flux map.

It would be ideal to calculate the heat flux from airborne thermal data or high-resolution satellite data and to validate the model results with eddy correlation heat flux data. A good candidate for the purpose is the BOREAS data set.

Latent heat flux

In principle latent heat flux can be obtained in a way analogous to the sensible heat flux. The lower boundary conditions would be roughness *and* surface humidity.

$$q-q_0=\frac{q_*}{\kappa}\left(\ln\left(\frac{z}{z_{0q}}\right)-\psi_E\left(\frac{z}{L}\right)\right) \qquad (169)$$

ψ_E depends on E, so iteration is needed before the humidity flux can be

calculated from $E=-\rho u_* q_*$ (eq 18). Here, however, q_0, is not readily available. A common way to get around the lack of q_0 is to estimate $\alpha q_{sat}(T_s)$ (section 4.7 and 6.6). An alternative may be to use the upper soil moisture measured from airborne radar data (section 4.7). It still needs some thoughts.

Latent heat flux can of course also be retrieved as the energy balance residual. It is likely, however, that the microscale aggregation model will do better than the simplified relationship. The reason is that the "constant c_3" (eqs 45 and 48) will be explicitly solved in the microscale model. So this error will not "end up" in the moisture flux.

Passive scalar fluxes

In principle fluxes of passive scalars can be calculated from the microscale aggregation model too. At this moment no remote sensors map surface concentrations of say, CO_2, NO, O_3, CH_4 or particulate matter. But in cases where a surface concentration can be inferred, a scalar flux version of the microscale model can be applied. It has to be assumed that a constant concentration is found above a certain height. The scalar exchange coefficient should be linear, ie excluding fast chemically reactive species (no flux divergence).

Trace gas exchanges differ from water vapour as the pathways are not identical. For example water vapour goes into stomata and soils whereas CO_2 enters stomata but typically is released from soils. The CO_2 contribution from soil to air is significant. Another example is that ozone not only enters stomata but also is deposited onto leaves. O_3 reacts with NO released from soil, ie the process reduces the surface concentration of ozone.

The interest of applying the microscale aggregation model for passive scalars is to be able to predict local deposition. We know that the "mean" pollution on a large scale is distributed very unevenly to a heterogeneous surface. An example is the momentum flux (figure 30). It also applies to scalar fluxes. The microscale model can be used to answer the question: How much pollutant will be deposited in a given location in a heterogeneous area? The questions is relevant for estimating the load to for example a vulnerable ecosystem.

In regard to local deposition two features of the atmospheric flow are important

1) the amount of pollutant
2) the deposition velocity

Both of these can have a strong directional dependency. The microscale model predicts a directional deposition velocity. Hence given a directional pollution concentration as input, the local deposition may be predicted for a given time period.

7.7 Summary on microscale aggregation

The microscale aggregation model is a physically based model. It predicts effective roughness, friction velocity and momentum flux in real terrain. The flow equations are linearized and only the diffusion term is modelled, as all other terms are thought to be of much less importance for the flow response over roughness step changes. The numerical solution is performed by the Fast Fourier Transform method.

Simple numerical test runs of the microscale model on artificial roughness terrain types, checkerboard and striped, show very promising results. All of the results are as expected from basic theory on the flow response over step changes. Prior to the numerical two-dimensional testing, analytic and numerical one-dimension model results were shown to closely follow higher-order closure models and experimental data (Jensen 1995).

The microscale model is applied to roughness maps with spatial resolutions of 25 m * 25 m and 30 m * 30 m. The roughness maps are based on classified ERS-1 SAR and Landsat TM satellite data from the Rhine Valley in Germany in 1992 and 1993. Appropriate local roughness values are assigned to the cover classes. The investigeated area along the valley floor is flat and highly heterogeneous.

Land surface friction velocity maps are calculated pixelwise for a 15 km * 15 km area. Momentum flux maps are also produced. Significant contrasts in the surface flux is noted both spatially and through season. Very large momentum fluxes are seen at the leading forest edges. In the lakes and rivers very low fluxes are observed. Friction velocity relaxation towards equilibrium is slow. In rough areas it far from reaches the equilibrium value. For the smoothest surface it unexpectedly does. One reason may be that the equilibrium flow results are calculated by the geostrophic drag law. This is not truly valid on the microscale. The typical horizontal length scale of roughness variation (measured from the Fourier spectra) is of the order of 650 m. However a large range of smaller length scales is present.

The wind directional dependence is also investigated. These results are compared to field data from a micrometeorological mast in Scherzheim. The field data of the ratio of the normalized friction velocity showed a strong directional dependence. The microscale model results are always within $\pm 50\%$ of the field data, but the model results do not clearly reveal the directional dependence. The most likely explanation is that the image data have a too low resolution in terrain with many single obstacles.

Future research on the microscale aggregation model tends towards validation with airborne eddy correlation momentum fluxes. Development of a scalar flux model version of the microscale model is envisaged.

8 Conclusion

Calculation of the surface fluxes in heterogeneous landscapes is a scientific challenge not yet fully accomplished. Utilizing satellite information in the calculation of land surface momentum flux is, however, a significant step forward.

Background summary

Surface fluxes in heterogeneous landscape can only be calculated using similarity theory, a method that is only truly valid for homogeneous terrain. The essence of the problem is to make the similarity relations work through area-averaged (effective) boundary conditions or alternatively area-averaged exchange coefficients (conductances or resistances).

The area-averaged roughness length for momentum is always larger than the logarithmic mean, the latter only being valid for surface flux prediction with equilibrium flow. Conversely, the area-averaged roughness length for temperature is usually smaller than the logarithmic mean. It is clear from theory and data that the ratio between area-averaged momentum and scalar roughness is strongly increased in heterogeneous terrain compared to homogeneous.

A key parameter in surface flux calculation is the horizontal landscape scale. Landscapes with patches of the size order up to 100 m are *homogeneous* as seen from "normal" (field mast) observation heights and similarity scaling describes boundary layer flow well. Conversely advective effects between *microscale* patches (100 to 1000 m) are significant. Two-dimensional models based on the blending height concept or the so-called texture analysis offer solutions for a limited number of idealized (geometric) terrain patterns. However two problems have hampered a practical real terrain solution; one was the lack of real terrain surface information, the other lack of a parametrization capable of treating arbitrary site specific roughness distributions.

The present work overcomes both problems and predicts roughness values useful for *mesoscale* treatment. In effect the new approach links microscale dynamics to high-resolution mesoscale models (10 to 100 km). The gap from microscale to mesoscale, namely between one to ten km, is thereby bridged.

Achievements

The present work demonstrates the application of a physically based flux aggregation model that predicts the effective roughness from satellite based roughness maps. The atmospheric flow equations are linearized and only the diffusion term is modelled. A Fast Fourier Transform is used to solve the equations. The microscale flux aggregation method was proposed by Jensen

(1994).

Part of the work focused on a two-dimensional sensitivity test on artificial heterogeneous landscapes of checkerboard and striped geometries. The results perform as expected according to current knowledge of the turbulent dynamic response to roughness step changes.

Data from the Upper Rhine Valley in Germany were used for the real terrain application part. The terrain investigated is flat but highly heterogeneous. Classified SAR and optical imagery were combined with micrometeorological field data of roughness lengths from a project on Transport of Pollutants over Complex Terrain (TRACT) conducted in September 1992. Currently satellite-based land surface roughness maps can only be attained reliably through classification processes. Direct roughness retrieval is still in its infancy.

The microscale model output from real terrain encompass the area-averaged (effective) roughness for momentum, area-averaged (effective) friction velocity and area-averaged momentum flux. At the same time high-resolution maps of friction velocity and momentum flux are calculated. From these maps site specific values can be read out. The maps seem to be the first of their kind.

Inverting the microscale model facilitates the prediction of site specific friction velocity and momentum flux. A comparison with results obtained using the geostrophic drag law shows very large differences in both rough and smooth terrain. However the drag law results are only valid for equilibrium flow.

Comparison of normalized friction velocity measured on a field site agrees within $\pm 50\%$ to the microscale model outputs. A directional dependence as a function of upwind roughness was pronounced in the field data, but not convincingly clear in the microscale model results. A likely reason is that tall, small-scale heterogeneity in the form of scattered trees, was present at the site (Scherzheim). These elements are smaller than the spatial resolution of both ERS-1 SAR and Landsat TM (25^2 m^2 and 30^2 m^2) respectively, and thus cannot be mapped.

Recommendations

Validation of momentum flux results by comparison to airborne eddy correlation data seems a natural next step.

A future scalar flux version of the microscale model will allow prediction of scalar fluxes in heterogeneous landscape. Sensible heat calculation require high-resolution thermal maps. It is anticipated that the results will be superior to estimates from the simplified relationship in heterogeneous terrain, as the nonlinear effects of wind and roughness on surface fluxes are parametrized through the physical description. Latent heat could be calculated as the energy balance residual, however, probably with less error propagation.

Moisture flux could be calculated directly by input of high-resolution soil moisture data in a scalar flux version model. Only airborne passive microwave

data have the required accuracy.

Passive scalar fluxes could be retrieved. However the most obvious use is to downscale these fluxes from known large-scale concentration values. That means to predict the deposition load of pollutants to given sites in a heterogeneous landscape.

Dansk sammendrag

Overflade fluxe i heterogent landskab beregnes udfra similaritets teori. Similaritets teorien er dog kun fuldt gyldig for homogent terræn. Similaritets relationerne anvendes derfor med brug af såkaldte *effektive* parametre. Det kan være arealmiddelværdier af grænsebetingelserne, dvs effektive ruhedslængder. Alternativt kan det være arealmiddelværdier af udvekslingskoefficienterne, dvs effektiv konduktans eller effektiv modstand.

I heterogent landskab vil den effektive arealmiddelværdi af ruhedslængden for momentum altid være større end det tilsvarende logaritmiske middel. Sidstnævnte middelværdi er gyldig ved beregning af overflade fluxen mellem overfladen og atmosfæren med ligevægtsstrømning. Den effektive ruhedslængde for temperatur er som regel mindre end det logaritmiske middel af ruhedslængderne for temperatur. Udfra både teori og data er det dermed klart at i heterogent landskab kan forholdet mellem de effektive ruhedslængder for momentum og temperatur afvige meget fra forholdet mellem disse ved ligevægtsstrømning.

Et landskabs heterogenitet kan beskrives udfra den typiske horisontale længdeskala. Landskaber med felter af størrelsesorden op til 100 m kan betegnes som homogene set fra "normal" observationshøjde (f.eks. mikrometeorologiske master) og similaritets teorien er gyldig. I kontrast til dette kan der være en stor advektiv effekt mellem mikroskala felter (100 til 1000 m). Beregning af overflade fluxe i landskab med mikroskala heterogenitet må derfor baseres på to-dimensionale modeller. "Blending height" konceptet og såkaldt "tekstur analyse" giver kun løsninger for idealiserede terræn typer med simple geometrier, ikke for naturligt landskab.

Kort sagt har to problemer hindret en praktisk anvendelig løsning for beregning af overflade fluxe i naturligt heterogent landskab med mikroskala felter: det ene er manglende kortlægning af de lokale og regionale grænsebetingelserne, det andet er manglen på en parametrizering (matematisk model), der er i stand til at løse for arbitrære stedbestemte ruhedsfordelinger objektivt og hurtigt.

Herværende projektarbejde giver en løsning på begge problemer. Dermed er det opnået at beregne effektive ruhedslængder til brug i mesoskala sammenhæng (5 til 100 km). Værdierne er beregnet for et heterogent landskab i Rhindalen, Tyskland. Opskalering af grænsebetingelsen for ruhed mellem mikroskala og større atmosfærisk skala er hermed løst.

Gennem arbejdet demonstreres det, hvorledes den fysisk baserede flux aggregerings model kan anvendes til at beregne den effektive ruhed udfra satellit-baserede ruhedskort. De atmosfæriske strømningsligninger er lineariserede og kun diffusionsledet er modelleret. En to-dimensional Fast Fourier Transform bruges til at løse ligningssættet. Ideen til mikroskala flux aggregerings metoden blev foreslået af Jensen (1994).

En del af arbejdet er fokuseret på en to-dimensional sensitivitets analyse for heterogent terræn med simple geometrier såsom skakbræt og striber. Alle

resultaterne svarer til de forventede udfra kendskabet til det turbulente atmosfæriske respons til abrupte ruhedsskift.

Feltdata og satellitdata fra Den Øvre Rhindal blev brugt ved analysen for naturligt landskab. Landskabet er fladt men meget heterogent med mange forskellige arealanvendelses typer og små felter i et stærkt varierende mønster. Klassificerede optiske og syntetiske apertur radar satellitbilleder blev kombineret med mikrometeorologiske feltdata af ruhedslængder. Disse data blev indsamlet i et Europæisk Union projekt kaldet "Transport of Pollutants over Complex Terrain" (TRACT) i September 1992. For nuværende kan satellit-baserede ruhedskort kun opnås med en rimelig sikkerhed gennem en klassifikations procedure og efterfølgende tildeling af kendte (feltmålte) ruhedslængder. Direkte ruhedslængde estimering fra satellitdata er attraktiv for vegetationsdækkede overflader, men er endnu ikke fuldt undersøgt.

Resultaterne fra mikroskala aggregerings modellen er arealmiddelværdien af ruhedslængden for momentum, arealmiddelværdien af friktions hastigheden og arealmiddelværdien af momentum fluxen. På samme tid beregnes to-dimensionale kort af friktions hastighed og momentum flux. Fra disse kort kan værdierne udlæses sted-specifikt med en høj rumlig opløselighed. Kortene er de første af deres slags.

Ved at invertere mikroskala modellen kan sted-specifikke værdier af friktions hastighed og momentum flux beregnes. Disse mikroskala model resultater er sammenlignet med de tilsvarende værdier, som fås ved at anvende "den geostrofisk drag law" metode. "Drag law" resultaterne er kun gyldige for ligevægtsstrømning og der ses meget store forskelle mellem de to metoder både i ru og glat terræn. Dette forhold indikerer betydningen af at inddrage den advektive turbulent effekt i beregningerne.

Ved at sammenligne den normaliserede friktions hastighed målt på en mark i Scherzheim i Rhindalen og mikroskala model resultaterne ses en rimelig overensstemmelse. Mikroskala model resultaterne afveg mindre end ± 50 % fra de målte data. Vindretningen viste sig at have stor betydning for friktions hastigheden i feltdata, men denne tendens kunne ikke klart genfindes i mikroskala model resultaterne. Forklaring antages at være at bl.a. enkeltstående træer ikke var korrekt repræsenteret udfra de tilgængelige satellitdata. Disse var Landsat TM på 30 m * 30 m pixels og ERS SAR på 25 m * 25 m. (Vigtige) elementer af sub-pixel størrelse kan mangle.

Det anbefales stærkt at validere mikroskala model resultaterne med flybårne momentum flux data. Det er meget vigtigt at sammenligne rumlige model resultater med rumlige data fremfor med punktmålte data især i heterogent landskab.

Mikroskala aggregerings metoden vil kunne anvendes til beregning af skalare fluxe som varme og vanddamp. Hertil kræves rumlige input af overflade temperatur og overflade fugtighed. Disse værdier vil kunne uddrages fra data fra eksisterende satellit- og flybårne billeddannende sensorer.

Acknowledgements

I would like to express my gratitude to Dr. Niels Otto Jensen of the Department of Meteorology and Wind Energy (Risø National Laboratory) for his very inspiring comments and suggestions. It has been a great pleasure to work under his continued positive and patient guidance. Professor Henrik Søgaard of the Institute of Geography (University of Copenhagen) encouraged me to undertake the research project of this dissertation. I am very grateful to him for giving me the oppurtunity to work with an interesting application of satellite imagery and for his support as supervisor.

The study under Professor Toby Carlson of the Department of Meteorology (the Pennsylvania State University) was a very fruitful and pleasant experience. Professor Carlson's warm and humorous personality made me feel at home immediately. His teaching on counter-intuitive system responses in SVAT modelling was extremely revealing to me. My sincere thanks also go to Dr. Rob Gillies, Dr. Bill Capehart and Mr. David Ripley for their kind and unfailing support through the six months I spent at Penn State. I would also like to thank Dr. Larry Hipps at the Department of Plants Soils and Biometeorology and Dr. Christopher Neale at the Department of Biological and Irrigation Engineering (Utah State University) for inspiring discussions at USU.

I would like to acknowledge Dr. Helmut Frank and Dr. Jakob Mann both of Risø for kind assistance and comments on the microscale model. Dr. Beki Barthelmie of Risø has given me other useful suggestions. Professor Larry Mahrt of Oregon State University has given me inspiration through his visits at Risø. I am grateful to Mrs. Birthe Skrumsager, Dr. Mike Courtney and Dr. Helmut Frank for reading my draft. I would like to thank all of my colleagues at Risø for their support.

I acknowledge Dr. Christoph Konrad and Dr. Wilhelm Hagg of Institut für Photogrammetrie und Fernerkundung (Universität Karlsruhe) for the classified Landsat TM and ERS SAR data. The airborne EMISAR data are from the Danish Multisensor Airborne Campaign (DANMAC) group.

I acknowledge the financial support by The Danish Environmental Research Programme and The Danish Research Academy for three years, including the additional expenses for me spending six months of these years at the Pennsylvania State University.

References

Adrian G. and F.Fiedler,1991. Simulation of unstationary wind and temperature fields over complex terrain and comparison with observations, Beitr.Phys.Atmosph,vol 64 no 1,27-48

Antoine J.Y. M.Derrien, L. Harang, P.Le Borgne, H.Le Gleau and C. Le Goas, 1992. Errors at large satellite zenith angles on AVHRR derived sea surface temperatures, Int.J.Remote Sensing, vol 13 no 9, 1797-1804

Astrup P. N.O.Jensen and T.Mikkelsen,1996. Surface roughness model for LINCOM,Risø Report-900, 31p

Avissar R.,1991. A statistical-dynamical approach to parameterize subgrid-scale land-surface heterogeneity in climate models,in E. Wood (ed.) Land Surface/Atmosphere Interactions for Climate Modeling, Kluwer Academic Pub., 155-178

Baldocchi D.D. R.J.Luxmoore and J.L.Hatfield,1991. Discerning the forest from the trees: an essay on scaling canopy stomatal conductance. Agriculture and Forest Meteorology 54, 197-226

Band L.E.,1991. Distributed parameterization of complex terrain. In E. Wood (ed.) Land Surface/Atmosphere Interactions for Climate Modeling, Kluwer Academic Pub., 249-270

Barthelmie R.J. and N.O.Jensen,1995. TRACT database #4:Surface measurements Station and data description, Risø Report-816, 54p

Becker F. and Z.-L.Li,1993. Surface temperature and emissivity at various scales. In T. Carlson et al. (eds) Thermal Remote Sensing ACTES-proc. Sep.93 France, 35-60

Beljaars A.C.M. and P.Viterbo, 1994. The sensitivity of winter evaporation to the formulation of aerodynamic resistance in the ECMWF model, Boundary-Layer Meteorology vol 71, 135-149

Beljaars A.C.M. and A.A.M.Holtslag, 1991. Flux parametrerization over land surfaces for atmospheric models, J. Applied Meteorology, 327-341

Blyth E.M. A.J.Dolman and N.Wood ,1993. Effective resistance to sensible- and latent-heat flux in heterogeneous terrain, Q.J.R.Meteorol.Soc. 199, 423-442

Blyth E.M and A.J.Dolman,1995. The roughness length for heat of sparse vegetation, J.Applied Meteorology vol 34, 583-585

Bougeault P. B.Bret, P.Lacarrere and J.Noilhan,1991. An example of spatial integration of a land-surface parameterization in a Meso-Beta-Scale model. In T.J.Schmugge and J.-C.Andre (eds) Land Surface Evaporation. Springer-Verlag. New York, 383-402

Bougeault P.,1991. Parameterization Schemes of Land-Surface Processes for Mesoscale Atmospheric Models. In T.J.Schmugge and J-C.André (eds) Land Surface Evaporation. Springer-Verlag. New York, 55-92

Bradley E.F.,1968. A micrometeorological study of velocity profiles and surface drag in the region modified by a change in surface roughness, Q.J.R.Meteorol.Soc. 94, 361-

Brutsaert W. and M.Sugita,1992. Regional surface fluxes from satellite-derived surface temperatures (AVHRR) and radiosonde profiles, Boundary-Layer Meteorology vol 58, 355-366

Brutsaert W. A.Y.Hsu and T.J.Schmugge, 1993. Parameterization of Surface Heat Fluxes above Forest with Satellite Thermal Sensing and Boundary-Layer Soundings, J.Applied Meteorology vol 32, 909-917

Brutsaert W.,1982. Evaporation into the Atmosphere.Theory History and Applications, D.Reidel Publishing Company London, 299p

Busch N.E.,1973. On the mechanics of atmospheric turbulence. In D.A.Haugen (ed) Workshop on micrometeorology , American Meteor.Soc, 1-65

Camillo P.J. R.J.Gurney and J.E.Devaney,1991. A Two-Dimensional Model of the Hydrological Response of a Hillslope. In T.J.Schmugge and J-C.André (eds) Land Surface Evaporation. Springer-Verlag New York, 121-136

Capehart W.J.H. and T.N.Carlson,1994. Estimating near-surface soil moisture availability using a meteorologically driven soil-water profile model, J. Hydrology vol 160, 1-20

Carlson T.N. R.R.Gillies and E.M.Perry,1994. A method to make use of thermal infrared temperature and NDVI measurements to infer surface soil water content and fractional vegetation cover, Remote Sensing Reviews vol 9, 161-173

Carlson T. O.Taconet, A.Vidal, S.Moran and R.Gillies (eds.),1993. Thermal remote sensing, ACTES-Proceedings, France, 31-32

Carlson T.N.,1991. Recent advances in modeling the infrared temperature of vegetation canopies, In T.J.Schmugge and J-C.André (eds) Land Surface Evaporation. Springer-Verlag. New York, 349-358

Carlson T.N. W.J.Capehart and R.R.Gillies,1995. A new look at the simplified method for remote sensing of daily evapotranspiration, Remote Sens. Environ. vol 54 no 2, 161-167

Carlson T.N. E.M.Perry and T.J.Schmugge, 1990. Remote estimation of soil moisture availability and fractional vegetation cover for agricultural fields, Agriculture and Forest Meteorology 52, 45-69

Carlson T.N. and M.Buffum, 1989. On Estimating Total Daily Evapotranspiration from Remote Surface Temperature Measurements, Remote Sens. Environ. 29 no 2, 197-207

Caselles V.,1993. Mapping actual evapotranspiration by combining Landsat-TM and NOAA-AVHRR images, In T.Carlson et al. (eds) Thermal Remote Sensing ACTES-proc. Sep.93 France, 309-312

Chamberlain A.C.,1968. Transport of gases to and from surfaces with bluff and wave-like roughness elements, Q.J.R.Meteorol.Soc. Met Soc 94, 318-332

Chehbouni A. E.G.Njoku, J.P.Lhomme and Y.H.Kerr, 1993. Aggregation techniques for estimating hydrologic flux controlling parameters:appl. to remotely sensed surface temp. In T.Carlson et al. Thermal Remote Sensing ACTES-Proc. Sep.93 France, 129-132

Choudhury B.J.,1994. Synergism of Multispectral Satellite Observations for estimation regional land surface evaporation, Remote Sens.Environ. 49, 264-274

Claussen M. and W.Klaassen,1992. On regional surface fluxes over partly forested areas,Max-Planck-Institut für Meteorologie Report no 82, 11p

Claussen M., 1991. Estimation of areally-averaged surface fluxes, Boundary-Layer Meteorology 54, 387-410

Claussen M.,1990. Area-averaging of surface fluxes in a neutrally stratified horizontally inhomogeneous atmospheric boundary layer, Atmospheric Environment vol 24A no 6, 1349--1360

Claussen M.,1992. Scale aggregation in semi-smooth flow, Max-Planck-Institut für Meteorologie Report no. 87, 21p

Coll C. V.Caselles, J.A.Sobrino and E.Valor,1994. On the atmospheric dependence of the split-window equation for land surface temperature, Int. J. Remote Sensing vol 15 no 1, 105-122

Crago R.D.,1996. Daytime evaporation from conservation of surface flux ratios. I J.Stewart J.B. E.T.Engman, R.A.Feddes and Y.Kerr (eds) Scaling up in hydrology using remote sensing, John Wiley and Sons, Chichester, 235-244

Curran P.J,1988. The semivariogram in remote sensing:An introduction, Remote Sens. Environ. 24, 493-507

de Bruin H.A.R. N.J.Bink and L.J.M.Kroon,1991. Fluxes in the Surface Layer Under Advective Conditions, In J.J.Schmugge and J-C.André (eds) Land Surface Evaporation. Springer-Verlag. New York, 157-170

Desjardins R.L. and J.I.MacPherson,1991. Water Vapor Flux measurements from Aircraft. In T.J.Schmugge and J-C.André (eds) Land Surface Evaporation. Springer-Verlag. New York, 245-260

Diak George R., 1990. Evaluation of heat flux moisture flux and aerodynamic roughness at the land surface from knowledge of the PBL height and satellite-derived skin temperatures, Agriculture and Forest Meteorology 52, 181-198

Diak G.R. and T.R.Stewart, 1989. Assessment of surface turbulent fluxes using geostationary satellite surface skin temperatures and a mixed layer planetary boundary layer scheme, J.Geophys.Research vol 94 no D5, 6357-6373

Diak G.R., 1993. Current and future methods for the remote sensing of the land-surface energy balance. In T.Carlson et al. (eds) Thermal Remote Sensing ACTES-Proc. Sep. 93 France, 261-264

Diak G.R. C.J.Scheuer, M.S.Whipple and W.L.Smith,1994. Remote sensing of land-surface energy balance using data from the High-Resolution Interferometer Sounder (HIS):A simulation Study, Remote Sens.Environ 48, 106-118

Dickenson R.E.,1995. Land Processes in Climate Models, Remote Sens. Environ. vol 51, 27-38

Dobson M.C. F.T.Ulaby and L.E.Pierce,1995. Land-cover classification and estimation of terrain attributes using synthetic aperture radar, Remote Sens.Environ. 51, 199-214

Dolman A.J.,1993. A multiple-source land surface energy balance model for use in general circulation models, Agriculture and Forest Meteorology 65, 21-45

Dolman A.J.,1992. A note on areally-averaged evaporation and the value of the effective surface conductance, J.Hydrology 138, 583-589

Dubois P. C.J.van Zyl and T.Engman,1995a. Measuring soil moisture with imaging radars, IEEE Trans.Geosc.and Remote Sens. vol 33 no 4, 915-926

Dubois P. C.J.van Zyl and T.Engman,1995b,Corrections to "Measuring soil moisture with imaging radars",IEEE Trans.Geosc. and Remote Sens. vol 33 no 6,1340

Dubois P. C.J.van Zyl and T.Engman,1995c. Measuring soil moisture with active microwave:effect of vegetation, Proc. IGARSS, IEEE vol.1, 495-497

Engman E.T., 1995. Microwave remote sensing of soil moisture. Progress potential and problems, Proc. IGARSS IEEE vol 1, 489-491

Engman E.T. and R.J.Gurney,1991. Remote Sensing in Hydrology, Chapman and Hall. London, 230p

Eymard L and O.Taconet, 1995. The methods for inferring surface fluxes from satellite data, and their use for atmosphere model validation, Int. J. Remote Sensing vol 16 no 11, 1907-1930

FAO Remote Sensing Centre,1993. Radar imagery:Theory and interpretation. Lecture Notes,ESA FAO Rom, 103p

Ferrazzoli P. S.Paloscia, P.Pampaloni, G.Schiavon, D.Solimini and P.Coppo,1992. Sensitivity of microwave measurements to vegetation biomass and soil moisture content:A case study, IEEE Trans.Geosc.and Remote Sens. vol 30 no 4, 750-755

Fiedler F.,1996. Heat, moisture and mass exchange processes on a regional scale in a non homogeneous terrain, Final report, Inst. Meteor. und Klimaforschung, Karlsruhe

Fiedler F.,1991. TRACT annual report 1990, EUROTRAC part 3, 18p

Fiedler F. J.Ebert, H.Noppel and G.Adrian,1994 .Heat exchange processes at sloping terrain, Annual report 1994, Universitat Karlsruhe, 42-73

Garratt J.R.,1978. Transfer characteristics for a heterogeneous surface of large aerodynamic roughness, Q.J.R.Meteorol.Soc 104, 491-502

Gash J.H.C., 1986, A note on estimating the effect of a limited fetch on micrometeorological evaporation measurements, Boundary-Layer Meteorology 35, 409-413

Gilabert M.A. C.Conese and F.Maselli,1994. An atmospheric correction method for the automatic retrieval of surface reflectances from TM images, Int. J. Remote Sensing vol 15 no 10, 2065-2086

Gash J.H.C.,1987. An analytical framework for extrapolating evaporation measurements by remote sensing surface temperature, Int. J. Remote sensing vol 8 no 8, 1245-1249

Goutorbe J.-P. and C.Tarrieu,1991. HAPEX-MOBILHY data base. In T.J.Schmugge and J-C.André (eds) Land Surface Evaporation. Springer-Verlag and J.-C.Andre, Springer-Verlag. New York, 403-410

Greeley R. and D.Blumberg,1995. Preliminary analysis of shuttle radar laboratory (SRL-1) data to study aeolian features and processes, IEEE Trans. Geosc. and Remote Sensing vol 33 no 4, 927-933

Greeley R. L. Gaddis, N.Lancaster A.Dobrovolskis, J.Iversen K.Rasmussen S.Saunders J.van Zyl, S.Wall H.Zebher and B.White,1991,Assessment of aerodynamic roughness via airborne radar observations, Acta Mechanica Suppl 2, 77-88

Greeley R. D.G.Blumberg, A.Dobrovolskis, L.R.Gaddis, J.D.Iversen, N.Lancaster, K.R.Rasmussen, R.S.Sauners, S.D.Wall and B.R.White,1995a. Potential transport of windblown sand:influence of surface roughness and assessment with radar data. In V.P.Tchakerian (ed.) Desert Aeolian Processes. Chapman and Hall, NY, 75-99

Greeley R. D.G.Blumberg, A.Dobrovolskis, J.D.Iversen, N.Lancaster, K.R.Rasmussen, S.D.Wall, B.R.White,1995b. Applications of spaceborne radar laboratory data to the study of aeolian processes,SRL Aeol. features, California, 32p

Gu X.F. and B.Seguin,1993. Evaluation of correction methods for atmospheric effects on temperature measured by ERS1-ATSR, NOAA11-AVHRR and Landsat 5-TM sensors. In T.Carlson et al. Thermal Remote Sensing ACTES-Proc. Sep. 93 France, 99-102

Hagg W. and M.Szies, 1994. Efficient speckle filtering of SAR images. Proc. IEEE IGARSS, Pasadena, USA, 2140-2142

Hall F.G. K.F.Huemmrich, S.J.Goetz, P.J.Sellers and J.E.Nickeson, 1992. Satellite Remote Sensing of Surface Energy Balance:Success, Failures, and Unresolved Issues in FIFE, J.Geophys.Research vol 97 no D17, 19061-19089

Hallikainen M.T. F.T.Ulaby, M.C.Dobson, M.A.El-Rayes and L-K. Wu,1985. Microwave dielectric behaviour of wet soil - Part 1:Empirical models and experimental observations. IEEE Trans.Geosc. and Remote Sensing vol 23 no 1, 25-34

Hansen L. N.K.Højerslev and H.Søgaard,1993. Temperature Monitoring of the Danish Marine Environment and the Baltic Sea, University of Copenhagen. Copenhagen, 77p

Hasager C.B. and N.O.Jensen, 1996a. Aggregation of roughness lengths for surface flux calculation. European Geophysical Society, XXI General Assembly. Annales Geophysicae, Suppl 14. Part II, C356

Hasager C.B. and N.O.Jensen,1996b. Scaling up roughness lengths from local scale to mesoscale for surface flux estimation. Oral presentation at Scaling up hydrological variables using remote sensing, at Institute of Hydrology, Wallingford, UK. 10-12 June 1996

Hasager C.B.,1993. Satellite remote sensing as a tool for spatial evapotranspiration estimation in vegetated areas, Geografisk Tidsskrift 93. bind, 56-62

Henderson-Sellers A. and A.J.Pitman,1992. Land-Surface Schemes for Future Climate Models:specification,Aggregation, and Heterogeneity, J. Geophysical Research vol 97 no D3, 2687-2696

Hildebrand P.H.,1991. Errors in eddy correlation turbulence measurements from aircraft:Application to HAPEX-MOBILHY. In T.J.Schmugge and J-C.André (eds) Land Surface Evaporation. Springer-Verlag NY, 231-244

Hipps L.E. D.Or and C.M.U.Neale,1996. Spatial structure and scaling of surface fluxes in a Great Basin ecosystem. In J.Stewart E.T.Engman R.A.Feddes and Y.Kerr (eds) Scaling up in hydrology using remote sensing,John Wiley and Sons, Chichester, 113-126

Holtslag A.A.M. and M.Ek, 1996. Simulation of surface fluxes and boundary layer development over the pine forest in HAPEX-MOBILHY, J.Applied Met. vol 3, 202-213

Hummelshøj P. K.Pilegaard and N.O.Jensen,1994. Flux measurements of O_3 and NO_2 over a regrown wheat field, Proc.EUROTRAC symposium 1994, 1-5

Hurtado E. A.Vidal and V.Caselles,1996. Comparison of two atmospheric correction methods from Landsat TM thermal band, Int.J.Remote Sens. vol 17 no 2, 237-247

Hurtado E. M.M.Artigao and V.Caselles,1994. Estimating maize evapotranspiration from NOAA-AVHRR thermal data in the Albacete area. Spain, Int.J.Remote Sensing vol 15 no 10, 2023-2037

Jackson R.D. R.J.Reginato and S.B.Idso, 1977. Wheat Canopy Temperature: A Practical Tool for Evaluating Water Requirements, Water Resources Research vol 13 no 3, 651-656

Jensen N.O.,1981. Studies of the atmospheric surface layer during change in surface conditions. In Colloque Construire avec le vent. Nantes Juni 1981 Tome 1, France,I-4-1-I-4_20

Jensen N.O.,1994. Flux-aggregation modelling, European Geophysical Society XIX General Assembly (Session OA18), Grenoble, France, April 1994

Jensen N.O.,1978. Change of surface roughness and the planetary boundary layer, Q.J.R.Meteorol.Soc.Met.Soc. 104, 351-356

Jensen N.O. C.B.Hasager, H.P.Frank, J.Mann and L.J.Mahrt,1996. Development of a microscale model for the averaging of surface fluxes in inhomogeneous terrain. In F.Fiedler (ed.) Final report, IMK, Karlsruhe, c1-c29

Jensen N.O. and H.P.Frank,1996. Linearized flow over variable roughnesses (unpublished)

Jensen N.O., 1988. Air flow over complex terrain - commentary. In: W.L.Steffen and O.T.Denmead (eds) Flow and transport in the natural environment:advances and applications. Springer-Verlag, 230-239

Jensen, N.O. E.L.Petersen and I.Troen, 1984. Extrapolation of mean wind statistics with special regard to wind energy applications, WMO,/TD-No.15, 1-85

Jensen N.O. and N.E.Busch,1982. Atmospheric turbulence. In E.J.Plate (ed) Engineering meteorology, Elsevier, Amsterdam, 179-231

Jensen N.O.,1995. Flux-aggregation Modelling, Annales Geophysicae (submitted)

Jensen N.O. and J.Mann,1995. An objective method for flux aggregation over inhomogeneous surfaces (unpublished)

Jensen N.O. and P.Hummelshøj,1995. Derivation of canopy resistance for water vapour fluxes over a spurce forest, using a new technique for the viscous sublayer resistance, Agriculture and Forest Meteorology 73, 339-352

Jensen N.O. and P.Hummelshøj,1997. ERRATUM. Derivation of canopy resistance for water vapour fluxes over a spurce forest, using a new technique for the viscous sublayer resistance, Agriculture and Forest Meteorology, submitted

Ji J. P.v.d.Keur A.Thomsen and H.Skriver,1995. Soil moisture retrieval using the Danish L- and C-band polarimetric SAR, Hydrological science 1996, 1-3

Ji J. A.Thomsen and H.Skriver,1995. Estimating soil moisture using the Danish polarimetric SAR, IEEE Proc. IGARSS vol.2, 942-947

Jochum A.M. C.S.Strodl H.Willeke and N.Entstrasser,1994. The transport of heat, moisture and ozone in the atmospheric boundary layer in the Upper Rhine Valley. In P.M.Borrell et al. (eds) Proc. of EUROTRACT Symp. '94, 766-769

Jochum A.M.,1993. Evaporation and energy fluxes during EFEDA:horizontal variability and area averaging. In H.-J.Bolle R.A.Feddes and J.D.Kalma (eds) IAHS publ. no. 212, 373-380

Kaimal J.C. and J.J.Finnigan,1994. Atmospheric Boundary Layer Flows. Their Structure and Measurement, Oxford University Press New York, 289p

Kidder S.Q. and T.H.V.Haar,1995. Satellite Meteorology. An introduction,Academic Press, San Diego, 466p

Klaasen W.,1992. Average fluxes from heterogeneous vegetated regions, Boundary-Layer Meteorology vol 58, 329-354

Klaassen W. and M.Claussen,1995. Landscape variability and surface flux parameterization in climate models, Agriculture and Forest Meteorology 73, 181-188

Kohsiek W. H.A.R.de Bruin, H.The and B.van den Hurk,1993. Estimation of the sensible heat flux of a semi-arid area using surface radiative temperature measurements, Boundary-Layer Meteorology vol 63, 213-230

Kondo J. and H.Yamazawa,1986. Aerodynamic roughness over an inhomogeneous ground surface, Boundary-Layer Met. 35, 331-348

Konrad C. K.Segl and J.Wiesel,1994. Multitemporal landuse classification of the Upper Rhine Valley and adjacent areas with Landsat TM image data. In F.Fiedler Final report, Institut für Meteorologie, University of Karlsruhe a1-a13

Koster R.D. and M.J.Suarez,1992. A Comparative analysis of Two Land Surface Heterogeneity Representations, J.Climate, 1379-1390

Kubota A. and M.Sugita,1994. Radiometrically determined skin temperature and scalar roughness to estimate surface heat flux Part I:Parameterization of radiometric scalar roughness, Boundary-Layer Meteorology 69, 397-416

Kustas W.P. B.J.Choudhury, M.S.Moran, R.J.Reginato, R.D.Jackson, L.W.Gay, H.L.Weaver,1989. Determination of sensible heat flux over sparse canopy using thermal infrared data, Agriculture and Forest Meteorology 44, 197-216

Kustas W.P. D.C. Goodrich, M.S.Moran and 33 co-authors,1991. An interdisciplinary study of the energy and water fluxes in the atmosphere-biosphere system over semiarid rangelands: Description and some preliminary results., Bull. Amer. Meteorol.Soc.,72, 1683-1705

Kustas W.P. M.S.Moran, K.S.Humes, D.I.Stannard, P.J.Pinter Jr., L.E.Hipps, E.Swiatek and D.C.Goodrich,1994a. Surface energy balance estimates at local and regional scales using optical remote sensing from an aircraft platform and atmospheric data collected over semiarid rangelands, Water Res.Research vol 30, no 5, 1241-1259

Kustas W.P. K.S.Humes, J.M.Norman and M.S.Moran,1996. Single- and dual-source modeling of surface energy fluxes with radiometric surface temperature, J.Applied Met. vol 35, 110-121

Kustas W.P. E.M.Perry, P.C.Doraiswamy and M.S.Moran,1994b. Using satellite remote sensing to extrapolate evapotranspiration estimates in time and space over a semiarid rangeland basin, Remote Sens. Environ. 49, 275-286

Lagouarde J.-P. and K.J.McAneney,1992. Daily sensible heat flux estimation from a single measurement of surface temperature and maximum air temperature, Boundary-Layer Met. 59, 341-362

Lagouarde J.-P., 1991. Use of NOAA AVHRR data combined with an agrometeorological model for evaporation mapping, Int. J. Remote Sensing vol 12 no 9, 1853-1864

Lagouarde J.P., 1993. Using mid-morning surface temperature in the framework of future TIR satellite systems. In T.Carlson et al. (eds) Thermal Remote Sensing ACTES-Proc. Sep. 93 France, 227-232

Lagouarde J.P. Y.Brunet and R.G.B.Andre,1993. A simple PBL approach for estimating actual evapotranspiration from TIR data over a Pine forest canopy. In T.Carlson et al. (eds) Thermal Remote Sensing ACTES-Proc. Sep. 93 France, 265-270

Larsen S.E.,1993. Observing and modelling the planetary boundary layer. In E.Raschke and D.Jacob (eds) NATO ASI series VOL I 5,, Springer-Verlag, Berlin, 365-418

Lee J.S. I.Jurkevich, P.Dewaele, P.Wambacq and A.Oosterlinck,1994. Speckle filtering of synthetic aperture radar images: a review, Remote Sensing Reviews vol 8, 313-340

Lettau H.,1969. Note on Aerodynamic Roughness-Parameter Estimation on the Basis of Roughness-Element Description, Journal Applied Meteorology vol 8, 828-832

Lhomme J.-P. A.Chehbouni and B.Monteny, 1994. Effective parameters of surface energy balance inheterogeneous landscape, Boundary-Layer Meteorology vol, 297-309

Lopes A. E.Nezry, R.Touzi & H.Laur,1993. Structure detection and statistical adaptive speckle filtering in SAR images, Int. J. Remote Sensing vol 14 no 9, 1735-1758

Louis J-F. 1979. A parametric model of vertical eddy fluxes in the atmosphere, Boundary-Layer Met. 17, 187-211

Mahrt L.,1991. Heat and Moisture Fluxes over the Pine Forest in HAPEX. In T.J.Schmugge and J-C.André (eds) Land Surface Evaporation. Springer-Verlag NY, 261-274

Mahrt L. and M.Ek,1993. Spatial variability of turbulent fluxes and roughness lengths in HAPEX-MOBILHY, Boundary-Layer Meteorology vol 65, 381-400

Mahrt L. and J.Sun, 1995. Dependence of surface exchange coefficients on averaging scale and grid size, Q.J.R.Meteorol.Soc.Meteorol.Soc 121, 1835-1852

Mahrt L.,1987. Grid-Averaged Surface Fluxes, Monthly Weather Review vol 115, 1550-1560

Mahrt L.,1996. The bulk aerodynamic formulation over heterogeneous surfaces, Boundary-Layer Meteorology 78, 87-119

Markham B.L. and J.L. Barker, 1987. Thematic Mapper bandpass solar exoatmospheric irradiances, Int. J. Remote Sensing vol 8 no 3, 517-523

Markham B.L. and J.L.Barker, 1985. Spectral characterization of the LANDSAT Thematic Mapper sensors, Int. J.Remote Sensing vol 6 no 5, 697-716

Markwitz W. T.Winter, D.Kosmann, M.Wiggenhagen, W.Hagg and M.Sties, 1995. Radarkarte Deutschland, Zeitschrift für Photogrammetrie und Fernerkundung 4, 150-159

Mason P.J.,1988. The formation of areally-averaged roughness lengths, Q.J.R.Meteorol.Soc.Meterorol.Soc 114, 399-420

McAneney K.J. and J.P.Lagouarde,1994. The patchwork problem:effects of sub-pixel scale non-uniformity on the spatially-averaged sensible heat flux, Int. J.Remote Sensing vol 15 no 8, 1687-1694

McNaughton K.G. and M.R.Raupach,1996. Responses of the convective boundary layer and the surface energy. In J.Stewart E.T.Engman, R.A.Feddes and Y.Kerr (eds) Scaling up in hydrology using remote sensing,John Wiley and Sons, Chichester, 171-182

Menenti M.,1993. Understanding land surface evapotranspiration with satellite multispectral measurements, Adv.Space Res. Vol 13 no 5, 89-100

Menenti M. J.C.Ritchie, K.S.Humes, R.Parryl, Y.Pachepsky, D.Gimenez and S.Leguizamon,1996. Estimation of aerodynamic roughness at various spatial scales. In J.Stewart E.T.Engman, R.A.Feddes and Y.Kerr (eds) Scaling up in hydrology using remote sensing,John Wiley and Sons, Chichester, 39-58

Menenti M. and J.C.Ritchie,1994. Estimation of effective aerodynamic roughness of Walnut Gulch watershed with laser altimeter measurements, Water Res. Research vol 30 no 5, 1329-1337

Menenti M. and B.J.Choudhury,1993. Parameterization of land surface evaporation by means of location dependent potential evaporation and surface temperature range,Exchange Processes at the Land Surface for a Range of Space and Time Scale, IAHS publ 211, 561-568

Menenti M. and J.C.Ritchie, 1992. Estimation of effective aerodynamic roughness with altimeter measurements, IGARSS Procee. Space Remote Sensing vol II, 12th Ann, 1508-1510

Milly P.C.D.,1991. A refinement of the combination equations for evaporation. In E.Wood (ed) Land Surface/Atmosphere Interactions for Climate Modeling, Kluwer Academic Pub., 145-154

Moore K.E. D.R.Fitzjarrald and J.A.Ritter,1993. How well can regional fluxes be derived from smaller-scale estimates?, J.Geoph.Res. vol98 no D4, 7187-7198

Moran M.S. T.R.Clarke, Y.Inoue and A.Vidal,1994. Estimating crop water deficit using the relation between surface-air temperature and spectral vegetation index, Remote Sens. Environ. vol 49 no 3, 246-263

Mortensen N.G. and U.S.Said, 1996, Wind Atlas for the Gulf of Suez, Risø National Laboratory, 110p

Nemani R.R. and S.W.Running, 1989. Estimation of Regional Surface Resistance to Evapotranspiration from NDVI and Thermal-IR AVHRR Data, Journal of Applied Meteorology vol 28, 276-284

Nezry E. A.Lopex & R.Touzi,1991. Detection of structural and textural features for SAR images filtering,IEEE Trans. Geosc. and Remote Sensing, 2169-2171

Nieuwenhuis G.J.A. E.H.Smidt and H.A.M.Thunnissen, 1985. Estimation of regional evapotranspiration of arable crops from thermal infrared images, Int. J. Remote Sensing vol 6 no 8, 1319-1334

Noilhan J. J.C.André, P.Bougeault, J.P.Goutorbe and P.Lacarrere, 1991. Some Aspects of the HAPEX-MOBILHY Programme. In E.Wood (ed) Land Surface/Atmosphere Interactions for Climate Modeling, Kluwer Academic Pub., 31-62

Noilhan J. and P.Lacarrere,1995. GCM grid-scale evaporation from mesoscale modeling, J.Climate vol 8, 206-223

Norman J.M., 1993. Estimation of surface fluxes from remote observations of directional IR temperature. In T.Carlson et al. (eds) Thermal Remote Sensing ACTES-Proc. Sep. 93 France, 281-292

Norman J.M. M.Divakarla and N.S.Goel,1995. Algorithms for extracting information from remote thermal-IR observations of the Earth's surface, Remote Sens. Environ. 51, 157-168

O'Neill P.E. A.Y.Hsu and J.C.Shi,1995. Soil moisture estimation using time-series radar measurements of bare and vegetated fields in Washita '92, Proc. IGARSS vol 1 IEEE, 498-500

Oevelen P.J. van D.H.Hoekman and R.A.Feddes,1996. Errors in estimation of area soil water content from SAR data. In J.Stewart E.T.Engman R.A.Feddes and Y.Kerr (eds) Scaling up in hydrology using remote sensing,John Wiley and Sons, Chichester, 207-220

Offiler D., 1994. The calibration of ERS-1 satellite scatterometer winds, J. Atmospheric and Oceanic Techn. vol 11, 1002-1017

Oke T.R.,1987. Boundary Layer Climates , Methuen, New York 2.ed., 435pp

Panofsky H.A. and J.A.Dutton,1984. Atmospheric Turbulence. Models and methods for engineering applications,John Wiley and Sons,New York, 397p

Paulson C.A.,1970. The Mathematical Representation of Wind Speed and Temperature Profiles in the Unstable Atmospheric Surface Layer, Boundary-Layer Met., 857-861

Perrier A. and A.Tuzet,1991. Land Surface Processes:Description, Theoretical Approaches and Physical laws Underlying Their measurements. In T.J.Schmugge and J-C.André (eds) Land Surface Evaporation. Springer-Verlag NY, 145-156

Peterson E.W.,1969. Modification of mean flow and turbulent energy by a change in surface roughness under conditions of neutral stability, Q.J.R.Meteorol.Soc. 95, 561-575

Pilegaard K. N.O.Jensen and P.Hummelshøj,1995. Deposition of nitrogen oxides and ozone to Danish forest sites. (G.J.Heij and J.W.Erisman (eds.)) Acid rain research:do we have enough answers?,Elsevier, 31-40

Pocket Webster School & Office Dictionary, 1990, The World Publishing Company, New York, 2nd ed.

Prevot L. I.Champion and G.Guyot,1993b. Estimating surface soil moisture and leaf area index of a wheat canopy using a dual-frequency (C and X bands) scatterometer, Remote Sens. Environ. 46, 331-339

Prevot L. Y.Brunet, K.T.Paw and B.Seguin, 1993a. Canopy modelling for estimating sensible heat flux from thermal infrared measurements. In T.Carlson et al. (eds) Thermal Remote Sensing ACTES-Proc. Sep. 93 France, 17-22

Rambal S. B.Lacaze, H.Mazurek and G.Debussche,1985. Comparison of hydrologically simulated and remotely sensed actual ET from some Mediterranean vegetation formations, Int.J.Remote Sens. vol 6 no 8, 1475-1481

Rao K.S. J.C.Wyngaard and O.R.Cote,1974. The structure of the two-dimensional internal boundary layer over a sudden change of surface roughness, J Atmosph.Sci.vol 31, 738-746

Raupach M.R.,1994. Simplified expressions for vegetation roughness length and zero-plane displacement as functions of canopy height and area index, Boundary-Layer Meteorology 71, 211-216

Raupach M.R.,1991. Vegetation-atmosphere interaction in homogeneous and heterogeneous terrain:some implications of mixed-layer dynamics, Vegetatio 91, 105-120

Raupach M.R.,1993. The averaging of surface flux densities in heterogeneous landscapes, in Eds. H.-J.Bolle R.A.Feddes and J.D.Kalma, IAHS publ. no. 212, 343-356

Reutter H. F.-S.Olesen and H.Fischer, 1994. Distribution of the brightness temperature of land surfaces determined from AVHRR data, Int. J. Remote sensing vol 15 no 1, 95-104

Riou C. B.Itier og B.Seguin,1988. The influence of surface roughness on the simplified relationship between daily evaporation and surface temperature, Int.J.Remote Sensing vol 9 no 9, 1529-1533

Ritchie J.C. D.L.Evans, D.Jacobs, J.H.Everitt and M.A.Weltz, 1993. Measuring canopy structure with an airborne laser altimeter, Transactions of the ASAE, vol 36 no 4, 1235-1238

Rowntree P.R.,1991. Atmospheric Parameterization Schemes for Evaporation over Land:Basic Concepts and Climate Modeling Aspects, in Land Surface Evaporation. In T.J.Schmugge and J-C.André (eds) Land Surface Evaporation. Springer-Verlag, 5-30

Rufenach C.,1995. A new relationship between radar cross-section and ocean surface wind speed using ERS-1 scatterometer and buoy measurements, Int. J.Remote Sensing vol 16 no 18, 3629-3647

Running S.W.,1991. Computer simulation of regional evapotranspiration by integration landscape biophysical attributes with satellite data. In T.J.Schmugge and J-C.André (eds) Land Surface Evaporation. Springer-Verlag NY, 359-370

Sandholt I. and H.S.Andersen,1993. Derivation of Actual Evapotranspiration in the Senegalese Sahel, Using NOAA-AVHRR Data during the 1987 Growing Season, Remote Sens. Environ. 46, 164-172

Schmid H.P. and B.Bunzli, 1995. The influence of surface texture on the effective roughness length, Q.J.R.Meteorol.Soc. 121, 1-21

Schmid H.P. and T.R.Oke,1990. A model to estimate the source area contributing to turbulent exchange in the surface layer over patchy terrain, Q.J.R.Meteorol.Soc.116, 965-988

Schmugge T.J. and F.Becker,1991. Remote sensing observations for the monitoring of land-surface fluxes and water budgets. In T.J.Schmugge and J-C.André (eds) Land Surface Evaporation. Springer-Verlag NY, 337-348

Schmugge T. T.J.Jackson, W.P.Kustas and J.R.Wang,1992. Passive microwave remote sensing of soil moisture:results from HAPEX, FIFE and MONSOON 90, J.Photogrammetry and Remote Sens. 47, 127-143

Schmugge T.J. and T.J.Jackson,1996. Soil moisture variability. In J.Stewart E.T.Engman, R.A.Feddes and Y.Kerr (eds) Scaling up in hydrology using remote sensing,John Wiley and Sons, Chichester, 183-192

Schmugge T.J. and T.J.Jackson,1992. A dielectric model of the vegetation effects on the microwave emission from soils,IEEE Trans.Geosc. and Remote Sens. vol 30 no 4, 757-760

Schmullius C.,1995. Dependence of X- C- and L-band measurements to soil moisture on vegetated fields. A comparison of airborne scatterometer and SAR data, Proc. IGARSS IEEE vol.1, 501-503

Schumann R.,1990. SAR Image Filtering,ESA Earthnet programme office, Rome 30p

Seguin B. 1996. oral presentation at International Workshop on Scaling up hydrology using remote sensing, Wallingford June 1996

Seguin B. D.Courault and M.Guérif, 1994. Surface temperature and evapotranspiration: Application of local scale methods to regional scales using satellite data, Remote Sens.Environ. 49, 287-295

Seguin B. D.Courault and M.Guerig,1994. Surface Temperature and Evapotranspiration:Application of Local Scale Methods to Regional Scales Using Satellite Data, Remote Sens. Environ. 49, 287-295

Seguin B. and B.Itier,1983. Using midday surface temperature to estimate daily evaporation from satellite thermal IR data, Int J. Remote Sensing vol 4 no 2, 371-383

Sellers P.J. J.A. Berry, G.J.Collatz, C.B.Field and F.G. Hall, 1992. Canopy reflectance, photosynthesis, and transpiration. III. A reanalysis using improved leaf models and a new canopy integration scheme., Remote Sens. Environ. 42, 187-216

Sellers P.J., 1989. Vegetation-canopy spectral reflectance and biophysical processes, in G. Asrar (Ed) Theory and Applications of Optical Remote Sensing. John Wiley & Sons. New York, 297-335

Sellers et al. (16 co-authors, 1995. Remote sensing of the land surface for studies of global change:Models-Algorithms-Experiments, Remote Sens. Environ. 51, 3-26

Seth A. F.Giorgi and R.E.Dickinson,1994. Simulating Fluxes from Heterogeneous Land Surfaces:Explicit Subgrid Method Employing the Biosphere-Atmosphere Transfer Scheme (BATS), J.Geophys.Research vol 99, 18651-18667

Shuttleworth W.J., 1988. Macrohydrology -The new challenge for process hydrology, J.Hydrology 100, 31-56

Shuttleworth W.J.,1991a. Insight from large-scale observational studies of land/atmosphere interactions. In E.Wood (ed) Land surface - atmosphere interactions for climate modeling. Kluwer Academic Press, 3-30

Shuttleworth W.J.,1991b. Evaporation Models in Hydrology. In T.J.Schmugge and J-C.André (eds) Land Surface Evaporation. Springer-Verlag NY, 93-120

Silva L.F.,1978. Radiation and instrumentation in remote sensing. In P.H.Swain P.H. and S.M. Davis (eds) Remote Sensing: The Quantitative Approach, McGraw Hill book company. Hamburg, 21-51

Stewart J.B. W.P.Kustas, K.S.Humes, W.K.Nichols, M.S.Moran and H.A.R. de Bruin, 1993. Sensible heat flux - radiometric surface temperature relationship for 8 semi-arid areas., In T.Carlson et al. (eds) Thermal Remote Sensing ACTES-Proc. Sep. 93 France, 27-30

Stewart J.B.,1993. Sensible heat flux derived from radiometric surface temperature of sparse prairie grass. In T.Carlson et al. (eds) Thermal Remote Sensing ACTES-Proc. Sep. 93 France, 23-26

Strebel D.E. P.J.Sellers and F.G.Hall,1991. The FIFE data. In T.J.Schmugge and J-C.André (eds) Land Surface Evaporation. Springer-Verlag NYa, 411-414

Stull R.B.,1991. An Introduction to Boundary layer Meteorology, Kluwer Academic Publishers, 666p

Sugita M. and W.Brutsaert,1990. Regional surface fluxes from remotely sensed skin temperature and lower boundary layer measurements, Water Res.Research vol 26 no 12, 2937-2944

Sugita M. and A.Kubota, 1994. Radiometrically determined skin temperature and scalar roughness to estimate surface heat flux Part II: Performance of parameterized scalar roughness for the determination of sensible heat, Boundary-Layer Meteorology 70, 1-12

Sun J. and L.Mahrt,1995. Relationship of surface hat flux to microscale temperature variations:application to BOREAS, Boundary-Layer Meteorology 76, 291-301

Søgaard H.,1992. Estimation of the Spatial Variation in Evapotranspiration based on Landsat TM and NOAA Satellite Imagery, Geografisk Tidsskrift bd 92, 80-85

Søgaard H. S.N.Madsen, A.Thomsen, C.B.Hasager and K.Wølders,1996. Estimation of surface aerodynamic roughness on the basis of C-band polarimetric SAR data (unpublished)

Søgaard H.,1988. Estimation of the surface energy balance in the Sahelian zone of Western Africa, Geografisk Tidsskrift bd 88, 108-115

Thomsen A. B.Fog, H.Skriver and M.Stjernholm,1994. The DANMAC Data Report 1994, Foulum, Denmark

Thomsen B.B.,1992. Anvendelse af SAR-data i forbindelse med landbrug, Electromagnetic Institute, DTU,Denmark

Troen I. and E.L.Petersen, 1989. European Wind Atlas, Risø National Laboratory, 656pp

Ulaby F.T. C.T.Allen and G. Eger III,1984. Relating the microwave backscattering coefficient to leaf area index, Remote Sens. Environ. 14, 113-133

Vidal A. C.Devaux-Ros and M.S.Moran, 1993. Calibration of Landsat TM thermal band using surface energy balance. In T.Carlson et al. (eds) Thermal Remote Sensing ACTES-Proc. Sep. 93 France, 83-88

Vidal A. and A.Perrier,1989. Technical note. Analysis of a simplified relation for estimating daily evapotranspiration from satellite thermal IR data, Int. J.Remote Sensing vol 10 no 8, 1327-1337

Vihma T. and H.Savijarvi,1991. On the effective roughness length for heterogeneous terrain, Q.J.R.Meteorol.Soc. 117, 399-407

Vining R.C. and B.L.Blad,1992. Estimation of sensible heat flux from remotely sensed canopy temperatures, J.Geophys.Research vol 97 no D17, 18951-18954

Vries A.C. de,1996. Forest edges and tree lines heights computed from shadows of SLAR images, Annales Geophysicae EGS vol 14, c362

Vries A.C.de J.W.van den Barg and W.Klaassen,1996. Estimation of a landscape scale parameter from Landsat TM data,Int.J.Remote Sens. (submitted)

Vugts H. A.F.G.Jacobs and W.Klaassen,1996. SLIMM-project,Annales Geophysicae EGS vol 14, c351

Vugts H.F. and F.Cannemeijer,1981. Measurements of drag coefficients and roughness length at a sea-beach interface, J.Applied Meteorol. vol 20 no 4, 335-340

Wieringa J.,1993. Representative roughness parameters for homogeneous terrain, Boundary-Layer Meteorology 63, 323-363

Wieringa J.,1986. Roughness-dependent geographical interpolation of surface wind speedaverages, Q.J.R.Meteorol.Soc. 122, 867-889

Wood N. and P.Mason,1991. The influence of static stability on the effective roughness lengths for momentum and heat transfer, Q.J.R.Meteorol.Soc.117, 1025-1056

Woodhouse I.H. and D.H.Hoekman,1996. Modelling of microwave backscatter using a tree-growth model fro boreal-type forest within the NOPEX test site, Annales Geophysicae EGS vol 14, c362

Wukelic G.E. D.E.Gibbons, L.O.M.Martucci og H.R.Foote,1989. Radiometric Calibration of Landsat Thematic Mapper Thermal Band, Remote Sens. Environ. 28, 339-347

Wyngaard J.C.,1991. On the maintenance and measurement of scalar fluxes. In T.J.Schmugge and J-C.André (eds) Land Surface Evaporation. Springer-Verlag NY, 199-230

Bibliographic Data Sheet **Risø-R-922(EN)**

Title and authors

Surface fluxes in heterogeneous landscape

Charlotte Bay Hasager

ISBN	ISSN
87-550-2218-9	0106-2840

Department or group	Date
Wind Energy and Atmospheric Physics	January 1997

Groups own reg. number(s)	Project/contract No(s)

Pages	Tables	Illustrations	References
180	10	49	223

Abstract (max. 2000 characters)

The surface fluxes in homogeneous landscapes are calculated by similarity scaling principles. The methodology is well established. In heterogeneous landscapes with spatial changes in the microscale range, ie from 100 m to 10 km, advective effects are significant. The present work focus on these effects in an agricultural countryside typical for the midlatitudes.

Meteorological and satellite data from a highly heterogeneous landscape in the Rhine Valley, Germany was collected in the large-scale field experiment TRACT (Transport of pollutants over complex terrain) in 1992. Classified satellite images, Landsat TM and ERS SAR, are used as basis for roughness maps. The roughnesses were measured at meteorological masts in the various cover classes and assigned pixel by pixel to the images.

The roughness maps are aggregated, ie spatially averaged, into so-called effective roughness lengths. This calculation is performed by a microscale aggregation model. The model solves the linearized atmospheric flow equations by a numerical (Fast Fourier Transform) method. This model also calculate maps of friction velocity and momentum flux pixelwise in heterogeneous landscapes.

It is indicated how the aggregation methodology can be used to calculate the heat fluxes based on the relevant satellite data ie temperature and soil moisture information.

Descriptors INIS/EDB

AIR-BIOSPHERE INTERACTIONS; BOUNDARY CONDITIONS; BOUNDARY LAYERS; ENVIRONMENTAL TRANSPORT; FLOW MODELS; FOURIER TRANSFORMATION; LANDSAT SATELLITES; MAPPING; REMOTE SENSING; ROUGHNESS; SYNTHETIC-APERTURE RADAR; TWO-DIMENSIONAL CALCULATIONS

Available on request from Information Service Department, Risø National Laboratory,
(Afdelingen for Informationsservice, Forskningscenter Risø), P.O.Box 49, DK-4000 Roskilde, Denmark.
Telephone +45 46 77 46 77, ext. 4004/4005, Telex 43 116, Telefax +45 46 75 56 27